

# Real-World Simulation Model for Advanced Analyses and Developments of Trolleybus Systems

Mohammed Abohat





# **Real-World Simulation Model for Advanced Analyses and Developments of Trolleybus Systems**

From the Department of  
Electrical, Information and Media Engineering  
University of Wuppertal

for the degree of  
**Doctor of Engineering Sciences**  
**(Dr.-Ing.)**

approved dissertation

by  
**Mohammed Abohat, M.Sc.**  
from Koblenz

Supervisor: Univ.-Prof. Dr.-Ing. Markus Zdrallek  
Co-supervisor: Univ.-Prof. Dr.-Ing. Benedikt Schmülling

Day of thesis defence: 12. May 2023

## **NEUE ENERGIE AUS WUPPERTAL**

Publication series of the Chair of Power Systems Engineering,  
University of Wuppertal

Publisher: Univ.-Prof. Dr.-Ing. Markus Zdrallek

### **Impressum**

Abohat, Mohammed:  
Real-World Simulation Model for Advanced Analyses and  
Developments of Trolleybus Systems  
Neue Energie aus Wuppertal, Volume 53, 1<sup>st</sup> Edition 2023

Copyright: © 2023 Mohammed Abohat. All rights reserved  
Print: epubli – a service of neopubli GmbH, Berlin, [www.epubli.de](http://www.epubli.de)  
Image source: [iStock.com/monsitj](https://iStock.com/monsitj) (Cover)

## **Acknowledgements**

This thesis is written as part of my work as a research assistant at the chair of Power Systems Engineering at the University of Wuppertal. The work presents essential results of research projects, which are carried out in cooperation of the chair with partner institutions and experts from the German electric and public transport sectors. I would like to take this opportunity to express my gratitude to those who accompanied, inspired, and supported me along the way.

First and foremost, I would like to express my deepest gratitude to Univ.-Prof. Dr.-Ing. Markus Zdrallek, head of the chair and the supervisor of this thesis, for his continuous motivating words and the freedom to work independently during the execution of my research activities at the chair. I would also like to thank him for all for the scientifically constructive discussions and the knowledge he provided. Furthermore, I would like to thank Univ.-Prof. Dr.-Ing. Benedikt Schmülling, head of the chair of Electro-Mobility and Energy Storage Systems at the University of Wuppertal, for his commitment to taking over the co-supervisor.

I would also like to thank all involved at the chair of Power Systems Engineering, who have always inspired and supported me along my work. I want to express my gratitude to all colleagues in the project group for the great scientific work we did together and for the information and ideas we shared. Special thanks go to Dr.-Ing. Mahjar Wazifehdust, Dr.-Ing. Dirk Baumeister, and Dr.-Ing. Philippe Steinbusch, without whose assistance, insightful discussions, and interesting and informative criticism, this work would not be accomplished.

I would also like to thank my closest friends, who have always been very understanding and provided the necessary balance and motivation.

My parents, brothers, and sister deserve a special mention for their ongoing support and encouragement, which have accompanied me on my way and helped my effort succeed inadvertently.

I would like to express my sincere gratitude to my wife, Dr. Rawya Al-Akam, for her tireless efforts over the years and the valuable guidance she has provided me throughout my work.

Wuppertal, May 2023

Mohammed Abohat



## **Abstract**

Climate change is one of the greatest challenges of the 21st century, and curbing it requires significant efforts from all sectors, including transportation. The city's public transport system is a crucial component of the transport sector. Trolleybuses, which have been used as a means of public transportation for decades, have gained renewed popularity. Combining the tried-and-true trolleybus technology with the state-of-the-art battery technology creates the battery-trolleybuses, which offer significant environmental benefits in the fight against fossil fuel pollution in cities.

The goal of this work is to develop a simulation model that can overcome limitations in accurately representing real-world conditions, such as traffic congestion, weather conditions, and passenger demand. The proposed simulation model considers various factors that affect the performance of trolleybus systems and is designed to be flexible and adaptable to different scenarios. This work also investigates the challenges of implementing many innovative features into modern trolleybus systems, such as battery-trolleybuses, photovoltaic systems, electric vehicle charging stations, and battery storage power stations.

The simulation model will take into account various factors from both the traffic and electrical network parts that can affect the performance of trolleybus systems. The model is based on a combination of electrical network simulation and vehicle (traffic network) simulation and is designed to be flexible and adaptable to different scenarios.

To calculate the bus propulsion power and location accurately, it is essential to simulate the bus's longitudinal dynamics and its corresponding speed profile. However, calculating a realistic bus speed profile that takes into consideration traffic situations and limitations while assuring a complete stop at the designated stops is presented with sophisticated modelling techniques.

The simulation model is a discrete-time model that identifies the trolleybus system state across time samples. As the buses move continuously, the topology of the traction network will vary with each time step. Thus, a new conductance matrix for the trolleybus traction network is determined at each time step. Furthermore, modelling the power consumption of the trolleybus system is critical. Thus, voltage rules for the traction network that protect the bus motor and keep the traction network stable is considered. Moreover, the presence of unidirectional traction substations results in significant voltage rises whenever surplus power is produced. A specific approach is implemented to effectively determine the traction network's steady-state.

Overall, this thesis makes a significant contribution to the fields of transportation and electric power engineering by introducing a novel simulation model. This model can help enhance the performance and efficiency of current trolleybus systems, support decision-making processes for public transportation authorities, and promote the transition towards more sustainable and environmentally friendly public transportation systems, specifically battery-trolleybus systems.



# Table of Contents

<b>Table of Contents .....</b>	<b>I</b>
<b>1 Introduction.....</b>	<b>1</b>
1.1 Motivation.....	2
1.2 Related Work .....	3
1.3 Aim and Structure of the work.....	6
<b>2 Conversion of a Trolleybus System into a Simulation Model .....</b>	<b>9</b>
2.1 Historical and Technical Overview.....	9
2.2 Sources and Loads.....	11
2.3 System Regulations.....	15
2.4 Development of a Simulation Model .....	17
2.5 Structure of the Simulation Model.....	19
2.6 Implementation Challenges.....	23
<b>3 Modelling the Traffic Network along with Buses.....</b>	<b>25</b>
3.1 Features of the Road Network.....	26
3.1.1 Traffic Nodes .....	26
3.1.2 Traffic Branches.....	29
3.2 Daily Timetable.....	32
3.3 Daily Travelling Route.....	33
3.4 Modelling of the Bus.....	41
3.4.1 Bus Specifications .....	42
3.4.2 Bus Speed/Power Profile.....	43
3.4.3 Stop-to-Stop Movement .....	55
<b>4 Modelling the AC/DC-Network .....</b>	<b>63</b>
4.1 Modelling the Traction network.....	64
4.1.1 Traction network Topology.....	64
4.1.2 Traction nodes.....	65

---

4.1.3	Traction branches .....	68
4.1.4	Traction Substation.....	70
4.1.5	Other Energy Sources.....	71
4.1.6	Loads .....	71
4.2	Modelling the AC-Network.....	72
4.3	Modelling the Traction Sources and Loads Power Profiles .....	74
4.3.1	Trolleybus and Battery-Trolleybus.....	74
4.3.2	Photovoltaic System .....	77
4.3.3	Electric Vehicle Charging Station .....	78
4.3.4	Battery Storage Power Station.....	79
<b>5</b>	<b>Modelling the Trolleybus System.....</b>	<b>83</b>
5.1	Applying Bus Movements to the DC Traction Network.....	84
5.2	Traction Network Steady-State Calculation .....	85
5.2.1	Simulation Process .....	86
5.2.2	Determination of Conductance Matrix .....	91
5.2.3	DC Power Flow .....	96
5.2.4	DC Power Flow with Unidirectional Traction Substations .....	99
5.2.5	Bus Power Control System.....	103
5.3	AC Network State Calculation .....	105
5.3.1	AC Power Flow .....	105
5.3.2	AC-DC Power Flow .....	107
<b>6</b>	<b>Evaluation and Validation of the Simulation Model.....</b>	<b>111</b>
6.1	Adapting the Input Parameters .....	111
6.1.1	GIS Data .....	111
6.1.2	Bus Daily Timetable.....	113
6.1.3	Trolleybuses and Battery-Trolleybuses .....	113
6.1.4	Traction Substations .....	113
6.1.5	Photovoltaic Systems .....	113
6.1.6	Electric Vehicle Charging Stations .....	114



---

6.1.7	Battery Storage Power Stations.....	114
6.1.8	General Input Data.....	114
6.2	Simulation Model with Various Scenarios.....	114
6.2.1	Bus Performance Against Travel Obstacles.....	114
6.2.2	Simulating with Innovative Features.....	116
6.2.3	Several Day Simulation.....	118
6.2.4	Simulating Future Scenarios .....	118
6.3	Quality and Accuracy of the Bus Movement.....	120
6.4	Quality and Accuracy of the Traffic Network State Calculation .....	121
6.5	Quality and Accuracy of the Traction Network State Calculation.....	125
6.6	Assessment of the Simulation Model.....	128
<b>7</b>	<b>Use Cases and Applications of the Simulation Model.....</b>	<b>133</b>
7.1	Operating and Planning a Trolleybus Systems .....	133
7.2	Integration of Photovoltaic Systems .....	134
7.3	Integration of Storage Systems .....	135
7.4	Monitoring and Control System.....	136
<b>8</b>	<b>Summary.....</b>	<b>139</b>
<b>9</b>	<b>References.....</b>	<b>143</b>
9.1	Bibliography.....	143
9.2	Publications of the author.....	165
<b>10</b>	<b>List of Symbols and Abbreviations.....</b>	<b>167</b>
10.1	Mathematical Formulas and Symbols.....	167
10.2	List of Symbols .....	169
10.3	Abbreviations .....	177
<b>11</b>	<b>Annex.....</b>	<b>179</b>
11.1	Solingen Digital Terrain Map .....	179
11.2	Real-World Outside Temperature Data.....	180
11.3	Bus Daily Timetable (Schedule).....	181
11.4	Buses Specifications.....	183

11.5	Traction Substations Specifications .....	184
11.6	Photovoltaic Systems Specifications .....	185
11.7	Electric Vehicle Charging Stations Specifications.....	186
11.8	Battery Storage Power Stations Specifications .....	186

# 1 Introduction

One of the greatest frustrations of the 21st century is climate change; consequently, curbing the climate change is considered the most challenging task. Increased atmospheric CO<sub>2</sub> concentrations are to blame for global warming and consequently climate change. In Germany, the average temperature has increased by 1.6 °C with compare to the pre-industrial period [1]. As a leading industrial country, Germany pursues the *Energy Transition*<sup>1</sup> since 2011 [2]. In addition, the Climate Action Plan 2050 outlines the basic principles for implementing Germany's long-term climate action strategy to achieve a largely greenhouse gas-neutral Germany in 2050. The main goals are to cut greenhouse gases (GHG) emissions 40% by 2020, 55% by 2030, 70% by 2040, and 80-95% by 2050 as compared to 1990 as the baseline year [3].

Following the manufacturing and energy industries, the transport sector can and is imposed on sustainably contribute to meeting the climate goals. The city's public transport system is an important element of the overall transport sector. To this day, most urban transport uses internal combustion engines as its principal energy source. The internal combustion engine is easy to operate, but it generates polluting emissions due to fuel burning. Pollutant gases contribute significantly to global warming and have negative impacts on human health. Transportation emits around 19% of the GHG emissions in Germany in 2018 [4].

Germany's climate strategy includes steps to change the transport sector. These – efforts include government-funded subsidies for replacing personal and commercial vehicles by electric vehicles and for the development of the essential charging infrastructure [5]. As a result, electric traction systems have gained renewed popularity. This entails a well-known focus on trolleybus technology, which remains to be constrained by the limitation of the overhead contact wires. As a means of public transport, the trolleybus has thrived for decades and continues to thrive in several parts of the world as new technological advancements open up new possibilities for its expansion [6, 7]. However, combining the well-engineered trolleybuses with state-of-the-art battery technology creates the designated battery-trolleybuses, which can operate fully electrical for even more ranges wire-free [8].

The trolleybuses/battery-trolleybuses offer significant environmental benefits in the fight against fossil fuel pollution in cities. As oil costs grow, the trolleybuses/battery-trolleybuses become more popular as a mode of transportation.

In conjunction with renewable energies, e-mobility makes it possible to achieve a structural shift in the fossil fuel-intensive transport sector and is a fundamental for achieving environmentally friendly transport systems [5]. Technically, this involves considerable adaptations to electric network infrastructure and control. Electric battery vehicles acquire charging power from a low-

---

<sup>1</sup> In German, famous as: Energiewende

voltage network, meanwhile battery-trolleybuses charge their on-board battery directly from the overhead contact wires while they are moving. However, the electric network's original design does not ensure the needed charging infrastructure.

## 1.1 Motivation

Cities, municipalities, and transport operators (in particular) are planned to play an essential role in the development of electric mobility in Europe [9]. Based on the associated energy policy and climate-related goals, the existing energy supply and transport systems are considered to play an essential role in the context of the emerging transformation processes. Even today, fossil fuels are used to run most public transport fleets, which adds to CO<sub>2</sub> emissions, especially in cities. Substituting diesel buses with electric buses in public transport services reduces local CO<sub>2</sub> emissions and worldwide GHG emissions, making them climate-friendly and sustainable public transport. Electrifying public transport vehicles in cities is possible and has been done effectively for decades using trolleybuses. Technological advances in battery and charging technologies enable the new electric battery bus to be deployed flexibly and offer a viable alternative to the already deployed trolleybus.

Nevertheless, battery electric buses (BEBs) are unreliable to totally overcome the challenge of wire-free driving, primarily due to their limited driving range and the battery's limited operating life and energy capacity, which raises further cost-benefit considerations [10]. One of the current solutions for this issue, which has high potential, is a hybrid trolleybus, which combines the cutting-edge battery storage technology with the tried-and-true trolleybus (TB) technology [11]. Many other terms, including: in-motion charging (IMC), electric battery-trolleybus (EBTB), battery-trolleybus<sup>2</sup> (BTB), and battery-powered trolleybus (BPTB), are used to denote the hybrid trolleybus.

Implementing power-intensive batteries eliminates the auxiliary diesel generator unit equated in conventional trolleybuses and provides extended driving range independent of the overhead contact wire infrastructure. Compared to conventional trolleybus systems, this could decrease investment costs through the targeted partial expansion of the routes to be traversed and enhances the flexibility of the route range. In this approach, it is possible for the BTB to recharge the on-board batteries while marching under the overhead contact wires or at bus stops where quick charging outlets are available, which could lead to maximising the utilisation of the existing trolleybus system infrastructure. The increased amount of energy used to charge the on-board batteries pushes the trolleybus system's capacity to its technological limits. Existing trolleybus systems can only tolerate a certain amount of equipment overloads and voltage violations, but the infrastructure of a newly designed trolleybus system (battery-trolleybus system) may be designed while considering the charging power already in the planning process. The increased network

---

<sup>2</sup> In German, famous as: Batterie-Oberleitungsbus (BOB)

load may trip protection mechanisms and damage operating equipment, compromising the trolleybus system's reliability [12].

The conventional trolleybus system has the potential to include more innovative features, i.e., photovoltaic (PV) systems, electric vehicle charging stations (EVCSs), and battery storage power stations (BSPSSs), making it even more comprehensive. Include these new features will add more strain on the trolleybus system. Decentralised feed-ins may easily exceed consumption demands, resulting in severe voltage violations; likewise, power demands may exceed equipment durability, especially at feeder cables and traction substations, causing internal overload problems. Theoretically, increasing system capacity can solve such difficulties. Thus, the direct current (DC) traction network may be enlarged, and the traction transformers improved. Due to its high cost, infrastructure expansion is however an expensive adaptation method. Even increasing nominal voltage to minimise line load is limited by traction system rules [13]. Using larger overhead contact wires exert more mechanical strain on the existing catenary framework, which is commonly attached to residential building walls in cities. DC traction network upgrades should be minimised [14, 15].

The context of this thesis is based on the current efforts regarding the environmentally friendly public transport systems transformation and is developed as part of a publicly funded research project and developed under joint cooperation with various project partners from the fields of academic research, electrical distribution, and the transport system operators. The expert knowledge from different sectors as well as the accessibility of a real trolleybus system contributed significantly to the practical approach and the overall quality of the obtained results.

## **1.2 Related Work**

Germany aims to achieve the highest level of sustainability by 2050 [3], so this work is mainly focused on the energy and transport sectors. In this context, the transport sector accounts for 24% of worldwide CO<sub>2</sub> emissions [16]. European Union regulations force transport operators to purchase certain percentages of vehicles that are environmentally friendly, which implies that transport operators have to cope with the present and future mobility technologies [17]. For the development of future-proof and sustainable trolleybus systems, a complete decarbonisation is essential. Especially in the case of existing trolleybus systems, this can be favoured using innovative and intelligent technologies. However, a complete fleet replacement is a challenging task, since an enhanced system infrastructure could be needed. With existing trolleybus systems, the challenge is to optimise the use of the existing infrastructure making sure that a reliable operation is maintained. Thus, the steady-state and adaptability of an existing trolleybus system must be further analysed based on its present characteristics and associated innovative features.

The aim of this work is to develop a trolleybus system simulation model (TBSSM) by employing novel approaches for traffic and electric network modelling and simulation. An overview of

scientific and practical efforts that examine the relevant scope of topics is presented below to contextualise the present work.

The proposed TBSSM, which is developed to analyse the above-mentioned problems, is a novel solution approach that has been the focus of numerous past and current efforts in research and development. Research on railway traction systems, however, has been the focus of the preceding trend [18–23]. Contrarily, trolleybus system modelling has very few concern, as in [24, 25]. Whereby, a trolleybus simulation model to analyse urban trolleybus performance is presented. Such simulation models never covered renewable energy sources, electric vehicle charging infrastructure, storage stations, and battery-trolleybuses since they are not obtained with any consideration. There are several publications of simulation models that address this subject as a consequence of the growing usage of buses with electric propulsion technology, such as BEB, TB, and BTB. Therefore, a TBSSM is crucial to evaluate the buses' energy consumption and traction network steady-state.

To effectively evaluate the impact of TBs and BTBs on a traction network, a realistic model of the traffic network with bus daily schedules, trolleybus longitudinal dynamics, and traction network infrastructure need to be combined into one comprehensive model. So far, the literatures on simultaneous traffic and traction network modelling of trolleybus systems are limited. For example, in [26], 125 software for modelling and evaluating electric vehicle effect on power networks are identified. Their evaluation comprises 23 traffic simulation tools. Yet, to investigate energy consumption and traction network steady-state, no simulation tool can model the traffic network, including vehicle dynamics, and electric traction network simultaneously.

Modelling the energy consumption for a real-world electric vehicle relies on vehicle type, speed profile, passenger loading and alighting (in case of electric bus), traffic situation, road topography, heating, ventilation and air conditioning (HVAC) operation, and auxiliary power [27–31]. Thus, reliable modelling and prediction of real-world traffic, TB and BTB advantages can be quantified. In [31–34], historical speed profile data from real-world driving are used to predicted the energy consumption. Alternatively, obtaining high-resolution speed profile data for big bus fleets is challenging, if not impossible [35]. Broad ranges of energy consumption rate (kWh/km) are reported. For example, in [36–38],  $E' = 1.2$  kWh/km to  $E' = 2.9$  kWh/km for BEBs. However, trolleybuses (with and without on-board battery) kWh/km of consumption are in the range of  $E' = 1.3$  kWh/km to  $E' = 2.52$  kWh/km [39, 40]. Several factors influence the energy consumption, and these broad ranges are attributed to different weather conditions (winter or summer), traffic volumes (regular or rush hours), and topography of the roads (flat or hilly).

A bus simulation model to establish energy consumption and predict optimal charging schemes for BEBs is presented in [41], where power consumption is impacted by weather and the type of day. The authors of [42] use a simulator tool to calculate BEB energy consumption. However, different HVAC operation conditions are not considered. Based on probabilistic speed profiles,

an energy demand analysis of electric buses is done in [43]. The heating and air conditioning demand are simulated in detail. The authors of [44] use a stochastic driver model based on a Markov chain to calculate electric bus torque at various speeds. The preceding simulation models do not include a sophisticated longitudinal dynamics model. Furthermore, none of the simulation models include additional calculation for a traction network. More researches which include vehicle longitudinal dynamics modelling are found in [45–48].

However, TBs and BTB modelling are considered in several works. In [49] the Monte Carlo method is used to model a trolleybus system, including daily route schedules, velocity profiles, and traction network characteristics. Using Matlab/Simulink, the authors of [50] develop a simulation model of two trolleybuses running in the same traction network section. The authors of [51] study the maximum possible energy saving that is achieved by using battery-trolleybuses.

Modelling the trolleybus traction network requires a power flow approach that can determine its steady-state. Owing to the passive traction network, the unidirectional behaviour of the traction substations demands special consideration. After establishing TBs and BTBs energy consumption and locations, the steady-state of the traction network may be simulated in order to evaluate any trolleybus system expansion. Also, TBs' and BTBs' contact positions with the traction network must be evaluated. Therefore, several simulation models have been created to calculate the steady-state of a traction network. The authors of [52] present a simulation model that determines train voltages at any position on a single railway track. Simscape, a MathWorks simulation programme, is used to represent the rail track system's mechanical and electrical features.

In [53], a new approach to simulating traction networks is presented. The suggested approach considers vehicle longitudinal dynamics as the traction network. The proposed model mimics the effect of voltage drops on vehicle acceleration dispose of any surplus regenerative braking energy. Nonetheless, the proposed model relies on reference speed profiles, which must be established in advance, and does not consider the traction network as a single mesh network, but rather splits it into several sections depending on traction substation feed-in points.

In [54], a neural network optimization is used to simulate the power demand of an urban trolleybus/battery-trolleybus system. A test ride of a BTB is used to train the neural network. More historical data from real-world driving, even considering daily traffic volumes, are planned for future work.

The author of [55] suggests a two-stage approach to solve the power flow problem. The first step uses a bisection method to find a scaling parameter, and the second step uses the Newton-Raphson method to check if the traction network can be solved. However, the proposed approach includes no provision for power regulation based on line voltage drops [56]. Instead, it simply considers the unsolvable load flow problem from a mathematical standpoint.

Consistently, the concept of modelling a traction network with sustainable features is presented in plausible works. The author of [57] studies the effect of using a battery storage power station on the traction network voltage profile. In [58], a PV system is presented in a traction network. Monte Carlo methods are used to address irradiation and traffic congestion uncertainties. In the follow-up work [59], two unique battery storage power station applications for urban mobility are presented. The studied applications try to reduce the peak demand of a traction substation or make the best use of solar energy by matching production with demand. In [60], PV and Wind systems are integrated into the traction network to optimise direct utilisation using a simulation model to prove different scaling and positioning situations.

### **1.3 Aim and Structure of the work**

The challenges that transport companies are currently confronted with are mainly related to the planning of new transport systems and operating models as well as the further development and technical upgrading of existing systems so that they are capable of adapting to fully electrified transport systems. The primary objective in this thesis is to develop a reliable simulation model that can mimic a real-life trolleybus system for the purpose of reliability evaluating in the presence of various modifications and other operational needs necessary to the long-term stability. Furthermore, all innovative features, such as battery-trolleybuses (BTBs), photovoltaic (PV) systems, electric vehicle charging stations (EVCSs), and battery storage power stations (BSPSs) are to be included in the proposed simulation model.

This associative thesis describes the development steps of the TBSSM. For this purpose, the historical background and the relevant technical information of trolleybuses are explained in Chapter 2. This includes the technical characteristics of TBs and BTBs as well as those of the traction network. The principle need for a TBSSM will be clarified afterwards. Furthermore, the overall structure of the proposed TBSSM will be presented. Finally, the challenges that could face the development of such a simulation model will be pointed out.

Chapter 3 will handle the process of developing both the traffic network model and the bus model. The traffic network model will include the final structure of the travel route that will be used by each bus during its daily operation. The model will also include the traffic situation that will affect the bus movement. The bus model will consist of the longitudinal dynamic model. Accordingly, speed, travel distance, and traction power will be calculated. The model will also incorporate the power consumption of the auxiliary systems. In the case of BTB, the on-board battery model will be incorporated.

Chapter 4 will cope with the modelling of the electric network and the innovative features. The electric network will be considered as both a traction network and the overlaying medium voltage alternating current (MVAC) network. The modelling of the power profiles for the innovative features will also be included. However, buses will not have a pre-defined power profile. For that,



the calculation process for the power consumption as well as bus location with respect to the traction network will be established.

Chapter 5 will outline the complete simulation model. The step-by-step process to determine the traction network steady-state will be elaborately described. The steps to determine the conductance matrix of the traction network after each topology change – due to bus movement – will be described. Due to the passive behaviour of the traction network, a novel approach that will solve this issue will also be described. Moreover, a power control model, which will hold bus motor current at the permitted voltage level, will be included in the simulation model. Lastly, a sequential AC-DC power flow calculation will be discussed too.

In Chapter 6, different scenarios will be tested using the TBSSM and real trolleybus system data. The results will be discussed and evaluated with real measured logs from the same trolleybus system.

In Chapter 7, four use cases of the TBSSM will be presented. The TBSSM will be used for different planning and operation cases.

Chapter 8 will summarise the work of this thesis.

Finally, the result of this work is aimed to make it easier to configure the future of existing trolleybus system, and consequently, adapts future planning and operation of trolleybus and battery-trolleybus systems.



## 2 Conversion of a Trolleybus System into a Simulation Model

Nowadays, trolleybuses (TBs) are often criticised for being inflexible, and their unsightly overhead contact wires are widely cited as a determining factor. They do, nevertheless, have a distinct advantage over public transport systems that employ buses with internal combustion engines. Innovative electric drive technologies, such as the battery-trolleybus (BTB) running on a smart trolleybus system, can compensate for the disadvantages of a trolleybus system and may introduce a new era of environmentally friendly transport systems.

### 2.1 Historical and Technical Overview

Essentially, the trolleybus as we understand it today is comprised of an electrical motor, a pair of overhead live wires, and a couple of rolling or sliding contacts. Over 130 years have passed since the first successful journey of the world's first electric trolleybus was successfully accomplished. In 1882, Werner von Siemens demonstrated his groundbreaking concept of an electric vehicle powered by a fixed source but capable of being directed like conventional road vehicles. The vehicle he designed, the *Electromote*, was completely without rails support and travelled the Kurfürstendamm in Berlin. The vehicle was driven by two electric motors with  $P = 2.2$  kW each fed by a flexible cable connected to a small eight-wheeled trolley (the contact assembly with the wires) running on two stranded copper wires that are supported by wooden poles along the roadside. The overhead contact line operated with a DC voltage of  $U = 550$  V. Even though the *trolleybus* is less expensive than rail vehicles, Werner von Siemens decided to halt the test as early as mid-June 1882. Most of this was due to poor road conditions, making it impossible for the vehicle to move without causing significant disruption. Additionally, there were no rubber tyres available for automobiles at the time. For the time being, "trolleybus" technology was obsolete. However, the concept survived: In cooperation with Siemens & Halske, the engineer Max Schiemann resumed construction and continued developing the *Elektromote*. The drive methods and current collectors were improved because of his efforts. In 1901, the world's first trolleybus route was established between Königstein and Bielatal in Dresden, Germany. From then on, Schiemann trolleybuses began to be seen on roads [61].

The development of the trolleybus may be traced back to its rise and fall periods [62], as shown in Figure 2-1. After its discovery in the 1880s, the first actual use of trolleybus technology lasted until 1915. Many countries around the world adopted the technology during that period. In Germany, 110 trolleybuses were built and used until 1911 [63].

After World War I, from 1921 to 1926, new pilot projects were carried through to establish trolleybus services. Several cities of North America and Europe embraced these services. Even though the early vehicles were primitive by today's standards in these projects, they were functional and helped with gaining experience and learning lessons [64].

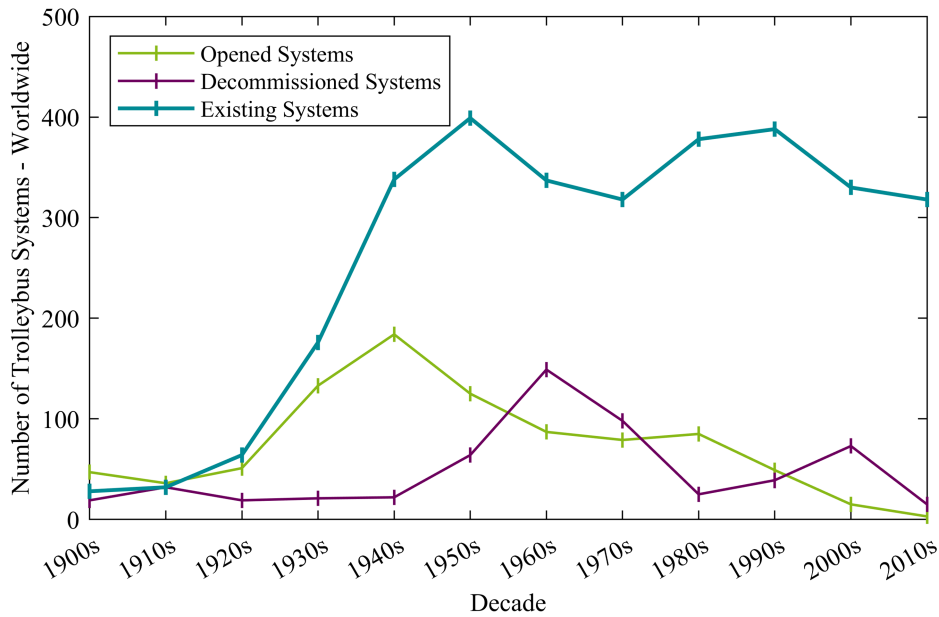


**Figure 2-1: Number of opened, decommissioned and existing trolleybus systems worldwide through decades [65] [66].**

In the late 1920s, a more appropriate vehicle was developed, which had a larger and more powerful motor, improved brakes, a workable pantograph, and pneumatic tyres. As a result of its further development, the trolleybus achieved its excellent deployment during this period, which lasted from 1927 to the early 1950s. At the beginning of this period, tram lines began to be viewed as obsolescent modes of transportation, and the trolleybuses began to take their place. However, the employment of trolleybus technology to transport trams quickly gained great popularity. Trolleybuses quickly emerged as the primary mode of public transit in several countries. In general, the number of trolleybuses on the road continued to rise, except for World War II from 1941 to 1945. A trolleybus powered by both electricity and gasoline was officially introduced in the early 1930s. On routes that were partly wired, the trolleybus was powered by electricity until it reached the end of the catenary. The gasoline engine then assisted the vehicle's operation for the remains of the route [6].

From the 1950s to the beginning of the 1970s, many problems began to emerge. One of these is the development of large diesel buses that accelerated the trolleybus' decline at a rate that almost matches its success before the 1950s. The decline continued despite the several upgrading of electric and electronic elements in the late 1960s. Power consumption was decreased significantly with the use of chopper control, which also ensured smooth speed transitions. Improved power connections and regenerative braking were included too. Trolleybus services were discontinued in nearly every country, notwithstanding the significant early development work. In particular, the procedure was criticised for being rigid and the overhead wires as being ugly. However, countries like Switzerland and Germany have modernised their trolleybus systems and extensively used them across the region. On 19 June 1952, the city of Solingen decided to end the tram service and replace it with a trolleybus system. The cheap operating and fuel expenses and

the extended service life of the trolleybuses influenced this choice. It took seven and a half years to transition tram lines to trolleybus service. In November 1959, the final tram line was decommissioned from operation. In contrast to many other German cities, Solingen has converted its entire public transportation system to trolleybuses rather than just minor parts. As of that time, it operated the third-largest German trolleybus network, running about 40 kilometres, and even led in terms of vehicle count [67].

A new era of trolleybus popularity began in the early 1970s. Relative price changes for diesel sparked a renewed interest in the trolleybuses. The oil crises of the 1970s, combined with growing concern about the environment and air pollution on city streets, resulted in a relatively small restored concern for trolleybuses as an alternative transportation system. Accordingly, several developing countries, especially those that are reluctant to import expensive oil fuels but can produce sufficient electrical energy, have embraced this form of public transportation service. [6]. Nevertheless, the number of trolleybus systems has continued to decline. Like the rest of the world, Germany's trolleybus era had faded. Almost all of the operating trolleybus systems were shut down, so that only three systems in Solingen, Eberswalde, and Esslingen are still in operation today [68, 69].

With the current push to minimise greenhouse-gas (GHG) emissions and improve air quality in cities, transportation operators are pressured to compensate their fleets with more zero-emission buses, such as the *battery-electric bus* (BEB) [70, 71]. This bus has the same operating concept as a trolleybus, but its electric motor obtains energy from an on-board battery pack and not directly from the overhead network. Improvements in battery technology have extended the BEB range to 300 km with a fully charged battery. Thus, the BEB has outsold all other types of electric vehicles on the market today, making it the best seller [71, 72]. However, the issue of charging the bus battery remains challenging. Optimistically, a *battery-trolleybus* (BTB) could open the opportunity for a *promising new era* of trolleybuses that combine the advantages of a trolleybus and battery-electric bus in a single-vehicle. The BTB is the most economical approach for large capacity routes when compared to other electric buses [73]. As concluded in [40], 33% to 50% of the travelling route must be electrified in order to operate BTBs. For existing trolleybus networks, it is possible to utilise *existing* overhead contact lines correlate with buses, which could be replaced by BTB, running on a variety of routes. This approach will allow for more efficient use of the existing infrastructure. Furthermore, in many circumstances, it may be practical to plan new traction systems based on the BTB technology.

## 2.2 Sources and Loads

Generally, the electrical infrastructure of a trolleybus system is composed of three main components: power supply sources, loads, and overhead contact wires. The traction substations serve as the primary power source, while the TBs operate mostly as the main loads for the system.

As one of the most essential components, overhead contact wires (OHCWs) are those that link the sources and loads. The connection and impact of each component on the overall trolleybus system are therefore vital to model a realistic simulation for a trolleybus system.

TBs utilise direct current (DC) through the OHCWs to power their electric propulsion and auxiliary system. The connection to the OHCW is facilitated by a *current collector* system (two trolley poles and two contact shoes) of about 6 m length mounted above the TB roof, at the rear, allowing a lateral movement of up to 4.5 m [74]. Additionally, a *combustion engine* – serving as a generator or a direct propulsion – is equipped to power the TB and enable it to travel autonomously; without contacting the OHCW or in the event of supply malfunction. Formerly, TBs were propelled by series wound DC traction motors; however, modern TBs are equipped with asynchronous motors powered by a three-phase DC to AC inverter [75]. Hence, the motor speed is controlled by altering the applied voltage and frequency. The low manufacture cost and their advantages, three-phase asynchronous motors with brushless squirrel-cage rotors are widely used in the automobile industry. A single, sometimes two, electric motor with a total power ranging between  $P_M = 165$  kW and  $P_M = 320$  kW is inducted in TBs, depending on their models ( $l = 12$  m single-decker or  $l = 18$  m articulated) [76, 77]. The maximum speed of a TB is usually  $v = 60$  km/h and in some model up to  $v = 80$  km/h [74].

The primary function of the OHCW is to provide energy to the TB fleet through overhead suspended *contact wires* distributed along the TB traffic routes. Sustain poles and anchors on buildings along the streets support the *longitudinal contact line equipment*, i.e., contact wires, messenger or catenary wires, droppers, and stitch wires. *Grooved contact wire*<sup>3</sup> (see Figure 2-2), which is a copper wire feature grooves on each side of the top section for clamping by clips, is preferred as overhead contact wires for the trolleybus system [78]. A cross-sectional area of 80 mm<sup>2</sup>, 100 mm<sup>2</sup>, 107 mm<sup>2</sup>, 120 mm<sup>2</sup>, or 150 mm<sup>2</sup> is considered (based on European Standard) for the overhead contact wires [79].

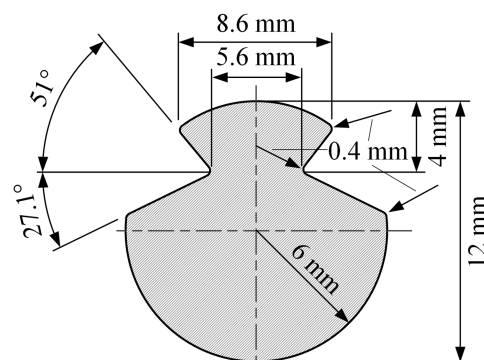


**Figure 2-2: Groove contact wire (type AC-100) cross section [78].**

<sup>3</sup> Abbreviated Ri (dt. Rillenfahdraht)

TBs, in contrast to trams, do not operate on rails and hence require a two-pole wire system. In most cases, the wire fixed on the outside – in direction of travel – is the negative wire, while the other is the positive and positioned on the inside. Accordingly, the two-pole overhead wires provide the complete path for the current to flow from the traction substation to the TB and back again. The TB load current is divided between the overhead contact wires – on both traffic directions – by *cross-couplings* which electrically interconnect these wires at regular intervals (see Figure 2-3). Since these couplings are integrated rapidly into the OHCW, particularly over long sections, power losses as well as voltage drops are minimised. As shown in Figure 2-4 the voltage drop conditions are compared for equivalent total loads between two substations. In addition, the graph of Figure 2-4 shows that increasing the number of *cross-couplings*  $k$  between traction substation improves the voltage conditions over the OHCWs of a traction network [80]. The traction substation supplies the OHCW with *feeder cables*, which connect the overhead contact wires with the traction substation busbar (see Figure 2-3).

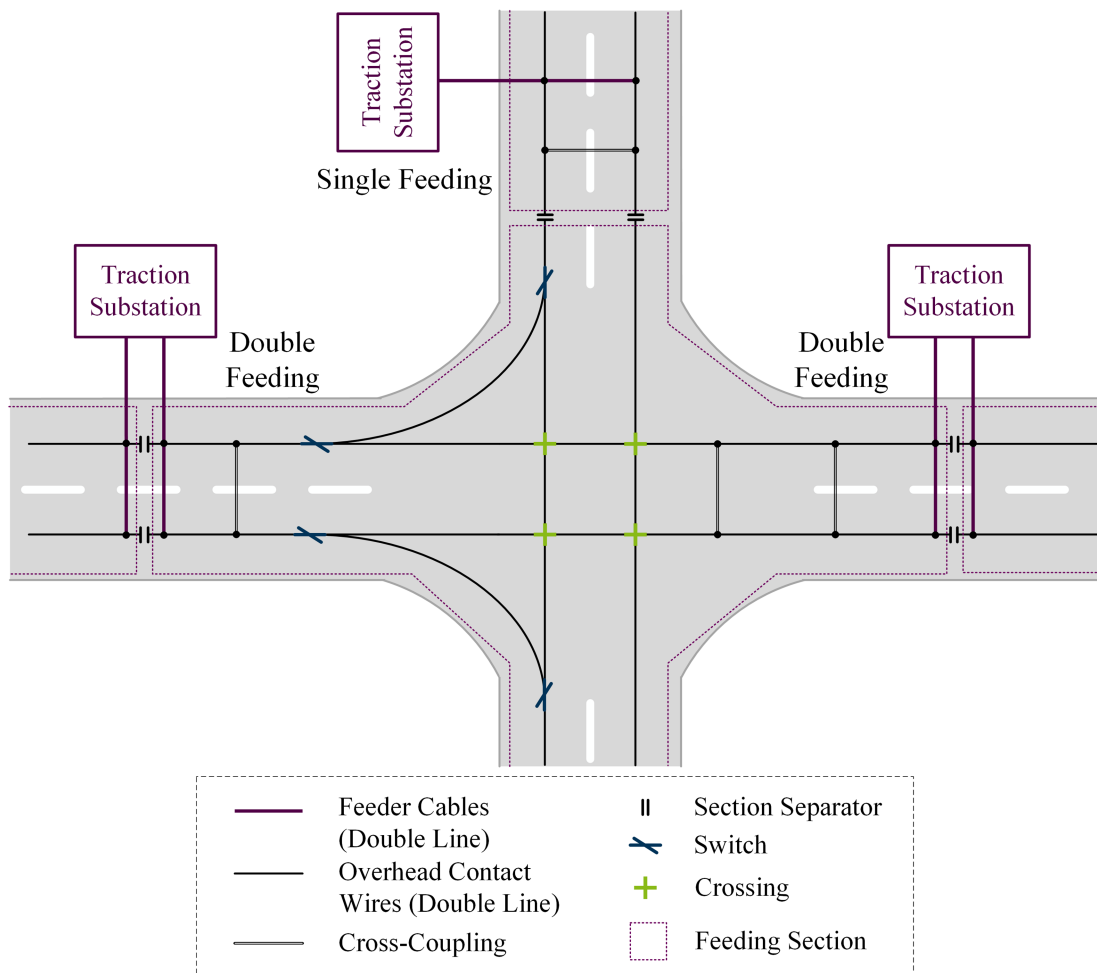


**Figure 2-3: Structure of a trolleybus traction network.**

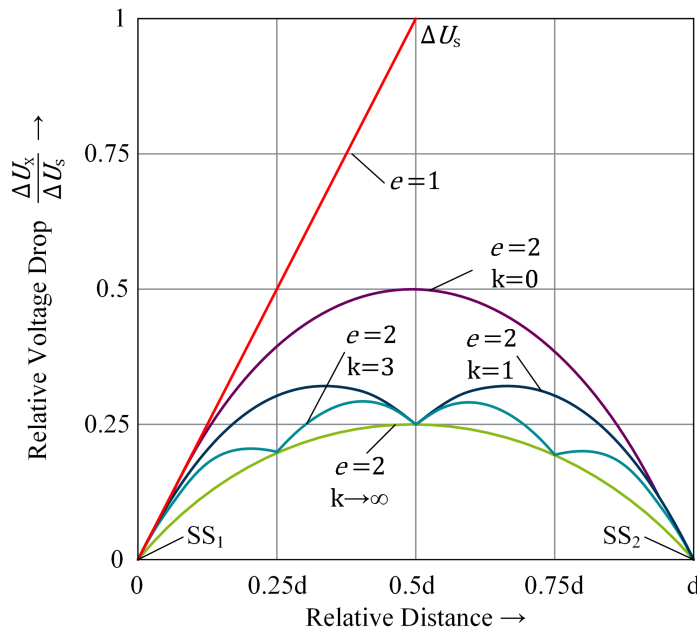


**Figure 2-4:** Voltage drop relative to the voltage drop  $\Delta U_s$  which occurring with single end feed and one load in the feed section for single end substation ( $e = 1$ ), and double end substations ( $e = 2$ ) with different number of cross-couplings  $k$  between the substations ( $SS_1$  and  $SS_2$ ). The distance from  $SS_1$  to  $SS_2$  is represented as  $d$  (compare to [80]).

The OHCW, in contrast, is not just utilized to provide electricity to the TBs. It is also used to distribute energy during brake applications and provide regenerative energy – TB as a power source – to other TBs in the same supply segment. The electric motor transforms the TB's kinetic energy into electricity while braking. The auxiliary equipment consumes the regenerative energy first, and if possible, the OHCW distributes the surplus energy; otherwise, it is converted into heat using a brake-resistor, and, thus, all voltage violations – due to this surplus energy – are restricted [81].

The function of *traction substation* is to supply electrical energy within voltages conforming with the nominal values used for the traction system. As shown in Figure 2-5, the traction substation draws energy from the upper stream medium voltage alternating current (MVAC) network. After stepping-down the voltage from the MVAC network by the *traction transformer*, the three-phase AC voltage is rectified into the nominal DC voltage of the traction network by the *traction power rectifier*.

The spacing of traction substations is determined based on calculations of voltage regulation and short circuit situation. This decision is made based on the technical performance of the trolleybus system. Nevertheless, other factors such as: availability of land, position of junctions and crossovers, and road access determine the final choice of the traction substation locations, and thus, influence the distance between the traction substations. As rule of thumb, most economical distance between traction substations is (2 km to 4 km) for the DC with  $U_n = 600$  V systems and (4 km to 6 km) for the DC with  $U_n = 750$  V systems.



As shown in Figure 2-3, each traction substation is responsible of supplying at less one *feeding section*. It is noteworthy that a feeding section may be supplied by one or multiple traction substation. A *section separator* is used to isolate adjacent feeding sections in such a way that they cannot be bridged by the OHLWs; although, the feeding sections are still connected through the *direct current busbars* of the traction substation. In this manner, regenerative energy can be distributed beyond the feeding section to other nearby feeding sections with power demands.

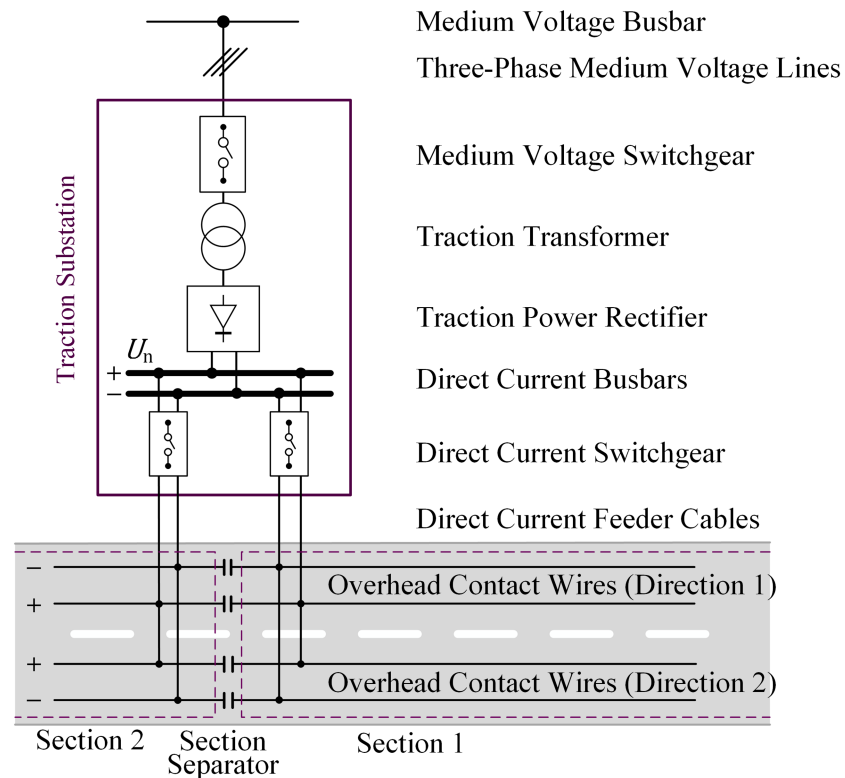


Figure 2-5: Schematic diagram of a traction substation (Adapted from [80] and [82]).

### 2.3 System Regulations

The electric traction system is powered by a direct current (DC). Concerning the voltage level restriction on city roads, a low voltage direct current (LVDC) system with a nominal voltage  $U_n = 600 \text{ V}$  or  $U_n = 750 \text{ V}$  is regulated according to IEC 60850:2014-11 [13]. For an appropriate bus operation, a considerable tolerance between the maximum and minimum voltage values is authorised (see Table 2-1). Greater current consumption may arise due to the low voltage level of the traction system, resulting in a significant voltage drop at the bus locations, which increases as a bus travel farther away from the substations. Nonetheless, the tolerable minimum voltage value ( $U_{\min 1} = 0.76 \cdot U_n$ ) permits the buses with greater feeding distances and minimises the need for additional substations. However, with the maximum voltage value ( $U_{\max 1} = 1.2 \cdot U_n$ ), the utilisation range of regenerative power is extended. Within 5 minutes, the maximum certified voltage  $U_{\max 1}$  may be extended to  $U_{\max 2}$  [13]. The system voltage must not exceed the highest non-permanent voltage  $U_{\max 2}$ ; accordingly, voltage increase during bus braking is regulated by

a *squeeze control* system, where the surplus energy is converted into heat using a *brake-resistor*, preventing the system voltage from acceding  $U_{\max 2}$  [83]. A system with higher nominal voltage  $U_n = 750$  V is reasonable in terms of supply ranges, short-circuit detectability, and power loss reduction. There are no different between the value of the lowest non-permanent voltage ( $U_{\min 2}$ ) and the lowest permanent voltage ( $U_{\min 1}$ ) with in the nominal voltage  $U_n = 600$  V and  $U_n = 750$  V as shown in Table 2-1; However, the values of  $U_{\min 2}$  and  $U_{\min 1}$  with higher nominal voltage according to IEC 60850:2014 [13].

**Table 2-1: Nominal voltages and their permissible limits in a trolleybus/battery-trolleybus traction system (based on IEC 60850:2014) [13].**

<b>Nominal voltage (<math>U_n</math>)</b>	600 V	750 V
<b>Lowest non-permanent voltage (<math>U_{\min 2}</math>)</b>	400 V	500 V
<b>Lowest permanent voltage (<math>U_{\min 1}</math>)</b>	400 V	500 V
<b>Highest permanent voltage (<math>U_{\max 1}</math>)</b>	720V	900 V
<b>Highest non-permanent voltage (<math>U_{\max 2}</math>)</b>	800 V	1000 V

The TB propulsion system is consisting of asynchronous motors which behave as constant power loads [84]. The TB motor power  $P_M$  is computed as follows:

$$P_M = I_M \cdot U_B \quad (2.1)$$

where  $I_M$  is the motor drawn current, and  $U_B$  is the bus voltage. The TB accumulates the required power (see Equation 2.1) from the OHCW to fulfil propulsion demands. Consequently, a high motor current  $I_M$  arises with a low voltage level provided by OHCW throw the bus current collector. An overcurrent protection mechanism is thus built into the bus, reducing power consumption while the bus is in traction mode. The regulation curve of the maximum allowable current – drawn by the TBs/BTBs – corresponding to the OHCW voltage is shown in Figure 2-6.

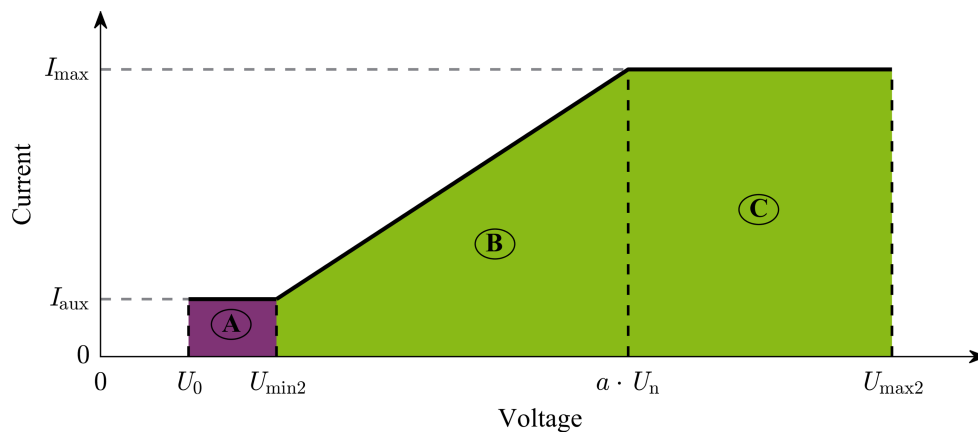


**Figure 2-6: Maximum consumption current against voltage (compare to [56]).**

- A: No traction power, only auxiliary current**
- B: Traction power with reduced current.**
- C: Maximum traction power.**

Based on voltage levels (see Table 2-1), the TB/BTB consumption current is regulated within three regions. The bus voltage  $U_B$  in region ① is less than the lowest non-permanent voltage  $U_{\min 2}$ ; thus, the current consumed by the bus  $I_{\text{aux}}$  is just used to power the auxiliary system, and the propulsion system is powered off  $P_M = 0$ . The overcurrent protection system is activated in region ② as the bus voltage swings between  $U_{\min 2}$  and  $\alpha \cdot U_n$ . Accordingly, the motor current is restricted, which reduces the motor's maximum power  $P_M \leq P_{M,\max}$ . In region ③, the bus voltage is higher than  $\alpha \cdot U_n$ ; hence, the bus operates normally with full motor power and a maximum current accumulated from the OHCW through the current collector system. The value of  $P_M$  in Equation 2.1 must not exceed the value of  $P_{M,\max}$  which is defined based on the regulation curve shown in Figure 2-6 as follows:

$$P_{M,\max} = \alpha_r \cdot P_M \quad (2.2)$$

$$\alpha_r = \begin{cases} 1, & U_B > \alpha \cdot U_n \\ \frac{U_B - U_{\min 2}}{\alpha \cdot U_n - U_{\min 2}}, & U_{\min 2} < U_B \leq \alpha \cdot U_n \\ 0, & U_B \leq U_{\min 2} \end{cases} \quad (2.3)$$

Where  $\alpha_r$  is a reduction factor,  $P_M$  is the maximum motor power as indicated by the TB specifications,  $P_{M,\max}$  is the maximum motor power based on the traction network state (as defined by [56]), and  $\alpha$  is the knee point factor, where  $\alpha = 0.8$  is considered for a system with nominal voltage  $U_n = 600$  V and  $U_n = 750$  V [56].

## 2.4 Development of a Simulation Model

Reducing GHG emissions and improving air quality in cities can be made possible with implementation of environmentally friendly public transport systems. The primary component contributing to this goal is the withdrawal of *diesel buses* by replacing them with *electric buses*. Although some cities already have a *trolleybus system* as part of their public transportation systems, which makes it even more sustainable to invest in replacing the remaining bus fleet with electric buses, specifically *battery-trolleybuses*, which combine the features of already efficient and reliable trolleybus technology with state-of-the-art storage technologies. Nevertheless, designing a new *battery-trolleybus system* should be taken into consideration too [85]. The BTBs, like conventional TBs, obtain their power directly from the overhead contact wires (OHCWs). Still, additional energy can be stored in their *on-board* battery even while moving (in-motion charging). Thanks to the energy provided by the on-board batteries, BTBs are more adaptable for travels beyond the traction network, which previously needed a diesel engine. The utilisation of BTBs, however, exposes the existing trolleybus system infrastructure to its technical limitations because of the extra energy needed to charge the on-board batteries. Thus, the existing trolleybus system is no longer guaranteed to operate reliably due to equipment overloads and voltage drops below the lower voltage limit [86].

It is possible to achieve a fully sustainable public transport system by assessing the potential of existing trolleybus systems. The conventional trolleybus system could be upgraded to include a range of innovative features, making it even more comprehensive. *Sustainable power sources*, i.e., PV systems, can be directly linked to the DC traction network. Accordingly, there will be fewer power losses when energy is transferred from PV systems to TBs/BTBs. Integrating PV systems directly into the DC traction network allows an efficiency improvement of the PV voltage from  $\eta = 90\%$  to  $\eta = 96\%$  [87]. Old traction substations can also be replaced with a promising concept for a bidirectional traction substation with *active front-end* converter [87, 88], which will allow surplus power produced by renewable sources or regenerative power during bus decelerations to be converted into the upper stream AC network. The *outdated* batteries from the BTBs can be as well repurposed to establish battery storage power stations (BSPSs) within the trolleybus system. Thus, more flexibility is added to the DC traction network. By using this approach, the average battery lifetime can be increased by several years. Additionally, multiple electric vehicle charging stations (EVCSs) can be linked to the DC traction network, giving city residents easy access to charge their electric vehicles.

The *existing trolleybus system* will be stretched to its threshold by these new load scenarios. Basically, decentralised feed-ins within the DC traction network may easily surpass the power consumption demands, resulting in severe local voltage violations above the allowed voltage range. However, the DC traction network may experience power demands that are greater than its equipment durability, particularly at feeder cables and traction substations, leading to internal overload conditions that cannot be recognised [15]. In theory, there are two methods for resolving these issues. Such problems can be solved by increasing the system's capacity. For example, the traction transformers can be upgraded to higher capacities, and the DC traction network can be expanded. Infrastructure expansion is still a costly adaptation strategy that can only be used to a limited extent due to its high cost. Due to the regulations established for traction systems [13], increasing the nominal voltage to reduce line current flow is only a restricted choice. Larger cross-section OHCWs provide a greater mechanical pressure on the existing catenary structure, which is often fixed on residential building walls in metropolitan locations. If the DC traction network is to be upgraded conventionally, it should be done to a limited degree [89]. Nevertheless, it must be remembered that the previously indicated overload situations are only present for short periods of time. Therefore, upgrading the trolleybus system with automation technologies and establishing a smart trolleybus system (STS) is a more viable option [86].

Taking into consideration the above conclusion, a *simulation model* is required to determine the reliability of a system under certain extensions and additional operational requirements that are necessary for stable operation. The model should incorporate both technical and operational considerations. For the purpose of this work, a trolleybus system simulation model (TBSSM) will be developed in order to mimic the regular activities of TBs and BTBs, as well as evaluate the

steady-state behaviour of a trolleybus system over a period of time. Consequently, a competitive trolleybus system can be adaptably planned and operated.

According to [86], a TBSSM can be used to contribute to the development of a predictive control and optimization algorithm for trolleybus systems. The proposed algorithm makes it possible to safely operate a trolleybus system that includes new techniques and network elements, i.e., BTBs, PV systems, EVCSs, BSPSs, and bidirectional traction substations, in the right way. Based on the features of the traction system and the associated challenges, which could be simulated using the TBSSM proposed in this work, the general process of establishing a central network automation system is explained [86]. In this context, the traction network steady-state forecast can be determined using a TBSSM [85]. The use of grid automation technology has already been proven to be an effective method for the practical upgrading of power systems. Accordingly, infrastructure expansion can be delayed or completely prevented, and thus, it makes sense to adapt these concepts to enable the implementation of the new network elements into the existing trolleybus system [86].

And furthermore, the steady-state of a traction network over time interval can be predicted by implementing a forecasting model with TBSSM [85]. The forecasting model mirrors TB and BTB locations, based on their GPS<sup>4</sup> information, into TBSSM and matches other available measures to their corresponding components in TBSSM. The steady-state of a traction network is forecasted for a given time frame and reported to the work of [86].

Based on [85], TBSSM is a great asset for planning a new battery-trolleybus system. The planning approach relies on successive simulation analyses, which are performed using TBSSM. In which, BTB energy demands are segmented along the travel route schedule. These simulated segment-specific energy data can be used to determine the required OHCWs for the new battery-trolleybus system. The contiguous segments, which are commuted for each potential solution of this optimization problem, are grouped into zones. For each of these zones, the number of traction substations needed is determined after considering all technical restrictions. Following successful optimization execution, the validation of the resulting battery-trolleybus system will be examined using TBSSM to conform the compliance with technical framework criteria and constraints.

## 2.5 Structure of the Simulation Model

A proper simulation model of a trolleybus system requires adequate modelling of the traction network infrastructure (traction network) and the public transport roads (traffic network) with bus daily schedules as well as buses movements and energy consumptions. The term *bus(es)* is used, in this work, to indicate *trolleybus(es)/battery-trolleybus(es)* or both. A traction network is highlighted by the fact that its loads are in motion. TBs and BTBs, which are connected to traction

---

<sup>4</sup> Global Positioning System

network's OHCW, change locations on a regular basis to fulfil their daily schedule. TBSSM is used to recreate in vitro the activity of a real-world trolleybus system. Whereby, mathematical equations and diagrams are utilised to explain the relationship between the system components, i.e., TBs, BTBs, PV systems, EVCSs, BPSs, and traction substations. During the simulation cycles, the dynamic behaviour of the trolleybus system and its state variables are solved over a specified time interval. The simulation time samples set  $\tau_s$  is defined as follows:

$$\tau_s = \{t_{ss}, (t_{ss} + \delta t), (t_{ss} + 2 \cdot \delta t), \dots, (t_{ss} + (n_s - 2) \cdot \delta t), t_{se}\} \quad (2.4)$$

where  $t_{ss}$  is the start time that correspond to real-world time,  $\delta t$  is the time step that represents the progress of the simulated trolleybus system over  $\tau_s$ ,  $t_{se}$  is the end time, which in the simulation cycles are concluded, and  $n_s$  is the number of discrete samples in  $\tau_s$ .

The start (date and time) set  $SM_{sd}$  is defined as follows:

$$SM_{sd} = \{Y_{sd}, M_{sd}, D_{sd}, h_{sd}, m_{sd}, s_{sd}\} \quad (2.5)$$

where  $Y_{sd}$ ,  $M_{sd}$ ,  $D_{sd}$ ,  $h_{sd}$ ,  $m_{sd}$ , and  $s_{sd}$  are the start year, month, day, hour, minute, and second, respectively. The values of  $Y_{sd}$ ,  $M_{sd}$ , and  $D_{sd}$  are used to identify the type of day, i.e., workdays, weekends, and public holidays. Moreover, the value of  $M_{sd}$  is used to identify the seasons of the year.

The simulation interval set  $SM_{int}$  is defined as follows:

$$SM_{int} = \{D_{int}, h_{int}, m_{int}, s_{int}\} \quad (2.6)$$

where  $D_{int}$ ,  $h_{int}$ ,  $m_{int}$ , and  $s_{int}$  are the number of days, hours, minutes, and seconds that are intended to be simulated, respectively.

Therefore, simulation starting time  $t_{ss}$  is determined as follows:

$$t_{ss} = (3600 \cdot h_{sd}) + (60 \cdot m_{sd}) + s_{sd} \quad (2.7)$$

and simulation end time  $t_{se}$  is determined as follows:

$$t_{se} = t_{ss} + \tau_{int} \quad (2.8)$$

where  $\tau_{int}$  the simulation interval in second and is calculated as follows:

$$\tau_{int} = (86400 \cdot D_{int}) + (3600 \cdot h_{int}) + (60 \cdot m_{int}) + s_{sd} \quad (2.9)$$

The number of discrete samples  $n_s$  is determined as follows:

$$n_s = \frac{\tau_{int}}{\delta t} \quad (2.10)$$

where  $\delta t$  is in second.

However, the sample elements in  $\tau_s$  do not represent the actual day time yet they are the advancing steps correspond to the start time  $t_{ss}$ . The actual day time can be determined as follows:

$$\tau_{rw} = \tau_s \bmod 86400 \quad (2.11)$$

where  $\tau_{rw}$  is the real-world time set and  $1 \text{ s} \leq \tau_{rw} \leq 86400 \text{ s}$ .

The TBSSM represents a discrete-time model, where the trolleybus system state is determined at each time step. Several models that are characterised by mathematical relationships are used to describe the connection between the trolleybus system features. Attribute sets and events are included as well in the model structure. A discrete-time model can be used to capture how the trolleybus system's features change over time. There are numerous parts of the TBSSM, such as the traffic network, that are treated as static entities, even though the trolleybus system is considered a dynamic system. Yet, despite the traffic network's static attributes, certain events still take place as a result of some dynamic behaviour, so the TBSSM is also a discrete-event model. An example of such a dynamic event is the traffic light, where the bus may stop for some time or may not. The process is not frequent with time but can happen when a bus arrives at a traffic light location. Contrarily, the bus motion that changes its point of contact with the OHCWs causes the traction network's topology to change with each time step, making the traction network show dynamic behaviour despite the static topology nature of the electric network. The bus model also changes frequently with time. Nevertheless, discrete-events can affect the behaviour of the bus model and last till the next discrete-event occurrence. For example, the bus weight depends on the number of passengers in the bus, which changes when a bus dwells at a bus stop and passengers board and alight the bus.

As shown in Figure 2-7, the TBSSM is divided into four blocks, which are explained in more details in the following chapters. There are four primary model blocks, each of which is distinguished in the trolleybus system model scheme by a different colour. The blocks are arranged in the same order as their corresponding entity appear in the real world. First, on the ground, is the road (Traffic Network Model), then the buses (Bus Model), and finally, on the top, the traction overhead contact wires (Traction Network Model).

The light green block (Traffic Network Model) represents the road network topology with traffic nodes and traffic branches. Both the traffic node and traffic branch models contain attributes that further characterise the road network's features. The model also includes bus schedules and traffic situations. The traffic network model defines the routes and events that impact bus movements. Chapter 3 – Sections 3.1, 3.2, and 3.3 elaborate on the traffic network model.

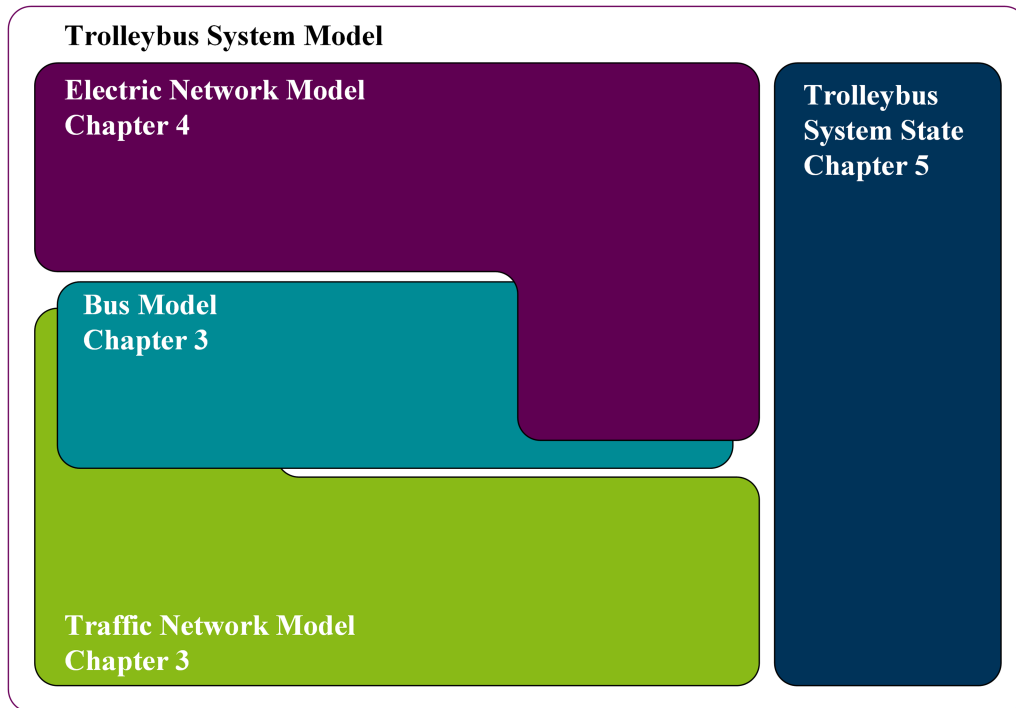


**Figure 2-7: Trolleybus system model scheme.**

The turquoise block (Bus Model) represents the bus model. As shown in Figure 2-7, it overlaps the traffic network block. The overlap resembles the dependence of the bus model on the traffic model. According to the daily travel route schedules, bus movements are calculated based on their mechanical and electrical specifications. The model also includes longitudinal equations of motion, which will be used to compute electrical traction power, bus speeds, and travel distances. Using the heat balance equation, the required amount of heat and the interior temperature of the bus are calculated discretely in time. In addition, basic auxiliary powers are determined. The bus position, based on the daily travel route schedule data, indicates whether it is under an overhead line, so the on-board batteries of the BTBs can be turned on or off as needed. Chapter 3 – Section 3.4 elaborates on the bus model.

The electric network is represented by the purple block (Electric Network Model). Figure 2-7 shows that it covers the bus block. The overlap is a visual representation of the link between the buses and the traction network. The electrical network includes the DC traction network and may optionally incorporate the upstream AC medium voltage network in the calculations. Based on traction network and AC network topology, node and branch models are featured. The electric network model also includes PV systems, electric vehicle charging stations, and battery storage power stations models. The traction network simulation model uses power flow calculations at each time sample (see Equation 2.4). Since each bus's location and power consumption fluctuate over time, stationary counterparts for moving loads are employed, where the buses are paused at each time samples in  $\tau_s$  in order to find the new locations and powers of the buses. The behaviour of the traction network needs to be evaluated once regenerative power is identified using the



proper power flow approach. The electric network model is described in more detail in Chapter 4 and Chapter 5.

The dark blue block (Trolleybus System State) represents the result block of the simulation model and includes the traction network steady-state as well as the TB and BTB. From the bus model, relevant process data such as position, speed, and interior temperature are stored. Yet, regarding the traction network, all node voltages, node powers, and branch current profiles are included in the output sets.

## 2.6 Implementation Challenges

When developing a realistic simulation model for trolleybus systems, it is necessary to consider the characteristics of the surrounding environment that have the potential to affect the movement of the TBs and BTBs. The following are some of the most challenging aspects of modelling the bus routes and bus movements:

- Bus movement progression is affected by traffic volume and the daily schedule. Traffic lights and bus stops force frequent stops, and also the bus's speed is limited by road speed restrictions and peak times. Accurately representing a bus's daily trips is a challenging task, particularly when dealing with the unpredictable nature of traffic and the demands of a bus's passengers. This problem will be directed in Sections 3.2 and 3.3.
- The approach to finding bus propulsion power and bus location is to mimic the bus's longitudinal dynamics and its corresponding speed profile. Motion regimes influence the speed at which the bus accelerates, steady drives, rolls, and decelerates (see Figure 3-6). It is incorrect, though, to use an optimal speed profile to depict the bus's movements on a road (between two stop points). Calculating a realistic bus speed profile (see Figure 3-10) that takes into consideration traffic situations and limitations while simultaneously assuring a complete stop at the intended stopping point is a difficult problem to solve in practise. This problem will be addressed in Sections 3.3, 3.4.2, and 3.4.3.
- An important factor in determining the topology of the traction network is the positions of the buses in reference to the OHCWs. However, bus movement is computed with respect to the road network and bus schedule. In order to determine and utilise the contact points of the buses with the OHCWs in the formulation of the traction network conductance matrix, the locations of the buses need to be mirrored on the traction network (see Figure 3-3). This problem will be handled in Sections 3.1.1, 3.1.2, and 3.3.

Correspondingly, the electric network model implies a different method of modelling entirely. Listed below are some of the issues that need to be addressed:

- The TBSSM, as aforementioned, is a discrete-time model that identifies the system state across particular time samples (see Equation 2.5). Owing to the buses' continuous

movements, the topology of the traction network will vary with each time step. Thus, determining a new conductance matrix for the traction network must be taken into account at each time step. This problem will be handled in Sections 5.1 and 5.2.2.

- In trolleybus systems, the presence of unidirectional traction substations results in significant voltage rises whenever surplus power is produced. This problem needs a specific approach in order to effectively anticipate the traction network's steady-state. This problem will be handled in Section 5.2.4.
- There are voltage rules for the traction structure (see Table 2-1 and Figure 2-4) that protect the bus motor and keep the traction network stable. Section 5.2.4 deals with voltage rises; however, for the steady-state calculations, voltage drops and their associated effect on bus motor current must be considered and correctly implemented. This issue will be directed in Section 5.2.5.

### 3 Modelling the Traffic Network along with Buses

One of the most promising approaches to developing realistic trolleybus system simulation model (TBSSM) is to mimic the real-world traffic flows of trolleybuses (TBs) as battery-trolleybuses (BTBs). The characteristics of the traffic network and the buses as well as the bus movements, need to be defined in considerable detail in order to develop appropriate speed and power profiles for all traffic situations.

A traffic network model (TNM) is the initial stage of the TBSSM. It is developed to characterise the travelling routes, with respect to traffic conditions and bus daily trip schedule, for trolleybus systems. As shown in Figure 3-1, TNM is composed of several models, which are responsible for describing the features of the road network. The road network is divided into two primary components, namely the traffic nodes and the traffic branches. This contributes to the description of how the travel roads are arranged depending on the topology of a road network. Both the traffic node and traffic branch models feature a number of attributes that are intended to assist in characterising the individuality of the elements that constitute the road network model (RNM). The mathematical expressions of the road network elements are described in Section 3.1.

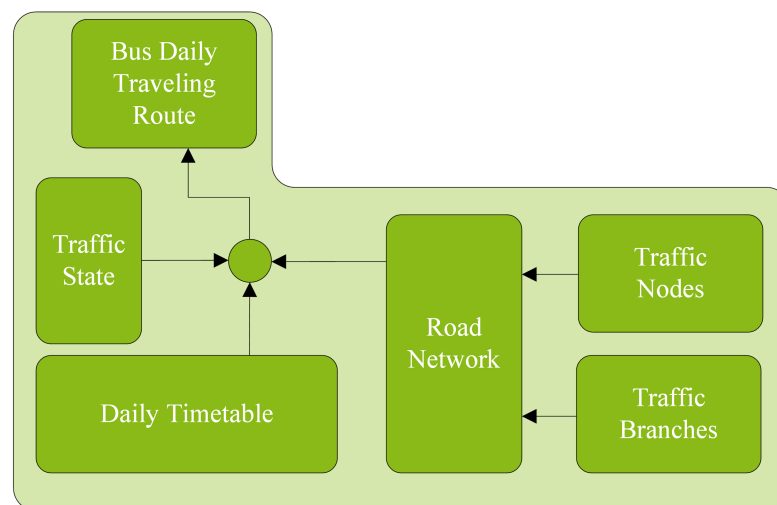


**Figure 3-1: Trolleybus traffic network model scheme which is part of the TBSSM scheme.**

In Section 3.2, the mathematical expressions for the daily timetable model (DTM) are developed in considerable detail. Afterwards, the bus daily travelling routes model (BDTRM) is presented in Section 3.3. In which, the formation of the road network as a distinct travel route for each bus is described. In consideration of this, the RNM, the DTM, and the traffic state model (TSM) are utilised in the modelling process of the bus daily travelling routes.

The objective of the TSM is to define the travelling routes and to characterise the events that have the potential to affect how buses travel throughout their daily schedules, e.g., probability of

dwelling at bus stops and traffic lights, dwelling time, passenger crowding, and speed limit reduction due to road crowds. The mathematical expressions for TSM are impeded in BDTRM.

### 3.1 Features of the Road Network

To accurately model a network, one needs comprehensive data that precisely represent the components of the network and the attributes of those components. Within the context of this simulation model, the TNM mimic the actual roads that the buses use throughout the course of their daily schedule. To that end, the RNM is represented by two basic elements, i.e., traffic node and traffic branch. Accordingly, the real-world road network is represented by collection of nodes linked by directed edges. Thus, the road network is structured as a directed graph  $G = (V, E)$ . In directed graph  $G$ , the nodes  $i \in V$  represent the points of interest in the network, so the edges (branches)  $(i, j) \in E$  indicate that two nodes  $i$  and  $j$  are connected by branch  $(i, j)$ , with  $(i, j) \neq (j, i)$  [90, 91]. The TNM has  $n_t$  traffic nodes and  $m_t$  traffic branches.

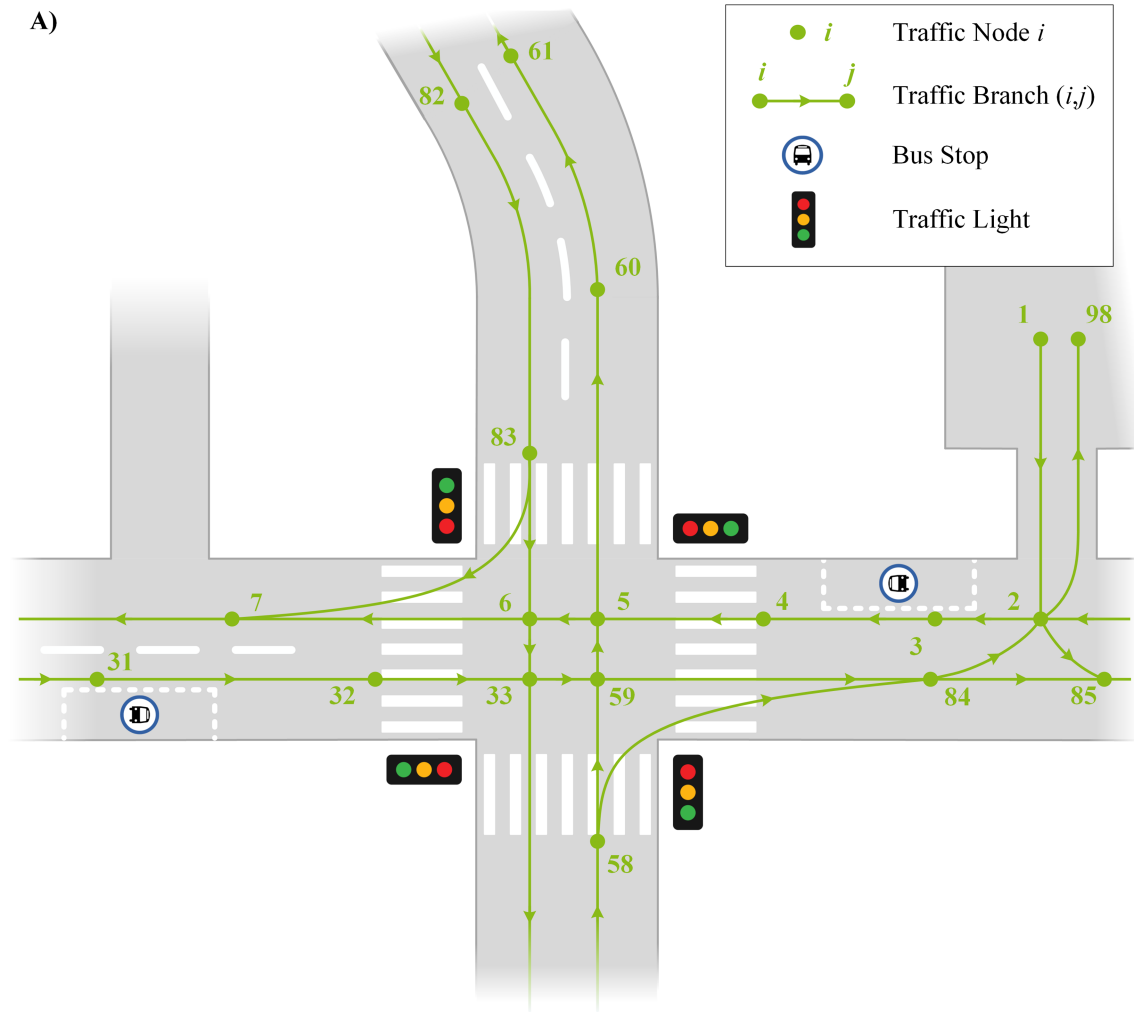
#### 3.1.1 Traffic Nodes

The traffic nodes represent specific locations in the road network; these nodes customise the RNM. In a standard road network, nodes represent the intersection points between roads. For the prepuce of this work, RNM must be defined with additional traffic nodes to make it more flexible and practical for simulating the bus movements (see Section 3.3). Intersections, turnouts, and bus terminus symbolise the primary traffic nodes in RNM; this group of nodes is not enough for modelling a correct bus speed-profile. In order to improve the bus speed-profile, more locations must be included. Bus stops and traffic lights are examples of important locations as a bus may reduce its speed or dwell at them. The road nature as the surface topography of the land effects the bus speed-profile as well. Consequently, additional types of traffic nodes must be defined in the RNM (see Figure 3-2).

The traffic nodes map the bus travelling paths (see Section 3.3); their locations predict possible changes in bus speed-profile likewise bus travel direction. Due to the individual of the traffic nodes, each one of them is represented with its own set of attributes. The traffic node attributes consist of several information such as geographic position and position type, e.g., bus stop, traffic light, road junction or roundabout. These attributes support tracking the location of traffic nodes within the RNM as well as projecting their locations into the real-world geographic position and vice versa. The attributes set of the traffic nodes  $TN_a$  can be presented as:

$$TN_a = \{TN_{a1}, TN_{a2}, TN_{a3}, \dots, TN_{ak}\} \quad (3.1)$$

where  $TN_a$  is the traffic node attribute set which includes several subsets. The number of attributes (subsets) for a traffic node is represented by the indicator  $k$ .



B)

Traffic Node Type	Traffic Node Id
Depot	{1,98}
Bus Stop	{3,31}
Traffic Light	{4,32,58,83}
Road Junction	{2,7,84,85}
Road Curve	{60,82}
Spare Node	{5,6,33,59,61}

**Figure 3-2: Trolleybus road network structure.**  
**A: Road network graphic.**  
**B: Traffic node types.**

Let  $I$  be an indexing set  $I = \{i \in \mathbb{N}_1 | i \leq n_t\}$ . If for each element  $i$  of  $I$  there is an associated object in each subset of  $TN_a$ , then the attribute set of a traffic node can be presented as:

$$TN_{a,i} = \{TN_{a1,i}, TN_{a2,i}, TN_{a3,i}, \dots, TN_{ak,i} | i \in \{1,2,3, \dots, n_t\}\} \tag{3.2}$$

The traffic node attributes are defined as follows:

### Node-Id

A unique number is assigned for each traffic node, where  $TN_{a1} = \{tn_{a1} | \mathbb{N}_1\}$  and  $|TN_{a1}| = n_t$ . Let  $tn_{a1,i} \in TN_{a1,i}$  and  $tn_{a1,j} \in TN_{a1,j}$ , if  $i \neq j$  and  $TN_{a1} = \bigcup_i^{n_t} TN_{a1,i}$ , then  $TN_{a1,i} \cap TN_{a1,j} = \emptyset$ . The node elements of the road network graph  $G_{tn}$  are denoted by the traffic node Id set  $TN_{a1}$ , i.e.,  $V_{tn} = TN_{a1}$ .

### Node Type

A type that represents the feature of a traffic node in the RNM is described based on its location in the real world: depot, bus stop, traffic light, road junction, road curve, or spare node. Except for road curves, which are represented by three different numbers dependent on the curve radius, each node type is represented by a unique number. If  $N_{type}$  is a set of the traffic node type numbers, then  $N_{type} = \{n_{type} \in \mathbb{N}_1 | 1 \leq n_{type} \leq 8\}$  and  $|N_{type}| = 8$ . The traffic node type spare node represents locations that are useful for the simulation but do not correspond to any of the other traffic node types. For example, the road slope may change multiple times between two distant traffic nodes, namely, a long traffic branch. The road slopes are correctly represented by placing additional nodes across the long traffic branch (see Section 3.3), which will split it into several short traffic branches. Moreover, certain traffic nodes of the type spare node are included in the RNM to form the connection points between the TNM and the electric network model (ENM) (see Section 3.3).

Node type attribute can be defined as  $TN_{a2} = \{TN_{a2,1}, TN_{a2,2}, TN_{a2,3}, \dots, TN_{a2,n}\}$ , where  $n = n_t$  and  $\forall i: TN_{a2,i} \subset N_{type}$ .

### Altitude

For each corresponding traffic node, the elevation above sea level is given in  $TN_{a3}$  in unit of meter  $m$ . Where  $TN_{a3} = \{TN_{a3,1}, TN_{a3,2}, TN_{a3,3}, \dots, TN_{a3,n}\}$ ,  $n = n_t$ , and  $\forall i: TN_{a3,i} \subset \mathbb{R}$ . The altitude attribute for each traffic node contributes to determining the slope angle between two nodes.

### Electric Node-Id

The TBSSM includes two network models, i.e., the TNM and the ENM. Over time, new bus locations are established on the TNM as a result of bus movements. These locations are projected onto the ENM using intersection points between the TNM and ENM (see Section 3.3). Since each bus location is projected onto the ENM, the traction network conductance matrix is calculated sequentially (see Section 5.3.2). The TNM is projected onto the ENM by intersecting all traction nodes with selected traffic nodes. Consequently, the traffic node attributes must include the adjacent electric node. If  $TEN_a$  is the traction node attribute set and  $TEN_{a1}$  is the node-Id set, then  $TN_{a4} = \{TN_{a4,1}, TN_{a4,2}, TN_{a4,3}, \dots, TN_{a4,n}\}$ , where  $n = n_t$ ,  $\exists i: TN_{a4,i} \subset TEN_{a1} \Leftrightarrow$  traction node overlap the traffic node  $i$ , and  $\exists i: TN_{a4,i} = \emptyset \Leftrightarrow$  no overlapped traction node.

### Overhead-Line Connection

In case of an accessible overhead-line, the traffic node is referred to as a connected node, as shown in Figure 3-3. The overhead-line connection attribute is  $TN_{a5} = \{TN_{a5,1}, TN_{a5,2}, TN_{a5,3}, \dots, TN_{a5,n}\}$ , where  $n = n_t$ ,  $\exists i: TN_{a5,i} = \{1\} \Leftrightarrow$  present of accessible overhead-line, and  $\exists i: TN_{a4,i} = \{0\} \Leftrightarrow$  no accessible overhead-line.

### X-Coordinate

The x-coordinate is a geographic reference that defines the longitude of the geographic point associated with a traffic node measured in decimal degrees. Where  $TN_{a6} = \{x | x \in \mathbb{R}\}$  and  $|TN_{a6}| = n_t$ .

### Y-Coordinate

The y-coordinate attribute specifies the latitude of the geographic point associated with the traffic node measured in decimal degrees. Where  $TN_{a7} = \{y | y \in \mathbb{R}\}$  and  $|TN_{a7}| = n_t$ .

Each traffic node in the RNM is projected to its location on earth and vice versa. Let  $x_i \in TN_{a6}$  and  $y_i \in TN_{a7}$  be the longitude and latitude of the same traffic node, respectively, where  $i$  is the traffic node index. If  $i = \{1, 2, 3, \dots, n_t\}$ , and  $\forall i (l_{xy,i} = (x_i, y_i))$ . Then the geographic coordinate set of the traffic nodes is  $L_{xy} = \{l_{xy,1}, l_{xy,2}, l_{xy,3}, \dots, l_{xy,n} | n = n_t\}$ .

### Bus Stop Name

For each traffic node type (bus stop) there is an associated bus stop name. Let  $BS_{name} = \{BS_{name,1}, BS_{name,2}, BS_{name,3}, \dots, BS_{name,n}\}$  be the set of bus stop names, then bus stop name attribute is  $TN_{a8} = \{TN_{a8,1}, TN_{a8,2}, TN_{a8,3}, \dots, TN_{a8,n}\}$ , where  $n = n_t$ ,  $\exists i: TN_{a8,i} \subset BS_{name} \Leftrightarrow TN_{a2,i} = \{\text{bus stop}\}$ , and  $\exists i: TN_{a8,i} = \emptyset \Leftrightarrow TN_{a2,i} \neq \{\text{bus stop}\}$ .

### Dwell Probability

The location of a bus stop has a significant role in determining whether a bus will dwell at that stop. In order to fulfil the requirements of this attribute, each bus stop is assigned with a specific dwell probability, which is used later in the daily travelling route (see Section 3.3) to determine whether a bus dwells at the bus stops that are on its daily trips in the course of a day. Let  $P_{dwell} = \left\{ \frac{x}{10} | x \in \mathbb{N}_1 \wedge 5 \leq x \leq 10 \right\}$  be the set of dwell probabilities, then the dwell probability attribute is  $TN_{a9} = \{TN_{a9,1}, TN_{a9,2}, TN_{a9,3}, \dots, TN_{a9,n}\}$ , where  $n = n_t$ ,  $\exists i: TN_{a9,i} \subset P_{dwell} \Leftrightarrow TN_{a8,i} \neq \emptyset$ , and  $\exists i: TN_{a9,i} = \emptyset \Leftrightarrow TN_{a8,i} = \emptyset$ .

### 3.1.2 Traffic Branches

Traffic nodes are distributed all over the road segments of the road network. For every pair of traffic nodes, an edge links them, referred to as a traffic branch in this simulation model. Traffic branches are unidirectional, which means that the traffic flow only goes in one direction, beginning at the start node and terminating at the end node of the traffic branch. Like the traffic

nodes, traffic branches are associated with several attributes that are insertional for bus movement (see Section 3.3 and 3.4.2) and the traction network state computing (see Section 5.2.2). The attributes set of the traffic branches  $TB_a$  is:

$$TB_a = \{TB_{a1}, TB_{a2}, TB_{a3}, \dots, TB_{ak}\} \quad (3.3)$$

where  $TB_a$  is the traffic branch attribute set which has several subsets. The number of attributes (subsets) for a traffic branch is represented by the indicator  $k$ .

If  $i$  indexes the traction branches in  $TB_a$ , then the attribute set of traffic branch  $i$  can be written as:

$$TB_{a,i} = \{TB_{a1,i}, TB_{a2,i}, TB_{a3,i}, \dots, TB_{ak,i} | i \in \{1, 2, 3, \dots, m_t\}\} \quad (3.4)$$

The traffic branch attributes are defined as follows:

### From-Node

This attribute denotes the traffic node at the start of the traffic branch. If  $TN_{a1}$  is the set of traffic node Ids, then traffic branch from-node set is  $TB_{a1} = \{TB_{a1,1}, TB_{a1,2}, TB_{a1,3}, \dots, TB_{a1,m}\}$ , where  $m = m_t$ , and  $\forall i: TB_{a1,i} \subset TN_{a1}$ .

### To-Node

This attribute denotes the traffic node at the end of the traffic branch. If  $TN_{a1}$  is the set of traffic node Ids, then traffic branch from node set is  $TB_{a2} = \{TB_{a2,1}, TB_{a2,2}, TB_{a2,3}, \dots, TB_{a2,m}\}$ , where  $m = m_t$ , and  $\forall i: TB_{a2,i} \subset TN_{a1}$ .

### Electric From-Node

To improve the simulation performance of the traffic and electric networks, two simulation models, TNM and ENM, are introduced. By linking specific traffic nodes to all traction nodes, the TNM may be mirrored in the ENM. The TNM has several traffic nodes to highlight the road topology and traffic situation, which are essential for simulating bus moves. However, the ENM has the least number of traction nodes. Thus, traffic nodes outnumber traction nodes, i.e.,  $n_t > n_{te}$ , while the traffic branches outnumber the traction branches, i.e.,  $m_t > m_{te}$ .

The electric from-node attribute of the traffic branch denotes the from-node Id of the overlapped traction branch. If  $TB_{a3}$  and  $TEB_{a1}$  are traffic branch and traction branch attribute sets, respectively, where  $TB_{a3} = \{TB_{a3,1}, TB_{a3,2}, TB_{a3,3}, \dots, TB_{a3,m}\}$  and  $m = m_t$ . Thus,  $\exists i: TB_{a3,i} \subset TEB_{a1} \Leftrightarrow$  traction branch overlaps the traffic branch, and  $\exists i: TB_{a3,i} = \emptyset \Leftrightarrow$  no overlapped traction branch with the traffic branch.

### Electric To-Node

As for the electric from-node, the electric to-node attribute of the traffic branch denotes the to-node Id of the overlapped traction branch. If  $TB_{a4}$  and  $TEB_{a2}$  are traffic branch and traction



branch attribute sets, respectively, where  $TB_{a4} = \{TB_{a4,1}, TB_{a4,2}, TB_{a4,3}, \dots, TB_{a4,m}\}$ , and  $m = m_t$ . Thus,  $\exists i: TB_{a4,i} \subset TEB_{a2} \Leftrightarrow$  traction branch overlaps the traffic branch, and  $\exists i: TB_{a4,i} = \emptyset \Leftrightarrow$  no overlapped traction branch with the traffic branch.

Figure 3-3 shows a traction branch being mirrored by multiple traffic branches when an OHCW is present, where the from-node (5) and to-node (6) of traction branch the (5,6) are defined as the electric from- and to-node of the traffic branches (25,26), (26,27), and (27,28), which have the indexes 1, 2, and 3, respectively. Whereas, the traffic branches 4, 5, and 6 have no values for the electric from- and to-node attributes, since no traction branches (OHCWs) exist over this part of the traffic road, i.e., electric from-node =  $\phi$  and electric to-node =  $\phi$  as well.

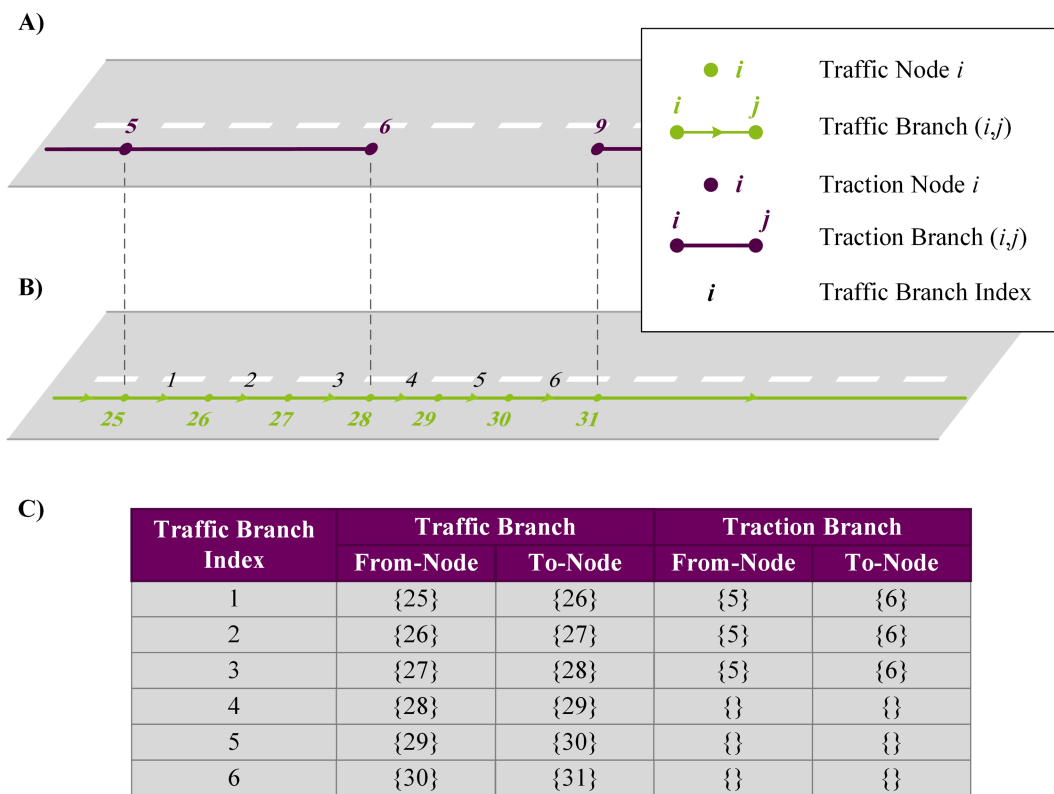


**Figure 3-3: Illustration of traffic- and electric network overlap.**  
**A: Electric traction network from ENM**  
**B: Road network from TNM**  
**C: Traction branch (from-/to-node) correspond to traffic branch (from-/to-node).**

**Length**

This attribute represents the distance between traffic branch from- and to-node. However, it is calculated across the roadway shapes, not from the shortest distance between the end nodes. Figure 3-1 shows that the distance between nodes 82 and 83 is not the shortest; instead, it is computed from the roadway shape, i.e., a curve road.

Length attribute is measured in units of metres and denoted as  $TB_{a5} = \{TB_{a5,1}, TB_{a5,2}, TB_{a5,3}, \dots, TB_{a5,m}\}$ , where  $m = m_t$  and  $\forall i: TB_{a5,i} \subset \mathbb{R}_{>0}$ .

### Speed Limit

It is noteworthy a maximum speed restriction is applied to particular stretch of roads according to the surrounding of the road, for example, residential zones 30 km/h, towns or cities 50 km/h, and arterial highways 70 km/h and above [92]. Since this speed limit impacts the bus movement and its speed profile, the maximum permitted speed for a particular road is included in the attributes of the traffic branch which represent that road. If  $S_{\max} = \{10x | x \in \mathbb{N}_1\}$  is the set of maximum speeds in km/h, then  $TB_{a6} = \{TB_{a6,1}, TB_{a6,2}, TB_{a6,3}, \dots, TB_{a6,m}\}$ , where  $m = m_t$  and  $\forall i: TB_{a6,i} \subset S_{\max}$ .

### 3.2 Daily Timetable

Daily bus schedules are represented by timetables that include estimated arrival and departure times at bus stops. A bus schedule is divided into several trips, so that every bus starts and ends its schedule at the bus depot. The departure trip begins from the depot and continues to the first bus stop (of the next trip) at the end of the departure trip. On subsequent inbound and outbound trips, the bus proceeds via a series of bus stops according to a predetermined schedule. Towards the conclusion of the day's schedule, the final journey from the last bus stop to the depot is established. The DTM is necessary to simulate bus movements in the road network; consequently, a daily travelling route (see Section 3.3) for the TNM is developed.

To implement the daily schedule of all buses into the simulation model, a set of all the trips during the daily schedule for bus  $k$  is defined as:

$$B_{\text{trips},k} = \{B_{t,k,1}, B_{t,k,2}, B_{t,k,3}, \dots, B_{t,k,n}\}, \quad (3.5)$$

$$n = n_{\text{bt},k} \wedge k \in \{1,2,3, \dots, n_{\text{bus}}\}$$

where  $B_{t,k,1}$  is the departure trip and  $B_{t,k,n}$  is the arrival trip,  $n_{\text{bt},k}$  is the total number of trips in the daily schedule of bus  $k$ ,  $n_{\text{bus}}$  is the total number of buses. If  $I = \{1,2,3, \dots, n_{\text{bt},k}\}$  and  $i \in I$  is an index for  $B_{\text{trips},k}$  elements, then for  $\forall i: (2 \leq i \leq (n_{\text{bt},k} - 1))$  are the inbound and outbound trips, consecutively. The minimum number of trips in a daily bus schedule  $B_{\text{trips},k}$  is four; departure, arrival, one inbound and one outbound trip.

The bus trip set  $B_{t,k,i}$  is defined as:

$$B_{t,k,i} = \{B_{\text{line},k,i}, T_{\text{start},k,i}, BS_{\text{start},k,i}, T_{\text{end},k,i}, BS_{\text{end},k,i}, BS_{\text{dis},k,i}\} \quad (3.6)$$

where  $i$  is the trip number,  $B_{\text{line},k,i}$  is the bus line number,  $T_{\text{start},k,i}$  is the starting time at the first bus stop of the trip,  $BS_{\text{start},k,i}$  is the name of the first bus stop,  $T_{\text{end},k,i}$  is the arriving time at the last bus stop in the trip,  $BS_{\text{end},k,i}$  is the name of the last bus stop, and  $BS_{\text{dis},k,i}$  is the whole trip distance.

Excluding the departure and arrival trips, which are driven directly away and toward the depot, a bus dwells at several bus stops along the route between the first and last bus stop of trip

$i$ , ( $2 \leq i \leq (n_{bt,k} - 1)$ ). A set of bus stop names, which contains the bus stops encountered along a bus trip, is necessary to depict the bus travel route thoroughly. Including the bus line number  $B_{line}$ , the name of the first bus stop  $BS_{start}$ , the name of the last bus stop  $BS_{end}$ , and the total trip distance  $BS_{dis}$ , the set of bus stop names along a bus trip is:

$$BS_{trip} = \{B_{line}, BS_{start}, BS_{end}, BS_{dis}, BS_{ts}\} \quad (3.7)$$

where  $BS_{ts}$  is a set of bus stop names, sorted so that the element sequence starts with the first bus stop name flowed by the series of consecutive bus stop names until the last bus stop name at the end of the set. The  $BS_{ts}$  is defined as:

$$BS_{ts} = \{bs_{n,1}, bs_{n,2}, bs_{n,3}, \dots, bs_{n,r}\}, \quad (3.8)$$

$$\forall i: (bs_{n,i} \in BS_{name} | i = \{1,2,3, \dots, r\})$$

where  $r$  is the number of bus stops in a trip, e.g.,  $r = 2$  in the departure and arrival trips, where only two bus stops are needed; one is the depot, and the other is either the destination or the departing bus stop.

If  $n_{bst}$  is the total number of the miscellaneous bus stop trips and  $BS_{trip,i} := BS_{trip}$  (see Equation 3.8) with  $i = \{1,2, \dots, n_{bst}\}$ , then:

$$BS_{trips} = \{BS_{trip,1}, BS_{trip,2}, BS_{trip,3}, \dots, BS_{trip,n}\}, n = n_{bst} \quad (3.9)$$

The daily schedule of all buses is defined as:

$$DS_{Buses} = \{B_{trips,1}, B_{trips,2}, B_{trips,3}, \dots, B_{trips,n}\}, n = n_{bus} \quad (3.10)$$

### 3.3 Daily Travelling Route

Throughout the day, each bus follows predetermined routes. Accordingly, a combination of the bus traffic network and daily schedule data is necessary to successfully mimic these routes, which will be later utilised by the bus model in order to simulate the bus movement (see Sections 3.4 and 4.3.1). BDTRM includes road topography, topology, and traffic data, i.e., road grades, traffic light and bus stop locations, road junctions, road curves, and road maximum speed. Furthermore, the OHCW data of the electric traction network are included as well.

The BDTRM of bus  $k$  is identified as  $\mathbf{B}_{TR,k}$ , however, for simplicity, the index  $k$  will be excluded. Thus,  $\mathbf{B}_{TR,k}$  is defined as:

$$\mathbf{B}_{TR} = \begin{bmatrix} btr_{11} & btr_{12} & \dots & btr_{1m} \\ btr_{21} & btr_{22} & \dots & btr_{2m} \\ \vdots & \vdots & \ddots & \vdots \\ btr_{n1} & btr_{n2} & \dots & btr_{nm} \end{bmatrix}, m = m_r, n = 12 \quad (3.11)$$

Where  $\mathbf{B}_{TR}$  is an  $n \times m$  matrix. The number of columns  $m_r$  represents the total number of the successive traffic nodes that are shaped from the daily travelling route of bus  $k$ , and the twelve rows represent the Ids of the successive traffic nodes that represent the bus daily travelling route,

traffic branch lengths, day time, road slope angles, road speed limits, bus stopping points, dwelling time at stop points, passenger crowding, distance to the next stopping point, electric traction branch from-nodes, electric traction branch to-nodes, and electric traction branch lengths, respectively. The structure and modelling of  $\mathbf{B}_{TR}$  are further described below:

### Route Nodes

The first row of  $\mathbf{B}_{TR}$  is computed using Equations 3.1, 3.5, and 3.9. The first group of traffic nodes is computed based on the first element of Equation 3.5 that is defined in Equation 3.6. Matching the element of the first bus trip in Equation 3.6, i.e.,  $B_{line,1}$ ,  $BS_{start,1}$ ,  $BS_{end,1}$ , and  $BS_{dis}$ , with the first four elements in  $(BS_{trip,i} | i = \{1,2,3, \dots, n_{bst}\})$  from Equation 3.9. The index  $i$  of the matched result is used to get  $BS_{ts}$ , which is the fifth element of  $BS_{trip,i}$ . After finding the corresponded bus stop names of the first trip, Equation 3.1 is used to find the equivalent traffic node Id of each bus stop in matched  $BS_{ts}$ . Each element in  $BS_{ts}$  is compared with the elements of  $TN_{a7}$  (see Equations 3.1). The index of the matched element is used to get the matched traffic node Id from  $TN_{a1}$ . With the same cardinality of  $BS_{ts}$ , a new set  $TN_{ts} = \{tn_{ts} | tn_{ts} \in TN_{a1}\}$  is computed.

If  $n_{bsn} = |TN_{ts}|$  and  $j$  is the index of  $TN_{ts}$  elements, then  $BS_{sp} = \{(tn_{ts,j}, tn_{ts,k}) | tn_{ts} \in TN_{ts}, j = [n_{bsn}] \wedge k = j - 1\}$  is a set of paired traffic nodes  $(tn_{ts,j} := bs_{n,j})$ , whose first traffic node represents the (from bus stop) and the second traffic node represents the (to bus stop.). The road network is modelled as a directed graph  $G_{tn}$  (see Section 3.1). By including the traffic branch lengths  $TB_{a5}$  as a weight assigned to the graph edges, i.e., traffic branches,  $G_{tn}$  can be denoted as  $G_{tnw} = (V_{tn}, E_{tn}, w_{tn})$ . The weight function  $w_{tn}$  maps the traffic branches  $E_{tn}$  to their lengths,  $w_{tn}: E_{tn} \rightarrow TB_{a5}$ .

Whenever a path connects two nodes in a network, a weighted graph can be used to determine the shortest route between them [90, 93]. Therefore, the shortest route for each element of  $BS_{sp}$  is determined using  $G_{tnw}$ . If  $R_{paths} = \{R_{path,1}, R_{path,2}, R_{path,3}, \dots, R_{path,n}\}$  is a set of the possible paths between bus stops in  $BS_{sp}$ , i.e.,  $(tn_{ts,j}, tn_{ts,k})$ , and  $D_{paths} = \{D_{path,1}, D_{path,2}, D_{path,3}, \dots, D_{path,n}\}$  is the corresponding distance of  $R_{paths}$ , then the minimum path distance is  $D_{path,min} = \min(D_{paths})$  and its corresponding route is  $R_{path,min}$ . The elements of  $R_{paths}$  include the traffic nodes sequence for the path between  $(tn_{ts,j}, tn_{ts,k})$ . If there are  $n$  route paths in  $R_{paths}$  and  $r$  is the index on each element in  $R_{paths}$ , then each element in  $R_{paths}$  can be defined as  $R_{path,r} = \{tn_{rp} | tn_{rp} \in TN_{a1}\}$ . Combining all minimum routes in  $BS_{sp}$ , i.e.,  $(R_{path,min,1}, R_{path,min,2}, \dots, R_{path,min,n})$ , will produce the corresponding traffic nodes sequence to the first trip  $BS_{ts}$ . In the combination procedure, the final traffic node in  $R_{path,min}$  must be removed excluding last route path in  $BS_{sp}$ . Therefore, repetition of traffic nodes – at the end of a route path and the beginning of the following route path – is avoided.

After computing the traffic nodes sequence of the first trip  $TN_{ts,i}$ ,  $i = 1$ , the same process will carry on with the remained bus trip in Equation 3.6. The daily route is modelled by combining all

traffic node sequences of the bus trips respectively using the prior process to avoid any repetition of traffic nodes in the end and start of the trips. Elements of the first row of  $\mathbf{B}_{TR}$  can be defined as:

$$\text{row}_1(\mathbf{B}_{TR}) = (rn_l | rn_l \in TN_{a1}), l = \{1, 2, 3, \dots, m_r\} \quad (3.12)$$

Where  $rn_l$  is a traffic node Id and  $\forall l: (btr_{1l} := rn_l)$ . Each consecutive pair in Equation 3.12 represents a traffic branch, i.e.,  $(rn_l, rn_{l+1}) \in E_{tn} \Leftrightarrow (l+1) \leq m_r$ .

### Branch Lengths

As mentioned above, each consecutive pair in Equation 3.12 represents a traffic branch, and  $(rn_{l-1}, rn_l)$  for  $l = \{2, 3, 4, \dots, m_r\}$  is the from- and to-node, respectively. If  $i$  is the index of traffic branch in Equation 3.4 and  $(rn_{(l-1)} \in TB_{a1,i} \wedge rn_l \in TB_{a2,i})$ , then the length of traffic branch  $i$  is  $tb_{L,l} = tb_{L,i}$ , where  $tb_{L,i} \in TB_{a5}$ . The length row can be defined as:

$$\mathbf{B}_{TR,2l} = \begin{cases} 0, & l = 1 \\ tb_l, & 2 \leq l \leq m_r \end{cases} \quad (3.13)$$

Where  $tb_{L,l}$  is the traffic branch length for the consecutive pair  $(rn_{l-1}, rn_l)$  from Equation 3.12.

### Day Time

In Equation 3.6, bus trip start time  $T_{start,i}$  and end time  $T_{end,i}$  are defined. After computing the traffic nodes sequence  $TN_{tns,i}$  of trip  $i$ , a time value, corresponding to each traffic node in  $TN_{tns,i}$ , is calculated. The first and end time are given, i.e.,  $T_{start,i}$  and  $T_{end,i}$ . If  $i = 1$ , the start index  $s = 1$ , and end index  $e = |TN_{tns,i}| - 1$ , then  $\mathbf{B}_{TR,3s} = T_{start,i}$  and  $\mathbf{B}_{TR,3e} = T_{end,i}$ . The corresponding time for the nodes between  $s$  and  $e$  is calculated as follows:

$$\mathbf{B}_{TR,3r} = \left( T_{start,i} + \frac{(T_{end,i} - T_{start,i})}{\sum_{k=s}^e \mathbf{B}_{TR,2k}} + \mathbf{B}_{TR,3r} \right), s \leq r \leq e \quad (3.14)$$

For the next trip  $(i+1)$ , the start and the end index are recalculated, where  $s = |TN_{tns,(i-1)}| - 1$ , and  $e = |TN_{tns,i}| - 1$  but not for last  $i$  in which  $e = |TN_{tns,i}|$ . Hereafter, Equation 3.14 will be repeated until all appropriate times are obtained. The elements of the day time row are defined as:

$$\text{row}_3(\mathbf{B}_{TR}) = (tr_{dt,l} | tr_{dt,l} \in H), l = \{1, 2, 3, \dots, m_r\} \quad (3.15)$$

where  $H = [00:00, 24:00)$ .

### Road Slope Angle

The road slope angle is calculated between every consecutive pair in Equation 3.12, i.e.,  $(rn_{l-1}, rn_l)$ , where  $l = \{2, 3, 4, \dots, m_r\}$ . The traffic node altitude can be found by using Equation 3.2. If  $rn_l \in TN_{a1,i}$ , then for the traffic node  $rn_l$  the attitude is  $tn_{z,l} = TN_{a3,i}$ . The row elements (road slope angle) can be computed as:

$$B_{TR,4l} = \begin{cases} 0 & , \quad l = 1 \\ \tan^{-1} \frac{(tn_{z,(l-1)} - tn_{z,l})}{tb_{L,l}} & , \quad 2 \leq l \leq m_r \end{cases} \quad (3.16)$$

Where  $tb_{L,l}$  is the length of traffic branch  $(rn_{l-1}, rn_l)$ .

### Road Speed Limit

After defining the traffic branch of every consecutive pair in Equation 3.12, i.e.,  $(rn_{l-1}, rn_l)$ , where  $l = \{2, 3, 4, \dots, m_r\}$ , the maximum permitted speed on these branches can be found by using Equation 3.4. If  $i$  is the index of traffic branch and  $(rn_{(l-1)} \in TB_{a1,i} \wedge rn_l \in TB_{a2,i})$ , then the maximum permitted speed on traffic branch  $i$  is  $tb_{SL,l} = tb_{SL,i}$ , where  $tb_{SL,i} \in TB_{a6}$ . The (road speed limit) row can be defined as:

$$B_{TR,5l} = \begin{cases} 0 & , \quad l = 1 \\ tb_{SL,l} & , \quad 2 \leq l \leq m_r \end{cases} \quad (3.17)$$

where  $tb_{SL,l}$  is the traffic branch speed limit for the consecutive pair  $(rn_{l-1}, rn_l)$  from Equation 3.12.

### Stopping Points

Each bus stop has a dwell probability (see Section 3.1.1). The dwell probability  $P_{dwell}$  is between 0.5 and 1, i.e.,  $P_{dwell} \in [0.5, 1]$ . Dwelling of buses at bus stops are not hold constant to the defined values in the dwell probability attribute of the traffic nodes over the course a of day, except for traffic nodes that are assigned with a dwell probability of  $P_{dwell} = 1$ . In other words, the defined dwell probability attribute is determined according to rush hour situation, and it needs to be adjusted for normal operation intervals. On workdays, three rush hour intervals are defined,  $RH_1 = [6: 30, 9: 00]$ ,  $RH_2 = [12: 00, 14: 00]$ , and  $RH_3 = [16: 00, 19: 00]$ , respectively. Otherwise, weekends have only two rush hour intervals; thus,  $RH_1 = \phi$ ,  $RH_2 = [12: 00, 14: 00]$ , and  $RH_3 = [16: 00, 19: 00]$ , respectively [94, 95]. The rush hours set can be defined as:

$$RH = RH_1 \cap RH_2 \cap RH_3 \quad (3.18)$$

In order to anticipate whether or not a bus may stop at bus stop, traffic light, or road junction, a random number  $0 \leq x_r \leq 1$  is generated for each traffic node in Equation 3.12, i.e.,  $x_{r,l} \in [0, 1]$ . Thereafter, identifying whether or not the corresponding traffic node in Equation 3.12 is a stopping traffic node is done by utilising Equation 3.2 as follows:

$$SP_{bs} = \{TN_{a1,i} | 1 \leq i \leq n_t \wedge TN_{a2,i} \in \{\text{bus stop}\}\} \quad (3.19)$$

$$SP_{tl} = \{TN_{a1,i} | 1 \leq i \leq n_t \wedge TN_{a2,i} \in \{\text{traffic light}\}\} \quad (3.20)$$

$$SP_{rj} = \{TN_{a1,i} | 1 \leq i \leq n_t \wedge TN_{a2,i} \in \{\text{road junction}\}\} \quad (3.21)$$

$$SP = SP_{bs} \cap SP_{tl} \cap SP_{rj} \quad (3.22)$$

and

$$x_{sp,l} = \begin{cases} 1, & rn_l \in SP \\ 0, & \text{otherwise} \end{cases}, l = \{1,2,3, \dots, m_r\} \quad (3.23)$$

where  $SP_{bs}$ ,  $SP_{tl}$ , and  $SP_{rj}$  are sets of traffic node Ids which their type attributes are bus stop, traffic light, and road junction, respectively,  $SP$  is a set in which all traffic node Ids in  $SP_{bs}$ ,  $SP_{tl}$ , and  $SP_{rj}$  are combined, and  $x_{sp,l}$  is an indicator which identifies possible stopping locations in the route nodes defined by Equation 3.12. Dwell probability  $x_{dp,l}$  for each bus stop in the route nodes defined by Equation 3.12 can be determined using Equation 3.2 as follows:

$$x_{dp,l} = \begin{cases} TN_{a9,i}, & TN_{a2,i} \subset \{\text{bus stop}\} \\ \emptyset, & \text{otherwise} \end{cases}, \quad (3.24)$$

$$l = \{1,2,3, \dots, m_r\}; i = \{1,2,3, \dots, n_t\}$$

where  $TN_{a2,i}$  and  $TN_{a9,i}$  are the traffic node attributes for node type and dwell probability, respectively (see Section 3.1.1). Bus dwelling corresponds to the route node (see Equation 3.12) can be determined as follows:

$$\mathbf{B}_{TR,6l} = \begin{cases} 1, & x_{r,l} \leq x_{dp,l} \wedge rn_l \in SP_{bs} \wedge tr_{dt,l} \in RH \\ 1, & x_{r,l} \leq (x_{dp,l} - 0.4) \wedge rn_l \in SP_{bs} \wedge tr_{dt,l} \notin RH \\ 1, & x_{dp,l} = 1 \wedge rn_l \in SP_{bs} \\ 1, & x_{r,l} \leq 0.5 \wedge rn_l \in SP_{tl} \wedge tr_{dt,l} \in RH \\ 1, & x_{r,l} \leq 0.3 \wedge rn_l \in SP_{tl} \wedge tr_{dt,l} \notin RH \\ 1, & x_{r,l} \leq 0.3 \wedge rn_l \in SP_{rj} \\ 0, & \text{otherwise} \end{cases} \quad (3.25)$$

$$l = \{1,2,3, \dots, m_r\}$$

and

$$\text{row}_6(\mathbf{B}_{TR}) = (sp_l | sp_l \in \{0,1\}), l = \{1,2,3, \dots, m_r\} \quad (3.26)$$

where  $sp_l$  is an element in  $\mathbf{B}_{TR}$ , and it represents where a bus will dwell during its daily schedule. The value of  $sp_l$  is determined as presented in Equation 3.25. Bus dwelling at traffic node of type bus stops  $rn_l \in SP_{bs}$  during rush hours  $tr_{dt,l} \in RH$  is determined based on defined dwell probability  $x_{dp,l}$  which is compared to a random generated number  $x_{r,l}$ . As a result,  $x_{dp,l}$  has a higher value, bus is more likely to dwell. The dwell probability at bus stops  $x_{dp,l}$  is heuristically found to be reduced  $(x_{dp,l} - 0.4)$  outside the rush hours  $tr_{dt,l} \notin RH$ ; however, with a dwell probability of one ( $x_{dp,l} = 1$ ), bus dwell is inevitable. Similarly, the probability to dwell at traffic lights  $rn_l \in SP_{tl}$  is when the value of random number  $x_{r,l}$  is below 0.5 and 0.3, i.e.,  $x_{r,l} \leq 0.5$  and  $x_{r,l} \leq 0.3$ , during rush hours  $tr_{dt,l} \in RH$  and regular hours  $tr_{dt,l} \notin RH$ , respectively. Regardless of day time, it is anticipated that buses have a dwell probability only when  $x_{r,l} \leq 0.3$  for road junctions  $rn_l \in SP_{rj}$ .

## Dwelling Time

To model the travel route, dwelling time at each element in the  $SP$  set needs to be considered. The dwelling time is a random variable whose range depends on several factors. The time spent waiting at a traffic light, for instance, is determined by the arrival time of a bus at a traffic light after the red light has been triggered. Similarly, dwelling time at a bus stop depends on the number of passengers boarding or alighting. Furthermore, no dwelling time will be considered for stopping at a road junction in the  $\mathbf{B}_{TR}$  matrix.

Let  $WT_{tl} = \{wt_{tl} \in \mathbb{N} | wt_{tl,min} \leq wt_{tl} \leq wt_{tl,max}\}$ , be a sequence of expected dwelling times at traffic lights with minimum and maximum dwelling times  $wt_{tl,min}$  and  $wt_{tl,max}$ , respectively, and  $WT_{bs} = \{wt_{bs} \in \mathbb{N} | wt_{bs,min} \leq wt_{bs} \leq wt_{bs,max}\}$ , be a sequence of expected dwelling times at bus stops with minimum and maximum dwelling times  $wt_{bs,min}$  and  $wt_{bs,max}$ , respectively. However, dwelling time at road junction is always considered to be zero as mentioned above; thus,  $WT_{rj} = \{0\}$ . The dwelling time at a traffic light is chosen at random with uniform probability distribution from  $WT_{tl}$ , i.e.,  $wt_{tl,r} \stackrel{R}{\leftarrow} WT_{tl}$ . Furthermore, dwelling time at a bus stop is likewise picked at random from  $WT_{bs}$ , but with a temporal constraint, so that there is a high likelihood of a long dwelling time during the rush hours and a short dwelling time throughout the rest of the day. Accordingly, the dwelling time at a bus stop is  $wt_{bs,r} \stackrel{R}{\leftarrow} WT_A(x)$ , which is the random process of obtaining  $wt_{bs,r}$  by running algorithm  $WT_A$  on input  $x$ . Where  $x$  is determined as follows:

$$x = \begin{cases} 1, & tr_{dt,l} \in RH \\ 0, & otherwise \end{cases}, l = \{1,2,3, \dots, m_r\} \quad (3.27)$$

Using Equations 3.19, 3.20, 3.21, and 3.26, the dwelling time row can be determined as follows:

$$\mathbf{B}_{TR,7l} = \begin{cases} wt_{tl,r}, & sp_l = 1 \wedge rn_l \in SP_{tl} \\ wt_{bs,r}, & sp_l = 1 \wedge rn_l \in SP_{bs}, \\ 0, & sp_l = 1 \wedge rn_l \in SP_{rj} \end{cases}, l = \{1,2,3, \dots, m_r\} \quad (3.28)$$

## Passenger Crowding

For every trip between two consecutive bus stops, a specified number of passengers on board of bus must be considered. Passenger count depends on the time of day and the location of bus stops. In this work, only the time influence is considered. For sake of a random distribution, passenger crowding may be represented as several discrete levels rather than absolute numbers. Four crowding levels are defined as follows:

$$P_C = \{P_{C1}, P_{C2}, P_{C3}, P_{C4}\} \quad (3.29)$$

where  $P_C$  is the set of passengers crowding intervals,  $P_{C1}$ ,  $P_{C2}$ ,  $P_{C3}$ , and  $P_{C4}$  are the low, low medium, high medium, and high crowding intervals, respectively. Each crowding level is represented as an interval  $[x_1, x_2]$ , where  $x_1$  indicates the lower number of passengers and  $x_2$



indicates the higher number of passengers corresponds to each crowding level. Equation 3.29 can be written as:

$$P_C = \{[x_{1,C1}, x_{2,C1}], [x_{1,C2}, x_{2,C2}], [x_{1,C3}, x_{2,C3}], [x_{1,C4}, x_{2,C4}]\} \quad (3.30)$$

The average passenger load over 24 hours is 37% and at peak time between 7:00 and 8:00 is 65% [96]. The crowding intervals are defined for a correspond day time:  $P_{C1}$  at  $t_{d,C1} = \{[22:00, 7:00]\}$ ,  $P_{C2}$  at  $t_{d,C2} = \{[9:00, 12:00], [14:00, 16:00], [19:00, 22:00]\}$ ,  $P_{C3}$  at  $t_{d,C3} = \{[12:00, 14:00]\}$ , and  $P_{C4}$  at  $t_{d,C4} = \{[7:00, 9:00], [16:00, 19:00]\}$ . If a random integer number is picked from the crowding level intervals ( $P_{C1}$ ,  $P_{C2}$ ,  $P_{C3}$ , and  $P_{C4}$ ) and defined as:

$$R_{P,c} \in \{x \in \mathbb{N}_1 | x_{1,c} \leq x \leq x_{2,c}\}, c = \{C1, C2, C3, C4\} \quad (3.31)$$

then the elements of the passenger crowding mass row can be computed based on the day time sets ( $t_{d,C1}$ ,  $t_{d,C2}$ ,  $t_{d,C3}$ , and  $t_{d,C4}$ ) and their corresponding crowding intervals as follows:

$$\mathbf{B}_{TR,8l} = \begin{cases} R_{P,C1}, & sp_l = 1 \wedge rn_l \in SP_{bs} \\ & \wedge tr_{dt,l} \in t_{d,C1} \\ R_{P,C2}, & sp_l = 1 \wedge rn_l \in SP_{bs} \\ & \wedge tr_{dt,l} \in t_{d,C2} \\ R_{P,C3}, & sp_l = 1 \wedge rn_l \in SP_{bs}, \\ & \wedge tr_{dt,l} \in t_{d,C3} \\ R_{P,C4}, & sp_l = 1 \wedge rn_l \in SP_{bs} \\ & \wedge tr_{dt,l} \in t_{d,C4} \end{cases}, \quad l = \{1, 2, 3, \dots, m_r\} \quad (3.32)$$

where  $R_{P,C1}$ ,  $R_{P,C2}$ ,  $R_{P,C3}$ , and  $R_{P,C4}$  are random integer numbers generated randomly (see Equation 3.31) from the crowding level intervals, ( $P_{C1}$ ,  $P_{C2}$ ,  $P_{C3}$ , and  $P_{C4}$ ), respectively. Based on Equation 3.32, all non-bus stops nodes ( $rn_l \neq \{\text{bus stop}\}$ ) are not assigned with a passenger number. To substitute the missing values between any two consecutive bus stops, the passenger number of the previous column is utilised in the subsequent blank columns.

If  $\mathbf{B}_{TR,8l} = \{tr_{p,1}, tr_{p,2}, tr_{p,3}, \dots, tr_{p,n}\}$ , and  $n = m_r$ , then Equation 3.32 can be rewritten as follows:

$$\mathbf{B}_{TR,8l} = \begin{cases} R_{P,C1}, & sp_l = 1 \wedge rn_l \in SP_{bs} \\ & \wedge tr_{dt,l} \in t_{d,C1} \\ R_{P,C2}, & sp_l = 1 \wedge rn_l \in SP_{bs} \\ & \wedge tr_{dt,l} \in t_{d,C2} \\ R_{P,C3}, & sp_l = 1 \wedge rn_l \in SP_{bs}, \\ & \wedge tr_{dt,l} \in t_{d,C3} \\ R_{P,C4}, & sp_l = 1 \wedge rn_l \in SP_{bs} \\ & \wedge tr_{dt,l} \in t_{d,C4} \\ tr_{p,l-1}, & \text{otherwise} \end{cases}, \quad l = \{1, 2, 3, \dots, m_r\} \quad (3.33)$$

### Stopping Distance

In this row, the interstation distance between two consecutive stop locations (with tag 1 in  $\mathbf{B}_{TR,4}$ ) is commuted as follows:

$$\mathbf{B}_{TR,9l} = \sum_{k=s}^e \mathbf{B}_{TR,2k}, s \leq l \leq e \quad (3.34)$$

where  $s$  and  $e$  are the indices of the departure and arrival bus stops, respectively. The values of  $s$  and  $e$  are updated for every consecutive bus stops. If  $l_1$  is the index of departure bus stop and  $l_2$  is the index of arrival bus stop, then  $s = l_1 + 1$  and  $e = l_2$ .

### Electric Traction Branch (From-node)

Every consecutive pair in Equation 3.12, i.e.,  $(rn_{l-1}, rn_l)$ , represents a traffic branch, where  $l = \{2, 3, 4, \dots, m_r\}$ . The electric traction branch (from-node) that is corresponded to a specific traffic branch (see Figure 3-3) can be determined using Equation 3.3 and the from- and to-node values of the traffic branch, which are in this case  $(rn_{l-1}, rn_l)$ , as follows:

$$teb_{fn,l} = \{TB_{a3,i} \Leftrightarrow (rn_{(l-1)} = TB_{a1,i} \wedge rn_l = TB_{a2,i}) | 1 \leq i \leq m_t\} \quad (3.35)$$

and the (electric traction branch (from-node)) row can be defined using Equation 3.35 as follows:

$$\mathbf{B}_{TR,10l} = \begin{cases} 0 & , \quad l = 1 \\ teb_{fn,l} & , \quad 2 \leq l \leq m_r \end{cases} \quad (3.36)$$

### Electric Traction Branch (To-Node)

The electric traction branch (to-node) can be find using the same process used to find the electric traction branch (from-node) of traffic branch  $(rn_{l-1}, rn_l)$ . Therefore,

$$teb_{tn,l} = \{TB_{a4,i} \Leftrightarrow (rn_{(l-1)} = TB_{a1,i} \wedge rn_l = TB_{a2,i}) | 1 \leq i \leq m_t\} \quad (3.37)$$

and the (electric traction branch (to-node)) row can be defined using Equation 3.37 as follows:

$$\mathbf{B}_{TR,11l} = \begin{cases} 0 & , \quad l = 1 \\ teb_{tn,l} & , \quad 2 \leq l \leq m_r \end{cases} \quad (3.38)$$

where  $teb_{tn,l}$  is the to-node of the electric traction branch that is correspond to traffic branch  $(rn_{l-1}, rn_l)$ , and  $teb_{tn,l} \in TB_{a4}$ .

### Electric Traction Branch Length

The elements in 10<sup>th</sup> row  $\mathbf{B}_{TR,10*}$  and 11<sup>th</sup> row  $\mathbf{B}_{TR,11*}$  are the electric traction branch from- and to-nodes, respectively. An electric traction branch can be represented as  $(teb_{fn,l}, teb_{tn,l}) \Leftrightarrow teb_{fn,l} \neq \emptyset \wedge teb_{tn,l} \neq \emptyset$ , where  $teb_{fn,l} \in \mathbf{B}_{TR,10*}$  and  $teb_{tn,l} \in \mathbf{B}_{TR,11*}$ , and  $l$  is the column

index of  $\mathbf{B}_{\text{TR}}$ . Using Equation 4.3 and the electric traction branch from- and to-node ( $teb_{\text{fn},l}, teb_{\text{tn},l}$ ), the electric traction branch length can be determined as follows:

$$teb_{L,l} = \{TEB_{a3,i} \Leftrightarrow (teb_{\text{fn},l} = TEB_{a1,i} \wedge teb_{\text{tn},l} = TEB_{a2,i}) | 1 \leq i \leq m_{\text{et}}\} \quad (3.39)$$

and the electric traction branch length row can be defined using Equation 3.40 as follows:

$$B_{\text{TR},12l} = \begin{cases} 0 & , \quad l = 1 \\ teb_{L,l} & , \quad 2 \leq l \leq m_r \end{cases} \quad (3.40)$$

As mentioned above, the BDTRM contains the road network information that is sorted according to bus daily travel routs. A bus starts its daily schedule from the second column in  $\mathbf{B}_{\text{TR}}$  and finish at column  $m_r$ . Thus, the data of each column in  $\mathbf{B}_{\text{TR}}$  represent a *travel segment* that is utilised by the bus model (see Sections 3.4 and 4.3.1) to simulate the continues move of a bus during the simulation interval  $\tau_s$ . Equation 3.41 defines a travel segment correspond to column  $i$  in  $\mathbf{B}_{\text{TR}}$ .

$$B_{\text{trs},i} = (btr_{1,i}, btr_{2,i}, btr_{3,i}, \dots, btr_{12,i}), i \in \{1,2,3, \dots, m_r\} \quad (3.41)$$

### 3.4 Modelling of the Bus

Basic information about the bus physical and technical specifications and its travelling routes is essential to calculate the speed/load profile that mimics the traffic condition and trolleybus/battery trolleybus behaviour in real-world scenarios. The bus speed/load profile is thus simulated using a bus model (BM) that accounts for road topography, traffic regulation and bus schedule, which are represented by BDTRM, as well as auxiliary loads, and the influence of weather conditions. The BM can be computed as follows:

$$BM_k = \{B_{\text{sp},i,k}, B_{\text{state},k}, B_{\text{trs},j,k}\}, k \in \{1,2,3, \dots, n_{\text{bus}}\} \quad (3.42)$$

where  $BM_k$  is the BM for bus  $k$ ,  $n_{\text{bus}}$  is the total number of buses,  $B_{\text{sp},i,k}$  is bus  $k$  mechanical and electrical speciation which will be described in section 3.4.1,  $B_{\text{state},k}$  is bus  $k$  state with respect to time  $t$ , i.e. bus consumption power, bus battery SOC, and bus location in TNM and ENM (see Sections 3.4.2 and 3.4.3), and  $B_{\text{trs},j,k}$  is the actual travelling route segment (see Equation 3.41).

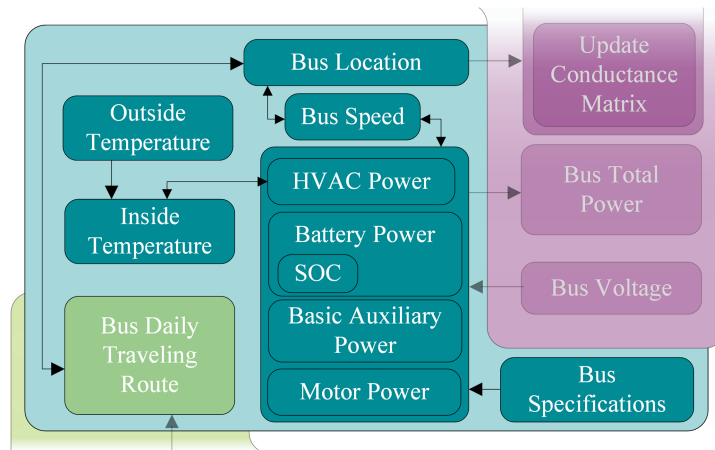


**Figure 3-4: TB/BTB model scheme which is part of the TBSSM scheme. The overlapped light green and purple parts represent the TNM and ENM, respectively.**

The block diagram of BM is shown in Figure 3-4. Through the BDTRM, which is a combination of road topography, traffic regulation, and bus schedules (see Section 3.3), the BM is interconnected to the TNM. With regards to BDTRM, the location of the bus is continuously updated based on the laws of motion while considering the impacts of mechanical and aerodynamic drag on the bus as well as the characteristics of the bus. Numerous motion regimes, including acceleration, constant-speed, rolling, and braking, are used to determine bus speed profile between two stop points (see Section 3.4.2). Nevertheless, bus speed is impacted by bus location (BDTRM), bus physical and technical specifications (see Sections 3.4.1 and 3.4.2), and the traction network status (see Section 5.2.5). The corresponding bus speed is determined following the calculation of bus longitudinal dynamics, and the updated location in the traffic network is simultaneously recorded and used to update the traction network conductance matrix (see Section 5.2.2). According to bus location in the traffic network, the battery operation may be changed – charging or discharging – depending on the availability of the OHCWs. When bus contact with OHCWs changes, the current operating state of the on-board battery is evaluated and changed if necessary. Temperature in the passenger compartment is regulated using a thermal balance calculation that considers the surrounding environment's temperature. Combining the auxiliary powers, which include heating, ventilation, air conditioning (HVAC) power, and basic auxiliary power, with the electric traction power – the motor power – defines the total amount of consumed power. If the on-board batteries of the bus are being charged, the charging power will be included in the total consumed power. Otherwise, the power demands of the bus will be met by the energy that has been stored in the on-board batteries.

### 3.4.1 Bus Specifications

To simulate the driving cycle of a TB or a BTB, mechanical and electrical specifications for these buses need to be considered. The bus specifications can be represented as following:

$$B_{sp,i} = \{b_{sp1,i}, b_{sp2,i}, b_{sp3,i}, \dots, b_{spk,i}\} \tag{3.43}$$

where  $B_{sp,i}$  is the specification set of a given bus maker, such as Premier AT 18, AG 300T, or Trolino 18.75 [97],  $i$  is the bus maker index, and  $(b_{sp1,i}$  to  $b_{spk,i})$  are the mechanical and electrical specifications of bus maker  $i$ . The elements of set  $B_{sp,i}$  are defined as shown in Table 3-1. There are 31 elements that represent the specifications of bus  $i$ , and, thus,  $k = 31$  in Equation 3.43. In case the bus variety is not a battery trolleybus, then  $b_{sp19,i} = b_{sp20,i} = b_{sp21,i} = b_{sp22,i} = \emptyset$ .

### 3.4.2 Bus Speed/Power Profile

It is necessary to have comprehensive information about both the physical and technical specifications of the bus (see Section 3.4.1) in order to mimic its realistic speed/power profile. In the following section dynamic models for the longitudinal motion of a bus are presented.

#### Longitudinal Dynamics Model

Bus propulsion system counteracts the effects of aerodynamic and mechanical drags on the bus. Figure 3-5 shows the forces impacting a bus moving on an inclining road. Based on Newton's second law of motion, the forces acting in the movement of the bus is computed as follows [98–102]:

$$F_T = F_{in} + F_R + F_A + F_S \tag{3.44}$$

where  $F_T$  is the tractive (traction) force,  $F_{in}$ ,  $F_R$ ,  $F_A$ , and  $F_S$  are the inertia force, rolling resistance forces, aerodynamic drag force, and grade (gravitational) force, respectively.

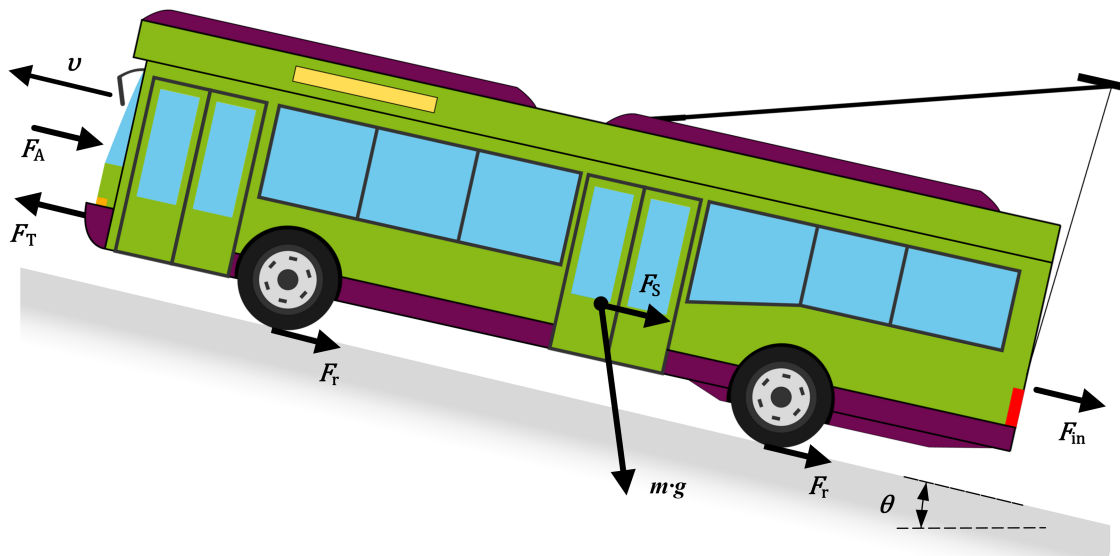


Figure 3-5: Acting forces on a moving bus (trolleybus/battery trolleybus) [103].

**Table 3-1: Trolleybus/battery trolleybus mechanical and electrical specifications (elements of Equation 3.43).**

Element Notation		Description	Unit
$b_{sp1,i}$	$B_{type}$	Bus variety	-
$b_{sp2,i}$	$m_{min}$	Minimum mass (without passengers)	kg
$b_{sp3,i}$	$m_{max}$	Maximum mass (with full passenger capacity)	kg
$b_{sp4,i}$	$\lambda_m$	Mass factor	percent
$b_{sp5,i}$	$L_b$	Length	m
$b_{sp6,i}$	$W_b$	Width	m
$b_{sp7,i}$	$H_m$	Height	m
$b_{sp8,i}$	$v_{bs}$	Maximum Speed	m/s
$b_{sp9,i}$	$pn_{max}$	Maximum passenger capacity	-
$b_{sp10,i}$	$a$	Acceleration	m/s <sup>2</sup>
$b_{sp11,i}$	$a'$	Deceleration	m/s <sup>2</sup>
$b_{sp12,i}$	$c_d$	Aerodynamic drag coefficient	-
$b_{sp13,i}$	$c_r$	Rolling resistance coefficient	-
$b_{sp14,i}$	$\eta_m$	Electrical motor efficiency	percent
$b_{sp15,i}$	$\eta_b$	Regenerative braking efficiency	percent
$b_{sp16,i}$	$P_m$	Motor maximum power	W
$b_{sp17,i}$	$P_{BH}$	Heating power	W
$b_{sp18,i}$	$P_{BAC}$	Air-condition power	W
$b_{sp19,i}$	$P'_V$	Ventilator power	W
$b_{sp20,i}$	$\eta_{hc}$	Heating/Cooling efficiency	percent
$b_{sp21,i}$	$P_{baux}$	Basic Auxiliary power	W
$b_{sp22,i}$	$\rho_{air}$	Air density	kg/m <sup>3</sup>
$b_{sp23,i}$	$C_p$	Air specific heat capacity	kJ/kgK
$b_{sp24,i}$	$L_g$	Window glass thickness	m
$b_{sp25,i}$	$L_c$	Chassis thickness	m
$b_{sp26,i}$	$k_g$	Glass thermal conductivity	W/m <sup>2</sup> K
$b_{sp27,i}$	$k_c$	Chassis thermal conductivity	W/m <sup>2</sup> K
$b_{sp28,i}$	$P_{bdis}$	Battery discharging power	W
$b_{sp29,i}$	$P_{bcha}$	Battery charging power	W
$b_{sp30,i}$	$E_{sc}$	Battery effective capacity	Wh
$b_{sp31,i}$	$SOC_{ini}$	Battery initial SOC	percent

The *inertia force*  $F_{in}$  is responsible of providing the bus linear acceleration, and can be defined from Newton's third law as follows:

$$F_{in} = \lambda_m \cdot M \cdot a \quad (3.45)$$

where  $\lambda_m := b_{sp4,i}$  (see Equation 3.43) is the factor to take into account the rotational masses,  $M$  is the total mass of the bus and calculated as shown in Section 4.3.1 and Equation 4.10, and  $a$  is the acceleration/deceleration of the bus,  $a := b_{sp10,i}$  for acceleration and  $a = a' := b_{sp11,i}$  for deceleration (see Equation 3.43).

The *rolling resistance forces*  $F_R$  is primarily influenced by the deformation and abrasion of the tires [104]. Moreover, friction in bearings and the gearing system also play their part. Considering the rolling resistance coefficient  $c_r := b_{sp13,i}$  (see Equation 3.43) and the gradient of the road  $\theta := b_{tr3,i}$  (see Equation 3.41), the rolling resistance force, which are distributed over the bus tyres, is the summation of the rolling resistance forces  $F_r$  that are applied on the bus tyres and can be mathematically expressed as in Equation 3.46.

$$F_R = \sum F_r = c_r \cdot M \cdot g \cdot \cos(\theta) \quad (3.46)$$

where  $g$  is the gravitational acceleration ( $g = 9.81 \text{ m/s}^2$ ). The rolling resistance coefficient  $c_r$  is determined experimentally and is impacted by road and tire conditions, and, thus, the rolling resistance depends on the tire's construction and the compounds used in its production.

The *aerodynamic drag force*  $F_A$  is the force caused by the friction of the bus body moving through air. This force is distributed over the bus surface and is influenced by many parameters: bus physical body, bus velocity and wind velocity, temperature, altitude, and humidity [105]. The aerodynamic drag force is expressed as:

$$F_A = \frac{1}{2} \cdot \rho_{air} \cdot c_d \cdot A_f \cdot v(t)^2 \quad (3.47)$$

where  $\rho_{air}$  is the air density in ( $\text{kg/m}^3$ ),  $c_d := b_{sp12,i}$  (see Equation 3.43) is the aerodynamic drag coefficient, which depends on the bus design,  $A_f = (W_b \cdot H_b)$  (see Equation 3.43) is frontal area of the bus in ( $\text{m}^2$ ), and  $v(t)$  (see Equation 3.52) is the bus speed in ( $\text{m/s}$ ) at simulation time  $t$ . In this simulation model, the airflow velocity around the bus is assumed to equal the bus speed; therefore, the wind speed is neglected. The value of ( $\rho_{air} = 1.225 \text{ kg/m}^3$ ) is considered for air density  $\rho_{air}$  in this work which is suitable for most cases, despite its dependence on temperature, altitude and humidity [105].

The *grade force*  $F_S$  is the force that the bus requires to drive on a slope. It is computed from the component bus total mass  $M$  acting along the slop and can be mathematically expressed as:

$$F_S = M \cdot g \cdot \sin(\theta) \quad (3.48)$$

where  $M$ ,  $g$ , and  $\theta$  are the bus total mass, gravitational acceleration, and gradient of the road, respectively. The bus will gain force when driving downhill ( $F_S < 0$  and  $\theta < 0$ ), and require additional force when driving uphill ( $F_S > 0$  and  $\theta > 0$ ). Otherwise,  $F_S = 0$  when  $\theta = 0$ .

The electric traction power of the trolleybus/battery trolleybus can be calculated from the resulting traction force  $F_T$  and the electrical motor efficiency  $\eta_m := b_{sp14,i}$  (Equation 3.43) [106].

$$P'_{TB} = F_T \cdot v(t') \quad (3.49)$$

$$P_{TB} = \frac{P'_{TB}}{\eta_m} \quad (3.50)$$

where  $P'_{TB}$ , and  $P_{TB}$  are the mechanical and electric traction power, respectively.  $v(t')$  is bus speed at simulation time  $t'$  (see Equation 3.52), and  $t'$  is the progress of the simulation time  $t$  after adding the time step  $\delta t$  to it ( $t' = t + \delta t$ ).

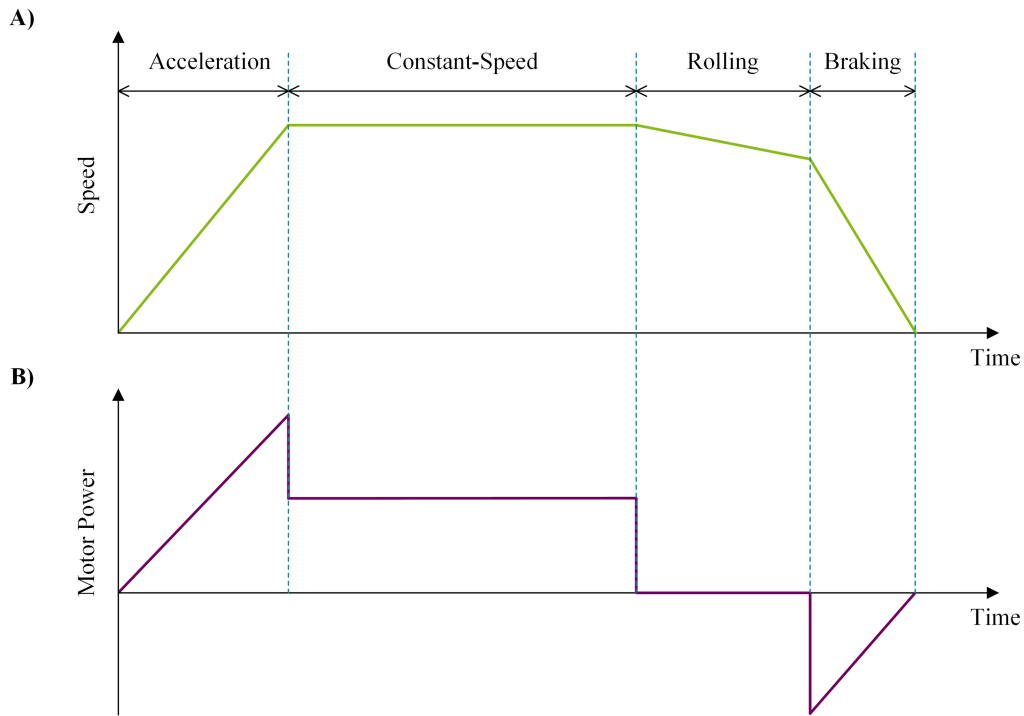


**Figure 3-6: Speed/power profile for a bus stop-to-stop driving cycles.**

**A) Optimal speed profile.**

**B) Optimal motor power profile.**

The motion regime of a bus travelling between two stops is critical since it directly affects the amount of energy a bus consumes, so it is essential to be aware of the motion regime at all simulated times. Bus stop-to-stop movement can be represented in four different regimes of motion: acceleration, constant-speed, rolling, and braking (see Figure 3-6) [107]. A regimes of motion variable  $M_B$  can be defined as follows:



$$M_B = \begin{cases} 1, & \text{Acceleration} \\ 2, & \text{Constant-speed} \\ 0, & \text{Rolling} \\ -1, & \text{Braking} \end{cases} \quad (3.51)$$

Figure 3-6 (A) shows an optimal bus speed progress between two bus stops with respect to each motion regime, while the corresponding motor power (bus traction power) with respect to these motion regimes is shown in Figure 3-6 (B).

In *acceleration regime* ( $M_B = 1$ ), more traction power is required to increase the bus speed. Accordingly, the bus traction force/power must be higher than the resistance force acting against the direction of motion ( $F_T(t') > 0, P_{TB}(t') > 0$ ). The bus speed – in acceleration regime – is calculated as follows:

$$v(t') = v(t) + a \cdot \delta t; t' = t + \delta t \quad (3.52)$$

where  $t$  is time,  $\delta t$  is the time step (change in time),  $v(t)$  is the former bus speed,  $v(t')$  is the new bus speed after  $\delta t$ , and  $a := b_{sp10,i}$  (see Equation 3.43) is the bus acceleration. At the starting of a driving cycle  $t = 0$ ,  $v(0) = 0$ , and  $d(0) = 0$ .

The displacement  $\delta d(t')$  is calculated as follows:

$$\delta d(t') = v(t) \cdot \delta t + \frac{1}{2} \cdot a \cdot \delta t^2; t' = t + \delta t \quad (3.53)$$

Thus, the travelled distance – between two consecutive traffic nodes –  $d$  is:

$$d(t') = d(t) + \delta d(t'); t' = t + \delta t \quad (3.54)$$

the travelled distance – between two consecutive stops –  $d'$  is:

$$d'(t') = d'(t) + \delta d(t'); t' = t + \delta t \quad (3.55)$$

and the travelled distance – between two consecutive traction nodes –  $d''$  is:

$$d''(t') = d''(t) + \delta d(t'); t' = t + \delta t \quad (3.56)$$

The three different, above mentioned, travelled distance, i.e.,  $d(t')$ ,  $d'(t')$ , and  $d''(t')$ , are used to calculate the bus progress with respect to the traffic branches and traction branches. These travelled distance are used to determine motion regimes with in a stop-to-stop movement (see Section 3.4.3), index  $i$  in Equation 3.41 (see Section 4.3.1), and traction network topology (see Sections 5.1).

In *constant-speed regime* ( $M_B = 2$ ), the bus stops accelerating ( $a = 0$ ) and keeps its driving speed constant. Specifically, the exact amount of traction force/power required to overcome the resistance force acting against the direction of motion ( $F_T(t') > 0, P_{TB}(t') > 0$ ) must be applied in this regime. The bus speed  $v(t')$  and displacement  $\delta d(t')$  in Equations 3.52 and 3.53, respectively, can be computed – in constant-speed regime – as follows:

$$v(t') = v(t), t' = t + \delta t \quad (3.57)$$

$$\delta d(t') = v(t) \cdot \delta t, t' = t + \delta t \quad (3.58)$$

and traction force  $F_T$  in Equation 3.44 as:

$$F_T = F_R + F_A + F_S \quad (3.59)$$

After determine the displacement  $\delta d(t')$  as shown in Equation 3.58, the travelled distances  $d(t')$ ,  $d'(t')$ , and  $d''(t')$  are calculated as defined in Equations 3.54, 3.55, and 3.56, respectively.

In *Rolling regime* ( $M_B = 0$ ), the bus speed progressively drops due to resistance force acting against the bus movement. While the bus is in rolling regime, no traction power is required to propel it forward. Therefore, the bus moves by its momentum and  $F_T = 0$ ; moreover, the bus acceleration  $a$  is calculated from Equations 3.44 and 3.45 as follows:

$$a_r = -\frac{(F_R + F_A + F_S)}{\lambda_m \cdot M} \quad (3.60)$$

with a road gradient  $\theta < 0$  (see Equation 3.48), the bus rolling deceleration rate  $a_r$  is positive and the bus will accelerate, e.g.,  $(F_A + F_S) > F_R$ , otherwise, the bus will deaccelerate and lose speed. The new bus speed  $v(t')$  and displacement  $\delta d(t')$  are calculated as in Equations 3.52 and 3.54, respectively. Where the calculated deceleration rate  $a_r$  (see Equation 3.60) is used to substitute  $a$ , i.e.,  $a := a_r$ .

In *braking regime* ( $M_B = -1$ ), the bus is forced to reduce its speed by reversing the operation direction of the traction motor. Consequently, the mechanical energy ( $P'_{TB}(t) < 0$ ) is utilized by converting the bus kinetic energy into electrical energy. The bus speed  $v(t')$ , displacement  $\delta d(t')$ , and tractive force  $F_T$  are calculated – in braking regime – using Equations 3.52, 3.53, and 3.44, respectively. The deceleration rate  $a' := b_{sp11,i}$  (see Equation 3.43) is used to substitute  $a$ , i.e.,  $a := a' := b_{sp11,i}$ .

The regenerative braking power is computed as follows:

$$P_{TB}(t') = P_b = \eta_b \cdot P'_{TB}(t') \quad (3.61)$$

where  $P_b$  is the regenerative braking power, and  $\eta_b := b_{sp15,i}$  (see Equation 3.43) is the regenerative braking efficiency.

### Auxiliaries

The power consumption of the auxiliary units must be considered in the BM, given the significant impact of some of these units on the bus power profile [108]. Heating, ventilation, and air conditioning (HVAC) systems, as other non-mechanical units (basic auxiliary units), define the auxiliary consumption power of a trolleybus/battery trolleybus.

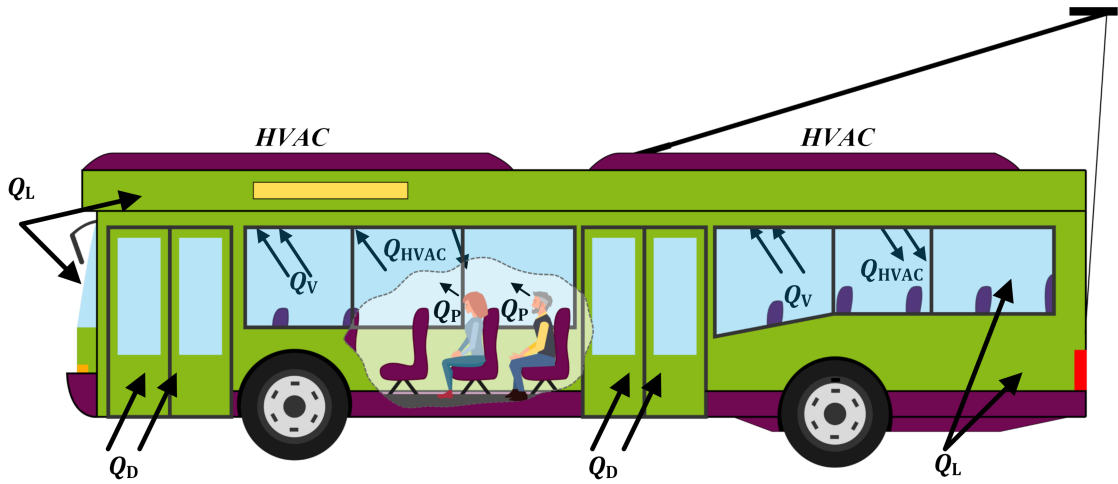


**Figure 3-7: Heat loads through the bus passenger compartment.**

The HVAC in the BM is computed using the heat balance equation of the air inside the passenger compartment as shown below [109, 110]:

$$\frac{(T_i(t') - T_i(t))}{\delta t} = \frac{(Q_{HVAC}(t') + Q_P(t') - Q_L(t') - Q_D(t') - Q_V(t'))}{V_b \cdot \rho_{air} \cdot C_p}, t' = t + \delta t \quad (3.62)$$

where  $C_p$  is the air specific heat capacity ( $C_p := b_{sp23,i}$ , see Equation 3.43),  $(V_b \cdot \rho_{air})$  is the air mass inside the bus in (kg) –  $V_b := (b_{sp5,i} \cdot b_{sp6,i} \cdot b_{sp7,i})$  and the air density  $\rho_{air} := b_{sp22,i}$  (see Equation 3.43),  $T_i(t)$  and  $T_i(t')$  are the temperature inside the bus at the last step time  $t$  and the given time  $t'$ , respectively,  $\delta t$  is the simulation time step,  $Q_{HVAC}(t')$  is the added HVAC thermal energy at  $t'$ ,  $Q_P(t')$  is the passengers heat energy at  $t'$ ,  $Q_L(t')$  is the conductive and convective thermal losses energy at  $t'$ ,  $Q_D(t')$  the energy loss due to the opening of the bus doors at  $t'$ , and  $Q_V(t')$  energy loss due to ventilation at  $t'$ . Figure 3-7 shows all the added heat energy and lost energy losses (see Equation 3.62) contributing to the thermal balance inside the passenger compartment are represented. The arrow directions are a symbolic for the impact of the heat energy on the passenger compartment.  $Q_D$  and  $Q_L$  represent the outside thermal energy coming from opening the bus doors and the contact with the bus windows and chassis, respectively. A small section of the bus side is removed to show the contribution of passengers' heat energy  $Q_P$  to the passenger compartment. The HVAC units are located on the roof of the bus, so  $Q_{HVAC}$  and  $Q_V$  are impacting the passenger compartment through the roof of the bus, as indicated by the arrow directions inside the bus.

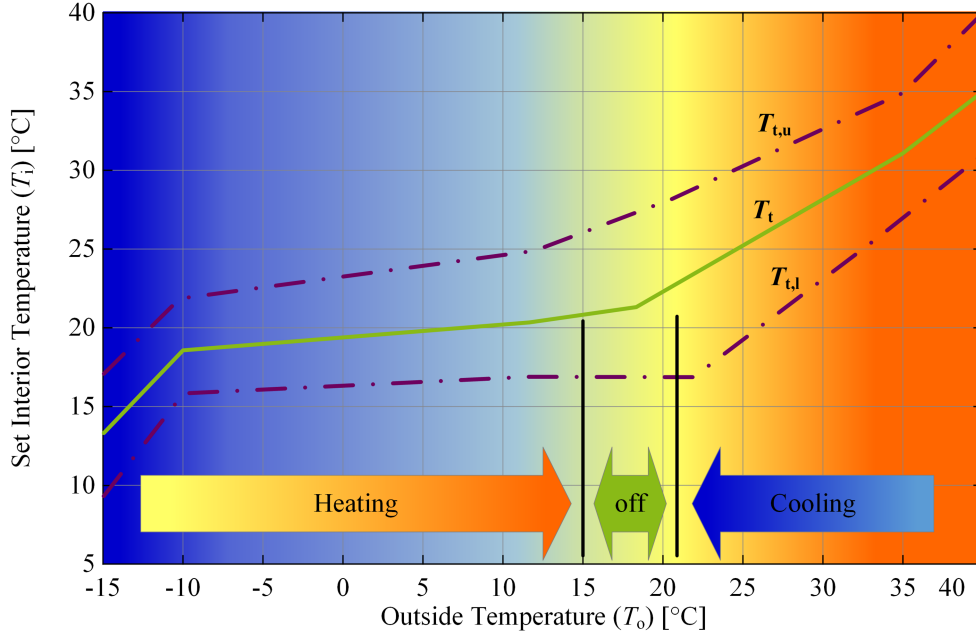


Figure 3-8: Comfort temperature range in the passenger compartment, in compliance with VDV<sup>5</sup> recommendation 236 [111].

Based on the bus internal temperature  $T_i$  and the target comfort temperature  $T_t$  setting (see Figure 3-8), the HVAC system of the bus runs in either *heating*-, *cooling*-, or *off*-mode, as follows:

$$Q_{\text{HVAC}}(t') = \begin{cases} -P_{\text{BH}} \cdot \delta t, & T_o(t') < 15^\circ \wedge M_{\text{hc}}(t') = 1 \\ P_{\text{BAC}} \cdot \delta t, & T_o(t') > 22^\circ \wedge M_{\text{hc}}(t') = 1 \\ 0, & M_{\text{hc}}(t') = 0 \end{cases} \quad (3.63)$$

$$M_{\text{hc}}(t') = \begin{cases} 1, & \begin{cases} (T_i(t) \leq T_{t,l}(t') \wedge T_o(t') < T_i(t)) \\ (T_i(t) \geq T_{t,u}(t') \wedge T_o(t') > T_{t,u}(t')) \end{cases} \\ 0, & \begin{cases} (T_i(t) \geq T_{t,u}(t') \wedge T_i(t - \delta t) < T_{t,u}(t')) \\ (T_i(t) \leq T_{t,l}(t') \wedge T_i(t - \delta t) > T_{t,l}(t')) \\ 15^\circ \leq T_o(t') \leq 22^\circ \end{cases} \\ M_{\text{hc}}(t), & \text{otherwise} \end{cases} \quad (3.64)$$

where  $P_{\text{BH}} := b_{\text{sp}17,i}$  and  $P_{\text{BAC}} := b_{\text{sp}18,i}$  are heating power and air-condition power (see Equation 3.43), respectively,  $T_o(t')$  is the outside temperature at  $t'$ ,  $\delta t$  is the time step, and  $M_{\text{hc}}$  is a control variable, which turns *on/off* the heating and cooling, and is determined as shown in Equation 3.64.  $M_{\text{hc}}(t')$  turn *off* the heating or cooling ( $M_{\text{hc}}(t') = 0$ ) when the outside temperature  $T_o(t')$  is between  $15^\circ\text{C}$  and  $22^\circ\text{C}$  (see Figure 3-8). Yet  $M_{\text{hc}}(t')$  turn *off* the heating ( $M_{\text{hc}}(t') = 0$ ) when the bus inside temperature  $T_i(t)$  reaches the upper comfort temperature  $T_{t,u}$  ( $T_i(t) \geq T_{t,u}(t') \wedge T_i(t - \delta t) < T_{t,u}(t')$ ) and turns it *on* ( $M_{\text{hc}}(t') = 1$ ) when  $T_i(t)$  drops below the lower comfort temperature  $T_{t,l}$  with an outside temperature  $T_o(t')$  less than  $T_i(t)$  ( $T_i(t) \leq T_{t,l}(t') \wedge T_o(t') < T_i(t)$ ), as it turn *off* the air-condition ( $M_{\text{hc}}(t') = 0$ ) when  $T_i(t)$  drop below the

<sup>5</sup> In German, famous as: Verband Deutscher Verkehrsunternehmen

lower comfort temperature  $T_{t,l}$  ( $T_i(t) \leq T_{t,l}(t') \wedge T_i(t - \delta t) > T_{t,l}(t')$ ) and turns it *on* once more ( $M_{hc}(t') = 1$ ) when  $T_i(t)$  reaches the upper comfort temperature  $T_{t,u}$  again ( $T_i(t) \geq T_{t,u}(t') \wedge T_o(t') > T_{t,u}(t')$ ). Otherwise,  $M_{hc}(t')$  hold its revues value from the last time step  $M_{hc}(t') = M_{hc}(t)$ . The initial value of  $M_{hc}$ , when the bus starts to move from depot, is  $M_{hc}(t_{b0}) = 1$ . Figure 3-8 outlines the recommended comfort temperature – lower and upper – curves in the passenger compartment,  $T_{t,l}$  and  $T_{t,u}$ , respectively.  $T_t$  is the regulated temperature in the passenger compartment. Moreover, the heating-, cooling-, and off-region, correspond to the outside temperature  $T_o(t')$ , are represented in Figure 3-8 as well. The upper and lower comfort temperature  $T_{t,u}(t')$  and  $T_{t,l}(t')$ , respectively, are defined using the upper and lower comfort temperature curves  $T_{t,u}$  and  $T_{t,l}$ , respectively, shown in in Figure 3-8 with correspond to the outside temperature  $T_o(t')$  at time  $t'$ .

The outside temperature  $T_o$  is determined using real-world temperature measurements collected on several days throughout the year (see Figure 11-2Annex 11.2).  $T_o$  can be represented as follows:

$$T_o = (T_o(t_1), T_o(t_2), T_o(t_3), \dots, T_o(t_n)), \quad (3.65)$$

$$n = |\tau_{rw}| \wedge t_i \in \tau_{rw}$$

where  $\tau_{rw}$  is a set of the real-world times that is utilised in this simulation model (see Equation 2.11), and  $|\tau_{rw}|$  is the number of elements in  $\tau_{rw}$ .

The passenger heat energy  $Q_p(t')$  in Equation 3.62 is calculated as:

$$Q_p(t') = q_p \cdot (n_p + 1) \quad (3.66)$$

$$q_p = \begin{cases} 100 & , & T_i(t') < 18 \\ \frac{10}{3} \cdot T_i(t') - 80, & 15 \leq T_i(t') < 24 \\ 5 \cdot T_i(t') - 40, & 24 \leq T_i(t') < 35 \\ 25 & , & T_i(t') \geq 35 \end{cases} \quad (3.67)$$

where  $q_p$  denotes the heat gained per passenger (W) based on the interior temperature of the bus cabin [112, 113], and  $n_p := btr_{8,i}$  (see Equation 3.41) denoted the number of passengers – plus one for the bus driver – in the bus cabin.

Heat transfer between the bus cabin and outside ambient temperature can be computed using the thermal resistance and conductance Equations [114, 115]. Thus, the conductive and convective thermal losses energy  $Q_L(t')$  is computed as follows:

$$Q_L(t') = \frac{1}{R_{th,tot}} \cdot (T_i(t') - T_o(t')), t' = t + \delta t \quad (3.68)$$

$$R_{th,tot} = \frac{1}{A_{BS} \cdot h_o} + \frac{L_g}{A_g \cdot k_g} + \frac{L_c}{A_c \cdot k_c} + \frac{1}{A_{BS} \cdot h_i} \quad (3.69)$$

where  $R_{th,tot}$  is the total thermal resistance,  $A_{BS}$ ,  $A_g$ , and  $A_c$  are the total surface area, the window glass area, and the chassis area of the bus in ( $m^2$ ), respectively.  $A_{BS} = (2 \cdot L_b \cdot W_b) + (2 \cdot L_b \cdot H_b) + (2 \cdot H_b \cdot W_b)$  is calculated using bus specification length  $L_b := b_{sp5,i}$ , width  $W_b := b_{sp6,i}$ , and height  $H_b := b_{sp7,i}$  (see Equation 3.43), accordingly, the window glass area is assumed to be third the total surface area  $A_g := \frac{1}{3}A_{BS}$ , and, therefore, the chassis area is  $A_c := \frac{2}{3}A_{BS}$ .  $L_g$ ,  $L_c$ ,  $k_g$ , and  $k_c$  are the glass thickness, the chassis thickness, glass thermal conductivity and chassis thermal conductivity, respectively, and their values are found in  $B_{sp,i}$  (see Equation 3.43 and Table 3-1).

The surface convective heat transfer coefficients  $h_o$  and  $h_i$  depend on the air velocity and thus are computed using the bus speed (from Equation 3.57) as follows [116]:

$$h_x = 0.6 + 6.64 \cdot \sqrt{v(t')}, \quad x \in \{o, i\} \quad (3.70)$$

where  $h_o$  and  $h_i$  are the outside and inside convection coefficients, respectively.

The energy loss due to opening the bus doors  $Q_D$  – during dwell time – can be estimated as follows [113, 117]:

$$Q_D(t') = \psi_{door} \cdot \mathcal{V}_d \cdot \rho_a \cdot C_p \cdot (T_i(t') - T_o(t')) \quad (3.71)$$

$$\psi_{door} = \begin{cases} 1, & v(t') = 0 \wedge btr_{1,i} := \{\text{bus stop}\} \\ 0, & v(t') > 0 \end{cases} \quad (3.72)$$

where  $\mathcal{V}_d$  is the air infiltration flow rate in ( $m^3/s$ ), based on [117],  $\mathcal{V}_d = 0.4 m^3/s$  is assumed in this simulation model, and  $\psi_{door}$  represents the condition of the bus doors. Accordingly, no thermal energy is lost when the bus is moving  $Q_D(t') = 0$  as  $v(t') > 0$ , however,  $\psi_{door} = 1$  when the bus stops at a traffic node  $btr_{1,i}$  (see Equations 3.41 and 3.42) that its type is *bus stop*.

The energy loss due to ventilation  $Q_V$  can be calculated as follows [113, 117]:

$$Q_V(t') = \psi_v(t') \cdot \mathcal{V}_v \cdot \rho_a \cdot C_p \cdot (T_i(t') - T_o(t')) \quad (3.73)$$

$$\psi_v(t') = \begin{cases} 1, & T_i(t) > T_t(t') \wedge M_{hc}(t') = 0 \\ 0, & \begin{cases} T_i(t) < T_{t1}(t') \wedge M_{hc}(t') = 0 \\ M_{hc}(t') = 1 \end{cases} \end{cases} \quad (3.74)$$

According to [117], HVAC air flow rate between  $\mathcal{V}_v = 0.05 m^3/s$  and  $\mathcal{V}_v = 0.3 m^3/s$  is measured depending on the operation mode of the HVAC system  $M_{hc}$ . A value of  $\mathcal{V}_d = 0.2 m^3/s$  is considered for all the ventilation mode in this simulation model.  $\psi_v$  indicates the ventilation system functional condition. Accordingly, the ventilation system is switched *on* ( $\psi_v(t') = 1$ ) when the bus cabin interior temperature  $T_i(t)$  at time  $t$  (see Figure 3-8) is more than the regulated temperature  $T_t(t')$  at time  $t'$  and the heating system is *off* ( $M_{hc}(t') = 0$ ), contrarily, the ventilation system is switched *off* ( $\psi_v(t') = 0$ ) whenever the heating/cooling system is *on* ( $M_{hc}(t') = 1$ ) or  $T_i(t)$  is less than  $T_{t1}(t')$  and ( $M_{hc}(t') = 0$ ). The regulated temperature  $T_t(t')$  is defined using the

regulated temperature  $T_t$  curve shown in in Figure 3-8 with correspond to the outside temperature  $T_o(t')$  at time  $t'$ .

The bus cabin interior temperature  $T_i$  is updated with every time step  $\delta t$  using Equations 3.62 - 3.83, the old  $T_i(t)$  – bus cabin interior temperature from last time step  $t = t' - \delta t$  – is used to find the functional mode of the heating, cooling or ventilation at time  $t'$  (see Equations 3.64 and 3.74). After determining the value of  $M_{hc}(t')$ , the power consumption of the HVAC system is:

$$P_{HC}(t') = \frac{1}{\eta_{hc}} \cdot \frac{|Q_{HVAC}(t')|}{\delta t} \quad (3.75)$$

where  $\eta_{hc} := b_{sp20,i}$  (Equation 3.43) denotes the thermal to electrical energy ratio. The power consumption of the HVAC Ventilator power  $P_V(t')$  is:

$$P_V(t') = \begin{cases} P'_V, & M_{hc}(t') \vee \psi_v(t') = 1 \\ 0, & M_{hc}(t') \wedge \psi_v(t') = 0 \end{cases} \quad (3.76)$$

where  $P'_V := b_{sp19,i}$  (see Equation 3.43) is the HVAC Ventilator power. The HVAC system total power  $P_{HVAC}$  is accordingly calculated as follows:

$$P_{HVAC}(t') = P_{HC}(t') + P_V(t') \quad (3.77)$$

More consumption power is contributed from other basic auxiliary units, besides the HVAC system, such as battery cooling, air compressor, steering pump, and lights [98]. The basic auxiliary power  $P_{baux}$  is computed using the bus specifications parameter  $b_{sp21,i}$  (see Equation 3.43) as below:

$$P_{baux}(t') = b_{sp21,i} \quad (3.78)$$

The TB power  $P'_B(t')$  – included in BM and presented in the next section – is calculated using: traction  $P_{TB}(t')$ , HVAC  $P_{HVAC}(t')$ , and basic auxiliary  $P_{baux}(t')$  power. Therefore, by using Equations 3.50, 3.61, 3.77, and 3.78, these powers can be accumulated as shown in Equation 3.79:

$$P'_B(t') = P_{TB}(t') + P_{HVAC}(t') + P_{baux}(t') \quad (3.79)$$

### Battery System

Most of the batteries used in electric vehicles are composed of lithium titanate (LTO), lithium iron phosphate (LiFePO<sub>4</sub>), and nickel-manganese-cobalt (NMC) cells. The high energy densities, high charge and discharge currents, and appropriate cycle stability of these batteries have shown great value in electro mobility applications [118].

For BTB, a battery system is associated with the BM (see Equation 3.43). Accordingly, the maximum charging ( $P_{bcha} := b_{sp29,i}$ ) and discharging ( $P_{bdis} := b_{sp28,i}$ ) powers are included in the battery model as well as the effective energy ( $E_{sc} := b_{sp30,i}$ ) and the initial state-of-charge SOC, i.e., the battery SOC when a BTB the first time states to move ( $SOC_{ini} := b_{sp31,i}$ ). In the

context of a battery, the term SOC refers to the percentage of its remaining energy to the actual rated energies. It shows how much charge is left in the battery, 100% fully charged and 0% completely drained. Various estimation approaches can be utilised to determine the SOC. In this simulation model, the Coulomb-Counting approach is used to calculate the new SOC. Accordingly, the battery's remaining capacity is estimated by measuring the power flowing in and out of the battery. The batteries new SOC is calculated as in the following Equation [119–121]:

$$SOC(t') = SOC(t) - \eta_c \cdot \frac{1}{E_{sc}} \cdot \int_0^{\delta t} P_{sc}(t) dt, \quad t' = t + \delta t \quad (3.80)$$

where  $SOC(t')$  is the new SOC,  $SOC(t)$  indicates the last SOC,  $\eta_c$  is the coulomb efficiency,  $E_{sc} := b_{sp30,i}$  (see Equation 3.43) is the battery effective capacity, and  $P_{sc}(t)$  is the charging/discharging power at time  $t'$  (positive for discharge and negative for charge).  $P_{sc}(t)$  is calculated as follows:

$$P_{sc}(t) = P'_{bat}(t') = \begin{cases} P'_B(t'), & \begin{cases} P'_B(t') \leq P_{bdis} \\ P'_B(t') \geq -P_{bcha} \end{cases} \\ P_{bdis}, & P'_B(t') > P_{bdis} \\ -P_{bcha}, & \begin{cases} P'_B(t') \leq -P_{bcha} \\ \psi_{bat} = 0 \end{cases} \\ 0, & \begin{cases} SOC(t) = 1 \wedge \psi_{bat} = 0 \\ SOC(t) = 0 \wedge \psi_{bat} = 1 \end{cases} \end{cases} \quad (3.81)$$

$$\psi_{bat} = \begin{cases} 1, & SOC(t) > 0 \wedge P'_B(t') > 0 \wedge btr_{12,i} = \emptyset \\ 0, & \begin{cases} P'_B(t') < 0 \\ SOC(t) < 1 \wedge btr_{12,i} \neq \emptyset \end{cases} \end{cases} \quad (3.82)$$

where  $P_{bat}(t')$  is the battery power,  $P'_B(t')$  is the TB power (see Equation 3.79), ( $P_{bdis} := b_{sp28,i}$ ), and ( $P_{bcha} := b_{sp29,i}$ ) are battery discharging and charging power as in bus specifications, respectively, (see Equation 3.43 and Table 3-1), and  $\psi_{bat}$  is the battery operating mode. As shown in Equation 3.81, the battery power is the same as the TB power  $P'_B(t')$  when the BTB is driving wire-free (no contact with OHCWs) and the TB power is less than the battery discharging power  $P'_B(t') \leq P_{bdis}$  (bus consuming power) or more than the battery charging power  $P'_B(t') \geq -P_{bcha}$  (bus generating power), otherwise, the battery discharges/charge with the maximum battery discharge/charge power.

The battery is in *discharging* mode ( $\psi_{bat} = 1$ ) when the battery  $SOC(t) > 0$  and  $P'_B(t') > 0$  with no available OHCW, where  $btr_{12,i}$  (see Equation 3.41) is the length of the electric traction branch, and in case of unavailability (no OHCW), its value is set to ( $\emptyset$ ). However, the battery is in *charging* mode ( $\psi_{bat} = 0$ ) when  $P'_B(t') < 0$  or when the battery  $SOC(t) < 1$  and the bus is under the OHCW, i.e.,  $btr_{12,i} \neq \emptyset$ .

The coulomb efficiency of the battery  $\eta_c$  is determined by experiments, e.g., lithium-ion battery has discharge efficiency  $\eta_c = 1$  and charging efficiency  $0.98 \leq \eta_c \leq 1$  [122]. When the battery



at time  $t$  is fully charged  $SOC(t) = 1$  and  $P_{sc}(t') < 0$ , then the battery SOC will maintain its level  $SOC(t') = 1$ . Similarly, for completely drained battery  $SOC(t) = 0$  and  $P_{sc}(t') > 0$ , the battery SOC will maintain its level  $SOC(t') = 0$ . Accordingly, Equation 3.80 can be formulated as follows:

$$SOC(t') = \begin{cases} 1 & , SOC(t) = 1 \wedge P_{sc}(t') < 0 \\ 0 & , SOC(t) = 0 \wedge P_{sc}(t') > 0 \\ SOC(t) - \eta_c \cdot \frac{\int_0^{\delta t} P_{sc}(t) dt}{E_{sc}} & , \text{otherwise} \end{cases} \quad (3.83)$$

The bus state set  $B_{state}$  (see Equation 3.42) can be defined as follows:

$$B_{state} = \{b_{s,1}, b_{s,2}, b_{s,3}, \dots b_{s,12}\} \quad (3.84)$$

The elements of set  $B_{state}$  are defined as shown in Table 3-2

**Table 3-2: Bus state.**

Element	Description	Equation
$b_{s,1}$	Bus regime of motion ( $M_B$ )	(3.51)
$b_{s,2}$	Bus Speed ( $v$ )	(3.52)
$b_{s,3}$	Travelled distance between two consecutive traffic nodes ( $d$ )	(3.54)
$b_{s,4}$	Travelled distance between two consecutive bus stops ( $d'$ )	(3.55)
$b_{s,5}$	Travelled distance between two consecutive traction nodes ( $d''$ )	(3.56)
$b_{s,6}$	Bus traction power ( $P_{TB}$ )	(3.50) or (3.61)
$b_{s,7}$	Bus HVAC power ( $P_{HVAC}$ )	(3.77)
$b_{s,8}$	Bus basic auxiliary power ( $P_{baux}$ )	(3.78)
$b_{s,9}$	Battery power ( $P_{bat}$ )	(3.81)
$b_{s,10}$	Battery SOC ( $SOC$ )	(3.83)
$b_{s,11}$	Heating/Cooling control ( $M_{hc}$ )	(3.64)
$b_{s,12}$	Bus cabin interior temperature ( $T_i$ )	(3.62)

### 3.4.3 Stop-to-Stop Movement

The third part provides a further explanation of the bus stop-to-stop movement and its corresponding regimes of motion. With the four possible regimes (acceleration ( $M_B = 1$ ), constant-speed ( $M_B = 2$ ), rolling ( $M_B = 0$ ) and braking ( $M_B = -1$ )), there are four basic cases of stop-to-stop movements (see Figure 3-9) [107].

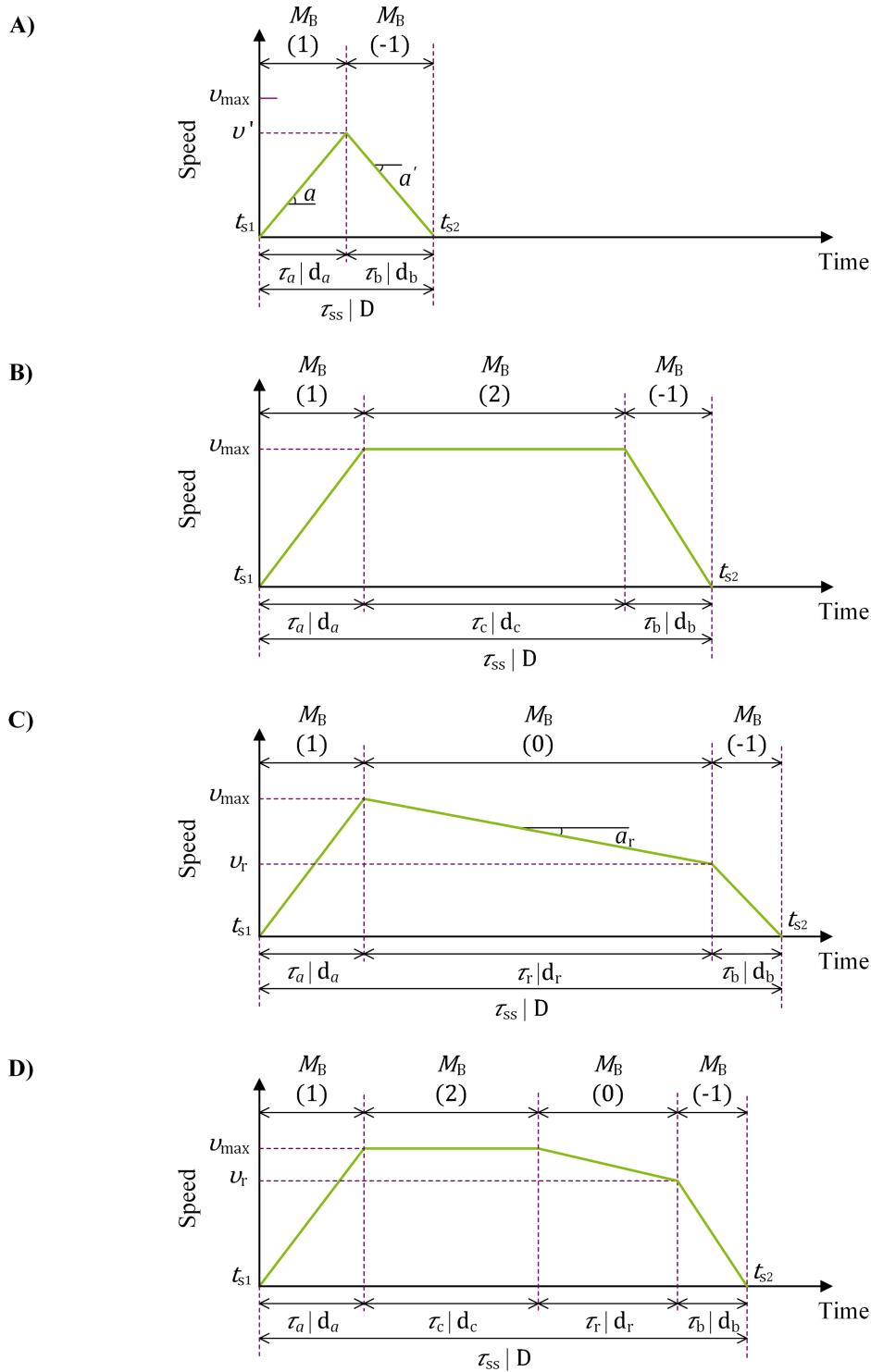


Figure 3-9: Cases of stop-to-stop movement regimes (adopted from [107]).

#### Case A:

In this case the distance between the two stop locations (bus stop or traffic light) is short, in which, the bus speed  $v' = v(t')$  does not reach the maximum permitted speed  $v_{\max}$ , where  $v_{\max}$  defines the maximum speed that is permitted by the road segment (see Equation 3.17) and bus maximum speed indicated in the bus specifications (see Equation 3.43). As shown in Figure 3-9 (A), only

two regimes of motion are expected, where the bus accelerates ( $M_B = 1$ ) until reaching  $v'$ . The bus travels the accelerating distance  $d_a$  over the accelerating time interval  $\tau_a$ . Afterwards it changes to braking regimes ( $M_B = -1$ ) directly and decelerates until settling at the end stop location. Through the braking regimes the bus travels the braking distance  $d_b$  over the braking time interval  $\tau_b$ . The total travel distance (stop-to-stop interstation distance) and total time interval (stop-to-stop travel interval) for case A are  $D = d_a + d_b$  and  $\tau_{ss} = \tau_a + \tau_b$ , respectively.

The x-axes in Figure 3-9 represent the time progress, where  $t_{s1}$  is the time when the bus start to move and  $t_{s2}$  is the time when the bus arrive at the stop location, thus,  $\tau_{ss} = t_{s2} - t_{s1}$ . The intervals remarked under the x-axes represent the time periods and distances that are correspond to each distinct regime of motion ( $M_B$ ).

To check if a bus could reach  $v_{max}$  within an interstation distance between two stops the following Equation is utilized [107].

$$v' = \sqrt{\frac{2 \cdot a \cdot |a'| \cdot D}{a + |a'|}} \quad (3.85)$$

where  $a$  is the acceleration rate,  $a'$  is the deceleration rate, and  $D$  is the distance between two consecutive stops (as calculated in Equation 3.34), i.e.,  $D = \mathbf{B}_{TR,9L}$ . If the calculated  $v'$  is less than  $v_{max}$ , the stop-to-stop interstation is considered as *case A* and braking regime ( $M_B = -1$ ) starts when the bus speed hits  $v'$ , i.e.,  $v(t') = v'$  and  $t' \geq t_{s1} + \tau_a$ . The  $\tau_a$  and  $\tau_b$  are calculated as follows [107]:

$$\tau_a = \frac{v}{a} \quad (3.86)$$

and

$$\tau_b = \frac{v}{|a'|} \quad (3.87)$$

where the bus speed  $v'$  can be substituted for the speed  $v$ .

Case A is utilised in the bus speed profile whenever an interstation distance is rather small. Traffic light with red light adjacent to a bus stop, or the other way around, is an example of this case.

### Case B:

In this case, the bus hits  $v_{max}$  and maintains moving at this speed until braking is required to stop at the coming stop station. As shown in Figure 3-9 (B), only three regimes of motion are utilised to simulate bus movement between the two stops. Acceleration interval  $\tau_a$  and braking interval  $\tau_b$  are determined using Equations 3.86 and 3.87 with  $v_{max}$  substitutes for the speed  $v$ . Yet, acceleration distance  $d_a$  and braking distance  $d_b$  are determined using Equation 3.53. Stop-to-stop travel interval  $\tau_{ss}$  consists in case B of acceleration, constant-speed, and braking intervals, i.e.,  $\tau_a$ ,  $\tau_c$ , and  $\tau_b$ .  $\tau_{ss}$  can be calculated as follows [107]:

$$\tau_{ss} = \frac{D}{v_{\max}} + \frac{v_{\max}}{2} \cdot \left( \frac{1}{a} + \frac{1}{|a'|} \right) \quad (3.88)$$

The constant-speed interval  $\tau_c$  can be determined also as follows:

$$\tau_c = \tau_{ss} - (\tau_a + \tau_b) = \frac{D}{v_{\max}} - \frac{v_{\max}}{2} \cdot \left( \frac{1}{a} + \frac{1}{|a'|} \right) \quad (3.89)$$

Thus, the following equation is used to determine when the braking regime ( $M_B = -1$ ) could be initiated:

$$t' \geq (t_{s1} + \tau_a + \tau_c) \quad (3.90)$$

As a consequence of a delay in bus schedule, case B is commonly implemented in the bus speed profile, where rolling regime ( $M_B = 0$ ) is omitted to avoid the additional delay caused by this regime.

### Case C:

The most efficient driving strategy in terms of energy utilisation is to accelerate ( $M_B = 1$ ) until  $v_{\max}$ , then roll ( $M_B = 0$ ) at the rolling deceleration rate  $a_r$  (see Figure 3-9 (C) and Equation 3.60) until braking ( $M_B = -1$ ) is required. Three regimes of motion are consisted in case C: acceleration, rolling, and braking regimes (see Figure 3-9 (C)). The rolling interval  $\tau_r$  is determined as follows [107]:

$$\tau_r = \frac{v_{\max} - v_r}{|a_r|} \quad (3.91)$$

and

$$v_r = \sqrt{\frac{(2 \cdot a \cdot |a'| \cdot |a_r| \cdot D) - (a' \cdot (a + |a_r|) \cdot v_{\max}^2)}{a \cdot (|a_r| - |a'|)}} \quad (3.92)$$

where  $v_r$  is the bus speed before switching from rolling regime ( $M_B = 0$ ) to braking regime ( $M_B = -1$ ). After determining the acceleration interval  $\tau_a$  as shown in Equation 3.88, the time when the braking regime ( $M_B = -1$ ) must be applied can be calculated as shown below:

$$t' \geq (t_{s1} + \tau_a + \tau_r) \quad (3.93)$$

The rolling regime is measured unlikely when the determined  $v_r$  is too low, in which instance a constant-speed regime must be implemented (see Case D). Equation 3.92 may be used to calculate  $\tau_r$  for a stop-to-stop interstation distance  $D$  only if  $v_r$  is determined to be acceptable. Case C is likely implemented for interstation distances that are relatively longer than interstation distance of case A.

**Case D:**

This case represents the optimal speed profile, where all four regimes of motion are involved (see Figure 3-9 (D)). For a long spacing between stops, case D is selected to determine the regimes of motion and their corresponding time intervals. The constant-speed time interval  $\tau_c$  for case D can be determined as follows [107]:

$$\tau_c = \frac{D}{v_{\max}} - \frac{v_{\max}}{2} \left( \frac{1}{a} + \frac{1}{|a_r|} \right) - \frac{v_r^2}{2 \cdot v_{\max}} \left( \frac{1}{|a'|} - \frac{1}{|a_r|} \right) \quad (3.94)$$

Moreover, the acceleration time interval  $\tau_a$  is determined using Equation 3.86 and the rolling time interval  $\tau_r$  is determined using Equation 3.91. The start of the braking regime is calculated as follows:

$$t' \geq (t_{s1} + \tau_a + \tau_c + \tau_r) \quad (3.95)$$

The  $v_r$  value is unknown in Equations 3.91 and 3.94. A value for  $v_r$  is selected to determine  $\tau_c$  and  $\tau_r$ . It is then checked to see whether a greater or smaller value of  $v_r$  would result in  $\tau_{ss}$  that match with the bus schedule. This process is repeated until an expectable  $\tau_{ss}$  is achieved.

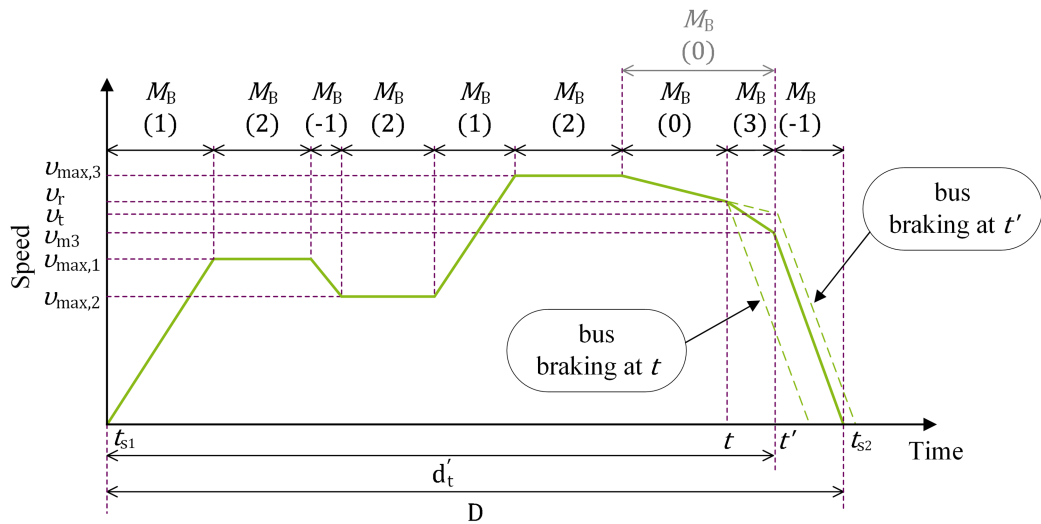


**Figure 3-10: Realistic bus speed profile for a stop-to-stop movement.**

The previously mentioned cases are simple and straightforward. In order to mimic a realistic bus speed profile (see Figure 3-10), it is not possible to use only the equations introduced for case D with an exact sequence of acceleration, constant-speed, rolling, and braking regimes; specifically, to determine the right time to activate braking regime and achieve exact stop location at the end of the stop-to-stop interstation distance  $D$ . As presented in Section 3.3, stop-to-stop can be consisted of several traffic branches. Thus, the permitted maximum speed  $v_{\max}$  is not fixed to a single value, it changes based on the permitted maximum speed of the traffic branches (see Equation 3.17 and Section 4.3.1 for bus motion continuity), leading to several  $v_{\max}$  and random sequence of motion regimes. As shown in Figure 3-10, during a stop-to-stop movement a bus may

encounter three distinct maximum speeds  $v_{\max,1}$ ,  $v_{\max,2}$  and  $v_{\max,3}$ , which correspond to the permitted maximum speed of the traffic branches.

Approaches and equations described for cases A to D can be used to predict the proper order of the motion regimes during a stop-to-stop movement. Acceleration regime ( $M_B = 1$ ) is used whenever there is a possibility to increase the bus speed ( $v(t) < v_{\max,i}$ , where  $i$  represents the sequence of the maximum speeds between a stop-to-stop movement and as shown in Figure 3-10  $i = \{1,2,3\}$ ). The bus retains its speed at  $v_{\max,i}$  and operates in constant-speed regime ( $M_B = 1$ ) as long as  $v_{\max,i}$  does not change, e.g., in Figure 3-10 the bus reduces its speed from  $v_{\max,1}$  to  $v_{\max,2}$  when the permitted maximum speed of the traffic branch is dropped to  $v_{\max,2}$  and subsequently accelerates when the permitted maximum speed changes to  $v_{\max,3}$ . The remained regimes are rolling regime ( $M_B = 0$ ) and braking regime ( $M_B = 0$ ), respectively, which come at the end of the regime cycles. However, intermediate braking regimes are essential once  $v_{\max,i}$  is dropped and the bus is moving at a speed  $v(t)$  above the new  $v_{\max,(i+1)}$ . As it is not possible to determine when exactly a rolling regime may be started (using Equations 3.91 and 3.92), a repetitive check with each time step  $\delta t$  is implemented. The value of an acceptable  $v_r$  is determined by utilising the trip time values (see Equation 3.15). The remaining time interval  $\tau_{rb}$  is determined using the time values in Equation 3.15.  $\tau_{rb}$  is considered to be the time interval for both rolling and braking regimes (see Figure 3-9 (D) – Figure 3-10 complicates concerns since it introduces a new motion regime  $M_B = 3$  which will be discussed in more detail below). Thus,  $\tau_{rb}$  is calculated as follows:

$$\tau_{rb} = \tau_r + \tau_b \quad (3.96)$$

The braking interval can be calculated using Equation 3.87 as follows:

$$\tau_b = \frac{v_r}{|a'|} \quad (3.97)$$

Substituting Equation 3.91 (after replacing  $v_{\max}$  by  $v(t)$ ) and Equation 3.97 into Equation 3.96 and solving for  $v_r$ , one obtains:

$$v_r = \frac{|a'| \cdot |a_r| \cdot \tau_{rb} - |a'| \cdot v(t)}{|a_r| - |a'|} \quad (3.98)$$

The remaining interstation distance is then compared to the distance that the anticipated rolling and braking regimes achieved. Utilising Equation 3.53 to determine the rolling distance  $d_r$  and braking distance  $d_b$ , one obtains:

$$d_r = \frac{1}{2} \cdot |a_r| \cdot \tau_r^2 \quad (3.99)$$

$$d_b = \frac{1}{2} \cdot |a'| \cdot \tau_b^2 \quad (3.100)$$

and

$$(d_r + d_b) \geq (D - d'(t)) \quad (3.101)$$

Switch to rolling regime (for simulation time  $t'$ ) is possible only when the condition of Equation 3.101 is satisfied. Once the rolling regime has been triggered, further checks are no longer necessary. Here it is worth mentioning that checking if a braking regime needs to be activated occurs before checking the rolling regime. In fact, braking regime check occurs before deciding any motion regime will be activated at  $t'$ . Therefore, braking distance  $d_b$  is determined as follows:

$$d_b = \frac{v(t)^2}{2 \cdot |a'|} \quad (3.102)$$

If the value of  $d_b$  satisfies the condition of Equation 3.101 (with  $d_r = 0$ ), then braking regime ( $M_B = -1$ ) for simulation time  $t'$  is activated and no more regime check is required.

Considering the frequent changes between the motion regimes and the uncertainty regarding the start time of the rolling regime, it is possible that a bus dwells before or after the stop destination. As shown in Figure 3-10, the bus stops before the stop destination when changing to braking regime at  $t$  (as represented by the first dotted light green line) and it stops after the stop destination when changing to braking regime at the next time step  $t'$  (as represented by the second dotted light green line and grey marking for the extended braking regime). Thus, a new motion regime  $M_B = 3$ , which occurs before the last braking regime, is implemented. In other words, the dotted light green lines in Figure 3-10 show where the bus could dwell without implementing the new motion regime. In  $M_B = 3$ , a deceleration rate more than  $a'$  is applied, which will enable the bus to move less than it would when applying the normal deceleration rate of the bus  $a'$ .

The decision to utilise this regime ( $M_B = 3$ ) is made as follows: As mentioned before, braking regime check is implemented with each  $\delta t$  and before deciding the motion regime for  $t'$ . This check will be repeated with a second check but after proceeding the bus movement with the previous motion regime (from simulation time  $t$ ). The resulted speed and travelled distance (at simulation time  $t'$  and deceleration rate  $a'$ ) are defined as  $v_t$  and  $d'_t$ , respectively (see Figure 3-10). After utilising  $v_t$  and  $d'_t$  into Equations 3.102 and 3.101, one obtains:

$$d_b = \frac{v_t^2}{2 \cdot |a'|} \quad (3.103)$$

$$d_b > (D - d'_t) \quad (3.104)$$

where  $D$  is the total travel distance (stop-to-stop interstation distance) and  $D = \mathbf{B}_{TR,9l}$  (as calculated in Equation 3.34). The total travel distance  $D$  is represented in Figure 3-10 under the x-axis, narrowed between the starting stop at time  $t_{s1}$  and the destination stop at time  $t_{s2}$ . The travelled distance  $d'_t$  (at simulation time  $t'$  and deceleration rate  $a'$ ) is also shown in Figure 3-10 under the x-axis.

If the condition of Equation 3.104 is satisfied (Equation 3.101 (with  $d_r = 0$ ) is not satisfied), the motion regime ( $M_B = 3$ ) will be activated for  $t'$ . This type of regime may occur before the last braking regime (during a stop-to-stop driving) and lasts for only one time step  $\delta t$ . The deceleration rate  $a_{m3}$  for this regime is calculated using object displacement equation (based on Equation 3.53) as follows:

$$a_{m3} = \frac{2 \cdot d_{m3} - v(t) \cdot \delta t}{\delta t^2} \quad (3.105)$$

where

$$d_{m3} = D - d'(t) - d_b \quad (3.106)$$

$$d_b = \frac{v_{m3}^2}{2 \cdot |a'|} \quad (3.107)$$

$$v_{m3} = \max(\{|a'| \cdot x \mid x \in \mathbb{N}_1 \wedge (|a'| \cdot x) < v_t\}) \quad (3.108)$$

and  $v_{m3}$  is the bus speed at the end of motion regime ( $M_B = 3$ ).

The bus speed  $v(t')$  and displacement  $\delta d(t')$  are calculated as in Equations 3.52 and 3.54, respectively. Where  $a_{m3}$  is substitute for  $a$ .

As summary, the implemented approaches to model the motion regimes of a stop-to-stop bus move can be described as follows. Accelerating and constant-speed regimes are standard and determined based on  $v_{\max,i}$  value. With each time step  $\delta t$  a check for a required braking regime is implemented as well as another braking regime checking is performed after assuming that the bus has moved (for one time step) with its current motion regime. Moreover, a check for an acceptable rolling regime (after passing the braking regime tests) is applied as well. Regime ( $M_B = 3$ ) is utilised only when correcting bus dwelling location (at the destination stop) is required.



## 4 Modelling the AC/DC-Network

To simulate a trolleybus system, the traffic network model (TNM) and bus model (BM) (see Chapter 3) must work with a suitable electric network model (ENM). To this end, this section describes the modelling of the *electric network*. Following that, modelling the *power profiles* of the traction network sources and loads are presented. Figure 4-1 represents the block diagram of ENM and indeed the relationships between its elements. The process as the determination of the admittance matrix, conductance matrix, traction substation power and voltage, and the electric network steady-state are presented in Chapter 5.

The ENM is divided into two segments. The first segment is the DC network, which consists of the trolleybus traction network. The term *traction network* will be used to denote the DC segment of ENM. The *AC network*, which powers the traction network, is the second segment of ENM. Since the trolleybus system can be operated at  $U_n = 600 \text{ V}$  or  $U_n = 750 \text{ V}$  (see Section 2.3), the traction network is classified as a low voltage direct current (LVDC) network. Hence, the AC network operates at a higher voltage level and is classified as a medium voltage (MV) network ( $1 \text{ kV} < U_{n,MV} < 52 \text{ kV}$ ) according to IEC 60071 [123, 124].

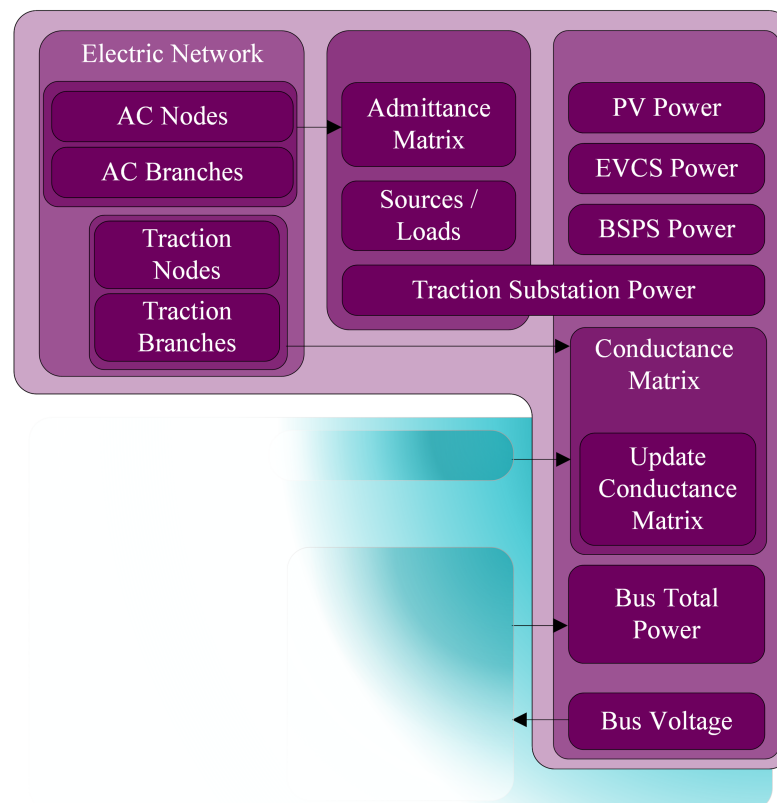


**Figure 4-1:** Trolleybus electric network model scheme which is part of the TBSSM scheme. The faded turquoise part represents the TB/BTB model and the arrows between the overlapped models show the direction of data exchanges.

The admittance matrix, sources, and loads of the AC network are determined using the AC nodes and AC branches models (see Section 4.2). However, the conductance matrix of the traction network is determined using the traction nodes and traction branches (see Section 5.2.2). A new conductance matrix will be created with each simulation time step  $\delta t$  (see Section 5.2.2), considering the bus's changing locations in the road network and therefore in the traction network (see Section 5.1).

Figure 4-1 also shows that the ENM has the photovoltaic (PV) system, the electric vehicle charging station (EVCS), and the battery storage power station (BSPS) models. These are the new innovative features which are intended to be integrated into the conventional trolleybus system (see Sections 1.1 and 2.4). The link between the AC network and the traction network is via the traction substations, whose model is presented in Section 4.1.4. The total power of the operational buses as their corresponding locations are determined (see Section 4.3.1) using the bus model presented in Section 3.4 and subsequently reformatted (see Section 5.1) to be used in the traction network steady-state calculation (see Chapter 5).

## 4.1 Modelling the Traction network

As shown in Figure 4-1, the traction network, which is part of the electric network block model, consist of two block models, i.e., the traction nodes and the traction branches. Later (see Section 5.2.2), the conductance matrix of the traction network is computed using these two models.

### 4.1.1 Traction network Topology

The overhead contact wires (OHCWs) are distributed over the road network, with the exception of some areas where no OHCWs are available to provide the required traction power, compelling the bus to use an auxiliary power source – auxiliary combustion engine or on-board battery – to power the electric motor, allowing it to travel autonomously. The *traction network* symbolises the trolleybus system's OHCWs, feeder cables, power sources, and loads as the equipment used to connect the various sections of the system together (see Figure 2-3). In comparison to traffic nodes, traction nodes have a much lower node count (see Section 6.1.1). When modelling the traction network, the primary consideration is to limit the number of nodes in the traction node model as much as possible. This is accomplished by modelling the traction network separately rather than a compact model that includes traffic and traction nodes in one model. Consequently, the conductance matrix (see Section 5.2.2) will be compact, which reduces the computational efforts. The traction network is modelled as a directional graph  $G = (V, E)$ . Wherein, the nodes  $i \in V$  represent the traction nodes of the traction network, so the edges (branches)  $(i, j) \in E$  indicate that two nodes  $i$  and  $j$  are connected by branch  $(i, j)$  forming the traction branches, with  $(i, j) \neq (j, i)$ . The traction network has  $n_{et}$  traction nodes and  $m_{et}$  traction branches “pairs of traction nodes” [125].

### 4.1.2 Traction nodes

The traction nodes represent incident points in the traction network. Source and load connections, disconnectors, change in line characteristics, junctions, and terminals are considered as traction nodes. Even though trolleybuses (TBs) and battery-trolleybuses (BTBs) can be symbolised as loads (see Section 4.3.1 4.1.6), they are not represented as traction nodes in the basic traction network – due to their dynamic nature – and are added to the basic traction network after their locations are calculated as described in sections 4.3.1 and 5.1. Thus, the basic traction network topology can be represented as shown in Figure 4-2 (A), in which the traction branches are considered as two lines (for the positive and negative wires) and the traction nodes outline the incident points in the traction network (see Figure 4-2 (B)). Like traffic nodes, each traction node has its individual attributes. The traction node attributes consist of information regarding their position and type. The node position helps to track the traction nodes based on the zone or feeding section consisting of them; further, geographic coordinates project their locations into the real-world and vice versa.

The attributes set of the traction nodes  $TEN_a$  is defined as shown in Equation 4.1:

$$TEN_{a,i} = \{TEN_{a1,i}, TEN_{a2,i}, TEN_{a3,i}, \dots, TEN_{ak,i}\} \quad (4.1)$$

where  $k$  indicates the number of attributes consisted with the traction node,  $i$  is the traffic nodes index and  $i \in I$ . The indexing set  $I$  is recognized as  $I = \{i \in \mathbb{N}_1 | i \leq n_{et}\}$ .

Each element of  $TEN_{a,i}$  represents a traction node attribute, the set elements are defined as follows:

#### Node-Id

For each traction node, a unique number is assigned. The node-Id set can be denoting as  $TEN_{a1} = \{ten_{a1} | \mathbb{N}_1\}$  with  $|TEN_{a1}| = n_{et}$ . Let  $ten_{a1,i} \in TEN_{a1,i}$  ( $i \in I$ ) and  $ten_{a1,j} \in TEN_{a1,j}$  ( $j \in I$ ), if  $i \neq j$  and  $TEN_{a1} = \bigcup_i^{n_{et}} TEN_{a1,i}$ . then  $TEN_{a1,i} \cap TEN_{a1,j} = \emptyset$ .

#### Node Type

Each traction node has unique characteristics. Essentially, traction nodes can be classified as either active or passive. The *active* traction nodes indicate points in the traction network where power exchanges occur, i.e., power is provided from the active traction nodes into the traction network and vice versa. Traction substations, PVs, EVCSs, and BSPSs are all examples of active nodes. Afterwards, TBs and BTBs are incorporated in the basic traction network (see Sections 4.3.1 and 5.1), in which they are also considered as active nodes.

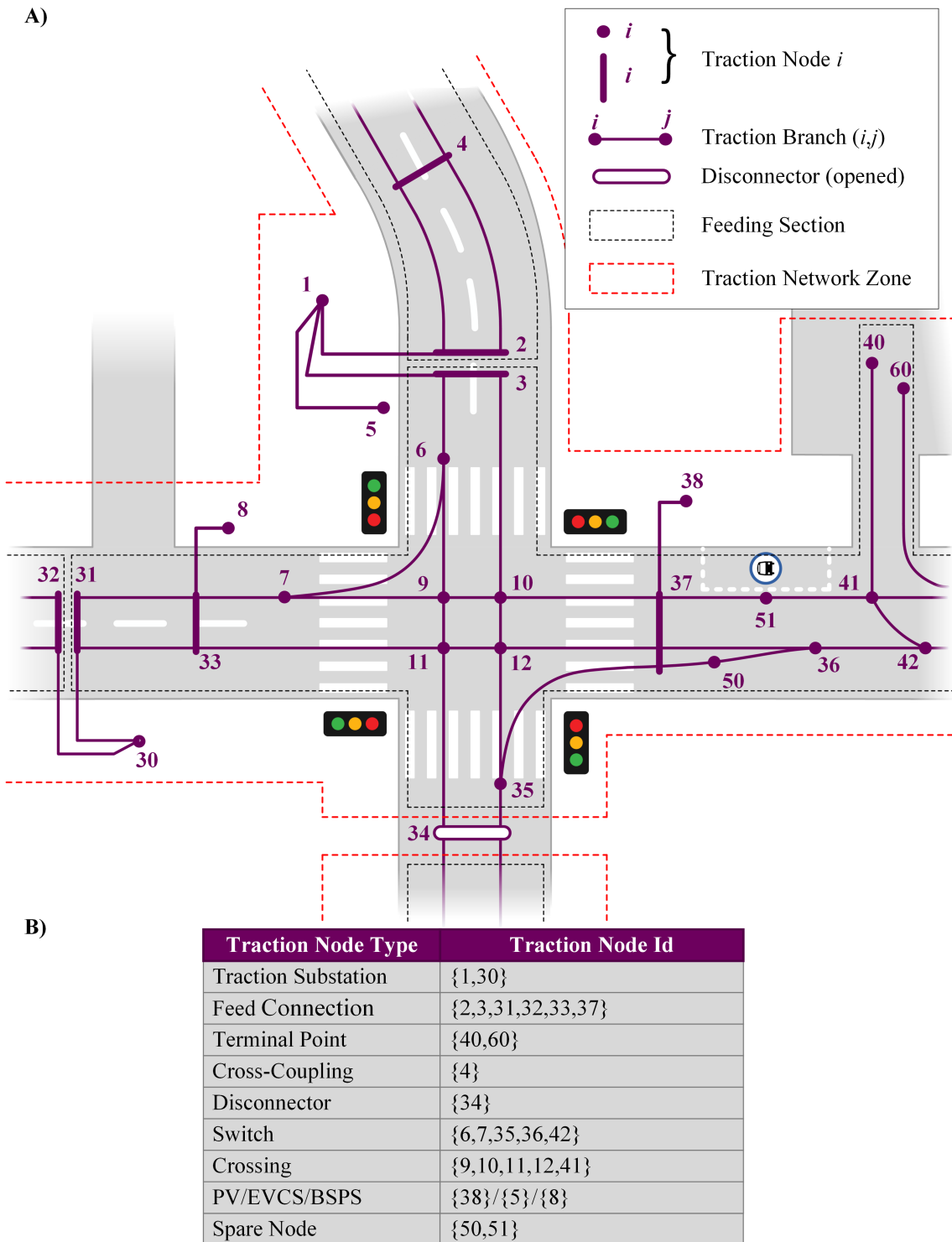


**Figure 4-2: Trolleybus traction network structure.**

**A: Basic traction network topology.**

**B: Traction node types.**

The *passive* traction nodes are points with no power exchanges; nevertheless, these nodes are essential to model the traction network topology. Any other points with no power exchanges are considered as passive nodes. In this simulation model the following traction node types are considered for the traction network: traction substation, PV, EVCS, BSPS, feed connection, cross-coupling, switch, crossing, disconnector, and spare node (see Figure 4-2 (B)). Technically, the

type *spare node* does not represent a physical element in the traction network. Indeed, providing spare nodes at some points in the traction network helps to eliminate redundant notation for traction branches. Moreover, traffic node locations, such as bus stops, that are essential to be included in the traction network, could also be represented as spare nodes (see Figure 4-2).

If each traction node type is represented with a unique number and  $n_{\text{type,et}}$  is the number of all traction node types, then a type description set  $TEN_{\text{type}}$  can be defined as follows:

$$TEN_{\text{type}} = \{(ten_D, ten_T)_i | 1 \leq i \leq n_{\text{type,et}}\} \quad (4.2)$$

Each element in  $TEN_{\text{type}}$  is a pair consist of an identification number  $ten_D$  and a corresponding name for the traction node type  $ten_T$ . The traction node type set can be defined as  $TEN_{\text{type,D}} = \{ten_D \in \mathbb{N}_1 | 1 \leq ten_D \leq n_{\text{type,et}}\}$ ; Accordingly, the node type attribute set for the traction nodes is modelled as  $TEN_{a2} = \{TEN_{a2,1}, TEN_{a2,2}, TEN_{a2,3}, \dots, TEN_{a2,n}\}$ , where  $n = n_{\text{et}}$  and  $\forall i: TEN_{a2,i} \subset TEN_{\text{type,D}}$ .

### Zone

Based on the disconnector state – closed or opened – the traction network could be divided into several zones. As shown in Figure 4-2 (A), two zones (encircled by the red dash line) are given for the shown traction network since disconnector {34} is opened. A number of traction nodes are associated with each zone (see Section 5.2.2). The zone attribute set can be defined as  $TEN_{a3} = \{TEN_{a3,1}, TEN_{a3,2}, TEN_{a3,3}, \dots, TEN_{a3,n}\}$ , where  $n = n_{\text{et}}$ ,  $i \in \{1,2,3, \dots, n_{\text{et}}\}$  and  $\forall i: (0 \leq TEN_{a3,i} \leq n_z)$ . The number of zones  $n_z$  is computed based on the disconnector settings. Zone attributes of traction nodes with opened disconnectors are defined as  $TEN_{a3,i} = 0$ , since they are not represented in either of the zones where they are located in between.

The number of traction nodes correspond to a zone is denoted as  $n_{\text{et,z}}$ , where  $z \in \{1, \dots, n_z\}$ . If there are any opened disconnector in the traction network, i.e.,  $\exists i: (TEN_{a3,i} = 0)$ , the sum of the zone nodes  $n_{\text{et,z}}$  is less than the total traction nodes number  $n_{\text{et}}$ , i.e.,  $\sum_{z=1}^{n_z} n_{\text{et,z}} < n_{\text{et}}$ .

### Section

As shown in Figure 4-2, a feeding section represents the traction network parts that are located between section separators or between a section separator and a line end. Section separators exist whenever two feed connections exist (see Figure 2-4). In Figure 4-2 (A) the section separators are the space between the close-up feed connections, i.e., {2} and {3} as well as {31} and {32}. Four sections (encircled by the black dash line) are given in Figure 4-2 (A). It is noteworthy that an opened disconnector divides the section. The section attributes of the traction nodes are defined as  $TEN_{a4} = \{TEN_{a4,1}, TEN_{a4,2}, TEN_{a4,3}, \dots, TEN_{a4,n}\}$ , where  $n = n_{\text{et}}$ . If  $S_n$  is the number of sections in the traction network, and  $i = \{1,2,3, \dots, n_{\text{et}}\}$ , then  $\forall i: (0 \leq TEN_{a4,i} \leq S_n)$ .

Traction substations can be connected to several sections (see Figure 4-2), making them share all the sections to which they are connected. Thus, section attributes for traction nodes of type

traction substations will be identified with zero, i.e., when  $TEN_{a2,i} = \{\text{traction station}\}$ , then  $TEN_{a4,i} = 0$ .

### X-Coordinate

The x-coordinate is a geographic reference that defines the longitude – in decimal degrees – of a traction node. The x-coordinate is measured in decimal degrees. The x-coordinate attribute is defined as  $TEN_{a5} = \{x|x \in \mathbb{R}\}$ , where the set cardinality is  $|TEN_{a5}| = n_{et}$ .

### Y-Coordinate

The y-coordinate is a geographic reference that defines the latitude – in decimal degrees – of a traction node. The y-coordinate is measured in decimal degrees. The y-coordinate attribute is defined as  $TEN_{a6} = \{y|y \in \mathbb{R}\}$ , where the set cardinality is  $|TEN_{a6}| = n_{et}$ .

### 4.1.3 Traction branches

Each pair of traction nodes forms an edge denoted as traction branch. The traction network model considers the traction branches to be directional, although electric edges are known to be bidirectional. A directional traction branch implies that swapping the Id of the terminal traction nodes (from- and to-node) will refer to a different traction branch. As shown in Figure 4-2, traction branch (33,31) is not the same as traction branch (31,33), i.e.,  $teb_{33,31} \neq teb_{31,33}$ . Each traction branch is associated with several attributes.

$TEB_{a,i}$  is the attributes set of traction branch  $i$  which can be defined as follows:

$$TEB_{a,i} = \{TEB_{a1,i}, TEB_{a2,i}, TEB_{a3,i}, \dots, TEB_{ak,i}\} \quad (4.3)$$

where  $k$  indicates the number of attributes consisted with the traction branch,  $i$  is the traffic nodes index and  $i \in I$ . The indexing set  $I$  is recognized as  $I = \{i \in \mathbb{N}_1 | i \leq m_{et}\}$ .

Each element of  $TEB_{a,i}$  represents an attribute associated with traction branch  $i$ , the elements of  $TEB_{a,i}$  are defined as follows:

#### From-Node

A traction branch represents a segment of the traction network, and it is denoted by two traction nodes. The first traction node is represented by the from-node. If  $TEN_{a1}$  is the set of traction node Ids, then  $TEB_{a1} = \{TEB_{a1,1}, TEB_{a1,2}, TEB_{a1,3}, \dots, TEB_{a1,m}\}$  is the traction branch from-node set with  $m = m_{et}$ . If  $i = \{1, 2, \dots, m_{et}\}$ , then  $\forall i: TEB_{a1,i} \subset TEN_{a1}$ .

#### To-Node

The second traction node that denotes the traction branch is the to-node. If  $TEN_{a1}$  is the set of traction node Ids, then the traction branch to-node set is  $TEB_{a2} = \{TEB_{a2,1}, TEB_{a2,2}, TEB_{a2,3}, \dots, TEB_{a2,m}\}$ , where  $m = m_{et}$ . If  $i = \{1, 2, \dots, m_{et}\}$ , then  $\forall i: TEB_{a2,i} \subset TEN_{a1}$ .

### Length

This attribute represents the distance between the traction branch ends (from- and to-node) which are distributed over the path of the traffic roads. The traction branch length is calculated based on the segment shapes, e.g., as in Figure 4-2 traction branch (01,05), (06,07), (04,02), and (41,42). The length attribute is measured in meters (m) and defined as  $TEB_{a3} = \{TEB_{a3,1}, TEB_{a3,2}, TEB_{a3,3}, \dots, TEB_{a3,m}\}$ , where  $m = m_{et}$  and  $\forall i: TEB_{a3,i} \in \mathbb{R}_{>0}$  with  $i = \{1, 2, \dots, m_{et}\}$ .

### Resistance

The electrical resistance per unit length  $R'$  of the overhead contact wires and the feeder cables are defined in this attribute. The resistance of the traction branch is identified based on the overhead contact wire or the feeder cable conductor type. Measured in ( $\Omega/\text{km}$ ), the set of the traction branch resistances per unit length  $R'$  is defined as  $TEB_{a4} = \{TEB_{a4,1}, TEB_{a4,2}, TEB_{a4,3}, \dots, TEB_{a4,m}\}$ , where  $m = m_{et}$  and  $\forall i: TEB_{a4,i} \in \mathbb{R}_{>0}$  with  $i = \{1, 2, \dots, m_{et}\}$ .

### Ampacity

This feature represents the maximum continuous current, measured in amperes (A), that an overhead contact wire or a feeder cable can carry under normal operating conditions without exceeding its temperature rating. The ampacity values of the overhead contact wires and the feeder cables are assigned to their corresponding traction branches. The attribute set of the traction branch ampacities is defined as  $TEB_{a5} = \{TEB_{a5,1}, TEB_{a5,2}, TEB_{a5,3}, \dots, TEB_{a5,m}\}$ , where  $m = m_{et}$  and  $\forall i: TEB_{a5,i} \in \mathbb{N}_1$  with  $i = \{1, 2, \dots, m_{et}\}$ .

### Zone

As previously mentioned in the zones attribute of the traction nodes, the traction network is divided into zones based on the disconnector state, i.e., closed or opened. The zone of a traction branch is established depending on the zone of its from- and to-node. The zone attribute of the traction branches is defined as  $TEB_{a6} = \{TEB_{a6,1}, TEB_{a6,2}, TEB_{a6,3}, \dots, TEB_{a6,m}\}$ , where  $m = m_{et}$ .

If  $i = \{1, 2, \dots, m_{et}\}$ , then  $TEB_{a1,i}$  and  $TEB_{a2,i}$  are the from- and to-node of traction branch  $i$ , respectively. Based on Equation 4.1, let  $TEN_{z,1}$  and  $TEN_{z,2}$  represents the zones of  $TEB_{a1,i}$  and  $TEB_{a2,i}$ , respectively, where  $TEN_{z,1} \wedge TEN_{z,2} \in TEN_{a3}$ , then  $\exists i: TEB_{a6,i} = TEN_{z,1} \Leftrightarrow TEN_{z,1} = TEN_{z,2}$ , otherwise,  $\exists i: TEB_{a6,i} = 0$ .

If  $n_z$  is the number of zones in the traction network, then the number of traction branches correspond to a zone is denoted as  $m_{et,z}$ , where  $z \in \{1, \dots, n_z\}$ .

### Section

Traction network can be divided into several sections depending on the number of traction substations and the associated section separators as well as disconnector state. Thus, several

groups of traction branches are identified with a specific section number. The section attribute set of the traction branches is defined as  $TEB_{a7} = \{TEB_{a7,1}, TEB_{a7,2}, TEB_{a7,3}, \dots, TEB_{a7,m}\}$ , where  $m = m_{et}$ .

If  $i = \{1, 2, \dots, m_{et}\}$ , then  $TEB_{a1,i}$  and  $TEB_{a2,i}$  are the from- and to-node of traction branch  $i$ , respectively. Based on Equation 4.1, let  $TEN_{s,1}$  and  $TEN_{s,2}$  represent the sections of  $TEB_{a1,i}$  and  $TEB_{a2,i}$ , respectively, where  $TEN_{z,1} \wedge TEN_{z,2} \in TEN_{a3}$ , then  $\forall i: TEB_{a7,i} = \{TEN_{s,1} \cup TEN_{s,2}\} \setminus \{0\}$ .

#### 4.1.4 Traction Substation

The traction substations are the primary energy sources of the traction network (see Figure 2-4 and Figure 2-5). They are divided into two essential parts: the *traction transformer*, which steps down the voltage level from medium voltage to low voltage, and the *traction power rectifier*, which converts the down stepped AC voltage into DC. The conventional traction substation is known to be unidirectional. Therefore, the traction network is a *passive network* with just one direction of power flow, namely from the MVAC network to the LVDC network.

Trolleybus systems might benefit from a promising concept: bidirectional traction substation with active front-end converter [87, 88], which will allow any surplus power produced by other energy sources (see Section 4.1.5) to be transferred into the upper stream AC network (MVAC). The traction substation model  $TPS_i$  can be defined as follows:

$$TPS_i = \{tps_{1,i}, tps_{2,i}, tps_{3,i}, \dots, tps_{5,i}\}, \quad i = \{1, 2, 3, \dots, n_{tps}\} \quad (4.4)$$

where  $i$  is the index of the traction substation,  $n_{tps}$  is the total number of traction substation, and  $tps_{1,i}$  to  $tps_{5,i}$  are the traction node Id ( $tps_{1,i} \in TEN_{a1}$ ), AC node Id ( $tps_{2,i} \in EN_{a1}$ ) – will be defined in Section 4.2, rectifier type (unidirectional = 0 or bidirectional = 1), count of the connected traction transformers, and capacity (in kVA) of traction substation  $i$ , respectively.

As illustrated in the electric network block diagram (see Figure 4-1), both the traction network and AC network models share the existences of traction substations in their model; consequently, two node Ids are assigned to each traction substation depending on the numbering scheme employed by each model. It is essential to know both node Ids of the traction substation in order to execute the DC-AC power flow (see Section 5.3). As each network – traction network an AC network – are modelled to be calculated with a separate power flow method (see Sections 5.2.3 and 5.3.1) and in order to simplify the connection between the AC network and the traction network, in this work, the total internal resistance of the traction substation is neglected.



#### 4.1.5 Other Energy Sources

Traction substations are the primary energy suppliers of the traction network. Yet, TBs and BTBs in braking mode are considered energy sources too, since the regenerative power can be used by the same bus to supply its auxiliary units and the surplus power could be used by nearby buses if the voltage limit  $U_{\max 1}$  is not exceeded. Furthermore, additional components which are intended to be included in the traction network, e.g., PVs and BSPSs, can be considered as additional energy sources (see Sections 4.3.2 and 4.3.4). As the TBs, BTBs, and BSPSs function both as energy sources and loads. By discharging its power, BSPS work as an energy source that intended to support the traction network by suppressing the traction network voltage from falling below the low voltage level.

#### 4.1.6 Loads

The basic loads in the traction network are TBs and the BTBs – in *braking mode* they supposedly act as energy sources (see Section 4.3.1). In case electric vehicle charging stations EVCSs are included in the traction network they are considered as loads as well (see Section 4.3.3). The last possible load could be represented by the presence of BSPSs in the traction network. Each of the pre-mentioned loads has its unique characteristic and behaviour. For instance, TBs and BTBs frequently change their location within the traction network while concurrently loading the traction network precisely when switching between acceleration and braking regimes; likewise, charging the on-board battery of BTBs may increase the load on the traction network and result in a significant voltage drop or overload. Thus, the anticipation of TB and BTB loadings on the traction network is a crucial process requiring extensive temporal and spatial information; moreover, the randomness of bus driver behaviours, passengers boarding and alighting, and traffic jams increase the errors when forecasting buses movement and power consumption over an extended timeframe. [85] deals with the anticipated forecast errors by projecting bus locations in real world into the simulation and predicts their movement and power consumption in a *short timeframe*. Once the simulation of the bus movements is completed, a new forecast is initiated after capturing the actual locations of the buses from the real world and simulating their movements again. A *forecast stock* is established as a result of this approach, which will prevent any accumulative errors from developing.

EVCS has more predictable load behaviour when compared to TB and BTB. During the time when an EVCS is utilized, its position in the traction network as well as the power it provides for the plugged-in electric vehicles are fixed. The charging power may shift somewhat over time, depending on the electric vehicle type and charge duration, although not as much as in the TB and BTB.

The last type of load in the traction network is the BSPS. As mentioned in the last section, BSPS can be considered as energy source when discharging. Nevertheless, when the batteries of the BSPS are being charged the BSPS is represented as a load. Unlike the other mentioned loads,

BSPS is a light-load as it charges when there is a light-load or no-load in the section where it is connected. Similarly, BSPS charges when the buses regenerate power or a PV system is feeding into the BSPS traction network section.

## 4.2 Modelling the AC-Network

The second segment of the electric network is the *AC network*, which supplies the traction network with power. The AC network is considered to operate at a medium voltage (MV) level. Figure 4-1 shows the block diagram model of the AC network; accordingly, the AC network is modelled based on its topology, represented by the AC nodes and AC branches, and the power profiles of the sources and loads at the MV level. The traction substations represent the connection points between the AC- and traction network. As shown in Figure 4-3, the traction network can be supplied by several traction substations which are distributed over different MV feeders.

The modelling of the AC network is based on the simulation model that was developed and used by [126, 127]. A solid data base of feeders' components, supplies, and demands are required to model a realistic AC network. In addition to data on all AC network feeders (see Figure 4-3), substantial data on all local AC network terminals such as linked low-voltage networks and their customers' data, spot loads, distributed generation, and photovoltaic systems are necessary for the initial stage of the AC network modelling. Switching and circuit breaker state are also included. The AC network model is determined in two parts after combining and processing all AC network information. More details on the input data and the process of the modelling of a medium voltage network can be found in [126, 127].

The first part of the AC network model consists of the static network parameters which represents the network topology in the form of *AC nodes* and *AC branches*. Equations 4.5 and 4.6 define the attribute sets of the AC nodes ( $EN_{a,i}$ ) and AC branches ( $EB_{a,j}$ ), respectively.

$$EN_{a,i} = \{EN_{a1,i}, EN_{a2,i}, EN_{a3,i}\}, \quad i = \{1,2,3, \dots, n_{en}\} \quad (4.5)$$

where  $i$  is the index of an AC node,  $n_{en}$  the total number of AC nodes, and  $EN_{a1,i}$  to  $EN_{a3,i}$  are the node Id, node type, and zone attribute, respectively. And

$$EB_{a,j} = \{EB_{a1,j}, EB_{a2,j}, \dots, EB_{a9,j}\}, \quad j = \{1,2,3, \dots, m_{eb}\} \quad (4.6)$$

where  $j$  is the index of an AC branch,  $n_{eb}$  the total number of AC branches, and  $EB_{a1,j}$  to  $EB_{a9,j}$  are the from-node ( $EB_{a1,j} \in EN_{a1}$ ), to-node ( $EB_{a2,j} \in EN_{a1}$ ), length, resistance, reactance, conductance capacitance, ampacity, and zone attribute, respectively

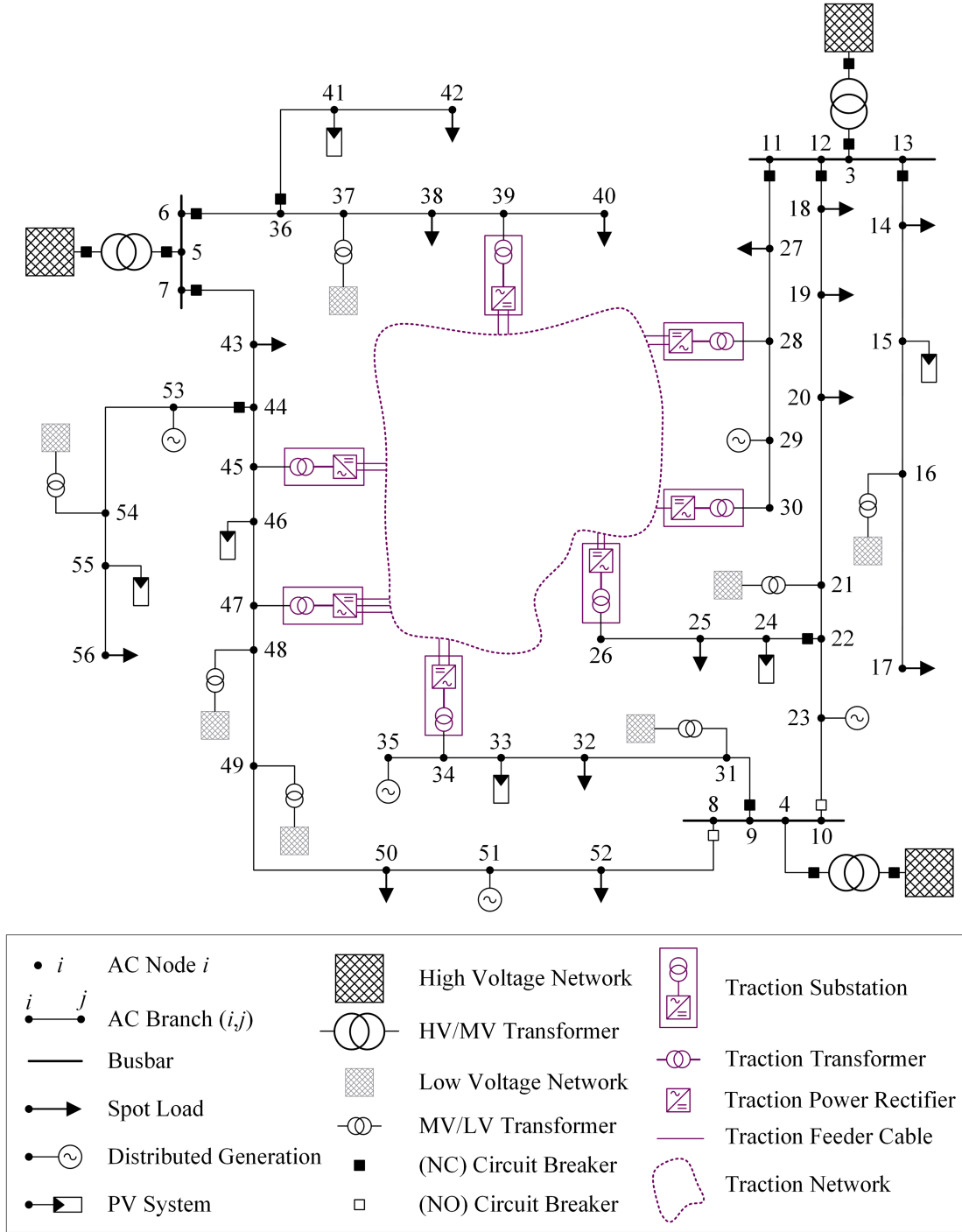


Figure 4-3: Medium voltage AC network structure.

The second part represents the dynamic parameters of the AC network. In this stage, it is necessary to provide the production and consumption power to model the AC network accurately. The attribute set of the AC network terminals  $EF_{a,k}$  is defined as follows:

$$EF_{a,k} = \{EF_{a1,k}, EF_{a2,k}, EF_{a3,k}, EF_{a4,k}\}, \quad k = \{1, 2, 3, \dots, n_{ef}\} \quad (4.7)$$

where  $k$  is the index of an AC network terminal,  $n_{ef}$  the total number of terminals, and  $EF_{a1,k}$  to  $EF_{a4,k}$  are the AC node Id ( $EF_{a1,k} \in EN_{a1}$ ), terminal type (HV/MV transformer, distributed

generation, PV system, spot load, MV/LV transformer, or traction substation), rated power, and utilization attribute, respectively.

Based on Equation 4.7, power profiles are developed for distributed generations and photovoltaic systems. Furthermore, consumer power profiles are developed for spot loads connected at the MV level and distributed loads linked in the low-voltage network. Realistic power profiles are simulated for every active AC node (terminal) in the AC network model, except the traction substation where the power is determined from the traction network (see Sections 5.2 and 5.3). The set of power profiles  $P_{ac}$  of the active AC nodes are defined as:

$$P_{ac,r} = \left( p_{ac,r}(t_1), p_{ac,r}(t_2), p_{ac,r}(t_3), \dots, p_{ac,r}(t_n) \right), n = n_{ss} \quad (4.8)$$

with

$$r = \{r_1, r_2, r_3, \dots, r_n\}, n = n_a \quad (4.9)$$

where the simulation is set to start at  $t_1$  and end at  $t_n$  with a time step  $\delta t$ . The index  $r$  is represented by the active AC node Ids, i.e.,  $r \subset EF_{a1}$ . The total number of active AC nodes is identified as  $n_a$ .

### 4.3 Modelling the Traction Sources and Loads Power Profiles

#### 4.3.1 Trolleybus and Battery-Trolleybus

The TB and BTB total consumption powers and locations are calculated respectively with each time step  $\delta t$  using the bus model (BM) and the bus daily travelling routes model (BDTRM) defined in Equation 3.42 and 3.11, respectively. With each time step  $\delta t$  buses move using the information in the daily travelling route (see Equation 3.11), and the concepts described in Section 3.4.2. The actual travelling route segment (see Equation 3.41) is denoted in  $BM_k$  as  $B_{trs,j}$  (see Equation 3.42).  $B_{trs,j}$  describes the traffic branch in which the location of bus  $k$  in the road network at time  $t$  is identified. To calculate the movement and power consumption of bus  $k$ , the specification model  $B_{sp,i}$  (see Equations 3.42 and 3.43) of bus  $k$  and the actual travelling route segment  $B_{trs,j}$  are required. The static data of bus  $k$  are defined by  $B_{sp,i}$ , while the dynamic data of the road network and bus  $k$  are defined by  $B_{trs,j}$ , e.g., road slope angle  $\theta = btr_{4,j}$ , road speed limit  $btr_{5,j}$ , and passenger crowding  $n_p = btr_{8,j}$ . Moreover, the actual travelling route segment  $B_{trs,j}$  contains information about the actual travelling route segment length  $btr_{2,j}$  (traffic branch length), stopping distance  $btr_{9,j}$ , dwelling time  $btr_{7,j}$ , traction branch (from-node and to-node)  $btr_{10,j}$  and  $btr_{11,j}$ , respectively, and traction branch length  $btr_{12,j}$ .

At the beginning of the simulation ( $t = t_{ss}$ ), the actual travelling route segment  $B_{trs,j}$  is corresponded to the second column of daily travelling route matrix  $\mathbf{B}_{TR}$ , i.e.,  $j = 2$ . When the simulation time  $t'$ , where  $t' = t + \delta t$ , reaches the departure time of bus  $k$ , i.e.,  $t' \geq btr_{3,j}$ , the motion regime  $M_B$  (see Equation 3.51) will be changed to acceleration regime ( $M_B = 1$ ). The

motion regime value is saved in bus state set  $B_{\text{state}}$  (see Equation 3.84), where  $b_{s,1} = M_B$ . The total mass  $M$  of bus  $k$  is calculated as follows:

$$M = m_{\min} + ((n_p + 1) \cdot aw_p) \quad (4.10)$$

where  $m_{\min} := b_{\text{sp}2,i}$  is the mass of bus  $k$  without passengers,  $(n_p + 1)$  is the number of passengers – plus one for the bus driver – in bus  $k$ , and  $aw_p$  is the average passenger weight. A weight between 65 kg and 75 kg is advised to be considered as the average passenger weight [128] or it is possible to use the bus specifications model  $B_{\text{sp},i}$  to calculate the average passenger weight by dividing the subtraction of the bus minimum mass  $m_{\min} := b_{\text{sp}2,i}$  from the bus maximum mass  $m_{\max} := b_{\text{sp}3,i}$  by bus maximum passenger capacity  $pn_{\max} := b_{\text{sp}9,i}$  (as specified by the manufacturer) plus the driver, as follows:

$$aw_p = \frac{(b_{\text{sp}3,i} - b_{\text{sp}2,i})}{(b_{\text{sp}9,i} + 1)} \quad (4.11)$$

After calculating the new speed  $v(t')$  and the change in distance  $\delta d(t')$  for bus  $k$ , its electrical traction power  $P_{\text{TB}}(t')$  is calculated (see Section 3.4.2). The auxiliary powers ( $P_{\text{HVAC}}(t')$  and  $P_{\text{baux}}(t')$ ) for bus  $k$ , i.e., HVAC, and the basic auxiliary power, are calculated as shown in Equations 3.62-3.78. If bus  $k$  variety is battery-trolleybus ( $b_{\text{sp}1,i} = \text{True}$ ), then bus  $k$  battery power  $P_{\text{bat}}(t')$  and battery state of charge  $SOC(t')$  are calculated using Equations 3.80-3.83. The three travelled distances  $d(t')$ ,  $d'(t')$ , and  $d''(t')$  (see Equation 3.54-3.56) are also updated. All previously mentioned variables, including motion regime, are stored in bus  $k$  state set  $B_{\text{state}}$  (see Equation 3.84 and Table 3-2). Based on the bus state set  $B_{\text{state}}$  of the operational buses, a bus profile matrix  $\mathbf{B}_{\text{profile}}$  is computed for each time step  $\delta t$ .

With each  $\delta t$ , a new  $B_{\text{state}}$  for bus  $k$  is computed. The motion regime  $M_B$  changes as shown in Section 3.4.3 until bus  $k$  reaches the next stopping traffic node. Several travelling route segments  $B_{\text{trs},j}$  are changed as bus  $k$  travels between two consecutive bus stops. If  $B_{\text{trs},j}$  defines the values of column  $j$  in the daily travelling route matrix  $\mathbf{B}_{\text{TR}}$ , then the new actual travelling route segment  $B_{\text{trs},j}$  will define the values of column  $(j + 1)$  in  $\mathbf{B}_{\text{TR}}$ . When the travelled distance between two consecutive traffic nodes  $d$  equals or surpasses the length of the traffic branch represented by the actual travelling route segment, the change of  $B_{\text{trs},j}$  is implemented. The previously specified condition is defined as follows:

$$d(t') \geq btr_{2,j} \quad (4.12)$$

The value of  $d(t)$  is adjusted as follows:

$$d(t) = d(t - \delta t) - btr_{2,j} \quad (4.13)$$

The value of  $d'(t)$  is adjusted to zero ( $d'(t) = 0$ ) when bus  $k$  stops ( $v(t) = 0$ ) and ( $d'(t - \delta t) = btr_{9,j}$ ). Based on the dwelling time  $btr_{7,j}$ , the position of bus  $k$  will remain unchanged, and thus no change in  $v(t')$  and  $\delta d(t')$  are given. During the dwelling time

$P_{TB}(t') = 0$  but  $P_{HVAC}(t')$ ,  $P_{baux}(t')$ ,  $P_{bat}(t')$ , and  $SOC(t')$  are computed as described in Section 3.4.2. The value of  $btr_{7,j}$  will be decreased by  $\delta t$ , with each new time step, until it reaches or decreases below zero. When  $btr_{7,j} \leq 0$ , the actual travelling route segment is switched with the new segment as described above. The motion regime  $M_B$  will be changed to acceleration mode ( $M_B = 1$ ), and bus  $k$  will resume the moving operation until it reaches the next stopping traffic node. Moving/stopping sequence will continue until the conclusion of bus  $k$  time schedule, i.e., the time at which bus  $k$  is scheduled to arrive at its depot ( $t' > btr_{7,j}$  and  $j = m_r$ ), or the simulation time  $t$  has reach its end ( $t = t_{se}$ ).

The third travel distance  $d''(t')$  denotes the distance travelled by bus  $k$  from the from-node  $btr_{10,j}$  of the traction branch. When  $d''(t')$  reaches or exceeds the length of the traction branch, which is defined in the actual travelling route segment  $B_{trs,j}$ , as shown below:

$$d''(t') \geq btr_{12,j} \quad (4.14)$$

the value of  $d''(t)$  is adjusted as follows:

$$d''(t) = d''(t - \delta t) - btr_{12,j} \quad (4.15)$$

The maximum speed of bus  $k$  is regulated by three factors, the first two factors are represented by the bus specification maximum speed  $b_{sp8,i}$  and the street speed limit defined in the actual travelling route segment  $B_{trs,j}$ , i.e.,  $btr_{5,j}$ . The third regulation factor is based on the limitations of the electric propulsion system. To prevent voltage drops from damaging the propulsion motor as recommended by IEC 62313:2009-04 [56], the overcurrent protection system reduces the propulsion motor's maximum power  $P_{M,max}$  (see Equation 2.30) to match the traction voltage level (see Section 5.2.5). The limitation of the electric propulsion system will restrict the bus speed; thus,  $b_{v,max}$  is bus  $k$  maximum permitted speed correspond to  $P_{M,max}$ .

Equation 4.16 is used to determine the maximum speed limit  $v_{max}(t')$  for bus  $k$ .

$$v_{max}(t') = \min(b_{sp8,i}, btr_{5,j}, b_{v,max}) \quad (4.16)$$

The buses that are currently operational are defined by their daily schedules. As shown in Equation 3.42,  $k$  is the index of trolleybuses and battery-trolleybuses operating in the trolleybus system, where  $k \in \{1, 2, 3, \dots, n_{bus}\}$ , and  $n_{bus}$  is the total number of the operating buses in the trolleybus system. Based on the index  $k$ , a set of departure time (from bus depot) for each bus can be defined as follows:

$$B_{dt} = (t_{db,1}, t_{db,2}, t_{db,3}, \dots, t_{db,n}), n = n_{bus} \quad (4.17)$$

and a set of arrival time (at bus depot) for each bus can be defined as follows:

$$B_{at} = (t_{ab,1}, t_{ab,2}, t_{ab,3}, \dots, t_{ab,n}), n = n_{bus} \quad (4.18)$$

$t_{db,k}$  and  $t_{ab,k}$  represent the departure and arrival times of bus  $k$ . Using Equations 4.17 and 4.18, the indices of the operational buses at  $t'$  are computed as follows:

$$K_{OB} = \{k | t_{db,k} \leq t' \leq t_{ab,k}\} \quad (4.19)$$

where  $K_{OB}$  is the set of the operational bus indices ( $k$ ) at time  $t'$

After determining the bus state  $B_{state}$  for each operational bus, a bus profile matrix  $B_{profile}$  is established (which is discussed in more detail in Section 5.1). The bus profile matrix  $B_{profile}$  include the indices of the operational buses and their corresponding information of the traction branch (from- and to-node), the total power, and the bus location to the traction branch.

### 4.3.2 Photovoltaic System

To simulate the power produced by a PV system, specific details as location, date, elevation, orientation, and installed capacity must be considered [129]. The PV specifications can be represented as following:

$$PV_{sp,i} = (pv_{sp1,i}, pv_{sp2,i}, pv_{sp3,i}, \dots, pv_{sp5,i}), 1 \leq i \leq n_{pv} \quad (4.20)$$

where  $pv_{sp1,i}$  is a number corresponding to the node-Id attribute of the traction nodes, i.e.,  $pv_{sp1,i} \in TEN_{a1}$ , the set elements from  $pv_{sp2,i}$  to  $pv_{sp5,i}$  are the installed power (in kW), the latitude (in decimal degrees), the altitude (in meters), and the azimuth (in degrees) of the PV system, respectively, and  $n_{pv}$  is the number of PV systems connected to the traction network. Figure 4-4 shows an ideal PV power profile computed from the global radiation of the sun using the PV specifications (see Equation 4.20) and the simulation corresponding real world time  $\tau_{rw}$  (see Equation 2.11). The ideal power profile  $P'_{PV,i}$  for each PV system ( $1 \leq i \leq n_{pv}$ ) can be represented as follows:

$$P'_{PV,i} = (p'_{pv1,i}, p'_{pv2,i}, p'_{pv3,i}, \dots, p'_{pvn,i}), n = n_s \quad (4.21)$$

where  $n_s$  is the number of discrete samples in  $\tau_s$  (see Equation 2.4), and  $p'_{pv1}$  to  $p'_{pv,n}$  are the ideal power produced by the PV system corresponded to each step along the total simulation time samples.

By applying a probability function to pre-measured data including cloud coverage information, the ideal power profile of the PV system is converted to a real-world power profile. An actual PV system was used to record the cloud indicator data, and several days over each month were taken into consideration. The cloud indicator data set  $PV_{cloud,i}$  is defined as:

$$PV_{cloud,i} = (pv_{c1,i}, pv_{c2,i}, pv_{c2,i}, \dots, pv_{cs,i}), 1 \leq i \leq n_{cloud} \quad (4.22)$$

where  $n_{cloud}$  is the number of the total recorded data sets ( $n_{cloud} \geq 12$ ),  $pv_{c1,i}$  and  $pv_{c2,i}$  are the date of the day and month of the recorded cloud indicator data, respectively, and  $pv_{c2,i}$  to  $pv_{cs,i}$  are the cloud indicator data assigned a value with in the interval  $[0,1]$ . Where zero indicates a cloudless sky and one a completely cloudy sky. The indicator  $s$  depends on the number of samples per day plus two (for  $pv_{c1,i}$  and  $pv_{c2,i}$ ), e.g., for a one-minute sampling ( $s = 1442$ ). As shown in Figure 4-4, a realistic power profile (associated with an ideal power profile) for a simulation

period of one day ( $n_s = 86400$  with  $\delta t = 1$  sec) is computed using Equation 4.21 and 4.22 and expressed as follows:

$$P_{PV,i} = (p_{pv,i}(t_1), p_{pv,i}(t_2), p_{pv,i}(t_3), \dots, p_{pv,i}(t_n)), n = n_s \quad (4.23)$$

where  $P_{PV,i}$  is the realistic power profile of PV system  $i$ , which is produced over the course of simulation time (from starting time  $t_1 = t_{ss} = 1$  to ending time  $t_n = t_{se} = 86400$ ). In Figure 4-4,  $t_1 = 00:00$  and  $t_n = 24:00$ .

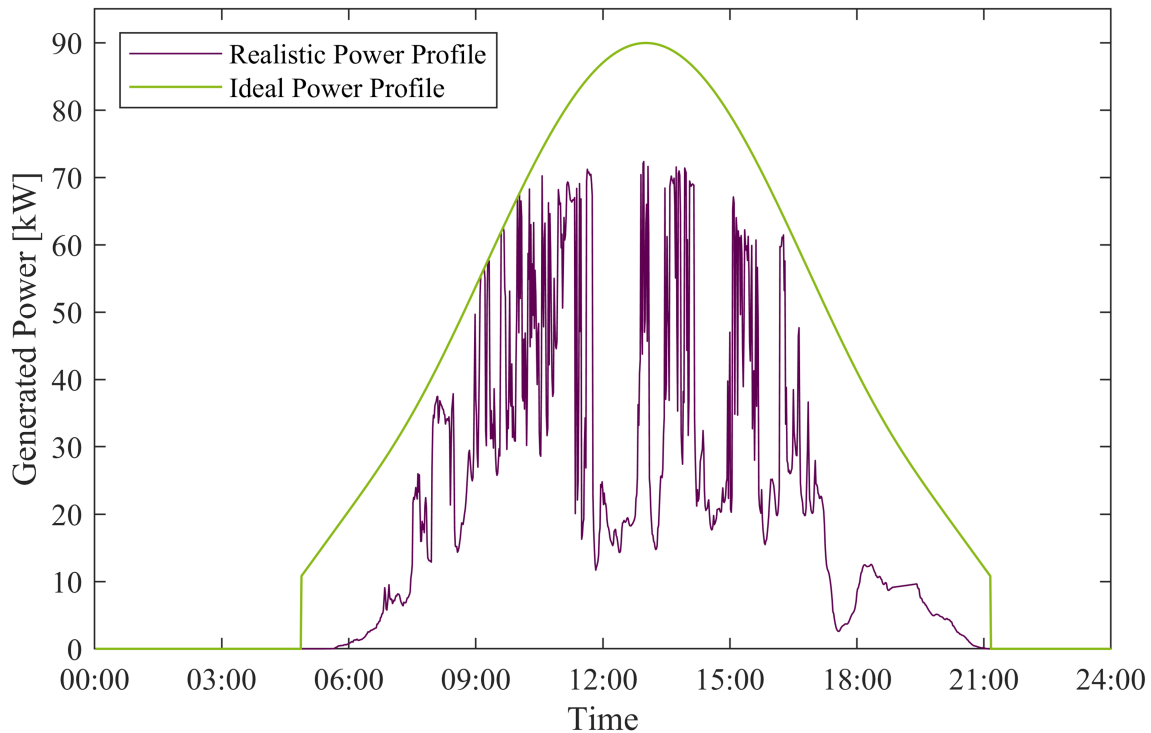


**Figure 4-4:** Generated power profiles of a photovoltaic system in the ideal case and when subjected to cloud coverage impact over one day.

### 4.3.3 Electric Vehicle Charging Station

Using electric vehicle parking profiles in terms of arrival and departure times, based on its battery state of charge –initial SOC– upon arrival, makes it possible to model the power profile of EVCSs throughout the course of the simulation time. Since representative battery SOCs are employed in the charging process, the time of the individual charging cycles and charging power might vary. Accordingly, the maximum charging power of the corresponding charging station is calculated based on the estimated initial SOC of the electric vehicle and the location of the charging station. The EVCS specifications can be represented as following:

$$CS_{sp,i} = (cs_{sp1,i}, cs_{sp2,i}, cs_{sp3,i}, cs_{sp4,i}), 1 \leq i \leq n_{cs} \quad (4.24)$$

where  $CS_{sp,i}$  is the specification set of EVCS  $i$ ,  $n_{cs}$  is the number of EVCSs connected to the traction network, and  $cs_{sp1,i}$  to  $cs_{sp4,i}$  are the traction node Id,  $cs_{sp1,i} \in TEN_{a1}$ , maximum



charging power (in kW), number of charging ports, location, and occupancy rate (in percent). In this model, the charging station location is considered one of three potential types: Residential area, shopping centre, and city centre. Consequently, the operating time of a charging station is determined. For example, a charging station close to a shopping centre is anticipated to be highly occupied from 09:00 to 22:00, however a charging station in a residential area is usually occupied from 16:00 to 08:00. Furthermore, the day type (weekday, weekend, or holiday) effects the operating time of a charging station [130–132].

The power profile of the EVCS is calculated using the data from Equation 4.24 and an estimated initial SOC based on a probability distribution of the daily driving distance of the charged electric vehicle [130, 133–136]. Equation 4.25 shows the expected power profile of electric vehicle charging station  $i$  over the course of the simulation time samples set  $\tau_s$  (see Equation 2.4).

$$P_{CS,i} = \left( p_{CS,i}(t_1), p_{CS,i}(t_2), p_{CS,i}(t_3), \dots, p_{CS,i}(t_n) \right), n = n_s \quad (4.25)$$

#### 4.3.4 Battery Storage Power Station

BSPS can be operated as both energy source and load (see Section 4.1.5 and 4.1.6). The mode of operation for a BSPS is defined based on several factors. In this work, the BSPS is modelled with three possible settings. The factors that are implemented based on these settings are the SOC of the BSPS combined with the traction network state. Moreover, a pre-defined operating mode based on a forecasting of the traction network state or energy market can be used to identify the BSPS settings during the simulation time samples set  $\tau_s$  (see Equation 2.4). The BSPS specifications  $SB_{sp,i}$  can be represented as following:

$$SB_{sp,i} = (sb_{sp1,i}, sb_{sp2,i}, sb_{sp3,i}, \dots, sb_{sp6,i}), 1 \leq i \leq n_{sb} \quad (4.26)$$

where  $n_{sb}$  is the total number of the BSPS connected to the traction network, and  $sb_{sp1,i}$  to  $sb_{sp6,i}$  are the traction node Id,  $sb_{sp1,i} \in TEN_{a1}$ , battery discharging power (in W), battery charging power (in W), battery effective capacity (in Wh), battery initial SOC (in percent), and BSPS operation setting ( $sb_{sp6,i} \in \{1,2,3\}$ ), respectively. BSPS is modelled in a manner comparable to the battery system of the BTB (see Section 3.4.2). Accordingly, the battery SOC of the BSPS is calculated as in Equation 3.80. The power of the BSPS  $P_{sb,i}$  for each  $t'$  is calculated as follows:

$$P_{SB,i}(t') = \begin{cases} sb_{sp2,i}, & \psi_{sb,i}(t') = 1 \\ -(\alpha_c \cdot sb_{sp3,i}), & \psi_{sb,i}(t') = -1 \\ 0, & \psi_{sb,i}(t') = 0 \end{cases} \quad (4.27)$$

$$\psi_{sb,i}(t') = \begin{cases} -1, & \text{charging} \\ 1, & \text{discharging} \\ 0, & \text{off} \end{cases} \quad (4.28)$$

The charge rate  $\alpha_c$  represent the decreases in charging capability corresponding to the battery SOC of the BSPS [137]. The influence of temperature on the performance of the BSPS is not taken into consideration in this work.  $\psi_{sb,i}(t')$  represents the operating mode of BSPS, which is

determined based on the defined setting  $sb_{sp6,i}$ . The operating modes are considered for the BSPS model. Thus, only one mode can be used (as defined in  $sb_{sp6,i}$ ) in order to compute the performance of the BSPS.

The first operating mode ( $sb_{sp6,i} = 1$ ) is solely dependent on the battery SOC of the BSPS, with the battery discharging – when the battery initial SOC (at the simulation start time  $t_{ss}$ ) is greater than zero ( $sb_{sp5,i} > 0$ ) – until its SOC drops to zero, and then charging until its SOC rises to one.  $\psi_{sb,i}(t')$  cycles between discharging and charging to the end of the simulation time  $t_{se}$ . Equation 4.28 can be computed with the first setting ( $sb_{sp6,i} = 1$ ) as follows:

$$\psi_{sb,i}(t') = \begin{cases} -1, & \begin{cases} SOC_{sb,i}(t) = 0 \\ \psi_{sb,i}(t) = -1 \end{cases} \\ 1, & \begin{cases} SOC_{sb,i}(t) > 0 \\ \psi_{sb,i}(t) = 1 \end{cases} \end{cases}, t' = t + \delta t \quad (4.29)$$

where  $t$  is the time of the last step,  $\delta t$  is the time step, and  $t'$  is the time of the current step.

In the second operating mode ( $sb_{sp6,i} = 2$ ),  $\psi_{sb,i}(t')$  is determined based on the voltage level at the BPS traction node (see Section 5.2.3). To manage the operating mode of the BPS with  $sb_{sp6,i} = 2$ , two voltage levels are defined. The batteries of BPS begin to charge when voltage  $U_{t,k}(t)$  at the connecting point of the BPS exceeds the defined upper voltage level  $U_{sb,up}$ , and discharge when their voltage  $U_{t,k}(t)$  falls below the defined lower voltage level  $U_{sb,low}$ . For  $sb_{sp6,i} = 2$ , Equation 4.28 can be computed as follows:

$$\psi_{sb,i}(t') = \begin{cases} -1, & U_{t,k}(t) > U_{sb,up} \\ 1, & U_{t,k}(t) < U_{sb,low} \\ 0, & \text{otherwise} \end{cases} \quad (4.30)$$

Equation 4.30 could be more refined by incorporating the battery SOC level  $SOC_{sb,i}(t')$ . Consequently, battery drain due to extensive discharging sessions is avoided since the charging margin is extended by decreasing  $U_{sb,up}$  when the battery SOC drops to a precise value  $SOC_{sb,c}$ .

In the third and last operating mode ( $sb_{sp6,i} = 3$ )  $\psi_{sb,i}(t')$  value is determined from a pre-defined operating mode. A forecast of the traction network state is used to set the operating mode  $\psi_{sb,i}(t')$  of the BPSs over the simulation time or for a specific timeframe. Equation 4.28 can be replaced with the pre-defined operating modes  $\Psi_{sb,i}$  as follows:

$$\Psi_{sb,i} = (\psi_{sb,i}(t) | t \in \tau_s \wedge t \forall: \psi_{sb,i} \in \{-1,0,1\}), |\Psi_{sb,i}| = n_s \quad (4.31)$$

where  $\tau_s$  is the set of simulation time samples (see Equation 2.4) and  $n_s$  is the number of discrete samples in  $\tau_s$ .

As previously stated, operating modes for a specified timeframe might be created and utilised for BPS (see [86]). The framed operating mode  $\Psi'_{sb,i}$  is defined as follows:

$$\Psi'_{sb,i} = (\psi'_{sb,i}(t) | t \in \tau_{sb,i} \wedge t \forall: \psi'_{sb,i} \in \{-1,0,1\}), |\Psi'_{sb,i}| = |\tau_{sb,i}| \quad (4.32)$$

$$\tau_{sb,i} = \{t_0, (t_0 + \delta t), (t_0 + 2 \cdot \delta t), \dots, (t_{ss} + (n - 2) \cdot \delta t), t_e\} \quad (4.33)$$

$$n = \frac{t_e - t_0}{\delta t} \quad (4.34)$$

where  $\tau_{sb,i}$  is the set of the timeframe time sequence,  $t_0$  is the starting of the timeframe,  $\delta t$  is the time step,  $t_e$  is the end of the timeframe, and  $n$  is the number of elements in  $\tau_{sb,i}$  and  $\Psi'_{sb,i}$ . The operating modes  $\Psi'_{sb,i}$  will override the value of  $\psi_{sb,i}(t')$  in Equations 4.30 and 4.31 when  $t' \in \tau_{sb,i}$ , i.e.,  $\psi_{sb,i}(t') := \psi'_{sb,i}(t) \Leftrightarrow t' = t \wedge t \in \tau_{sb,i}$ .



## 5 Modelling the Trolleybus System

The mathematical model of the electric trolleybus system is essential for studying and analysing the trolleybus system in its present condition, as for any plans to expand the system in the future. Precisely, a *conductance matrix* is used to represent the traction network topology, which is restricted to the trolleybuses (TBs) and battery-trolleybuses (BTBs) movement.

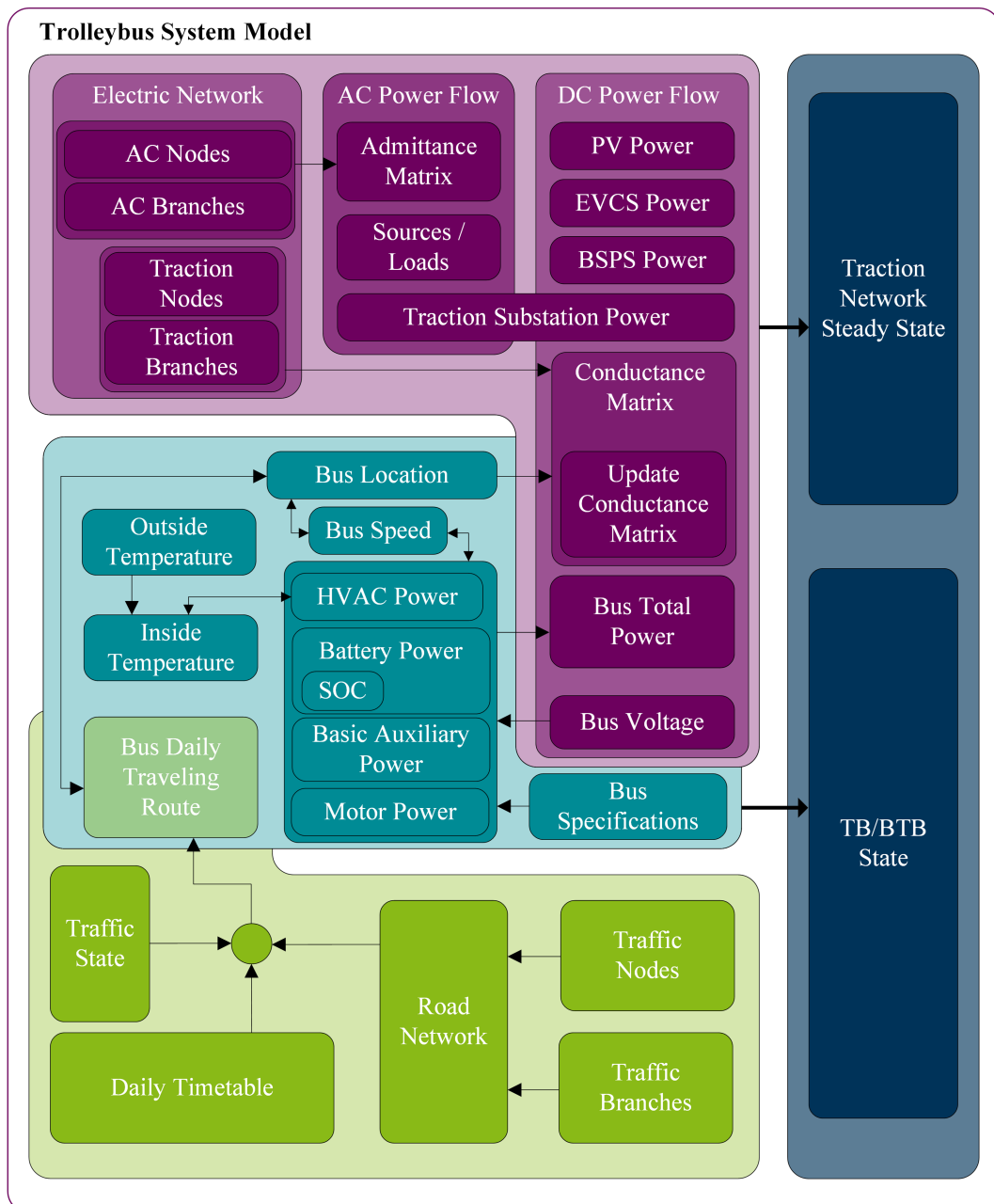


**Figure 5-1: Trolleybus system model scheme.**

The trolleybus system model shown in Figure 5-1 is a formation of three essential models, namely the traffic network model (TNM), the bus model (BS), and the electric network model (ENM).

The fourth block represents the calculated states for both traction network and buses (the AC network state is not included in the meant block). TNM and BS are elaborately described in Chapter 3, while ENM is presented in Chapter 4. The ENM is linked to the TNM by the BM, which projects all bus locations and powers from the road network to the traction network. When a bus moves under the overhead contact wires (OHCWs), the corresponding traction branch is adjusted. Consequently, the traction network gains an additional traction node for each bus. However, when many buses move within the same traction branch, several segments will be developed from the involved traction branch (see Section 5.2.2). With each simulation time step  $\delta t$ , the conductance matrix of the basic traction network is modified as a consequence of the bus movements (see Section 5.2.2). The steady-state of the trolleybus system may be calculated using either DC power flow or AC-DC power flow once the conductance matrix is modified (see Sections 5.2 and 5.3).

Finally, all node voltages, branch currents, and consequent powers of all traction substations, buses, and additional network sources and loads are determined and recorded. Furthermore, TB and BTB states, as indicated by their consumed power, location, speed, passenger crowding, outside temperature, and passenger compartment temperature, are all been recorded for further analysis and evaluation.

## 5.1 Applying Bus Movements to the DC Traction Network

After determining the bus state  $B_{\text{state}}$  for each operational bus as presented in Section 4.3.1, a bus profile matrix  $\mathbf{B}_{\text{profile}}$  is established as expressed below:

$$\mathbf{B}_{\text{profile}} = \begin{bmatrix} b_{p,11} & b_{p,12} & b_{p,13} & \cdots & b_{p,15} \\ b_{p,21} & b_{p,22} & b_{p,23} & \cdots & b_{p,25} \\ b_{p,31} & b_{p,32} & b_{p,33} & \cdots & b_{p,35} \\ b_{p,41} & b_{p,42} & b_{p,43} & \cdots & b_{p,45} \\ \vdots & \vdots & \vdots & \vdots & \vdots \\ b_{p,m1} & b_{p,m2} & b_{p,m3} & \cdots & b_{p,m5} \end{bmatrix}, m = |K_{\text{OB}}| \quad (5.1)$$

where  $|K_{\text{OB}}|$  is the number of the operational buses ( $K_{\text{OB}}$  is defined in Equation 4.19), and  $b_{p,ij}$  represents the elements of  $\mathbf{B}_{\text{profile}}$ . The first column of  $\mathbf{B}_{\text{profile}}$  denotes the operational bus indices, i.e.,  $\text{column}_1(\mathbf{B}_{\text{profile}}) = b_{p,i1} = K_{\text{OB}}$  with  $i = \{1, 2, \dots, |K_{\text{OB}}|\}$ . The second and third column of  $\mathbf{B}_{\text{profile}}$  denote the traction branch (from- and to-node) where the corresponding bus in  $b_{p,i1}$  are operating, respectively.

The fourth column of  $\mathbf{B}_{\text{profile}}$  denotes the total power  $P_{T,k}$  of the corresponding bus in  $b_{p,i1}$ .

The fourth column  $b_{p,i4}$  is calculated as follows:

$$P_{T,k} = b_{s,6} + b_{s,7} + b_{s,8} + b_{s,9} \quad (5.2)$$

and

$$b_{p,i4} = P_{T,k} \Leftrightarrow b_{p,i1} = k \quad (5.3)$$

The variables ( $b_{s,6}$  to  $b_{s,9}$ ) of Equation 5.2 are defined in Table 3-2.

The fifth column of  $\mathbf{B}_{\text{profile}}$  represents the ratio between travelled distance  $b_{s,5}$  – correspond to each bus in  $b_{p,i1}$  – and the traction branch length  $btr_{12,j}$ . The following equations are used to compute the element of the fifth column.

$$b_{p,k} = \frac{b_{s,5}}{btr_{12,j}} \cdot 100\% \quad (5.4)$$

and

$$b_{p,i5} = b_{p,k} \Leftrightarrow b_{p,i1} = k \quad (5.5)$$

with each time step  $\delta t$ , a new bus profile matrix  $\mathbf{B}_{\text{profile}}$  is computed. The number of rows in  $\mathbf{B}_{\text{profile}}$  depends on the number of the operational buses at  $t'$ .

## 5.2 Traction Network Steady-State Calculation

Resolving the steady-states of a traction network is critical in planning or determining the future growth of a trolleybus system as well as optimising the system's actual performance. The developed model of the traction network, which defines the interconnection of its various components (see Section 4.1), is utilized in order to determine the mathematical relations between the traction network components.

The node voltage and loop current approaches are often used to analyse power systems. Whereby, both approaches use simultaneous equations. Node equations are becoming more often used in power system analysis. To model the node equation of the traction network as shown in Equation 5.6, Kirchoff's current law is used [138]:

$$\mathbf{I}_{t,z} = \mathbf{G}_{t,z} \cdot \mathbf{U}_{t,z} \quad (5.6)$$

Here  $\mathbf{I}_{t,z}$  is the nodal injection current,  $\mathbf{U}_{t,z}$  is the nodal voltage, and  $\mathbf{G}_{t,z}$  is the nodal conductance matrix of traction network zone (TNZ). Each zone (see Section 4.1.2) in the traction network is modelled with its equivalent nodal equations, which reduce the number of nodes in the nodal equations to the number of nodes  $n_{\text{et},z}$  in a zone. The vector form of Equation 5.6 can be defined as shown below:

$$\begin{bmatrix} I_{z,1} \\ I_{z,2} \\ \vdots \\ I_{z,n} \end{bmatrix} = \begin{bmatrix} G_{z,11} & G_{z,12} & \cdots & G_{z,1n} \\ G_{z,21} & G_{z,22} & \cdots & G_{z,2n} \\ \vdots & \vdots & \ddots & \vdots \\ G_{z,n1} & G_{z,n2} & \cdots & G_{z,nn} \end{bmatrix} \cdot \begin{bmatrix} U_{z,1} \\ U_{z,2} \\ \vdots \\ U_{z,n} \end{bmatrix}, \quad n = n_{\text{et},z} \quad (5.7)$$

The current injection into node  $i$  (see Equation 5.7) is calculated as follows:

$$I_{z,i} = \sum_{j=1}^n G_{z,ij} \cdot U_{z,j}, \quad n = n_{et,z} \quad (5.8)$$

As shown in Equation 5.9, node voltage and injected node power can be used to express the injected current into node  $i$ .

$$I_{z,i} = \frac{P_{z,i}}{U_{z,i}} \quad (5.9)$$

where  $P_{z,i}$  is the power injected into node  $i$ . The following expression is obtained from Equations 5.8 and 5.9 .

$$P_{z,i} = U_{z,i} \cdot \sum_{j=1}^n G_{z,ij} \cdot U_{z,j}, \quad n = n_{et,z} \quad (5.10)$$

The general algorithm used to obtain the instantaneous steady-state solution of the DC traction network based on the location and total power of TBs and BTBs is described in the following subsections. Other power sources and loads, such as photovoltaics (PVs), electric vehicle charging stations (EVCSs), and battery storage power stations (BSPSs), are also evaluated in the simulation process.

### 5.2.1 Simulation Process

After modelling the bus specification (see Section 3.4.1), bus daily travelling path (see Section 3.3), traction network (see Sections 4.1.2 and 4.1.3), and the traction source and load power profiles (see Section 4.3), the process to calculate the traction network steady-state is accomplished as shown in Figure 5-2.

To avoid processing a large number of nodes and reduce computational effort, it is necessary to repeat the simulation process for each TNZ. In order to do this, a renumbering scheme for the node Ids is implemented for each zone. Based on Equation 4.1,  $TEN_{a1,i}$  is the standard node Id and  $TEN_{a3,i}$  is its corresponding zone. Using  $TEN_{a1}$  and  $TEN_{a3}$ , new groups of node Ids based on zone can be established. The groups of node Ids are defined as in Equations 5.11 and 5.12. Each group is presented with two sets; the first set has the new node Ids  $N_{zn,z}$ , while the second set has their corresponding standard node Ids  $N_{zs,z}$ .



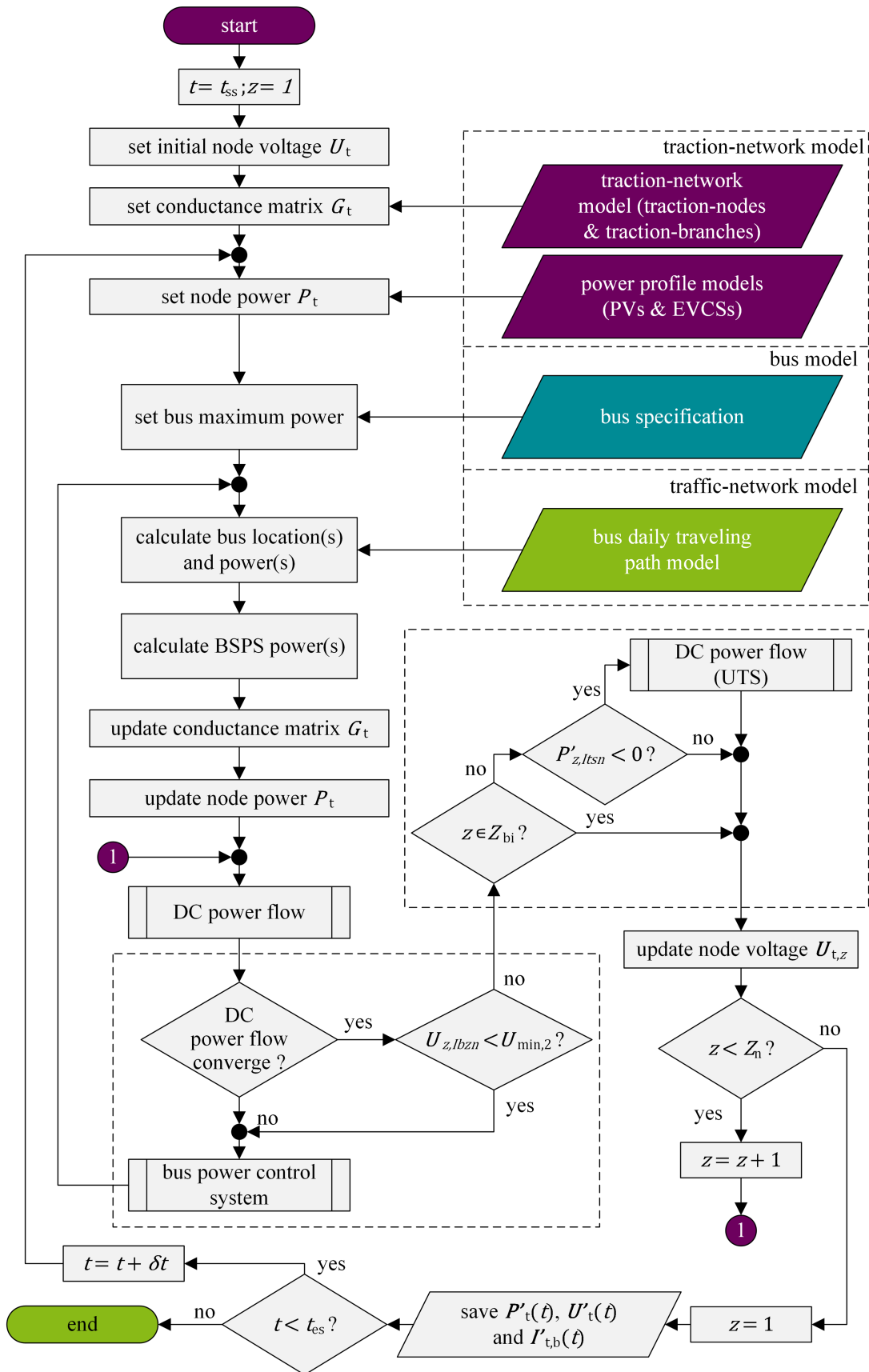


Figure 5-2: Sequence of the traction network steady-state calculation.

$$N_Z = \{N_{Z,z} | z = (1, 2, \dots, n_z)\} \quad (5.11)$$

$$N_{z,z} = \{N_{zn,z}, N_{zs,z}\}, z = (1, 2, \dots, n_z) \quad (5.12)$$

The number of nodes in zone  $z$  is denoted as  $n_{et,z}$ , therefore, the set of new node Ids can be defined as  $N_{zn,z} = \{1, 2, 3, \dots, n_{et,z}\}$ . On the other hand,  $N_{zs,z} \subset TEN_{a1}$ .

At the beginning, simulation time counter  $t$  is set to  $t_{ss}$ , which corresponds to the comparable day time as indicated in Equation 2.1. The initial nodal voltages correspond to each zone is set as  $U_t = \{U_{t,1}, U_{t,2}, U_{t,3}, \dots, U_{t,z}\}$ , where

$$U_{t,z} = \begin{bmatrix} U_{z,1} \\ U_{z,2} \\ \vdots \\ U_{z,n} \end{bmatrix}, n = n_{et,z} \quad (5.13)$$

$$U_{z,zn} = U_n, zn = N_{zn,z} \quad (5.14)$$

The basic conductance matrices  $G_t$  for each TNZ is initialised using the basic traction nodes and traction branches model, where  $G_t = \{G_{t,1}, G_{t,2}, \dots, G_{t,z}\}$ . For more information on how the conductance matrix is determined see Section 5.2.2. Equations 4.20, 4.23, 4.24, and 4.25 are used to determine the power values for any available PVs and EVCSs in the traction network. Using the new zone node Id and the simulation time counter  $t$ , the powers  $P_{PV,i}(t)$  and  $P_{CS,i}(t)$  are then sorted into their corresponding zone node power vector.

The node power vector of the complete traction network at time  $t$  can be defined as:

$$P_t = \begin{bmatrix} p_{t,1}(t) \\ p_{t,2}(t) \\ \vdots \\ p_{t,n}(t) \end{bmatrix}, n = n_{et} \quad (5.15)$$

where  $p_{t,1}(t)$  to  $p_{t,n}(t)$  denote the injected power at traction nodes (1 to  $n_{et}$ ), respectively. On the other hand, the set of zone power vector can be defined as  $P_t = \{P_{t,1}, P_{t,2}, \dots, P_{t,z}\}$ . Using the new node Ids  $N_{zn,z}$  defined in Equation 5.12, the node power vector of zone  $z$  is:

$$P_{t,z} = \begin{bmatrix} P_{z,1} \\ P_{z,2} \\ \vdots \\ P_{z,n} \end{bmatrix}, n = n_{et,z} \quad (5.16)$$

where  $P_{z,1}$  to  $P_{z,n}$  denote the injected power at traction nodes (1 to  $n_{et,z}$ ), respectively, in zone  $z$  and  $P_{t,z} \subset P_t$ .

If  $P_{PV,lpvz}(t)$  represents the output powers of PV systems  $lpvz$ , where  $lpvz$  indicate the traction node Ids of the PV systems in zone  $z$ , i.e.,  $lpvz = \{TEN_{a1,i} \Leftrightarrow TEN_{a2,i} := \{PV\} \wedge TEN_{a3,i} = z | 1 \leq i \leq n_{et}\}$  (see Section 4.1.2), and  $lpvzn$  represent the new node Ids corresponding to PV systems  $lpvz$  (see Equation 5.12), then  $P_{t,z}$  is updated with the PV powers as follows:

$$P_{z,lpvzn} = P_{PV,lpvz}(t) \quad (5.17)$$

Same for EVCSs, the node Ids of EVCSs in zone  $z$  are defined as in the following equation  $I_{csz} = \{TEN_{a1,i} \Leftrightarrow TEN_{a2,i} := \{EVCS\} \wedge TEN_{a3,i} = z | 1 \leq i \leq n_{et}\}$  (see Section 4.1.2) and their corresponding new node Ids are defined as  $I_{cszn}$  (see Equation 5.1). The EVCS node powers are computed into  $\mathbf{P}_{t,z}$  as follows:

$$P_{z,Icszn} = P_{CS,Icsz}(t) \quad (5.18)$$

According to IEC 62313:2009-04 [56] and as illustrated in Figure 2-6, the TBs and BTBs motor powers must be regulated as defined in Equation 2.2. Using the bus specifications' model (see Equation 3.43) and the bus voltage values  $U_{z,lbzn}$ , the maximum permitted motor power for each bus is calculated (as shown in Figure 5-2 using *bus power control system* block – to which Section 5.2.5 provides further detail).  $lbzn$  represent buses corresponding new node Ids in zone  $z$  and is described further below. The nominal voltage  $U_n$  is utilised as the starting voltage of the traction nodes at the start of the simulation ( $t = t_{ss}$ ). After calculating the traction network steady-state for each new time step  $\delta t$ , the nodal voltage of each zone  $U_t$  is adjusted, and the maximum permitted motor power of the buses are recalculated.

Using the bus daily travelling routes model (BDTRM) (see Equation 3.11) and bus model (BM) (see Equation 3.42), the powers and locations of the operational buses at time  $t$  are calculated as described in Section 4.3.1. With each time step  $\delta t$ , a new *bus profile* matrix  $\mathbf{B}_{profile}$  is computed (see Equation 5.1). The number of rows in  $\mathbf{B}_{profile}$  depends on the number of the operational buses at time  $t$ . After computing the bus movements, the calculation of BSPS powers takes place. Based on the operating setting of the BSPSs, the power and SOC of the BSPSs are calculated as described in Section 4.3.4.

By using the data computed in  $\mathbf{B}_{profile}$ , the conductance matrix  $\mathbf{G}_{t,z}$  is updated (see Section 5.2.2). Suppose one or several buses operate in a TNZ, as stated in  $\mathbf{B}_{profile}$ . In that case, the operational buses will be defined with new traction nodes which divide the traction branches, they are positioned on, into two traction branches or more, depending on the number of buses on a traction branch. After computing the power of the operational buses and BSPSs, the node power vector  $\mathbf{P}_{t,z}$  of each zone in the traction network is updated with these powers after referencing the operational buses and BSPSs to their corresponding zone. If  $lbz$  define the indices of the operational buses in zone  $z$ , then  $lbzn$  represent their corresponding new node Ids in zone  $z$ , and can be computed as follows:

$$lbzn = \{(1, \dots, |lbz|) + n_{et,z}\} \quad (5.19)$$

where

$$lbz \subset \{\text{column}_1(\mathbf{B}_{profile})\} \quad (5.20)$$

The traction node Ids of BSPSs in zone  $z$  are defined as  $Isbz = \{TEN_{a1,i} \Leftrightarrow TEN_{a2,i} := \{\text{BSPS}\} \wedge TEN_{a3,i} = z | 1 \leq i \leq n_{et}\}$  (see Section 4.1.2), and  $Isbzn$  represent the new node Ids corresponding to BSPSs  $Isbz$  (see Equation 5.12). If  $P_{B,lbz}(t)$  and  $P_{SB,icsz}(t)$  are the powers of the operational buses and BSPSs in zone  $z$ , respectively, then the elements of the node power vector  $\mathbf{P}_{t,z}$  are updated as follows:

$$P_{z,lbzn} = -P_{B,lbz}(t) \quad (5.21)$$

$$P_{z,icszn} = P_{SB,icsz}(t) \quad (5.22)$$

Calculating the steady-state of each TNZ using the *DC power flow* (see Section 5.2.3) will start once the nodal voltage vector, the node power vector, and the conductance matrix are formed for all TNZs. If the DC power flow converges, the resulted bus voltages ( $U_{B,lbz} := U'_{z,lbzn}$ ) will be evaluated for voltage violations. With any unsuccessful DC power flow or voltage violation, a *bus power control system* (see Section 5.2.5) will be initiated. If no voltage violation occurs, the calculated powers of the traction substations  $P'_{z,itsn}$  are evaluated for any feedback powers. Only zones with unidirectional traction substations  $Z_{uni}$  will be subjected to the evaluation. TNZs supplied by unidirectional traction substations will be resolved using an adapted DC power flow algorithm that can cope with feedback power (see Section 5.2.4). Once all anticipated violations have been resolved, the nodal voltages of zone  $z$  (see Equation 5.13) will be adjusted as follows:

$$\mathbf{U}_{t,z} = [U'_{z,zn}], zn = N_{zn,z} \quad (5.23)$$

where  $U'_{z,zn}$  is the DC power flow solution of the nodal voltage for zone  $z$ , and  $zn$  is the set of new traction node Ids  $N_{zn,z}$  for zone  $z$  (see Equation 5.12).

The DC power flow calculation process will be repeated for the following TNZ until the steady-states of all TNZs are established. After correctly identifying the steady-state of the traction network at time  $t$ , the zone index  $z$  is reset to its original configuration. The computed steady-state of the traction network at time  $t$ , characterised by the traction node powers  $\mathbf{P}'_t$ , the traction node voltages  $\mathbf{U}'_t$ , and the traction branch currents  $\mathbf{I}'_{t,b}$ , is saved as follows:

$$\mathbf{P}'_t = \begin{bmatrix} p'_{t,1}(t) \\ \vdots \\ p'_{t,n}(t) \\ \text{---} \\ p'_{t,n+1}(t) \\ \vdots \\ p'_{t,n+m}(t) \end{bmatrix} \quad (5.24)$$

$$\mathbf{U}'_t = \begin{bmatrix} u'_{t,1}(t) \\ \vdots \\ u'_{t,n}(t) \\ \text{---} \\ u'_{t,n+1}(t) \\ \vdots \\ u'_{t,n+m}(t) \end{bmatrix} \quad (5.25)$$

$$\mathbf{I}'_{t,b} = \begin{bmatrix} i'_{11} & \cdots & i'_{1n} & i'_{1(n+1)} & \cdots & i'_{1(n+m)} \\ \vdots & \ddots & \vdots & \vdots & \ddots & \vdots \\ i'_{n1} & \cdots & i'_{nn} & i'_{n(n+1)} & \cdots & i'_{n(n+m)} \\ \hline i'_{(n+1)1} & \cdots & i'_{(n+1)n} & i'_{(n+1)(n+1)} & \cdots & i'_{(n+1)(n+m)} \\ \vdots & \ddots & \vdots & \vdots & \ddots & \vdots \\ i'_{(n+m)1} & \cdots & i'_{(n+m)n} & i'_{(n+m)(n+1)} & \cdots & i'_{(n+m)(n+m)} \end{bmatrix} \quad (5.26)$$

and

$$i'_{ij} = \begin{cases} \frac{(u'_{t,i}(t) - u'_{t,j}(t))}{R_{ij}}, & A_{ij} = 1 \\ 0, & A_{ij} = 0 \end{cases} \quad (5.27)$$

The arrays in Equations 5.24 and 5.25 are divided into two parts. The upper part represents the traction nodes, indexed from 1 to  $(n := n_{\text{et}})$  as defined in Equation 4.1, while the lower part represents the TBs and BTBs, indexed by adding the bus indices (1 to  $(m := n_{\text{bus}})$ ) to the total number of traction nodes  $n_{\text{et}}$ . The indices of the matrix in Equation 5.26 have the same definition as of Equations 5.24 and 5.25, where the bus indices are represented on the right end and down end of the matrix after the traction node indices. The matrix in Equation 5.26 is divided into four parts: The first part (upper left) represents the current flows between the basic traction nodes (1 to  $n$  where  $n := n_{\text{et}}$ ), the second and third parts (upper right and lower left, respectively) represent the current flows between the basic traction nodes (1 to  $n$  where  $n := n_{\text{et}}$ ) and the bus nodes ( $n + 1$  to  $n + m$  where  $n := n_{\text{et}}$  and  $m := n_{\text{bus}}$ ), and the fourth part (lower right) represents the current flows between bus nodes ( $n + 1$  to  $n + m$  where  $n := n_{\text{et}}$  and  $m := n_{\text{bus}}$ ). The elements of Equation 5.26 are computed as shown in Equation 5.27, where  $i$  and  $j$  denote the from- and to-node of the traction branches, respectively, and  $A_{ij}$  denotes the elements of the traction network adjacency matrix  $\mathbf{A}$  at time  $t$ . Elements of  $\mathbf{A}$  indicate whether or not adjacent pairs of traction nodes  $(i,j)$  form a traction branch. If  $A_{ij} = 1$ , traction branches exist between  $i$  and  $j$ , and thus there are no traction branches when  $A_{ij} = 0$ .

After determining the steady-state of the traction network at time  $t$ , the simulation process will proceed with the following time step  $\delta t$  until the simulation time  $t$  reaches its conclusion at  $t_{\text{es}}$ . At that point, the simulation process will terminate.

### 5.2.2 Determination of Conductance Matrix

The trolleybus system has a significant number of sparse nodes, i.e., the traffic nodes and the traction nodes. The number of nodes required to construct an accurate nodal conductance matrix could be minimised using sparsity techniques to improve the computational effort. The node equation, which can be found in Equation 5.6, is used in the evaluation of the traction network steady-state. A nodal conductance matrix is a mathematical abstraction of a DC electric network topology and parameters; hence it may be interpreted as the mathematical representation of a

traction network, more specific, TNZ. If there are  $n$  traction nodes in a TNZ, the nodal conductance matrix  $\mathbf{G}_{t,z}$  of the traction zone  $z$  can be defined as:

$$\mathbf{G}_{t,z} = \begin{bmatrix} g_{z,11} & g_{z,12} & \cdots & g_{z,1n} \\ g_{z,21} & g_{z,22} & \cdots & g_{z,2n} \\ \vdots & \vdots & \ddots & \vdots \\ g_{z,n1} & g_{z,n2} & \cdots & g_{z,nn} \end{bmatrix}, \quad n = n_{et,z} \quad (5.28)$$

The conductance matrix can be simply created once the traction network topology (see Section 4.1) is determined. If  $i$  and  $j$  represent two traction nodes in zone  $z$  ( $i \wedge j \in \{1,2,3, \dots, n_{et,z}\}$ ), then the diagonal element  $g_{z,ii}$  represents the nodal self-conductance that can be computed as follows:

$$g_{z,ii} = - \sum_{\substack{j=1 \\ j \neq i}}^n g_{z,ij}, \quad n = n_{et,z} \quad (5.29)$$

while the off-diagonal element  $g_{z,ij}$  represents the mutual conductance between nodes  $i$  and  $j$  (traction branch  $(i,j)$ ). Traction branches are represented only by their ohmic resistance. In DC networks the shunt capacitance and reactance of the overhead lines are absent. In general, DC system is a two wires system and logically has no transformer. Based on Equation 4.3, the traction branches are organised into groups and given new traction node Ids. These new Id numbers depend on the traction zones that are indicated in  $TEB_{a6}$  (see Section 4.1.3).

$$Br_t = \{Br_{t,1}, Br_{t,2}, Br_{t,3}, \dots, Br_{t,z}\} \quad (5.30)$$

The elements of Equation 5.30 represent the traction branches for each zone in the traction network. After renumbering the traction nodes – corresponding to each traction zone,  $Br_{t,z}$  can be recognized as an  $(n \times m)$  matrix. The first and second columns of  $Br_{t,z}$  represent the standard traction node Ids of the traction branch (from- and to-node), yet the third and fourth columns of  $Br_{t,z}$  are the new traction node Ids correspond to the traction zone (see Equations 5.11 and 5.12). The fifth and sixth columns are the length in (m) and electrical resistance per unit length  $R'$  in ( $\Omega/m$ ) of the traction branch, respectively.

$$Br_{t,z} = \begin{bmatrix} N_{of,z,1} & N_{ot,z,1} & N_{nf,z,1} & N_{nt,z,1} & l_{b,z,1} & r_{b,z,1} \\ N_{of,z,2} & N_{ot,z,2} & N_{nf,z,2} & N_{nt,z,2} & l_{b,z,2} & r_{b,z,2} \\ \vdots & \vdots & \vdots & \vdots & \vdots & \vdots \\ N_{of,z,n} & N_{ot,z,n} & N_{nf,z,n} & N_{nt,z,n} & l_{b,z,n} & r_{b,z,n} \end{bmatrix}, \quad (5.31)$$

$n = n_{tn,z}$

Using the matrix of Equation 5.31, the off-diagonal element of Equation 5.28 can be calculated as follows:

$$\left. \begin{aligned} R_{z,ij} &= l_{b,z,k} \times r_{b,z,k} \\ i &= N_{nf,z,k} \\ j &= N_{nt,z,k} \end{aligned} \right\}, \quad k = \{1,2,3, \dots, n_{tn,z}\} \quad (5.32)$$

$$g_{z,ij} = \frac{-1}{R_{z,ij}} \quad (5.33)$$

The conductance matrix  $\mathbf{G}_{t,z}$  is constructed without considering TBs and BTBs locations in the traction network; owing to the changes in the traction network topology over time as these buses move. Hence, the dynamic behaviour of the buses results in a significant variance when it comes to the calculations for the steady-state of the traction network. Alternating network topology are comparable to contrasting new conductance matrix, which must be considered with each power flow calculation.

At any sample in  $\tau_s$  (see Equation 2.4), each TB and BTB is related to a specific location on the bus route. Bus locations under the OHCWs are listed as stated in Equation 5.1 After rearranging the buses to their corresponding zone by comparing the second and third columns of  $B_{\text{profile}}$  (see Equation 5.1) to the first and second columns of  $Br_{t,z}$  (see Equation 5.31),  $B_{\text{profile}}$  is redefined as follows:

$$B'_{\text{profile}} = \{B_{\text{pro},1}, B_{\text{pro},2}, B_{\text{pro},3}, \dots, B_{\text{pro},z}\} \quad (5.34)$$

and

$$B_{\text{pro},z} = \begin{bmatrix} b_{p,z,11} & b_{p,z,12} & b_{p,z,13} & \dots & b_{p,z,15} \\ b_{p,z,21} & b_{p,z,22} & b_{p,z,23} & \dots & b_{p,z,25} \\ \vdots & \vdots & \vdots & \dots & \vdots \\ b_{p,z,m1} & b_{p,z,m2} & b_{p,z,m3} & \dots & b_{p,z,m5} \end{bmatrix}, m = n_{\text{op},z} \quad (5.35)$$

where  $n_{\text{op},z}$  is number of operational buses in zone  $z$ .

A new Id will be assigned to each bus and elements of Equation 5.1 are updated as follows:

$$N'_{z,z} = \{N'_{zn,z}, N'_{zs,z}\} \quad (5.36)$$

The set of new node Ids is defined as  $N'_{zn,z} = \{1, 2, 3, \dots, n'_{\text{et},z}\}$ , where  $n'_{\text{et},z} = n_{\text{et},z} + n_{\text{op},z}$ . Yet,  $N'_{zs,z}$  represent zone  $z$  standard traction node Ids and operational bus indices (see Equation 5.1). Bus new node Ids and bus indices are listed at the end of  $N'_{zn,z}$  and  $N'_{zs,z}$ , respectively.

A new matrix  $Br'_{t,z}$  is computed from Equation 5.31 and Equation 5.35, where the element of  $Br_{t,z}$  are updated based on the *new nodes* that are founded in-between the existing traction branches. These *new nodes* represent bus locations in the traction zone  $z$ . Due to the fact that the presence of buses in between traction branch  $(i,j)$  will only impact the self and mutual conductance of traction nodes  $i$  and  $j$ , the new conductance matrix can be determined for the new state by adjusting the original conductance matrix  $\mathbf{G}_{t,z}$ . Since  $Br'_{t,z}$  is constricted based on  $Br_{t,z}$  and  $B_{\text{pro},z}$ , the rows of  $Br'_{t,z}$  will present the new network topology taking into account buses existence. Initially, all traction branches that do not include buses in  $Br_{t,z}$  will be included in  $Br'_{t,z}$ . The first and second columns of  $Br_{t,z}$  will be compared to the second and third columns of  $B_{\text{pro},z}$

in order to select all traction branches that do not include buses in  $Br_{t,z}$  and a new matrix  $Br'_{t,z}$  is thus formed. Furthermore, new traction branches will be added into  $Br'_{t,z}$  as follows:

**One bus in-between a traction branch (two traction branches are constructed)**

1. Identify the terminals (traction nodes) of the new traction branches. The first constructed traction branch has the same from-node Id as the original traction branch  $b_{p,z,i2}$  and its to-node Id will be indicated by the bus index  $b_{p,z,i1}$ . The second constructed traction branch will have the bus index  $b_{p,z,i1}$  as its from-node Id and the original traction branch to-node Id  $b_{p,z,i3}$  will be its to-node.
2. Using Equation 5.36, the new traction node Ids, which correspond to traction zone  $z$ , will be included in  $Br'_{t,z}$  to represent zone traction node Ids for the new constructed traction branches.
3. The lengths of the constructed traction branches will be calculated using  $b_{p,z,i5}$  and the length of the original traction branch. If  $o$  is the row index of the original traction branch, when  $b_{p,z,o1} = b_{p,z,i2} \wedge b_{p,z,o2} = b_{p,z,i3}$ , then  $l_{b,z,o}$  is the length of the original traction branch. Yet, let  $c$  be the row index of the new constructed branch, then the length of the first constructed traction branch is equal to ( $l_{b,z,c} = l_{b,z,o} \cdot b_{p,z,i5}$ ), while the length of the second constructed traction branch is equal to ( $l_{b,z,c} = l_{b,z,o} \cdot (1 - b_{p,z,i5})$ ).
4. The electrical resistance per length unit  $R'$  of the newly constructed traction branches is identical to that of the original traction branch. It is possible to utilise the same approach that was conducted in step three to find out the electrical resistance of the initial traction branch, i.e., when  $b_{p,z,o1} = b_{p,z,i2} \wedge b_{p,z,o2} = b_{p,z,i3}$  then  $r_{b,z,o}$  is the electrical resistance of the original traction branch.

**Several buses in-between a traction branch (three or more traction branches are constructed)**

1. Buses sharing the same traction branch will be sorted based on the values of  $b_{p,z,i5}$ , where  $i \in I_{bs}$  and  $I_{bs}$  represents the row of indices (based on matrix  $B_{pro,z}$ ) of buses that share the same traction branch. The first bus in the sequence is that with the smallest  $b_{p,z,i5}$  value; afterwards, it will be followed by the bus that has the next higher  $b_{p,z,i5}$  value, and the sequence will continue until the bus with the highest  $b_{p,z,i5}$  value comes at last.  $I_{bs}$  will be reordered as  $I'_{bs} = (i_{bs,1}, i_{bs,2}, \dots, i_{bs,n})$ , where  $i_{bs,1}$  denotes the index of the bus that has the lowest  $b_{p,z,i5}$  value and  $i_{bs,n}$  denotes the index of the bus that has the highest  $b_{p,z,i5}$  value. The number of the new constructed traction branches is determined as  $(|I_{bs}| + 1)$ .
2. Terminals (traction nodes) of the new traction branches will be defined based on the bus sequence or rather  $I'_{bs}$ . The original traction branch from- and to-node Ids will denote the from-node Id of the first constructed traction branch and the to-node Id of the last new constructed traction branch, respectively. The bus index  $b_{p,z,i1}$  of the *first* bus in the



sequence ( $i := i_{bs,1}$ ) will be used as the to-node Id of the *first* constructed traction branch as well as the from-node Id of the next adjacent traction branch, which is in this case the *second* constructed traction branch. In the same way, the index of next bus in the sequence will be used as the to-node Id of the constructed traction branch that has the *same sequence order* as the bus and the from-node Id next adjacent traction branch. The procedure will be proceeded until all bus indices are implemented as terminals of the new traction branches. The last bus index  $b_{p,z,i1}$ , where  $i := i_{bs,n}$ , will be utilised as the from-node of the last constructed traction branch.

3. Using Equation 5.36, the new traction node Ids, which correspond to traction zone  $z$ , will be used to identify the terminals of the newly constructed traction branches.
4. The length of the original traction branch is utilised using the same approach that was conducted in step three (One bus in-between a traction branch). With  $l_{b,z,o}$  defining the length of the original traction branch, the length of the first constructed traction branch is calculated as ( $l_{b,z,c} = l_{b,z,o} \cdot b_{p,z,i5}$ ) and  $i := i_{bs,1}$ , while the length of the last constructed traction branch is calculated as ( $l_{b,z,c} = l_{b,z,o} \cdot (1 - b_{p,z,i5})$ ) and  $i := i_{bs,n}$ . The lengths of the other constructed traction branch are calculated as ( $l_{b,z,c} = l_{b,z,o} \cdot (b_{p,z,i5} - b_{p,z,j5})$ ) with  $i = (i_{bs,2}, \dots, i_{bs,n})$  and  $j = (i_{bs,1}, \dots, i_{bs,(n-1)})$ . For example, the length of the second constructed traction branch is calculated with  $i = i_{bs,2}$  and  $j = i_{bs,1}$ , for the third  $i = i_{bs,3}$  and  $j = i_{bs,2}$ , and so forth.
5. As in step four (One bus in-between a traction branch), The electrical resistance per length unit  $R'$  of the newly constructed traction branches is identical to that of the original traction branch. Thus, when  $b_{p,z,o1} = b_{p,z,i2} \wedge b_{p,z,o2} = b_{p,z,i3}$  then  $r_{b,z,o}$  is the electrical resistance of the original traction branch.

After eliminating all traction branches that include buses and adding the new traction branches,  $Br'_{t,z}$  can be recognised as follows:

$$Br'_{t,z} = \begin{bmatrix} N'_{of,z,1} & N'_{ot,z,1} & N'_{nf,z,1} & N'_{nt,z,1} & l'_{b,z,1} & r'_{b,z,1} \\ N'_{of,z,2} & N'_{ot,z,2} & N'_{nf,z,2} & N'_{nt,z,2} & l'_{b,z,2} & r'_{b,z,2} \\ \vdots & \vdots & \vdots & \vdots & \vdots & \vdots \\ N'_{of,z,m} & N'_{ot,z,m} & N'_{nf,z,m} & N'_{nt,z,m} & l'_{b,z,m} & r'_{b,z,m} \\ \vdots & \vdots & \vdots & \vdots & \vdots & \vdots \\ N'_{of,z,l} & N'_{ot,z,l} & N'_{nf,z,l} & N'_{nt,z,l} & l'_{b,z,l} & r'_{b,z,l} \end{bmatrix} \quad (5.37)$$

where  $m$  is the number of traction branches in zone  $z$  after eliminating all traction branches that include buses, and  $l$  is the number of traction branches in zone  $z$ , which do not have active buses, plus the new constructed traction branches.

### 5.2.3 DC Power Flow

The steady-state solution of an electrical power network is commonly computed using a power flow calculation. Because of the non-linear formulation of the power flow equations, an iterative solution is required [139–149]. The popular DC power flow, that is utilised in standard AC power system calculations, is a linearisation of the non-linear AC power flow equations [150] and is unlike the *DC power flow* utilised in DC system calculations. Although it is possible to implement AC power flow methods to DC power systems, there are significant distinctions to consider. Analytical approaches like Gauss-Seidel (GS), Newton-Raphson (NR), or Backward-Forward (BF) sweeps are often used to solve *DC power flow* problems [151–160]. The *DC power flow* equations are non-linear, non-affine, and non-convex. Furthermore, the state variables are volts rather than angles, which are missing in DC networks.

This section explains how the *DC power flow* equations are developed and utilized to determine the steady-state operating conditions of the traction network. Generally, the primary purpose of a power flow approach is to identify the node voltages and the flow of power through system branches with given injected and consumed powers of every single node.

The mathematical formulation of a DC traction network may be simplified due to the absence of reactive power and voltage angle. As shown in Equation 5.10, two variables, i.e., injected power ( $P$ ) and node voltage ( $U$ ), are required to identify the traction network steady-state. Equivalently, one of Equation 5.1 variables should be specified for each traction node to solve the power flow equation and determine the other variable. There are three types of traction nodes that are grouped according to the variable ( $P$  or  $U$ ) they provide, namely: constant voltage, constant power, and passive nodes. Constant voltage nodes denote the traction-substations, which serve as the primary power supply for the traction network. However, the traction-substations are expected to maintain traction network nominal voltage  $U_n$  and provide enough power to ensure the system stability; thus, the voltage ( $U$ ) values are specified for constant voltage nodes. Conversely, the power ( $P$ ) values are specified for constant power nodes, and therefore, trolleybuses and battery-trolleybuses, as well as PVs, EVCSs, and BSPSs, are examples of constant power nodes. In this context, any node that does not provide or absorb power is considered a passive node.

Each TNZ is modelled as a set of nodes  $N_{tn} = N_{zn,z} = \{1, 2, 3, \dots, n_{et,z}\}$  (see Equation 5.12), which is separated into three subsets, i.e.,  $N_{tn} = \{PC, PA, VC\}$ , based on the type of the traction node, i.e., constant voltage ( $VC$ ), constant power ( $PC$ ), and passive node ( $PA$ ). In order to compute a reliable DC power flow calculation, it is essential to have at least one constant voltage node ( $|VC| \geq 1$ ) and one constant power node ( $|PC| \geq 1$ ) [151].

To solve Equation 5.10, a simplified version of the standard Newton-Raphson (NR) power flow calculation is adapted to be utilised for DC networks. Instead of commonly applied power mismatches, the utilised method uses non-linear current mismatch equations to reduce overall

equation complexity. With identical convergence properties, the *Simplified Newton-Raphson* (SNR) approach takes less time to execute than the standard NR method, which saves computation time [161].

The non-linear mismatch current equation for traction node  $k$ , based on Equations 5.9 and 5.10 as well as the Tellegen's theorem [162], can be expressed as follows:

$$\Delta I_{z,k} = \frac{P_{z,k}}{U_{z,k}} - \sum_{i=1}^n G_{z,ki} \cdot U_{z,i} = 0, \quad n = n_{et,z} \quad (5.38)$$

or in vector form

$$\Delta \mathbf{I}_z = \mathbf{P}_{t,z} \oslash \mathbf{U}_{t,z} - \mathbf{G}_{t,z} \cdot \mathbf{U}_{t,z} \quad (5.39)$$

where  $\mathbf{P}_{t,z}$  is the vector power,  $\mathbf{U}_{t,z}$  is the vector voltage,  $\mathbf{G}_{t,z}$  is the conductance matrix, and  $\Delta \mathbf{I}_z$  is the calculated mismatch current, all of which represent traction network zone  $z$ .

When all of the unknown node voltages  $\mathbf{U}_{t,z}$  are successfully gained, the mismatches will be equal to zero,  $\Delta I_{z,k} = 0$ . Equation 5.38 must be expanded using Taylor series in order to determine a set of voltage solutions using the NR method [161].

$$\Delta I_{z,k} = \sum_{\substack{i=1 \\ i \neq VC}}^n \frac{\partial \Delta I_{z,k}}{\partial U_{z,i}} \cdot \Delta U_{z,i}, \quad n = n_{et,z} \quad (5.40)$$

As the constant voltage nodes  $VC$  control the traction network voltage and the constant power nodes  $PC$  control the injected power, a compact matrix form used to update the mismatches current can be expressed as in Equation 5.41.

To simplify notation, the TNZ slack nodes (constant voltage nodes  $VC$ ) are excluded, while the constant power and passive nodes, i.e.,  $PP = PC \cup PA$ , are the defined mismatches currents. Thus, the vector form of Equation 5.40 can be defined as shown below:

$$[\Delta I_{z,PP}] = [J][\Delta U_{z,PP}] \quad (5.41)$$

The Jacobian matrix  $[J]$  from Equation 5.41 (same from Equation 5.40) may thus be constructed in a way identical to that of the normal NR approach, and their elements can be defined as follows:

$$\frac{\partial \Delta I_{z,k}}{\partial U_{z,i}} = \begin{cases} G_{z,ki} & , \quad k \neq i \\ G_{z,ii} + \frac{P_{z,k}}{U_{z,k}^2} & , \quad k = i \end{cases} \quad (5.42)$$

or in vector form

$$[J] = \mathbf{G}_{z,pp} \quad (5.43)$$

$$\text{diag}([J]) = \text{diag}(\mathbf{G}_{z,pp}) + ([P_{z,PP}] \oslash ([U_{z,PP}] \odot [U_{z,PP}])) \quad (5.44)$$

where  $\mathbf{G}_{z,pp}$  is zone  $z$  conductance matrix after removing the TNZ slack nodes ( $VC$ ) from  $\mathbf{G}_{t,z}$ , i.e.,  $\mathbf{G}_{z,pp} \subset \mathbf{G}_{t,z}$ . And the same for the other vectors that include only TNZ nodes  $PP$ , i.e.,  $[P_{z,PP}] \subset P_{t,z}$ ,  $[\Delta I_{z,PP}] \subset \Delta I_z$ , and  $[U_{z,PP}] \subset U_{t,z}$ .

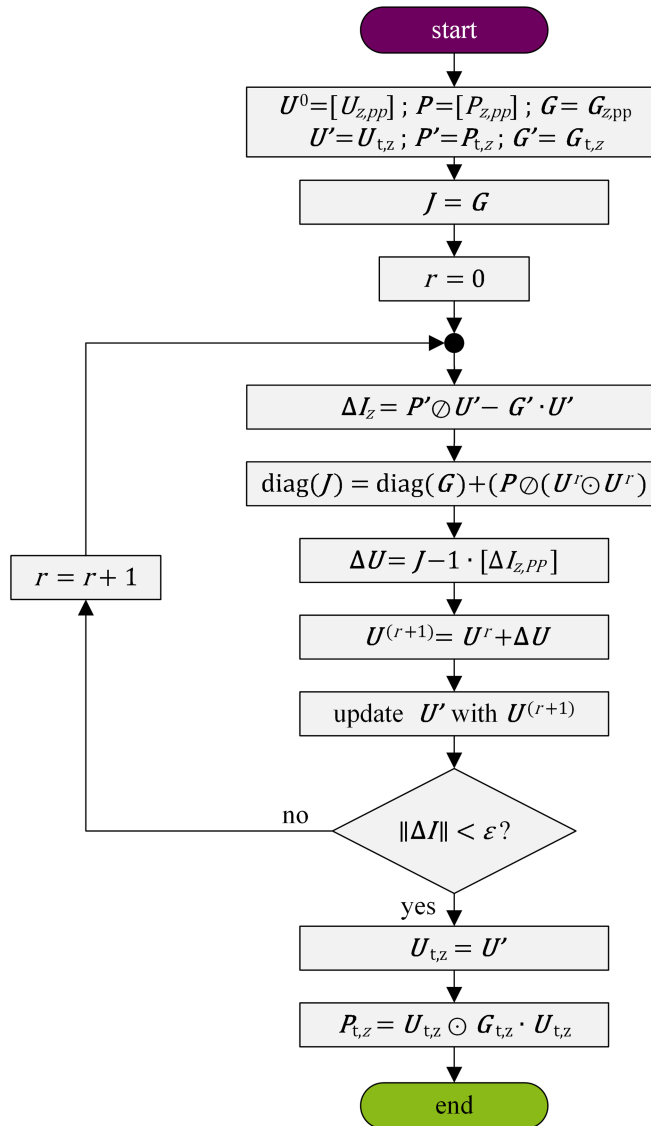


**Figure 5-3: Sequence of DC power flow with (Simplified Newton-Raphson).**

Equation 5.41 is repeatedly solved for  $\Delta U_{z,PP}$ , as shown in Equation 5.45. The voltage solution is successfully fulfilled if the norm of computed current mismatches  $\Delta I_{z,PP}$  is less than the specified mismatch tolerance  $\varepsilon$ , i.e.,  $\|\Delta I_{z,PP}\| < \varepsilon$ . If this is not the case, the voltage solution at the current iteration  $r$  must be adjusted for the following iteration  $r + 1$ , as seen in Figure 5-3

$$[\Delta U_{z,PP}] = [J]^{-1} [\Delta I_{z,PP}] \quad (5.45)$$

$$[U_{z,PP}]^{r+1} = [U_{z,PP}]^r + [\Delta U_{z,PP}]^r \quad (5.46)$$

The TNZ node power vector  $\mathbf{P}_{t,z}$  is calculated at the end after updating zone  $z$  voltage vector  $\mathbf{U}_{t,z}$  with the computed voltages  $[U_{z,PP}]^{r+1}$ . The TNZ slack nodes ( $VC$ ) have constant voltage and are not subject to the update.

#### 5.2.4 DC Power Flow with Unidirectional Traction Substations<sup>6</sup>

An adapted power flow method is proposed to compute traction network steady-state as well as buses behaviour during surplus power present in the TNZ. Traction substations are unidirectional; therefore, they prevent the surplus power produced by PV systems and decelerating buses from being transmitted to the AC network (see Section 4.1.4), the power flow is thus only in one direction that is from the medium voltage AC network to the low voltage (traction) DC network. Suppose the surplus power is not utilised by other moving buses, EVCSs, or BSPSs that are either too far away from the surplus power source (PV systems and decelerating buses) or have low power demands. In that case, the TNZ voltage rises at the source location. Following IEC 60850:2014-11 standard [13], the buses are protected by a *squeeze control* system ensuring that the traction network voltage remains within the permissible range (see Table 2-1) during bus decelerating by forcing the remaining power to dissipate in brake-resistor. Similarly, an *active power controller* in PV system is responsible for determining the amount of injected power [164]. When a PV voltage exceeds  $U_{\max 1}$ , the injected power of the PV system is dropped by a percentage level (active power curtailment) until the voltage value is reduced below the highest permanent voltage  $U_{\max 1}$  (see Table 2-1).

Throughout this section, the proposed algorithm steps are thoroughly explained. When the traction network has any unidirectional traction substation, standard power flow approaches fail to represent the actual steady-state of the TNZ. Given the presence of an active PV system or decelerating buses, and the fact that there is low power demand in the traction network, the traction substations will thus be calculated with negative power inputs (power flows from the traction DC network to the medium voltage AC network). To deal with this problem, a *three-block* process is developed to determine the actual traction network steady-state when there is surplus power in a TNZ.

In *block one* as shown in Figure 5-4, a power flow (see Section 5.2.3) is initiated after defining all inputs (constant voltage nodes  $VC'$ , constant power and passive nodes  $PP'$ , node powers  $\mathbf{P}_{in}$ , and node voltages  $\mathbf{U}_{in}$ ) of the traction network zone that is being calculated. The node voltages  $\mathbf{U}_{in}$  are set to the system nominal voltage  $U_n$ . All traction substation nodes are denoted as constant voltage nodes  $VC' = VC$  (slack nodes), while the other nodes are denoted as  $PP'$ , which indicates the constant power and the passive nodes ( $PP' = PC \cup PA$ ). The node power array  $\mathbf{P}_{in}$  denotes injected and absorbed power for  $PP'$ . Power flow calculations are evaluated to ensure that all traction substation nodes  $VC'$  have positive power values. If a negative power is identified, the

<sup>6</sup> The work of this section is published in [163] by the author of this thesis

corresponding traction substation with negative power ( $\forall i \in VC': P_{\text{cal},i} < 0$ ) will be modified as passive node and its power is set to zero, as shown below:

$$PP'^{(\text{new})} = PP' \cup \{i | \forall i \in VC': P_{\text{cal},i} < 0\} \quad (5.47)$$

$$VC'^{(\text{new})} = VC' \setminus \{i | \forall i \in VC': P_{\text{cal},i} < 0\} \quad (5.48)$$

where  $PP'^{(\text{new})}$  and  $VC'^{(\text{new})}$  represent the new constant power and passive nodes, and constant voltage nodes, respectively. The values of  $PP'$  and  $VC'$  are subsequently replaced by the new node sets  $PP'^{(\text{new})}$  and  $VC'^{(\text{new})}$  values.

When all traction substations are eliminated  $VC' = \emptyset$ , the simulation will proceed into *block two*. Otherwise, new  $VC'$  and  $PP'$  are defined, i.e.,  $PP' = PP'^{(\text{new})}$  and  $VC' = VC'^{(\text{new})}$ , and a new power flow is sequentially executed. When there is no more traction substation with negative calculated powers ( $\forall i \in VC': P_{\text{cal},i} < 0$ ), the cycle of *block one* is ended. The calculated voltages at  $PP'$  are evaluated for any violations ( $\forall i \in PP': U_{\text{cal},i} \geq U_{\text{max}1}$ ). If all voltages are under the highest permanent voltage  $U_{\text{max}1}$  (see Table 2-1), the approach concludes, and the TNZ steady-state is determined; otherwise, *block three* will begin its cycle.

Given the possibility of eliminating all constant voltage nodes  $VC' = \emptyset$  throughout *block one* cycle, the power flow calculation (see Section 5.2.3) cannot converge properly since no slack node is identified. It is essential to solve the problem with the approach shown in *block two*. Since all traction substations are being converted to constant power nodes  $PP'$ , new constant voltage nodes (slack nodes) must be established, as previously stated.

It is possible to utilise decelerating bus and PV system nodes as the new constant voltage nodes  $VC'$ . Their initial voltage value will be set to  $U_{\text{max}1}$  (see Table 2-1). As shown in Figure 5-4, redefining the system nodes and determining their initial values are executed at the beginning of *block two* and is computed as follows:

$$VC' = \{i | \forall i \in PP': P_{\text{in},i} > 0\}, k = |VC'| \quad (5.49)$$

$$PP'^{(\text{new})} = PP' \setminus VC' \quad (5.50)$$

and

$$[U_{\text{in},i}] = U_{\text{max}1} \quad (5.51)$$

$$P'_{\text{in}} = P_{\text{in}} \quad (5.52)$$

$$[P'_{\text{in},i}] = 0, \quad i = VC' \quad (5.53)$$

The value of  $PP'$  is subsequently replaced by the new node set  $PP'^{(\text{new})}$  value, i.e.,  $PP' = PP'^{(\text{new})}$ , and  $k$  is the count of the new constant voltage nodes  $VC'$ .

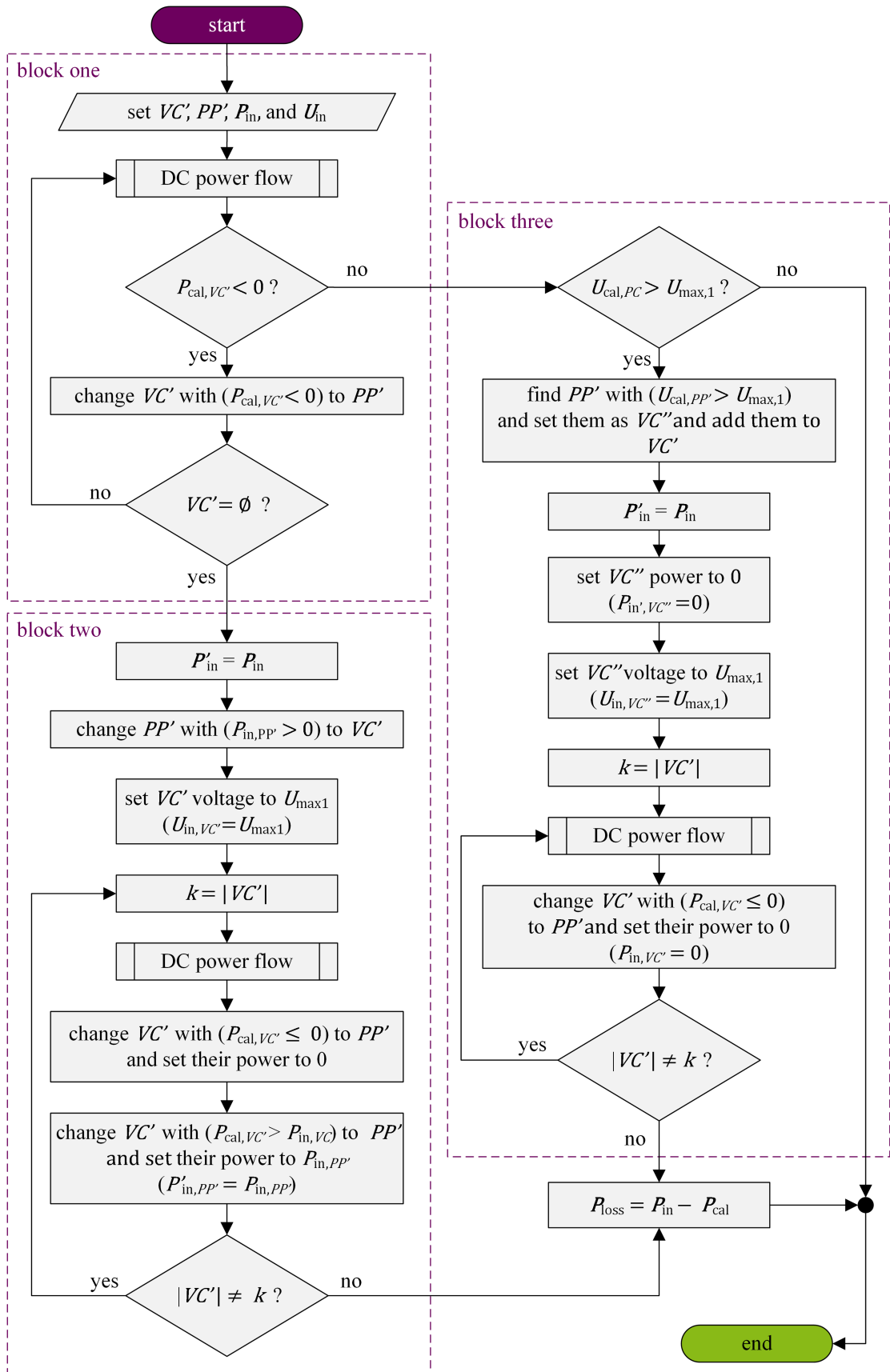


Figure 5-4: Sequence of DC power flow with unidirectional traction substations.

This approach makes it possible to calculate voltage rises when there are surplus power and unidirectional traction substations in a TNZ. With the new defined  $VC'$  (see Equation 5.49), a new power flow is executed. The calculated power ( $P_{cal,i} \Leftrightarrow i \in VC'$ ) is evaluated; whenever, a negative or zero power is computed the corresponding constant voltage node ( $i \in VC'$ ) will be modified as passive node and its power is set to zero, as defined in Equations 5.47 and 5.48.  $VC'$  is subjected to a second check to ensure that no calculated powers ( $P_{cal,i} \Leftrightarrow i \in VC'$ ) are more than their actual injected powers ( $P_{cal,i} \leq P_{in,i} \Leftrightarrow i \in VC'$ ). In cases of high demand,  $VC'$  with greater demand is reset back as  $PP'$  and retains the initial injected power, as shown below:

$$[P'_{in,i}] = P_{in,i}, \quad \forall i \in VC': P_{cal,i} \geq P_{in,i} \quad (5.54)$$

and

$$PP'^{(new)} = PP' \cup \{i | \forall i \in VC': P_{cal,i} \geq P_{in,i}\} \quad (5.55)$$

$$VC'^{(new)} = VC' \setminus \{i | \forall i \in VC': P_{cal,i} \geq P_{in,i}\} \quad (5.56)$$

The values of  $PP'$  and  $VC'$  are subsequently replaced by the new node sets  $PP'^{(new)}$  and  $VC'^{(new)}$  values, i.e.,  $PP' = PP'^{(new)}$  and  $VC' = VC'^{(new)}$ . In the event of a forced change in node types ( $VC'$  to  $PP'$ ) and  $|VC'| \neq k$ , *block two* cycle will be repeated with  $k$  been updated with the count of the new constant voltage nodes ( $k = |VC'|$ ); otherwise, the final power results  $P_{cal}$  is compared with the original power array  $P_{in}$ , and as shown in Equation 5.57 the difference between them  $P_{loss}$  denotes the wasted powers.

$$P_{loss} = P_{in} - P_{cal} \quad (5.57)$$

After the outcome of *block one* cycle, the calculated voltages at  $PP'$  are evaluated for any violations. When a voltage violation is discovered, *block three* will be started. Voltage rise at decelerating bus or PV system nodes may occur after eliminating traction substations with negative calculated powers ( $\forall i \in VC': P_{cal,i} < 0$ ). At the beginning of *block three*, constant power nodes with calculated voltages exceeding  $U_{max1}$  (see Table 2-1) will be converted into constant voltage nodes and added to the residual  $VC'$  set.

$$VC'' = \{i | \forall i \in PP': U_{cal,i} > U_{max1}\} \quad (5.58)$$

$$VC'^{(new)} = VC' \cup VC'', k = |VC'| \quad (5.59)$$

$$PP'^{(new)} = PP' \setminus VC'' \quad (5.60)$$

and

$$P'_{in} = P_{in} \quad (5.61)$$

$$[U_{in,i}] = U_{max1}, \quad i = VC'' \quad (5.62)$$

$$[P'_{in,i}] = 0, \quad i = VC'' \quad (5.63)$$



The value of  $PP'$  is subsequently replaced by the new node set  $PP'^{(\text{new})}$  value, i.e.,  $PP' = PP'^{(\text{new})}$ , i.e.,  $PP' = PP'^{(\text{new})}$  and  $VC' = VC'^{(\text{new})}$ , and  $k$  is the count of the new constant voltage nodes  $VC'$ .

The adjustment procedure for the node types' sets is defined by Equations 5.58-5.60. As stated in Equations 5.62 and 5.63, the voltage of the added  $VC''$  is set to  $U_{\text{max}1}$  and their power is set to zero. As shown in Figure 5-4, after defining the new  $VC'$  and  $PP'$  as well as the input voltage and power arrays, new power flow is initiated. The calculated power ( $P_{\text{cal},i} \Leftrightarrow i \in VC'$ ) is evaluated; anytime a negative or zero power is computed, the associated constant voltage node ( $i \in VC'$ ) will be modified as a passive node as described in Equations 5.47 and 5.48. As shown in Equation 5.63, the powers of the modified nodes have already been set to zero. The cycle of block three is repeated until no change in node types ( $VC'$  to  $PP'$ ) is detected. Finally, wasted powers  $P_{\text{loss}}$  are calculated as defined in Equation 5.57.

Using the proposed algorithm, it is now possible to calculate the amount of burnt energy that is dissipated into the brake-resistor, as well as the amount of curtailed energy that is reduced by active power controllers in PV systems. Moreover, it is now possible to determine the voltage of the traction network up to the maximum voltage level  $U_{\text{max}1}$  when no regeneration power is returned to the AC network.

### 5.2.5 Bus Power Control System<sup>7</sup>

To model the bus power control system, *three different approaches* have been implemented. With regard to the integrated overcurrent protection mechanism introduced in [83], the management of voltage drop is handled by reducing the consumed power when bus is in traction mode (see Section 2.3). Based on the functionality of this mechanism, all buses are modelled to maintain the consumption current in accordance with the voltage limits specified in IEC 62313:2009-04 [56]. The *first approach* is handled by using  $U_{t,z}$  (computed node voltages at time  $t$ ) and Equation 2.2. The power control system will regulate the trolleybuses and battery-trolleybuses maximum permeated motor powers (see Figure 5-5). Based on the bus voltage, a reduction factor  $\alpha_r$  (see Equation 2.3) is used to regulate the bus motor power consumption. The set  $Ib$  represents the operating buses indices, and the set  $ii$  represent the indices of buses with voltage  $U_b \leq \alpha \cdot U_n$ , where  $U_n$  is the traction network nominal voltage, and  $\alpha$  is the knee point factor (see Section 2.3). However, power flow convergence issues are caused by the substantial fluctuations in bus power consumption and location shifting. The solution of the traction network steady-state may not be achievable in certain circumstances, particularly those in which the power demands of some buses are very large.

<sup>7</sup> The work of this section is published in [165] by the author of this research



power reduction will be applied on that bus and its index is removed from the set of operating buses ( $Ib^{(new)} = Ib \setminus i$ ). Otherwise, the reduction process will be repeated until the DC power flow converge. When the reduced powers of all selected buses drop under the lower operating limit, the next bus with highest power divergence is selected and added to the set of selected buses  $ii$ . This process is also repeated until a convergent state is reached.

As previously mentioned, power consumptions or locations of certain buses may shift significantly in between simulation time steps. In this scenario, the simulation model may compute some buses with a voltage lower than  $U_{min2}$ , which is not permitted by system regulation and is effectively avoided in real life by the overcurrent protection mechanism incorporated in bus. The *third approach* is developed to cope with any uncounted voltage violations. After a successful DC power flow, as well as after a power reduction approach, bus voltages will be compared for any voltage violations (see Figure 5-5). Buses that have violated the voltage will be identified and their power progressively reduced until the bus voltage is increased above the  $U_{min2}$  threshold.

Finally, indices and new power values of buses that had a power reduction, granting a DC power flow converge or rather voltage adjustment, are saved and will be utilised to recalculate bus locations and the traction network steady-state, respectively (see Figure 5-2).

### 5.3 AC Network State Calculation

The voltage value of a traction substation (on the AC side of the substation) is affected by both the amount of the injected power into the traction network and the AC network steady-state, which implies that a various voltage – not fixed to the traction network nominal voltage  $U_n$  – could appear on the DC side of the traction substation. Thus, each traction substation on the traction network could have a different voltage value. This voltage difference between the traction substation will modify the load distribution on the traction network as well as the voltages at load and supply nodes, i.e., trolleybuses, battery-trolleybuses, PV systems, EVCSs, and BSPSs.

All of these considerations lead to the conclusion that when the medium voltage AC network is considered in the electric model, the determining of the traction network steady-state will be more realistic.

#### 5.3.1 AC Power Flow

The AC power flow method models the nonlinear relation between power injections, power demands, as well as node voltages and angles, with regard to the network topology. The mathematical description of the AC network can be formulated using several methods; however, nodal voltage method, which is based on Kirchoff's current law, is generally utilised for power system analyses. The topology can be described by the  $N \times N$  nodal admittance matrix  $Y_{ac}$  that is computed, as in Equation 5.64, from the incidence matrix  $K$  and the diagonal matrix constituted

by the primitive admittance matrix  $\mathbf{Y}_{ac,B}$ . The diagonal elements of the matrix  $\mathbf{Y}_{ac,B}$  represents the self-admittances and off-diagonal elements of the matrix  $\mathbf{Y}_{ac,B}$  represents the mutual admittances of the AC branches [126].

$$\mathbf{Y}_{ac} = \mathbf{K} \cdot \mathbf{Y}_{ac,B} \cdot \mathbf{K}^T \quad (5.64)$$

It is possible to identify an electric network's topology just by using an incidence matrix. Incident matrix  $\mathbf{K}$  is independent of the particular values of the branch parameters and has only three possible values, i.e., if  $k_{ij}$  is an element in  $\mathbf{K}$  then  $k_{ij} \in \{-1,0,1\}$ . The numbers of rows in the incidence matrix correspond to network node numbers, while the numbers of columns correspond to its branch numbers. Branch current directed away and toward a node are represented by  $k_{ij} = 1$  and  $k_{ij} = -1$ , respectively. Otherwise,  $k_{ij} = 0$  indicates no contact between the node and branch. The row numbers of the non-zero elements ( $k_{ij} = 1$  and  $k_{ij} = -1$ ) in each column (only two in each column) represent the ending node numbers of the relevant branch [138].

The nodal voltage vector  $\mathbf{U}_{ac}$  and the nodal current vector  $\mathbf{I}_{ac}$  form a set of nodal equations that can represent an electric AC network (see Figure 4-3) steady-state as follows:

$$\mathbf{I}_{ac} = \mathbf{Y}_{ac} \cdot \mathbf{U}_{ac} \quad (5.65)$$

It is possible to determine the power flow in an AC-network, which is represented by a non-linear set of equations, by using an iterative solution. The Newton-Raphson and Gauss-Seidel methods, for example, are practical approaches for the power flow calculation. In this simulation model, the Newton-Raphson method is used to calculate power flow in AC network due to its excellent convergence capabilities as well as the low number of iteration cycles [126]. In steady-state operation, node voltages are dependent on the balance between the combined powers being injected into an AC node (active  $\mathbf{P}_{ac,inj}$  and reactive  $\mathbf{Q}_{ac,inj}$  power) and calculated powers at the same node (active  $\mathbf{P}_{ac,calc}$  and reactive  $\mathbf{Q}_{ac,calc}$  power).

$$\mathbf{P}_{ac,inj} - \mathbf{P}_{ac,calc} = \Delta \mathbf{P}_{ac} = 0 \quad (5.66)$$

$$\mathbf{Q}_{ac,inj} - \mathbf{Q}_{ac,calc} = \Delta \mathbf{Q}_{ac} = 0 \quad (5.67)$$

Following a Taylor development, the Newton-Raphson method is used to solve Equations 5.66 and 5.67 iteratively for a given voltage reference at the slack node and other node powers  $\mathbf{P}_{ac,inj}$  and  $\mathbf{Q}_{ac,inj}$ . The nodal voltage  $\mathbf{U}_{ac}$  is divided into the voltage magnitude  $|\mathbf{U}_{ac}|$  and the voltage angles  $\boldsymbol{\delta}$  for this purpose. With each iteration step  $k$ , the power equations are linearised and approximated to the solution until the convergence limit is reached. As shown in Equation 5.68, The solution is calculated with each iteration step  $k$  by linearising the power equations until the convergence limit is reached.

$$\begin{bmatrix} \Delta \mathbf{P}_{ac}^{(k)} \\ \Delta \mathbf{Q}_{ac}^{(k)} \end{bmatrix} = \mathbf{J}^{(k)} \cdot \begin{bmatrix} \Delta |\mathbf{U}_{ac}|^{(k+1)} \\ \Delta \boldsymbol{\delta}^{(k+1)} \end{bmatrix} \quad (5.68)$$

$$J = \begin{bmatrix} \frac{\partial \Delta P_{ac}}{\partial \Delta \delta} & \frac{\partial \Delta P_{ac}}{\partial \Delta |U_{ac}|} \\ \frac{\partial \Delta Q_{ac}}{\partial \Delta \delta} & \frac{\partial \Delta Q_{ac}}{\partial \Delta |U_{ac}|} \end{bmatrix} \quad (5.69)$$

A new Jacobi matrix  $J$ , is computed with each iteration step  $k$ . In order to calculate the power flow during that operational point, an approximation approach is utilised with the help of a sensitivity matrix, which is defined as the inverse of the Jacobi matrix  $J^{-1}$ . However, the inversion of large matrices is time consuming. Particularly in medium-voltage grids, where the number of nodes might exceed several hundred, this results in a significant amount of computing work, which grows exponentially with the size of the electric network [126].

The AC network model thus receives the voltage at the slack node (MV busbar voltage at the HV/MV transformer  $U_{n,ac}$ ) and the active and reactive powers ( $P_{ac,sch}$  and  $Q_{ac,sch}$ ) as input variables  $\mathbf{v}$ . The output variables  $\mathbf{r}$  of the AC network are the node voltages and branch currents ( $U_{ac}$  and  $I_{ac,B}$ ), where the voltage values at the traction substation nodes are the focus of the AC power flow task (see Figure 5-6).

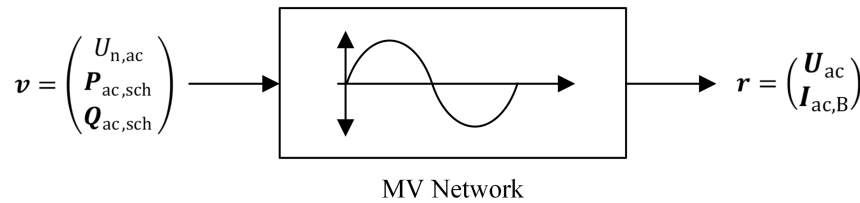


**Figure 5-6:** AC medium-voltage network schematic representation (linearisation approximated by a proportional element). (Adapted from [126])

### 5.3.2 AC-DC Power Flow

For traction system modelling, a unified AC-DC power flow has been the primary goal of many studies [166–171]. However, the inclusion of a heavily meshed traction network model, as well as the incorporation of unidirectional traction substations in the traction network, present a difficulty with the previously mentioned unified AC-DC power flow approaches.

Here, an approach for sequential AC-DC power flow is explained, in which the complete electric network is simulated at the same time and the features of the traction network are maintained. As shown in Figure 4-3, the traction substations are the primary parts that are shared by both AC network and DC traction networks. Traction substations play a critical part in the development of a sequential AC-DC power flow. A traction substation, as previously stated in Section 4.1.4, consists of traction transformer as well as rectifier. Traction substation is subjected to internal voltage drop that is caused by three core elements: rectifier resistance, traction transformer resistance, and traction transformer reactance [172]. In this work, the DC traction network is modelled and simulated separately from the AC network, and to simplify the calculation and the connection between the two networks, the total internal resistance of the traction substation is

excluded. The basic relationship between the AC input voltage and the DC output voltage of the traction substation can be defined as:

$$U_{t,p} = \frac{U_{ac,r}}{N_{tps,r}} \quad (5.70)$$

where  $N_{tps} = \frac{N_p}{N_s}$  is the traction transformer turns ratio with number of turns  $N_p$  on the primary side and number of turns  $N_s$  on the secondary side,  $r = \{tps_2\}$  (see Equation 4.4) is the set of traction substation node Ids (AC side), and  $p = \{tps_1\}$  (see Equation 4.4) is the set of traction substation node Ids (DC traction side).

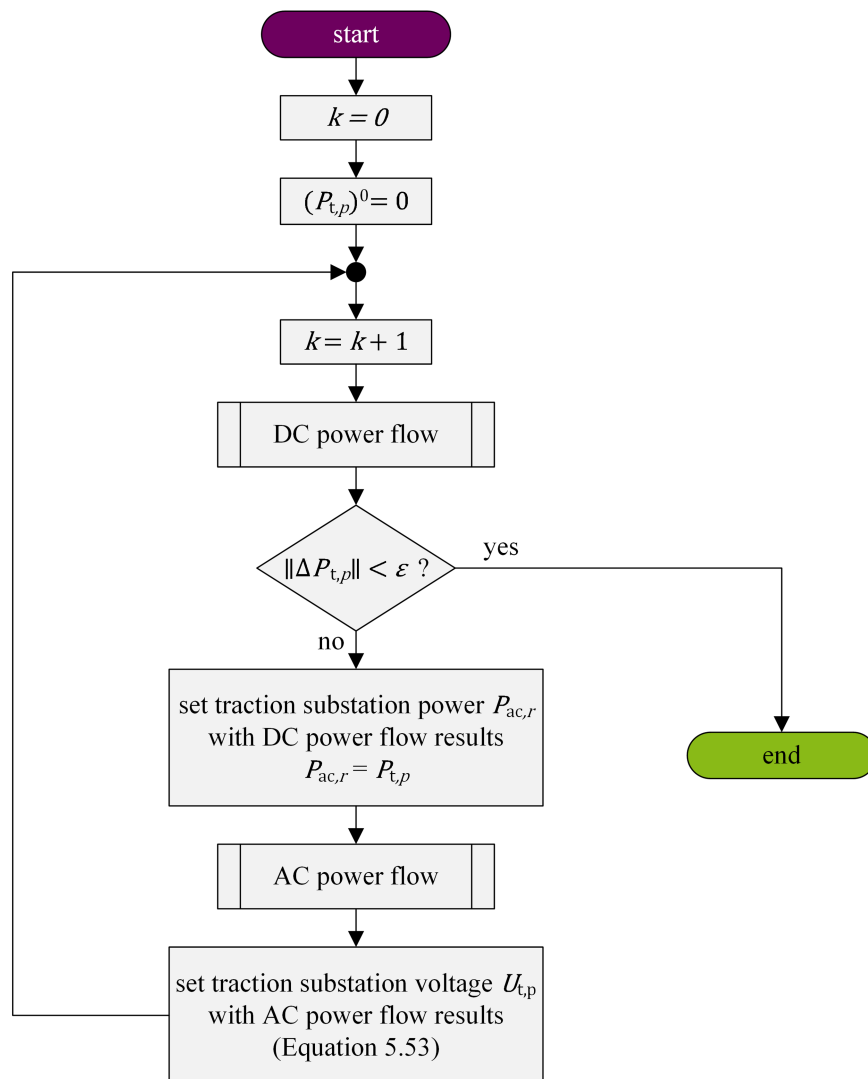


**Figure 5-7:** Sequence of sequential AC-DC power flow.

It is necessary to maintain a constant balance between input and output powers of the traction substations in order to establish a relationship between the AC and DC traction networks at any given time. When losses are not taken into account, the traction substation active AC power equals the DC power as follows:

$$P_{ac,r} = P_{t,p} \quad (5.71)$$

Following the calculation of the powers of TBs, BTBs, PV systems, EVCSs, and BSPSs, the steady-state of the traction network is computed as described in Section 5.2. Active powers at AC side of the traction substations are computed using Equation 5.71 depending on the outcomes of the DC power flow calculation (see Figure 5-7). After that, the calculation of the AC power flow can be performed (see Section 5.3.1). As a consequence of the AC power flow results, the new voltage values for each traction substation, which is calculated using Equation 5.70 are utilised with the new DC power flow.

AC and DC power flows are iterated (see Figure 5-7) until the norm of computed power mismatches  $\|\Delta P_{t,p}\|$ , i.e.,  $\Delta P_{t,p} = (P_{t,p})^k - (P_{t,p})^{k+1}$ , is less than the specified mismatch tolerance  $\varepsilon$ . As soon as an optimal solution for the traction network is determined, the simulation process continues although it reaches its conclusion.





## 6 Evaluation and Validation of the Simulation Model

Solingen's trolleybus system serves as the guide to this work. To this day, Solingen is known for owning Germany's largest trolleybus system. As of 2016, 50 electrically propelled trolleybuses equipped with auxiliary combustion engines have been operating six bus routes. Since 2018, a new, 7<sup>th</sup> bus route, which is operated by four BOBs, is introduced. The city traction network includes 22 unidirectional traction substations that are responsible for powering around 102 km of overhead contact wires; additionally, a separate traction substation is added at the new bus route terminal to charge BOB's on-board batteries during the dwelling times, although the BOB's on-board batteries are also charged during the bus motion under existing overhead contact wires (OHCWs). Solingen trolleybus system runs on a DC with  $U_n = 660$  V provided by the 22 unidirectional traction substations that link the DC network to the upstream AC network ( $U_n = 10$  kV) [14, 63]

### 6.1 Adapting the Input Parameters

For the objective of this simulation model, the spatial data, technical specifications, and the means necessary for the modelling and analysing of a trolleybus system are outlined in the following sections.

#### 6.1.1 GIS Data

Use of geographical information system (GIS) for modelling mobility and transportation projects has received considerable interest in recent years [173–175]. Modelling the trolleybus system requires the integration of spatial and non-spatial data, which may be accomplished using GIS software such as *QGIS* (open-source software [176, 177]). By integrating *OpenStreetMap* [178] and *Google Maps* [179], georeferencing important points in the trolleybus system is thus made possible; furthermore, the elevation data of the terrain are determined from the *Digital Terrain Map Model* (DTMM) of the target city (see Figure 11-1). Implementing trolleybus system in *QGIS* is accomplished by creating *shapefiles* of type *point* to represent the traffic nodes and the traction nodes and of type *line* to represent the traffic branches and traction branches. Actually, the *point features* in the road network are picked all over the trolleybus and BOB routes realising all locations (node types) defined in Section 3.1.1, just as the *point features* in the traction network are picked to denote the traction network topology and realise the node types defined in Section 4.1.2. Here it is worth mentioning that *line features* in both traffic- and traction network are created between consecutive *point features* in the traffic- and traction network, respectively.

The *attribute fields* of the road network point features are defined based on elements of the traffic node set (see Equation 3.2); likewise, *attribute fields* of the traction network point features are defined based on elements of the traction node set (see Equation 4.1). In fact, *QGIS* build-in tools

help with filling the spatial data of the point features. For instance, the *altitude* field, for road network point features, is determined using the DTM of Solingen and the location of the point feature (traffic node). However, the *x-* and *y-coordination* fields for both traffic- and traction network point features are determined based on the coordination system and the location of the point feature.

Equations 3.4 and 4.3 are used to define the *attribute fields* of the line features (traffic- and traction branches) in the road network and traction network, respectively. As utilized for the point features, QGIS build-in tools are used to determine the lengths of the line features in both traffic- and traction network.

After being modelled in QGIS, the Solingen trolleybus system can be seen in Figure 6-1 (A) and (B), where both traffic- and traction network are shown, respectively. It is remarkable that the total number of point and line features in the road network are 3908 and 4022 with total length 119.65 km, respectively; however, the total number of point and line features in the traction network are 377 and 626 thereof 103.27 km of overhead contact wires, respectively.

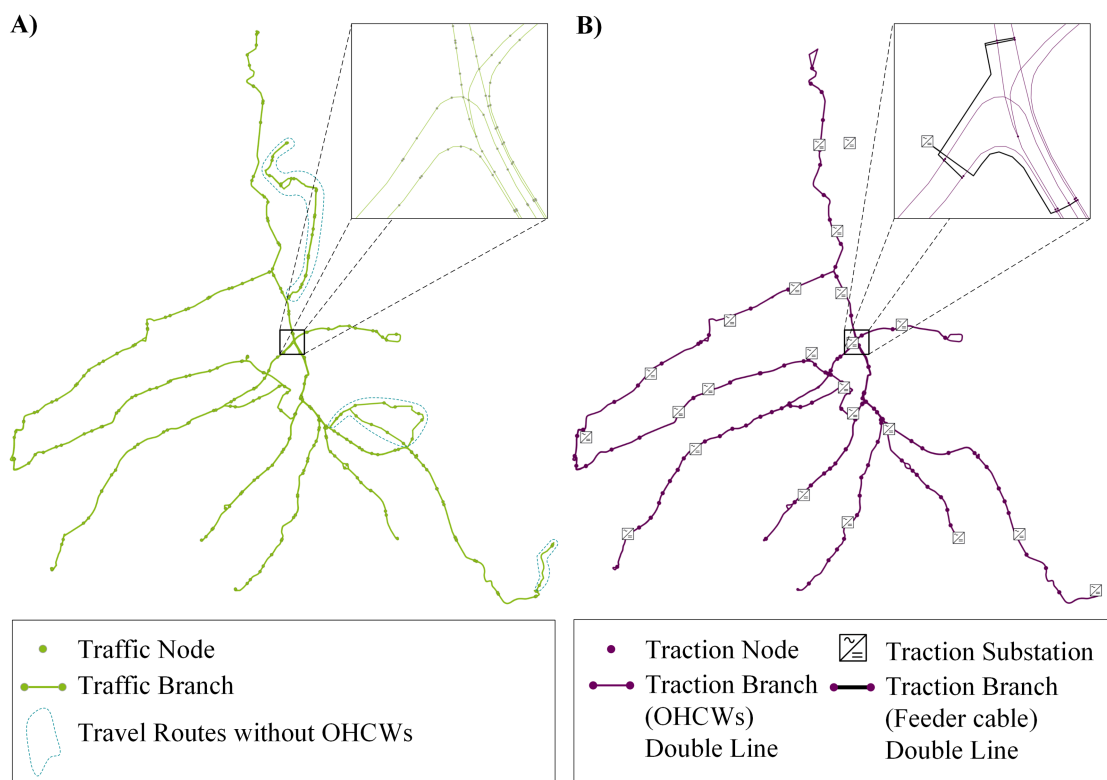


**Figure 6-1: Overview of Solingen trolleybus road and traction network topology.**

**A: Road network.**

**B: Traction network.**

As shown in Figure 6-1 (A), the traffic roads enclosed by the dashed turquoise line represent the travel routes without OHCWs. Accordingly, these parts from the road network are not represented in the traction network shown in Figure 6-1 (B).

The attribute fields of the road network point and line features (*traffic nodes* and *traffic branches*) as well as the traction network point and line features (*traction nodes* and *traction branches*) are exported into four individual CVS (comma-separated values) files which can be read by the simulation model and subsequently defined as Equations 3.2, 3.4, 4.1, and 4.3, respectively.

### **6.1.2 Bus Daily Timetable**

Two Excel spreadsheets [180] are used to describe the timetable of Solingen bus lines (681 to 686 and 695), in which, the daily schedules, with up to 50 trolleybuses and 4 BOBs, and the bus travel routes are defined. An illustrative example of the daily schedule as the bus travel route information is presented in Annex 11.3. The data, in the first Excel spreadsheet, include the daily schedules of all buses that serve the bus lines (681 to 686 and 695). Moreover, three individual daily schedules (worksheets) for workdays, Saturday, and Sunday/Holiday are included in the excel spreadsheet. However, the data of the daily schedules' file are structured in accordance with Equations 3.5, 3.6, and 3.10. The second Excel spreadsheet includes the information of the bus travel routes which is structured in accordance with Equations 3.7 and 3.8.

### **6.1.3 Trolleybuses and Battery-Trolleybuses**

The Solingen trolleybus system includes three models of trolleybuses and one model of BOB. The trolleybus fleet consists of 15 “Berkhof: Premier AT 18”, 15 “Carrosserie Hess: Swisstrolley 3 / BGT-N 2 C”, and 20 “Van Hool: AG 300 T” articulated buses. All 4 BOBs are “Solaris: Trollino 18.75” articulated buses [97]. The technical specifications of Solingen electric bus fleet (see Table 11-3 in Annex 11.4) are defined in an Excel spreadsheet. The specifications data realise the elements of Equation 3.43.

### **6.1.4 Traction Substations**

The number of traction substations that serve the Solingen traction system is 23 (including the new added traction substation at the terminal of bus line 695), which is divided between three traction zones. As shown in Figure 6-14, the 23 traction substations are divided as follows: 10 traction substations for the upper part of the network, 12 traction substations for the lower part of the network, and one traction substation at the terminal of bus line 695. The specifications of the traction substations (see Table 11-4 in Annex 11.5) are defined in an Excel spreadsheet, in which, the elements of Equation 4.4 are fulfilled.

### **6.1.5 Photovoltaic Systems**

PV systems are not present in the existing trolleybus system of Solingen. The integration of PV systems in the DC traction network is under study. 16 pre-exist PV systems, already connected to the AC MV network of Solingen, have the potential to be switched into the DC traction network. To implement the potential PV systems into the simulation model, elements of Equation 4.20

must be defined with the required data (see Table 11-5 in Annex 11.6). To define the required specifications for the PV systems, an Excel spreadsheet is used as input tool.

### 6.1.6 Electric Vehicle Charging Stations

The specifications of the EVCSs, which are planned to be implanted in the Solingen trolleybus system, are defined in Excel spreadsheet (see Table 11-6 in Annex 11.7) and structured in accordance with Equation 4.24.

### 6.1.7 Battery Storage Power Stations

An Excel spreadsheet (see Table 11-7 in Annex 11.8) is therefore needed to define the BSPSs' specifications which are planned to be used in the Solingen trolleybus system. These specifications are organised according to Equation 4.26.

### 6.1.8 General Input Data

To add more flexibility to the simulation model, an Excel spreadsheet with multiple worksheets is utilised. The date and starting time  $SM_{sd}$ , and duration  $SM_{int}$ , as well as the simulation time step  $\delta t$ , are all essential data of the simulation model. These data are included in one of the Excel worksheets and will be implemented by the simulation model to form Equations 2.4 to 2.11.

Other data that could be forced to override the default values or setting of the trolleybus system components are contained as *general input data*. For example, outside temperature  $T_o$ , bus interior temperature  $T_i$ , passenger crowding, and bus variety can be forced into the simulation model. Moreover, PV, EVCS, BSPS, and the DC traction network settings are configurable as well.

## 6.2 Simulation Model with Various Scenarios

This section aims to analyse the Solingen trolleybus system using the proposed simulation model; furthermore, the simulation result will be illustrated and evaluated. The proposed real-world trolleybus simulation model is coded and simulated using MATLAB [181]. The existing trolleybus system as well as the understudy new components, i.e., additional BTBs, PVs, EVCSs, and BSPSs specifications, are accessible via Excel spreadsheets (see Section 6.1). All input values for the Solingen trolleybus system are shown in Annex 11.

### 6.2.1 Bus Performance Against Travel Obstacles

To assess the effect of the traffic situation on the bus model (BM), three simulations with free, congested, and normal traffic are considered. The different traffic situations are realised within the BDTRM (see Section 3.3). The free traffic situation is modelled by omitting all rush hour intervals, which allows buses to operate at the maximum road speed limits as well as minimum stopping and dwelling times at traffic lights and bus stops. Conversely, the congested traffic situation is modelled by extending the rush hour intervals, which reduces the maximum road

speed limits, making the buses drive even slower during their trip. Furthermore, the stopping and dwelling times are increased. The third traffic situation (normal traffic) is modelled with the standard rush hour intervals at standard probability of dwelling at a traffic lights and bus stops in and outside the standard rush hour intervals. Likewise, the dwell time is also computed for the normal traffic situation as introduced in Section 3.3.

As shown in Figure 6-2 (A), which depicts the free traffic situation, buses from all eight bus lines (one bus operates on both lines 681 and 682 and the same applies for lines 685 and 686) arrive mostly on time or up to two minutes ahead of schedule. Nonetheless, there are cases where the bus arrives up to 17 minutes early. Considering this, a long dwell period is established between the inbound and outbound trips on the bus schedule. However, due to the congested traffic situation, buses swapping between lines 681 and 682 often has delays surpassed 40 minutes (see Figure 6-2 (B)). In a normal traffic situation (see Figure 6-2 (C)), there are still some delays, but they are no longer than 12 minutes, that is shown for buses swapping between lines 681 and 682. In contrast to congested traffic situation, being ahead of schedule occurs several times during the normal traffic situation, which on some bus lines exceeded 10 minutes.

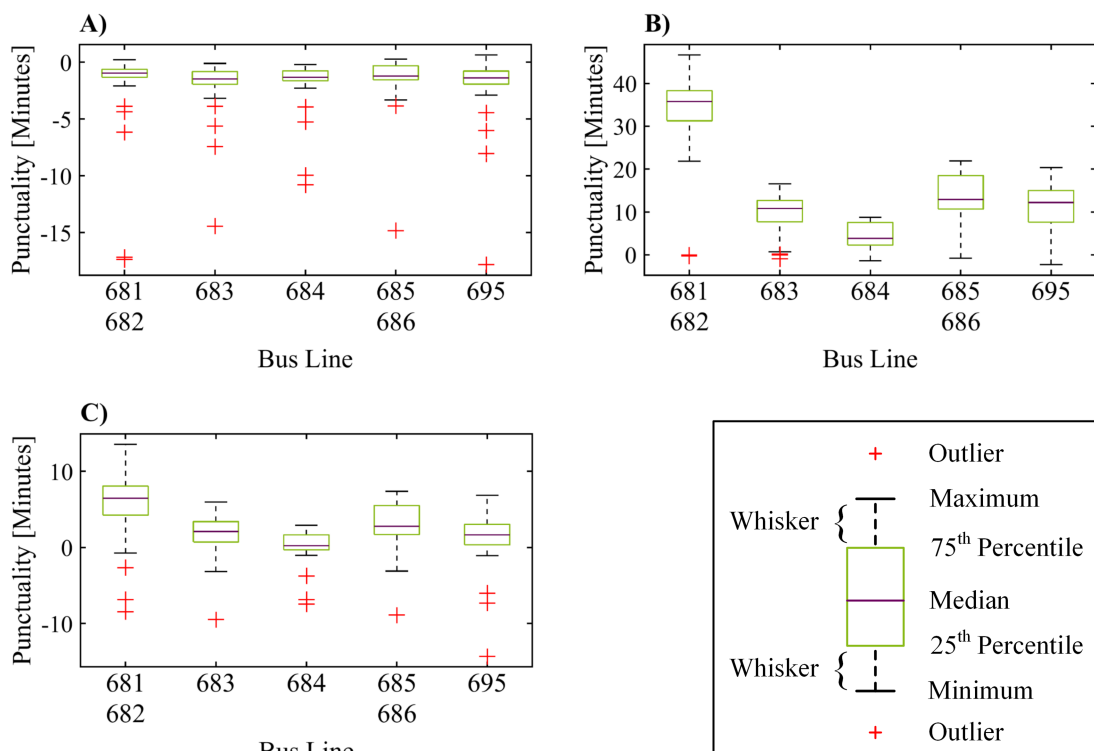


**Figure 6-2: Buses punctuality with respect to traffic situation. The simulation parameters are: Three traffic situations (free, congested, and normal), no HVAC, and only bus variety 3 (Annex 11.4).**  
**A: Free traffic.**  
**B: Congested traffic.**  
**C: Normal traffic.**

The topography of the travel routes effects the performance of the bus. Also, as shown in Figure 6-3, the traction power  $P_{TB}$  increases exponentially as bus speed and road slope increase (no deceleration power is considered). In consideration of the simulation results, the bus is

restricted to a specific speed on certain road slopes. As soon as the motor's maximum power  $P_M$  is reached, the bus's acceleration is capped at that moment, and it cannot go any faster. According to the simulation results, a bus requires around to  $P_{TB} = 250$  kW of electric power to travel  $v = 65$  km/h on a level road. It's also worth noting that the bus motor operates at its peak power at  $v = 20$  km/h on a 11% slope and  $v = 65$  km/h on a 2% slope.

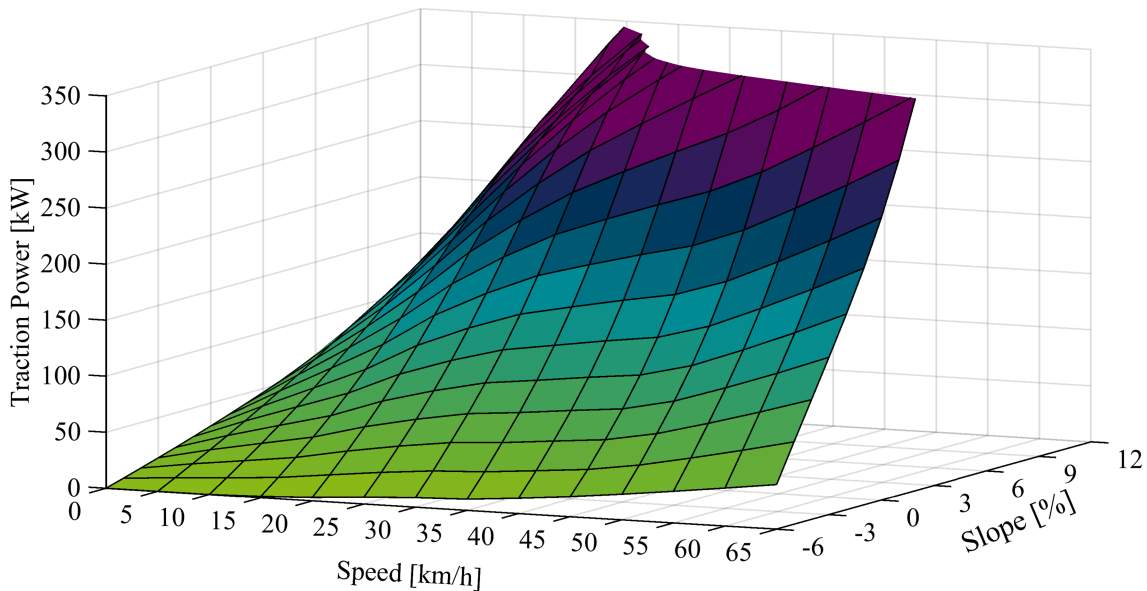


**Figure 6-3: Simulated bus power at different speeds and slopes. The simulation parameters are: free traffic situation, no HVAC, and empty buses from all bus variety (Annex 11.4).**

The surface plot of Figure 6-3 is based on several simulation outputs, in which, an empty bus and no power for HVAC is considered. Moreover, all simulations are conducted in a free traffic situation to avoid any speed limit restrictions.

## 6.2.2 Simulating with Innovative Features

The Solingen trolleybus system will be put under higher stress if innovative features like PV systems and EVCSs are integrated into the existing trolleybus system. As mentioned in Section 6.1.5, 16 pre-exist PV systems (connected to the MVAC network) are being looked at to connect directly to Solingen's traction network (see Annex 11.6). Furthermore, 18 EVCS locations are implemented in the simulation test (see Annex 11.7). The outside temperature is assumed to be between  $T_0 = 15$  °C and  $T_0 = 22$  °C. Thus, no HVAC power is included. Normal traffic volume on a workday is defined for this simulation as well as all four bus variety (see Annex 11.4) are included in this simulation test. The duration of the simulation test is 24 hours.

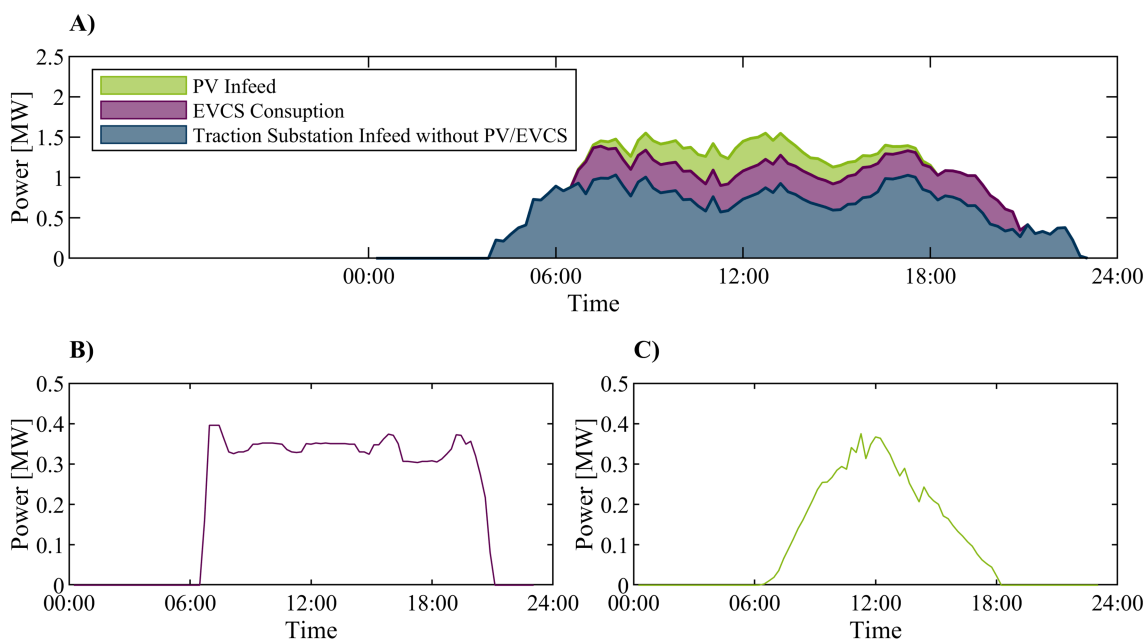


**Figure 6-4:** Solingen trolleybus system energy profiles with innovative features implemented in the system. The simulation parameters are: 16 PV systems (Annex 11.6), 18 EVCSs (Annex 11.7), no HVAC power, normal traffic for workday, and all 4 bus variety (Annex 11.4).  
**A:** Energy shares between system innovative features and the traction substations.  
**B:** Energy consumption of the implemented EVCSs.  
**C:** Energy produced by the implemented PV systems.

The simulation results can be seen in Figure 6-4. The consumed power of the 13 EVCSs is shown in Figure 6-4 (B) and the produced power from the 16 PV systems is shown in Figure 6-4 (C). Figure 6-4 (A) shows the total simulated power usage, where the light green area represents the energy contributed by the 16 PV systems. Thus, the PV systems have shifted the supply power of the traction substations and reduced their infeed power. In other terms, without the PV systems, more power is produced by the traction substations, so the blue area would be increased with the light green area. Over the course of 24 hours, the 18 EVCSs drew in the total energy shown in the purple area. Without solar PV systems and EVCSs, the infeed energy from the substations is shown as the blue area. The total infeed and consumed energy, as well as the energy lost by PV systems due to overvoltage protection, are all shown in Table 6-1.

**Table 6-1:** Simulation results of the energy shares of the implemented features and the existing traction substation as well as energy loss from PV systems. The simulation parameters are: 16 PV systems (Annex 11.6), 18 EVCSs (Annex 11.7), no HVAC power, normal traffic for workday, and with all 4 bus variety (Annex 11.4).

Energy	kWh
Substations Infeed	234.15
PV systems Infeed	47.26
EVCSs consumption	82.89
PV system lost	0.29

### 6.2.3 Several Day Simulation

The total power consumption in a trolleybus system depends on the number of operating buses and the power demands. The number of operating buses corresponds to the bus schedules. The TBSSM can simulate even for multiple days based on the input values in the simulation interval set (see Equations 2.4-2.11).

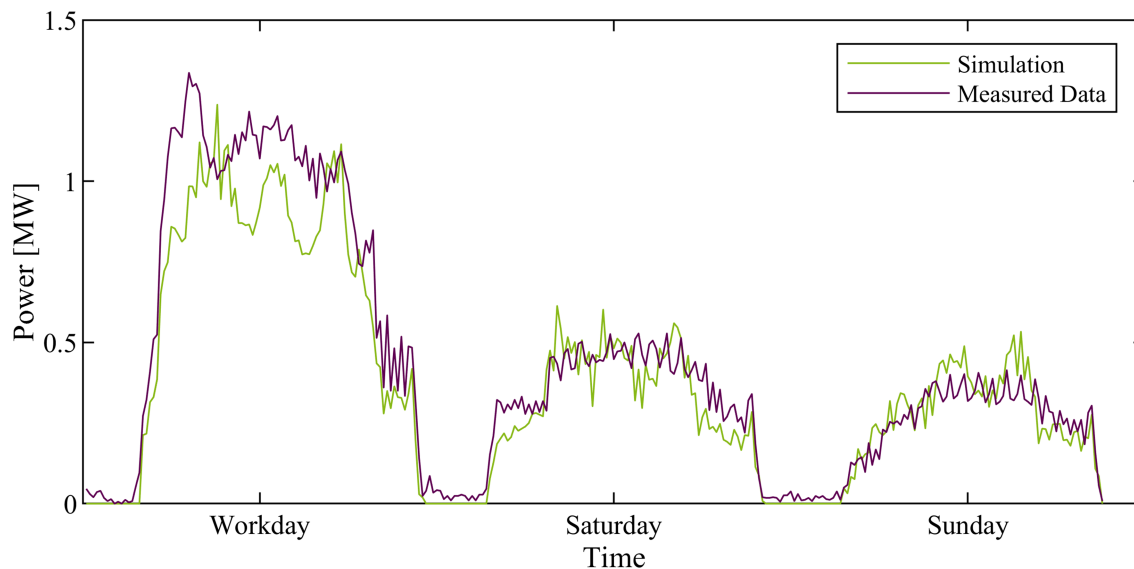


**Figure 6-5:** Total traction substation infeed power of the Solingen trolleybus system generated from a simulation of three different day types and compared to real measured logs. The simulation parameters are: normal traffic for three day types (workday, weekend, and public holiday), normal HVAC operation, and only the 3 TB variety (Annex 11.4).

As shown in Figure 6-5, three distinct bus schedules are simulated over the course of a three-day period. A real-world date, collected and provided by Solingen municipal utilities SWS<sup>8</sup>, are used to compare the simulation results. The simulated and measured data represent the infeed power of the 22 traction substations that power the Solingen trolley system (new added traction substation at the terminal of bus line 695 is not considered in this simulation test). Simulation results were averaged every 15 minutes to match the measured data since the simulation time step is 1 second and measurements were recorded every 15 minutes. The difference between the measurement date and the simulation results can be attributed to a possible difference between the bus timetable at the time of measurement and the bus timetable used in this simulation test, since the measurement data does not provide a precise bus timetable at the time of measurement. However, the simulation results for three different day types succeed in capturing the different power consumption during the different days.

### 6.2.4 Simulating Future Scenarios

It is necessary to do further research and analysis before expanding an existing trolleybus system. The TBSSM offers the necessary tools to evaluate the expansion of a trolleybus system with future

<sup>8</sup> In German, famous as: Stadtwerke Solingen



scenarios. Solingen's trolleybus system is evaluated in 2020, 2030 and 2050 with three different scenarios. The future trolleybus system (in 2030 and 2050) is expected to be expanding with more BTBs, bidirectional traction substations, PV systems, and EVCSs. Table 6-2 provides a summary of the present state of the trolleybus system and the future adjustments that are planned to be implemented in Solingen trolleybus system.

**Table 6-2: Number of the innovative features that are considered in the simulated scenarios.**

Scenario		2020	2030	2050
Traction Substation	Unidirectional	22	20	20
	Bidirectional	0	2	2
Buses	Trolleybuses	50	32	0
	Battery-Trolleybuses	0	36	100
Innovateve Features	EVCSs	0	10	10
	PV systems	0	1	1

Figure 6 shows the simulation results for the two potential future scenarios with the simulation of the existing system in 2020 and with measured data from 2016. The three simulation results as well as the measured data from 2016 represent the overall power consumption of the traction network. The total power is supplied by 22 traction substation and a single PV system (in 2030 and 2050 two unidirectional traction substations are replaced by bidirectional traction substations and the single PV system is integrated into the system). At this point it is worth mentioning that the simulation results as well as the measurement data are for the wintertime.

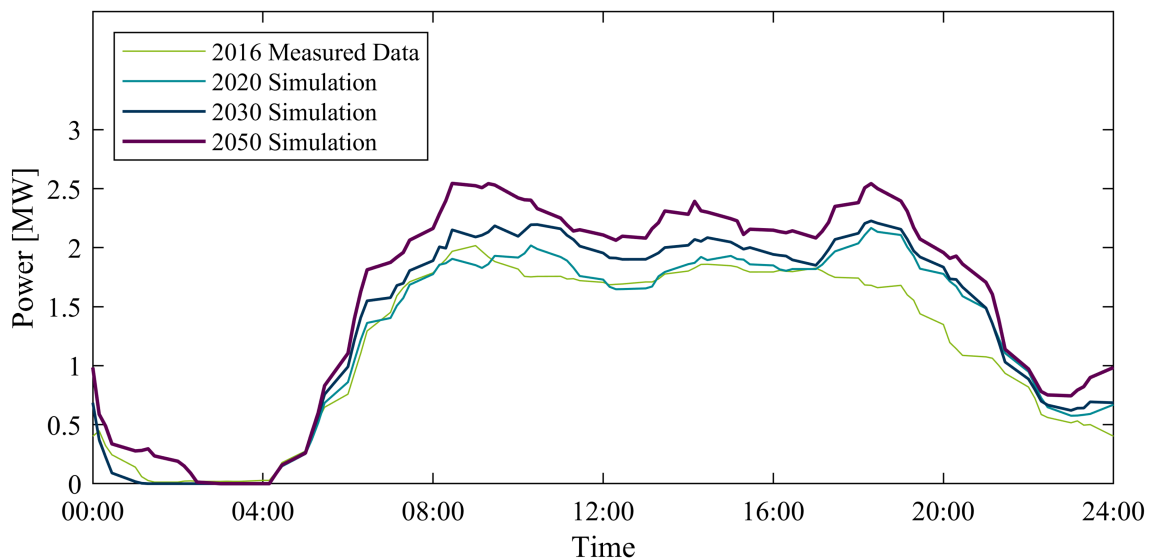


**Figure 6-6: Total traction substation infeed power of the Solingen trolleybus system from several simulation scenarios and real measured data. The simulation parameters are: normal traffic situation, normal HVAC operation for wintertime, all buses variety (Annex 11.4) considering Table 6-2, traction substation (Annex 11.5) considering Table 6-2, and PV systems from (Annex 11.6) and EVCSs from (Annex 11.7) considering Table 6-2.**

### 6.3 Quality and Accuracy of the Bus Movement

Additional assessment for the BM can be accomplished by comparing the power profile and state-of-charge progression of a BTB that is running on line 695 with those obtained from an actual driving test conducted on the same line [34]. Both simulated and test drive SOC progression are shown side by side in Figure 6-7 (A). Also, the SOC can be simulated with high accuracy using the trolleybus system simulation model and its base model (BM), and hence may be utilised reliably. Despite the delay in SOC progression shown by the test drive, which is due to a variety of reasons, such as congested traffic, roadworks, and the numerous pauses required to inspect the air conditioning system during the test drive. Figure 6-7 (B) shows the simulated SOC progression after compensating the waiting interval (increase the dwelling time at that stopping point) into the BDTRM.

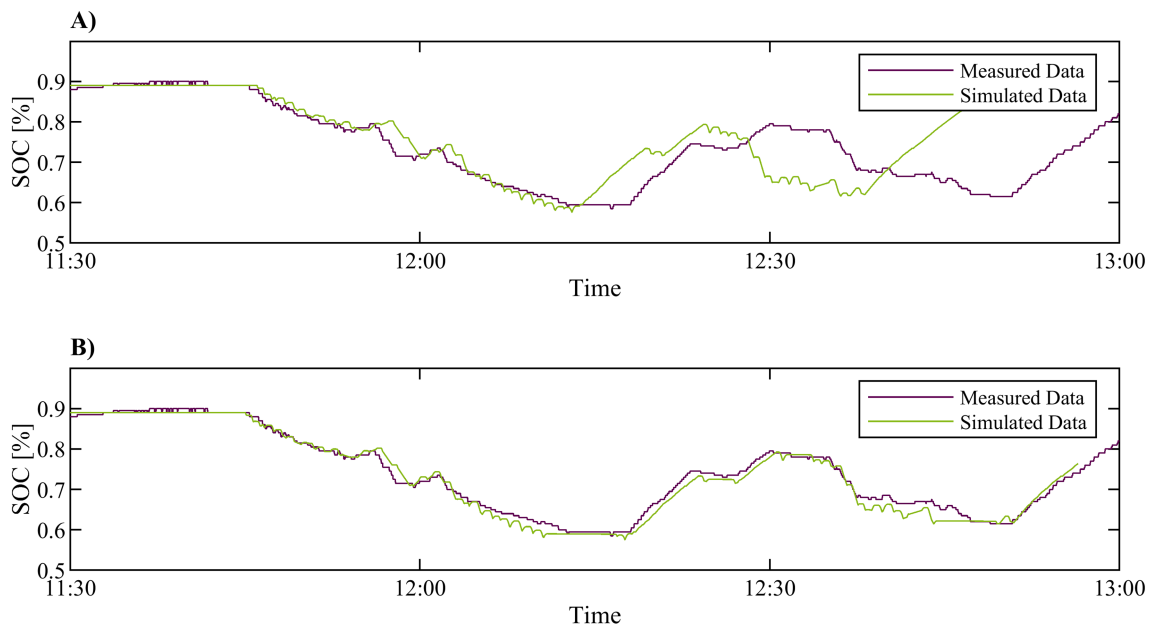


**Figure 6-7: Comparison of simulated and test drive SOC progression on line 695. The simulation parameters are: no HVAC power, normal traffic for workday, and only one full BTB (Annex 11.4).**

**A: No delay adjustment (Original test drive).**

**B: With delay adjustment.**

The power profiles of the simulation and the test drive are contrasted in Figure 6-8 (A). Between the two curves, there is a time and value shift. This is because a second-based measurement ( $\delta t = 1$  sec) can't be precisely matched. The simulated power profile is highly dependent on the topographical conditions, outside temperatures, passenger crowding, and traffic situations. Both power profiles have been smoothed using a moving average filter as shown in Figure 6-8 (B). The consistency of the simulated and test power profiles indicates that the trolleybus system simulation model can be used to determine TB and BTB power consumption as well as their instant states and implement them within other special-purpose analyses and applications (see Chapter 7).

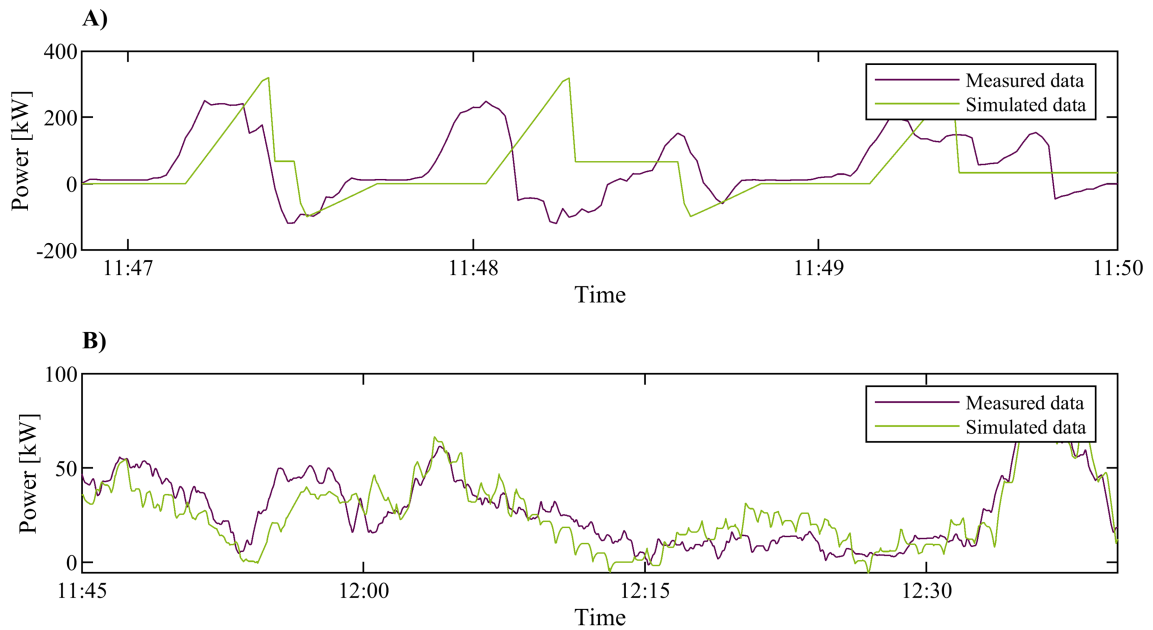


**Figure 6-8: Comparison of simulated and test drive power consumption on line 695. The simulation parameters are: no HVAC power, normal traffic for workday, and only one full BTB (Annex 11.4).**

**A: No filter applied.**

**B: Smoothed by moving average filter.**

## 6.4 Quality and Accuracy of the Traffic Network State Calculation

Energy consumption is measured by energy utilised per unit of output, e.g., travel distance. Energy consumption measured in (kWh/km) can be used to compare vehicles with comparable capacities and performance of the same type but operated differently (route topography, outside temperature, and traffic conditions). Wide energy consumption (kWh/km) ranges are reported by several research (see Section 1.2). Nevertheless, the estimation of the energy consumption ranges should reflect the high variability of the real-world situations. Therefore, it is essential to produce stochastic data for the purpose of studying whether the bus model and its consumption of energy are affected by uncertainties in different circumstances, for example, weather and traffic conditions.

Verifying the longitudinal dynamic model and the HVAC system in the bus model (see Section 3.4) requires multiple simulations under various weather and traffic scenarios. Buses are restricted in their stop-to-stop movements by the BDTRMs, in which the bus schedule and the traffic conditions are pre-defined (see Section 3.3). The histograms in Figure 6-9 depict three different simulation scenarios for buses with different operating situation. Normal workday traffic is considered for all simulation scenarios (pre-generated in BDTRM). Figure 6-9 (A), (B), and (C) shows the traction motor energy consumption in (kWh/km) for empty buses, full buses, and buses with a random number of passengers on-board, respectively. Traction motor energy consumption ranges between  $E_{CB} = 1$  kWh/km to  $E_{CB} = 1.8$  kWh/km for empty buses,  $E_{CB} = 1.51$  kWh/km to  $E_{CB} = 2.5$  kWh/km for full buses, and  $E_{CB} = 1.11$  kWh/km to

$E_{CB} = 2 \text{ kWh/km}$  for buses with a random passenger number. The lower energy consumption is seen in both empty and random number of passengers on-board situations. While the highest energy consumption is listed with a full bus situation.

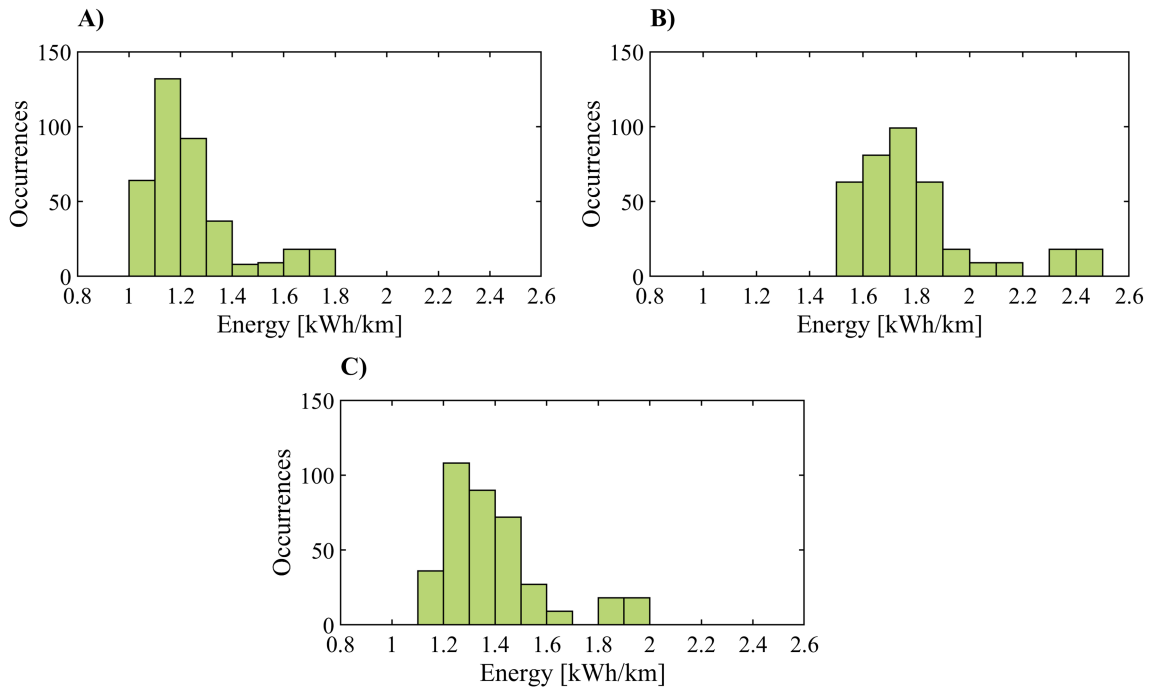


**Figure 6-9: Traction motor energy consumption based on three different scenarios. The simulation parameters are: normal traffic for workday, normal HVAC operation for several days from different seasons, and only bus variety 2 (Annex 11.4) with three different scenarios:.**  
**A: Empty buses (no passengers on-board).**  
**B: Full buses (maximum passengers on-board).**  
**C: Buses with random number of passengers on-board.**

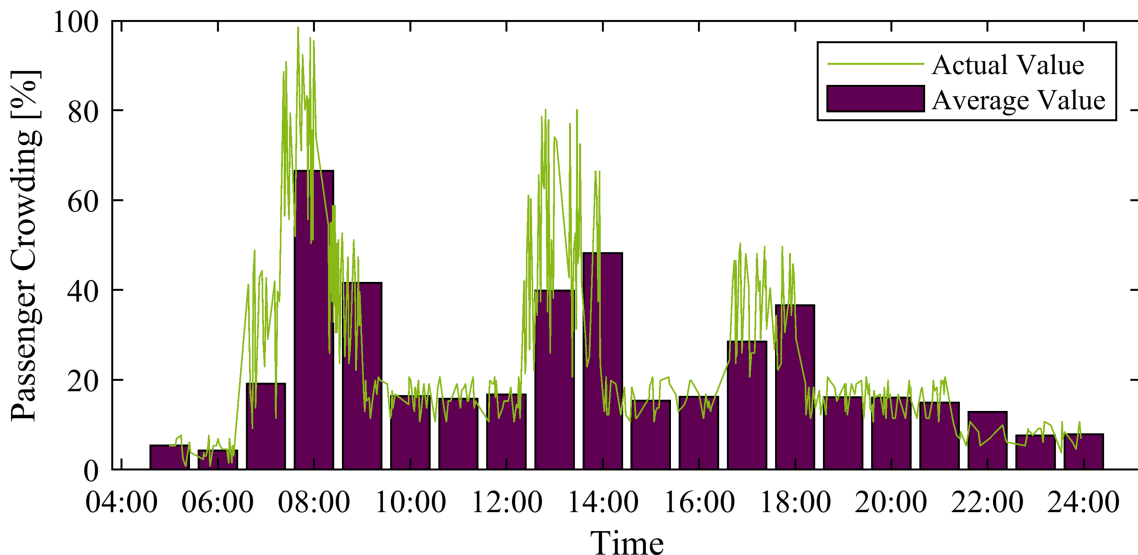


**Figure 6-10: Number of passenger on-board a bus as computed in the BDTRSM. The simulation parameters are: normal traffic for workday, normal HVAC operation, and only bus variety 2 (Annex 11.4) with random number of passengers on-board and operation on line 683.**

Figure 6-10 shows a histogram of the number of passengers on a bus throughout its daily schedule. In addition, the actual number of passengers is also presented by the curve. In this model, there

are three peak-time periods that are considered. Passengers are more likely to be on the bus during peak hours. Otherwise, there are fewer than 20% on board, and that number drops to less than 10% at dawn.

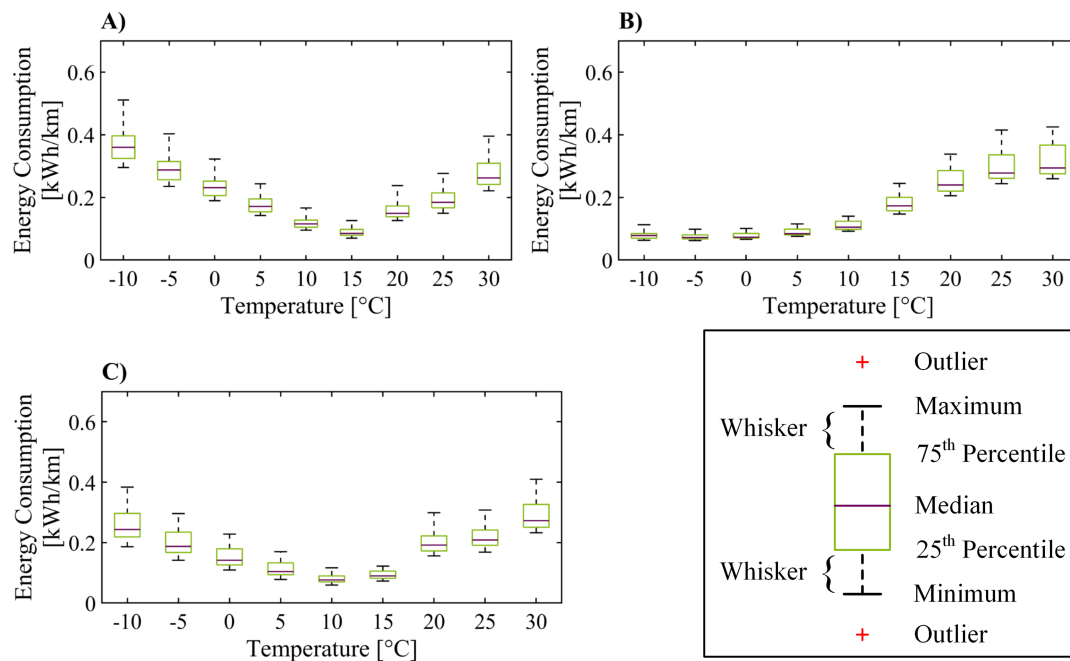
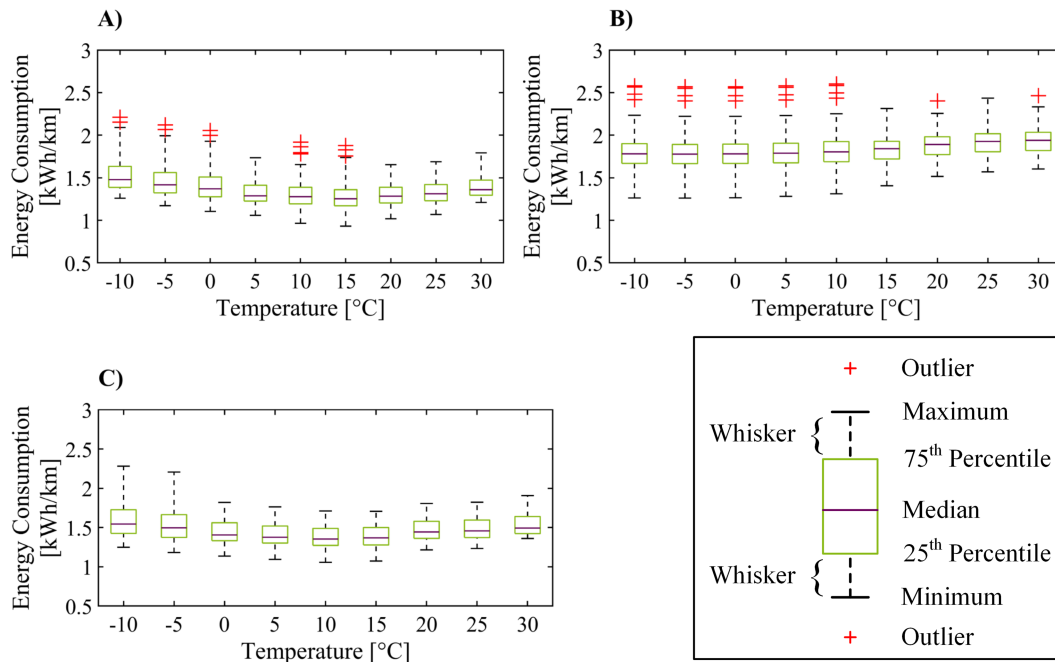


**Figure 6-11: Auxiliary energy consumption at different temperatures with three different scenarios. The simulation parameters are: normal traffic for workday, normal HVAC operation for several days from different seasons, and only bus variety 2 (Annex 11.4) with three different scenarios: A: Empty buses (no passengers on-board). B: Full buses (maximum passengers on-board). C: Buses with random number of passengers on-board.**

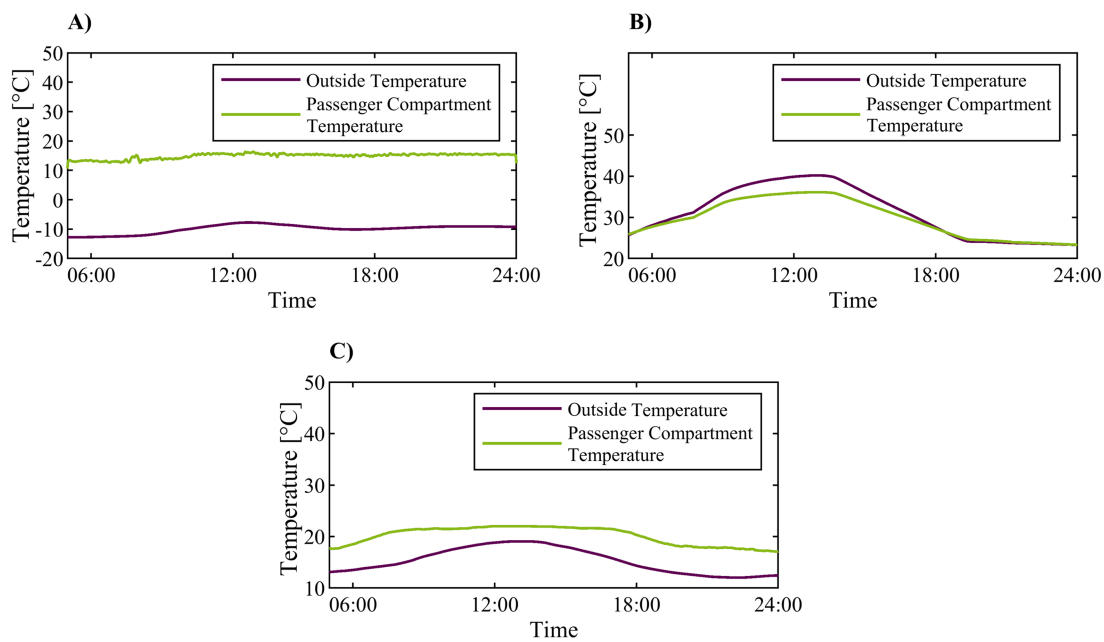
This passenger model, which is pre-determined in BDTRSM, is unique and corresponds only to one specific bus. In other words, each bus has its unique traffic situation which is different from the traffic situation of other buses using the same travel road, i.e., operating on the same line.

Figure 6-11 and Figure 6-12 depict the distribution of the auxiliary energy consumption (HVAC system and basic auxiliary) and the total energy consumption by buses at various outdoor temperatures, respectively. The central purple mark represents the median of the energy consumption, while the box top and bottom edges represent the 75th and 25th percentiles of the resulting energy consumption from the several simulations, respectively. The (A), (B), and (C) markers in Figure 6-11 and Figure 6-12 depict empty, full, and random bus occupancy, respectively.

As shown in Figure 6-11(A), more auxiliary energy is required in cold temperatures when compared to (B) and (C) of the same figure. The reason behind that is the absence of the on-board passengers, where no heat energy from passengers is thus contributed to the heating system. On the other hand, with high temperatures, less energy is required to cool down the passenger compartment when the bus is empty and more energy when it is full (see Figure 6-11 (A) and (B)).



**Figure 6-12: Total energy consumption at different temperatures with three different scenarios. The simulation parameters are: normal traffic for workday, normal HVAC operation for several days from different seasons, and only bus variety 2 (Annex 11.4) with three different scenarios:**  
**A: Empty buses (no passengers on-board).**  
**B: Full buses (maximum passengers on-board).**  
**C: Buses with random number of passengers on-board.**



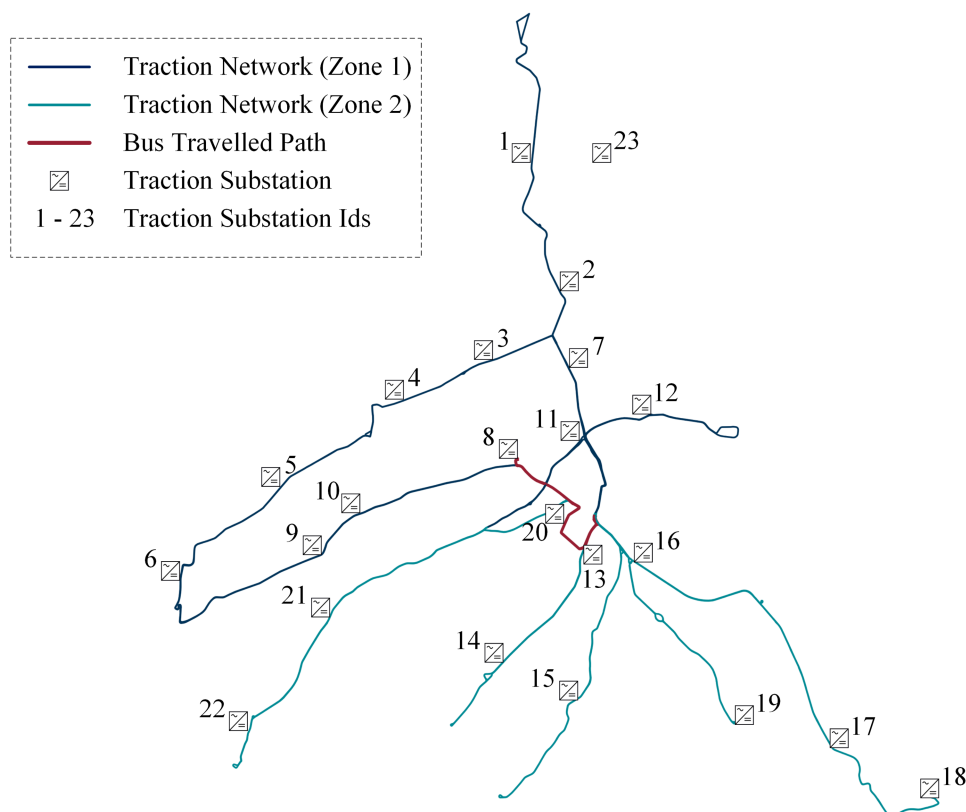
**Figure 6-13: Simulated passenger compartment temperatures compare to the outside temperature. The simulation parameters are: normal traffic for workday, only bus variety 4 (Annex 11.4) with random number of passengers on-board, and normal HVAC operation for different days from:**  
**A: Winter season.**  
**B: Summer season.**  
**C: Spring/Autumn season.**

Figure 6-13 depicts the operation of the HVAC system in one of the simulated buses with three different outside temperature values. The bus passenger compartment temperature is regulated

with respect to the outside temperatures and as defined in the VDV recommendation 236 [111] (see Figure 3-8).

## 6.5 Quality and Accuracy of the Traction Network State Calculation

In this section, the results of the steady-state calculation of the traction network are presented. As introduced in Chapter 4, the DC traction network is a passive network in which the traction substations are unidirectional with only one direction of power flow, i.e., from the medium voltage AC network to the DC traction network. Any surplus energy in the DC traction network is therefore associated with an increase in voltage. The voltage increase is damped by a squeeze control system implemented in the buses, where the surplus energy is converted into heat using a brake-resistor, preventing the system voltage from exceeding the maximum permanent voltage  $U_{\max 1}$  as defined in IEC 60850:2014-11 [13]. In order to calculate the steady-state of the traction network as well as the buses behaving during the occurrence of surplus energy in the traction network, an adapted power flow method is implemented (see Section 5.2.4).



**Figure 6-14:** The Solingen traction network zones and the travelled path of two trolleybus.

In order to show the results of the simulation process (defined in Section 5.2), a path as shown in Figure 6-14 is selected and only two buses are simulated. Although TBSSM has the option to simulate several bus movements simultaneously, only two buses are simulated travelling on this path to keep clear the behaviour of the traction substation to bus movements as well as the voltage

state in case of surplus power in the traction network. As shown in Figure 6-14, the Solingen traction network is divided into two zones.

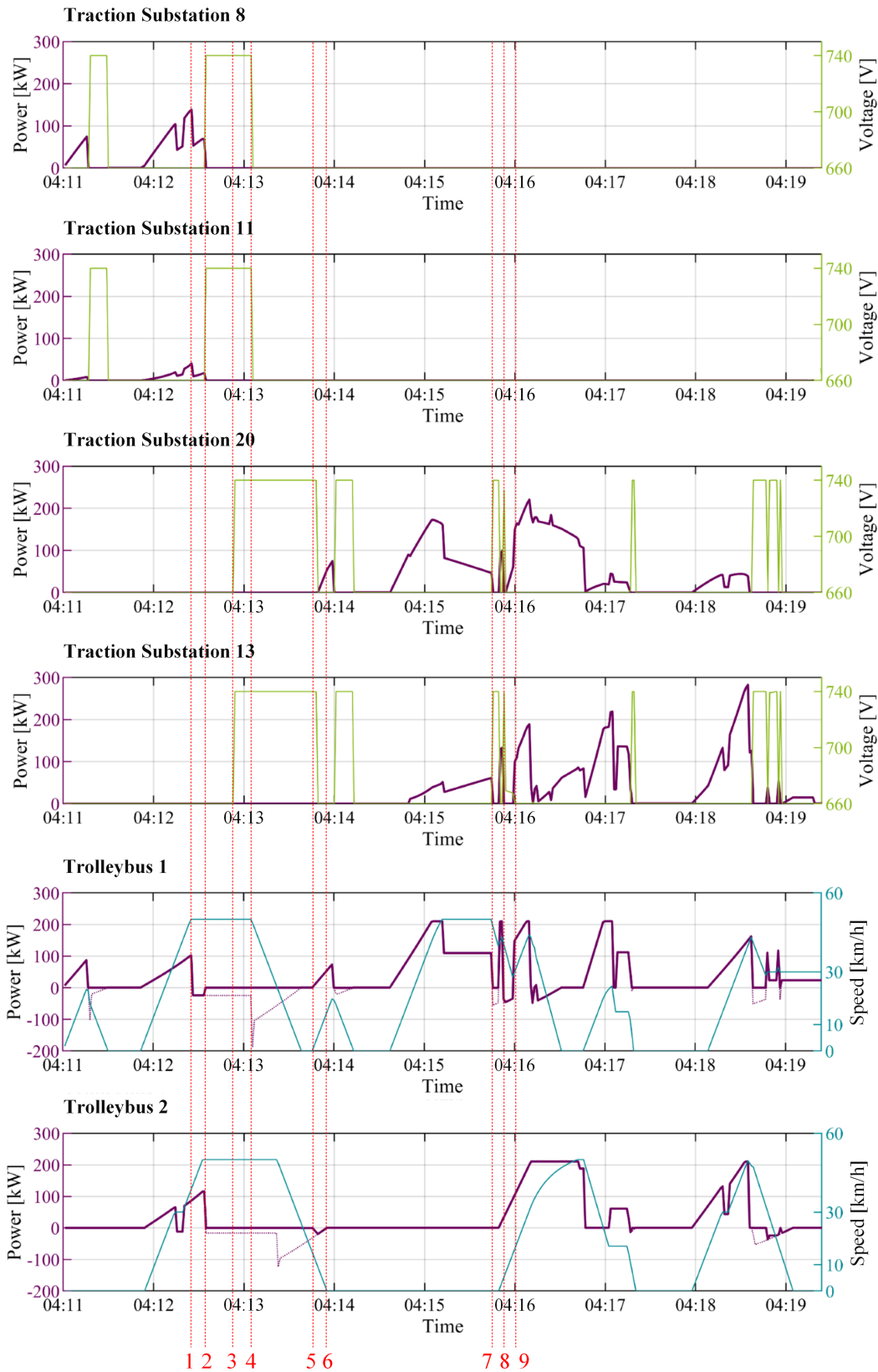


Figure 6-15: Traction network steady-state at selected traction substation and the two trolleybuses driving the path of Figure 6-14.



The buses start in zone 1 and end in zone 2. The power supply for the bus movements is mainly provided by the traction substations close to the bus route, i.e., traction substations 8, 11, 20 and 13. Traction substations 10, 14 and 16 are expected to make a very small contribution to the power supply. However, traction substations 10, 14 and 16 are excluded from the results discussion. As shown in Figure 6-15, the power and voltage at traction substations 8, 11, 20 and 13 are given the purple and light green curves, respectively. In addition, the total power (as considered by the traction network), the motor power (as calculated by the bus) and the speed of trolleybuses 1 and 2 are given the purple, dotted purple and turquoise curves, respectively. The vertical red lines are added to Figure 6-15 to represent the start and end of some critical changes for the bus and traction substation states.

At 04:11 o'clock trolleybus 1 starts to move. As the starting location of trolleybus 1 (as trolleybus 2) is in zone 1, no supplied powers are indicated in zone 2 (traction substation 20 and 13). Traction substation 8 and 11, per contra, supply the buses demand in zone 1. As traction substation 8 is the nearest to the bus positions, the highest supplied power is supplied by it. Before 04:12 o'clock trolleybus 1 deaccelerate (need to dwell at a traffic light) and because it is the only bus in zone 1 the regenerated deaccelerating power must be eliminated to keep the system voltage under the maximum permeated value (for Solingen's traction network  $U_{\max 1} = 740 \text{ V}$ ).

As shown in Figure 6-15 the traction network considers the trolleybus with no power  $P = 0 \text{ W}$ , as the auxiliary power of the bus is fulfilled from the regenerated deaccelerating power and all the surplus energy is burned using the brake-resistor. The dotted purple curve shows how the traction motor power is not considered in the traction network state. The purple curve shows how the traction network considers trolleybus 1 power (after using the adapted power flow calculation). The first voltage surge in zone 1 is given during this time.

When trolleybus 2 starts moving the regenerated power by trolleybus 1 is distributed to trolleybus 2 as long as trolleybus 2 is consuming power and in fare distance. In the time between red lines 1 and 2 as shown in Figure 6-15, trolleybus 1 start to generate power at red line 1 and trolleybus 2 consume the generated power until it stops accelerating. The power generated by trolleybus 1 is not due to deceleration to stop the bus, but to speed damping to keep the bus speed at  $v = 50 \text{ km/h}$  while the bus is travelling down slop. At red line 2, trolleybus 2 stops accelerating as it starts to drive down slope and thus regenerating power to maintain its speed at  $v = 50 \text{ km/h}$  (both buses are driving down slop). The regenerated power by trolleybus 2 is immediately burned (as given by the dotted purple and purple curve). Simultaneously, the regenerated power from trolleybus 1 is burned to remove the voltage surge from zone 1. Between red lines 2 and 3, the voltage surge in zone 1 is given at traction substation 8 and 11 by the light green curve. At red line 3, trolleybus 1 changes zones and enters zone 2. Thus, the voltage surge is given in zone 2 since trolleybus 1 is still driving down slope and regenerating power (as shown by the light green curve from traction substation 20 and 13 in Figure 6-15). However, the voltage surge continues

at zone 1 as long as trolleybus 2 is regenerating power and connected to zone 1 (as shown by the light green curve from traction substation 8 and 11 in between red lines 3 and 4 in Figure 6-15). At red line 4 both buses are in zone 2 and thus no more supplied powers or voltage segues are given by traction substation 8 and 11.

At red line 5, trolleybus 1 starts to accelerate and observe some of the regenerated power by trolleybus 2. As shown in Figure 6-15, the regenerated power by trolleybus 2 is feed into the traction network and delivered to trolleybus 1 (dotted purple curve is covered by purple curve). With trolleybus 1 continues accelerating, the regenerated power by trolleybus 2 becomes not enough to supply trolleybus 1 demands. Thus, traction substation starts to supply power into the traction network as soon as the voltage level drops to  $U = 660 \text{ V}$  (see Figure 6-15).

Between red lines 7 and 8 a voltage surge occurs in zone 2 as trolleybus 1 is decelerating and trolleybus 2 is dwelling. The regenerated power by trolleybus 1 is burned and excluded from the traction network steady-state calculation, as given by the dotted purple and purple curve of trolleybus 1 in Figure 6-15. As soon as trolleybus 2 starts to accelerate (shortly before red line 8) the voltage surge in zone 2 gradually diminishes. Thus, in the time between red lines 8 and 9 no dotted purple cure can be seen for trolleybus 1 since all regenerated energy is consumed by trolleybus 2.

In this context, it is worth pointing out that although trolleybuses 1 and 2 follow the same route (as shown in Figure 6-14), their speed curves (profiles) are not the same (as shown by the turquoise curves of trolleybuses 1 and 2 in Figure 6-15). Therefore, each trolleybus faces a different traffic situation. For example, trolleybus 1 stopped for some time at a traffic light immediately after leaving the depot, whereas trolleybus 2 did not have to stop at the same traffic light. The two speed profiles in Figure 6-15 show how each trolleybus is presented with a unique traffic situation. Of course, the traffic situation depends on the type of day, the time of day and the location of the bus stop.

## 6.6 Assessment of the Simulation Model

A comprehensive trolleybus system simulation model (TBSSM), in which trolleybuses and battery-trolleybuses collect energy from overhead wires to operate according to their daily schedules, requires extensive modelling of the buses, the traffic system and the traction system infrastructure. Battery-trolleybuses also charge their on-board battery while driving under the overhead contact wires or at bus stops where quick-charging stations are available, which challenges the reliability of the electric traction network. Besides, the implementation of innovative features, i.e., photovoltaic (PV) systems, electric vehicle charging stations (EVCSs) and battery storage power stations (BSPSSs) in the traction network, increases the load on the trolleybus system. To this end, the TBSSM developed in this thesis mimics the regular activities of a real-world trolleybus system to assist in the evaluation of the steady-state behaviour of the

electric traction network and the operating TBs and BTBs over a period of time. Consequently, a comprehensive, environmentally friendly, and competitive trolleybus system can be planned and operated in an adaptive manner.

By focusing on the extensive correlations between its components, the TBSSM is suitable for analysing the short- and long-term performance of a trolleybus system. As outlined in Chapters 3, 4, and 5, the TBSSM consists of four model blocks, namely the traffic network model, the bus model, the electrical network model, and the trolleybus system state model. In this way, TBSSM made it possible to implement a public transport system simulator together with a reliable power system simulator in a single simulation model. Both simulators are important for simulating the steady-state behaviour of a trolleybus network. The TBSSM offers the possibility to do the following:

1. The implementation of the road network, which defines the travel routes for the TB and BTB fleet.
2. Characterising the individual elements of the traffic and electrical network with numerous features making it convenient to associate them.
3. Establishing the Bus Daily Travelling Routes Model (BDTRM) from the road topology, traffic regulations, and bus timetables. The BDTRM defines the guidelines for each bus's routing and includes the following information:
  - The sequence of points (traffic nodes) that the bus passes through during a day.
  - The distance between the successive points (traffic branches).
  - The stopping points (bus stops, traffic lights, and junctions) where the bus will dwell.
  - Stop-to-stop distance.
  - Dwelling time.
  - Number of passengers between successive bus stops.
  - Speed limits over the travel roads.
  - Road topography.
  - Time progress correspond to the successive points (traffic nodes).
  - Traction network information (length, from-node, and to-node) correspond to travel roads (traffic branches).
4. Calculating the amount of traction power necessary to propel a bus over four different motion regimes (acceleration, constant-speed, rolling, and braking) during a standard stop-to-stop driving cycle. In addition, the required power for basic auxiliary and heating or cooling are calculated. Battery power is also calculated for BTB.
5. Determine the topology of the traction network and modifying it with each bus movement.
6. Considering the passive behaviour of the traction network when calculating the steady-state of the traction network, as well as the TB and BTB states.

7. regulating the system voltages and the buses' current consumption as recommended by IEC 60850:2014-11 [13] and IEC 62313:2009-04 [56], respectively.

According to Section 6.2.1, the TBSSM can compute the bus performance in under a variety of traffic conditions, which allows different traffic situations to be simulated. The traffic situation is unpredictable and impacted by a variety of factors. For example, the type of traffic and the time of day affect the traffic situation. Thus, to determine the traffic situation over the course of a day, the TBSSM utilises a random function that depends on a predetermined probability variable, as well as the type and time of the day, to define the stop-to-stop motion and the allowable maximum speed on the roads. According to [85], using TBSSM to forecast the trolleybus steady-state could diverge with a longer forecast, and for that reason, the forecasting procedure should be repeated as soon as the real steady-state of the trolleybus system is satisfied. In fact, it could be possible to use real-time traffic information, depending on availability, from internet sources such as Google Maps or TomTom to improve the accuracy of the forecast window. Furthermore, traffic accidents that disrupt the traffic flow can be considered in the TBSSM. However, for planning purposes, a wide range of power consumption is required to cover all situations that influence the system state. As shown in Section 6.2.1 and Figure 6-3, different motor powers are obtained for different speeds and road gradients. In addition, different auxiliary powers (HVAC system and basic auxiliary) that vary with the outside temperature (see Figure 6-11) are determined and included in the total power consumption of the buses (see Figure 6-12).

The calculation of the motion regimes between a stop-to-stop movement (see Section 3.4.3) depends mainly on the distance between successive stops and the speed regulation, which is determined by the road speed limit, the traffic situation, and the traction network regulation. However, different behavioural profiles of the bus driver, which include different tempos for acceleration, rolling and braking regimes, can be implemented to add more diversity to the calculation of motion regimes. Incorporating these profiles into the motion regime calculation can increase the diversity of motor power consumption. However, driver behaviour is random and associated with the traffic situation as well as the driver mode, which makes it impractical to determine such profiles and include them in the motion regime calculations. The approach developed in TBSSM for determining the motion regimes and their associated motor power consumption is adequate to account for the anticipated power consumption diversity.

The dynamic nature of the traction network, caused by the continuous movement of buses, presents a challenge to the calculation and implementation of the traction network conductance matrix. Moreover, the existence of unidirectional traction substations makes conventional power flow methods inadequate. As can be seen in sections 5.1 and 5.2.2, the TBSSM determines the conductance matrix of the traction network, taking into account the change in network topology due to bus movements. When determining the steady-state of the traction network, the TBSSM implements a modified power flow approach (see section 5.2.4), which allows it to compensate

for the unidirectional nature of the traction substations. As shown in Section 6.5, the steady-state of the traction network is very well represented, where all voltage surges due to surplus power in the traction network are captured and the squeeze control system used by the buses to dump any unacceptable voltage rise is conveniently represented by the TBSSM.

The TBSSM is basically developed to study a trolleybus system. However, it is always an option to adapt the TBSSM to simulate a tram system due to the similarity between the two systems. As the TBSSM is flexible, different input parameters can be changed. The tram system is even easier to calculate in terms of stop-to-stop motion. However, the calculation of the conductance matrix needs to be adapted because the trolleybus traction network is operated with a two-wire system, whereas the tram traction network is operated with a single wire system, and the tram tracks are used for the traction current return.

By considering the complexity, the advantages of TBSSM and the challenges of evaluating its performance remain unmatched. Furthermore, the simulation duration and expansion adaptability are also to be considered for the benefit of adopting the TBSSM in planning and operation works [85, 86]. The developed TBSSM represents the state of the art in simulation tools. It is a development derived from previous experience in the field of traction systems (see Section 1.2). The TBSSM represents a unique combination of the traffic network and the electric network of a trolleybus system, which opens several new research horizons to be explored. This simulation model allows the investigation of cases that cannot be directly considered with standard simulation tools [26], it allows the verification of the traffic network parameters, the bus specifications, and the detailed behaviour of the corresponding electrical traction network. It also provides a basis for planning and analysis of existing and newly developed trolleybus/battery-trolleybus systems.



## 7 Use Cases and Applications of the Simulation Model

The trolleybus system simulation model (TBSSM) is developed in such a form that it can adapt to environmental changes and be easily adjusted to mimic several scenarios within the trolleybus system. The TBSSM is constructed upon three fundamental models: the traffic network model (TNM), bus model (BM), and electric network model (ENM). It is necessary, however, to fully comprehend both the operating buses and the steady-state of the traction network in order to properly study and analyse a trolleybus system. A trolleybus system's potential should be evaluated before it can be expanded to include more innovative features. Thus, new *innovative features*, such as photovoltaic (PV) systems, electric vehicle charging stations (EVCSs), and battery storage power stations (BSPSs), are modelled within the ENM and are therefore implemented within the simulation of the trolleybus system. To accomplish these objectives, the TBSSM provides a complete solution that simultaneously simulates the movement of the whole trolleybus (TB) fleet, including even the battery-trolleybuses (BTBs), and simultaneously updates the bus positions within the traction network; the TBSSM can also manage the passive behaviour of the traction system. All voltage increases in the traction network are monitored, and any surplus power is eliminated. Some examples of potential use cases for the TBSSM will be explained in the following sections.

### 7.1 Operating and Planning a Trolleybus Systems

The author of [85] proposes innovative approaches to *operate* and *plan* a trolleybus system. In the *first* part of his work, he concentrates on the operating level of an *existing* trolleybus system. Accordingly, predicting how the TBs and BTBs will progress is necessary for forecasting the state of the trolleybus network, which is based on the TBSSM proposed in this thesis. The adopted TBSSM is set with *one-second* time step. However, the TBSSM only needs a fraction of a second to execute a simulation cycle in order to determine the trolleybus system's steady-state. Therefore, after determining the steady-state of the traction network, the TBSSM is paused until a *real-life* second has passed. Modifying the TBSSM in this way allows it to simulate a *real-time* trolleybus system. In TBSSM, the steady-state calculation covers the locations and powers of the operating TBs and BTBs in accordance with their schedules, as well as the power and voltage of all the components included in the traction network. A proposed guiding system utilises the modified TBSSM to generate *pseudo-measurements*, which are later used to generate a 10-minute forecast for the trolleybus system. A new TBSSM (unmodified with pause simulation cycle) is started in order to simulate the 10-minute forecast. The guiding system then mirrors the bus locations – which are given by the pseudo-measurements – into the corresponding locations in the new TBSSM. Simultaneously, operating buses' speed and power consumption are computed. The trolleybus system specifications, which are implemented in the new TBSSM, are used to figure

out where the buses are, how fast they are going, and how much power they consume. Once the 10-minute forecast, which takes less than 10 minutes to be simulated, is complete, a fresh 10-minute forecast is newly started based on the actual pseudo-measurements and the same pre-process will be repeated. The pseudo-measurements and 10-minute forecast data will be utilised by the intelligent control system, which is responsible for the reliable operation of the trolleybus system (see Section 7.4).

In the *second* part of the work, [85] handles two planning situations with very different baseline circumstances. Planning to expand an existing trolleybus system therefore necessitates the specifications of the *existing* infrastructure (brown-field scenario). Contrarily, no such information is needed when planning a *new* battery-trolleybus system (green-field scenario). Thus, a novel approach to plan a battery-trolleybus system is presented. An important consideration in planning a battery-trolleybus route is determining which segments of the route should be electrified, such that there are as few overhead contact wires as possible for the battery-trolleybus system to be reliably operated. Planning can be carried out with the help of the TBSSM, which utilises the existing information of the road network, bus daily schedules, construction restrictions, and trolleybus system infrastructure. The TBSSM is responsible for simulating the energy requirements of the operating buses during their daily schedules. Additionally, the SOC for the battery-trolleybuses is considered. The optimization algorithm will use all power demands to estimate the minimal overhead contact wires and traction substation needed to operate a reliable battery-trolleybus system. The optimised solution is then verified via an evaluation task by utilising the TBSSM. The new trolleybus system must satisfy all technical requirements. The battery-trolleybus SOC is also considered.

Two case study are implemented in [85], so that the optimisation algorithm is tested for both green-field and brown-field scenario.

## 7.2 Integration of Photovoltaic Systems

To develop a truly sustainable public transportation system, the actual implementation of renewable energy technologies into trolleybus networks is crucial. For this reason, this section presents an approach to determine the best *locations* and *sizes* of photovoltaic systems that are intended to operate on a passive DC traction network [182]. According to research, direct integration of PV systems into such DC traction network allows an increase in PV system voltage efficiency from  $\eta = 90\%$  to around  $\eta = 96\%$  while also improving power quality, increasing system reliability, and lowering system costs [87]. However, the traction network's passive behaviour may result in active power curtailment of the PV systems. For this purpose, the TBSSM is used to determine the traction network steady-state.

The proposed approach for choosing the best location for the PV systems is divided into several steps. In the beginning, existing traction substations are eliminated from the traction network



(traction network zone), i.e.,  $PA = PA \cup VC$  and  $VC = \emptyset$  (see Section 5.2.3). In the next step, traction nodes with feed-in accessibility are defined as the new power source of the traction network. If  $N_{PVP}$  represent the set of traction nodes with feed-in accessibility, then  $PA = PA \setminus N_{PVP}$  and  $VC = N_{PVP}$ . After that, the TBSSM is started with the new defined constant voltage ( $VC$ ) and passive node ( $PA$ ) set. The feed-in energy of the selected traction nodes set  $N_{PVP}$  will be computed over the simulation interval  $\tau_s$ . Then, each traction node in  $N_{PVP}$  is grouped with the electrically linked traction nodes. The groups of traction nodes can be determined by using the traction network model, which is included in TBSSM, and a defined distance. For example, all electrically linked traction nodes that are located within the defined distance range will be included in these groups. In the last step, the computed feed-in energy of  $N_{PVP}$  is summed up for each pre-defined group. This is followed by a check to identify the group that has the highest feed-in potential. The traction node that represents the selected group will be considered for the optimal PV system location.

Once the optimal locations for the PV systems are identified, maximum efficiency can be reached by finding its optimum capacity for the corresponding PV systems. The selected group total feed-in energy is compared to several power profiles generated for PV systems with varied capacity. Then, a utilisation factor for each comparison is calculated. The ideal capacity for the PV systems is determined by the best calculated utilisation factor.

The proposed approach in [183] was verified with a test trolleybus system.

### 7.3 Integration of Storage Systems<sup>9</sup>

This section introduces a method for determining the optimal placement for a battery storage power station (BSPS) in a passive DC traction network incorporating photovoltaic systems. A passive system is known for no possibility of power transfer into the adjacent systems. To balance the power flow within the trolleybus system, a BSPS is proposed to be included into the traction network. The TBSSM is used to determine the optimal BSPS location that can compensate the operating bus demands and PV systems power productions.

The BSPSs are implemented to utilise the regenerative power produced during bus decelerations and thus enhance the traction network stability. Additionally, they are used to minimise the active power curtailment of the PV systems and, as a result, enhance the utilisation rate of the PV systems. To meet these expectations, BSPSs must be located optimally. Since optimum position assessment needs to include not only a single time step but also all conceivable situations and circumstances during the trolleybus system's operating time, TBSSM is adopted and considered the leading platform. First, the traction network steady-state is obtained and summarised for all traction nodes. Accordingly, all nodal voltages and powers are determined, as well as the branch

---

<sup>9</sup> The work of this section is published in [183] by the author of this thesis

currents. It is important to find out what the current values are because buses and PV systems have voltage-controlled actuators that prevent the voltage from rising too high. Therefore, attention should be paid to branch currents and their limits. The residual currents are found by comparing the actual branch current to the maximum current permitted by the respective overhead contact wires. Based on the calculated residual currents, a sensitivity analysis is then used to determine how much power can be injected into the traction nodes. Finally, the injected power sets of the traction nodes are compared and ranked using a simple weighting function to determine the node potential coefficient.

The proposed approach in [183] was verified with a test trolleybus system.

## 7.4 Monitoring and Control System

To transfer a trolleybus system to become a fully sustainable public transportation system, the existing trolleybus systems will need to be updated with several new features, such as BTBs, PV systems, EVCSs, and BSOSs. The integration of these features is expected to challenge the existing trolleybus system's reliability. Excessive loads like BTB come with a significant impact on the existing traction network, which was not designed to handle such loads in the first place. Because of this, more voltage drops, and current overloads are likely to occur on the traction network. To resolve the problems associated with the expanded trolleybus system, the new features must be intelligently controlled by a smart network automation system. This can be done by using cutting-edge monitoring and control system methods. The author of [86] develops innovative algorithms for an *intelligent network control system* of a trolleybus system. In addition to the optimised planning of new battery-trolleybus system according to [85] (see Section 7.1), the approach followed in [86] makes it possible to promote the transformation with a reliable operation for expanded trolleybus systems. Based on the characteristics of the traction network and the corresponding challenges, the overall development process of a core intelligent network control system, which is to be used as a supplemental element controlling an developed trolleybus system, is explained in detail in [86].

A simulation model of existing trolleybus system will advantage the investigation of the impact of new battery-trolleybuses as well as the influence of other innovative features. The TBSSM is used to simulate the steady-state of the expanding trolleybus system. Furthermore, it will be used for the analysis of the traction network and as a development tool for the intelligent network control system.

In this context, the availability of predicted information regarding the traction network steady-state is essential. The intelligent network control system contains three essential stages, of which the network state identification and the network state forecast are part of [85] (see Section 7.1).

After establishing the TBSSM with the expanding trolleybus system's input characteristics, a wide range of scenarios with different configurations can be simulated. The TBSSM can continually

identify the steady-state of the traction network with a one-second time step even if the topology of the network is constantly changing because of excessive bus movements. In terms of providing results, the simulated output, especially the nodal voltages, nodal powers, and branch currents, and all incorporated sub-models information are of the highest importance. As a result, the real-world trolleybus system can be mimicked by the TBSSM after being defined with the appropriate specifications, providing a foundation for several scenarios to be analysed.

A case study for the trolleybus system of Solingen is implemented in [86], so that the developed intelligent network control system of a trolleybus system is tested and evaluated.



## 8 Summary

The work in this thesis presented a novel trolleybus system simulation model (TBSSM) that can mimic a real-world trolleybus system in its existing configuration and even with other additional innovative features, such as battery-trolleybuses (BTB), photovoltaic (PV) systems, electric vehicle charging stations (EVCSs), and battery storage power stations (BSPSs), and thus it is a solid framework to pave the way to a more sustainable and climate-friendly future across the transport sector. Electrification of public transport system, particularly bus transportation, necessitates a greater focus on analysis and evaluations. Transport operators are thus confronted with the extraordinary challenge of making their current bus fleet sustainable and, as a result, decreasing greenhouse gas (GHG) emissions (see Chapter 1).

Chapter 2 introduced the trolleybus system with a brief overview. From a historical point of view, trolleybuses are an outmoded kind of transportation. Despite rising oil costs, greater environmental awareness, and concerns about air pollution on city streets, the number of trolleybus networks had decreased globally, even in Germany. Optimistically, a battery-trolleybus might usher in a new era of trolleybuses that combine the benefits of a trolleybus and a battery-electric bus (see Section 2.1). In the next section (see Section 2.2), the technological underpinnings of the trolleybus system were discussed. These were broken down into the various trolleybus vehicle concepts, as well as the traction substation and traction network of trolleybus systems. In addition, the voltage system that is used to power a traction network as well as the operating regulations for a trolleybus system were described (see Section 2.3). The anticipated change of trolleybus systems and, as a result, the introduction of innovative features will also need additional evaluation from both the operational and technical points of view. To this end, a trolleybus system simulation model (TBSSM) was planned to be developed in order to mimic the regular activities of TBs and BTBs, as well as to evaluate the steady-state behaviour of a trolleybus system over a period of time. Consequently, a competitive trolleybus system can be adaptably planned and operated (see Section 2.4). In the following section, the basic concepts of the TBSSM were presented. The three fundamental layers, i.e., the traffic network model, bus model, and electric network model, were introduced (see Section 2.5). The last section in Chapter 2 addressed the challenges that stand against in the development of a traction simulation model (see Section 2.6).

Chapter 3 handled the process of developing both the traffic network model (TNM) and the bus model (BM). The road network was divided into two essential elements; the traffic nodes and traffic branches (see Section 3.1). The attributes' sets for both traffic nodes and traffic branches were described in Sections 3.1.1 and 3.1.2, respectively. Important spatial and geometrical information was considered for both road network elements. Later, the implemented attributes had significant benefits for the development of the bus daily travelling routes. In Section 3.2, the

construction of the bus timetables (schedules) was defined. After utilising the road network as a weighted directional graph, the process of developing the bus daily travelling routes model (BDTRM) was discussed in Section 3.3. In BDTRM, the basic elements that constructed a bus's long travel route for its daily operation were both the bus schedule and road network information. Bus dwellings at bus stops or traffic lights as well as the dwelling time were included in the BDTRM. Furthermore, the number of passengers on-board the bus was also defined in the model. Road topography, traffic restrictions, and even the availability of the traction network were implemented in the BDTRM.

The second part of Chapter 3 was aimed at the modelling steps of the BM. In Section 3.4, the mathematical representation and the block diagram of the BM were introduced. After defining the mechanical and electrical specifications of the bus (see Section 3.4.1), the mathematical steps to compute the bus speed and power profile were presented in Section 3.4.2. Using a bus longitudinal dynamic model was the key to calculating the propulsion motor power that is required to move the bus. Bus speed and travel distance were also calculated. However, four regimes of motion were used to determine bus progress between two consecutive stops. Bus power consumption is not limited only to the traction motor. Auxiliary power from both the heating, ventilation, and air conditioning (HVAC) system and basic auxiliary were also considered in the BM. The on-board battery model for a BTB was specified and included of the BM too. More details on the possible sequence of the motion regimes during a stop-to-stop movement were discussed in Section 3.4.3. The challenge of modelling a realistic bus speed profile was also brought up and handled.

The electric network model (ENM) was defined in Chapter 4. The traction network model was divided based on the traction network topology into traction nodes and traction branches (see Sections 4.1.1 and 4.1.2). The traction nodes and traction branches were used to define the traction network conductance matrix. The AC network model was defined in Section 4.2. Modelling the power profiles of the innovative features as well as TBs'/BTBs' power consumption and locations with respect to the traction network was elaborately described in Section 4.3. Calculating buses' power consumptions and locations is a repetitive process which is done with each simulation cycle. Section 4.3.1 described the process steps for calculating buses' power consumptions and locations. The calculation results were used to update the traction network conductance matrix. Sections 4.3.2 and 4.3.3 presented both the PV system and EVCS models. Whereby, the calculation of the power profile for both models was defined. Furthermore, the BSPS model was also introduced (see Section 4.3.4).

Chapter 5 outlined the complete simulation model. The step-by-step process to determine the traction network steady-state was elaborately described. In section 5.2 the mathematical equities of the traction network, or rather the traction network zone, were defined. The simulation process in general was clarified in Section 5.2.1. Due to the moving behaviour of the buses, the traction

network topology changes with each simulation cycle. In Section 5.2.2 the challenging task of determining the actual conductance matrix of the traction network zone was simplified. However, not only determining the conductance matrix was challenging but also calculating the traction power flow in a passive network. The simplified Newton-Raphson (SNR) approach was found to be the most practical way to solve a DC power flow problem (see Section 5.2.3). In Section 5.2.4, a novel approach of using the SNR power flow method to solve the power flow problem for passive traction networks with other power sources, such as regenerative braking power and PV systems, was shown. Keeping the bus motor current within the limits that are specified in traction network norms required a bus power control system to be implemented into the simulation process of the traction network. Section 5.2.5 described the aforementioned problem and the proposed control process that could handle it. Lastly, the chapter was finished with a proposed sequential AC-DC power flow used to simultaneously perform a sequential power flow for both the AC network and the traction network (see Section 5.3).

In Chapter 6, the trolleybus system of Solingen was presented to evaluate the developed TBSSM. The road network and the traction network were implemented using QGIS. The other input parameters for Solingen's trolleybus system were also defined and included in the TBSSM (see Section 6.1). Finally, the developed TBSSM was used to simulate several scenarios (see Sections 6.2, 6.3, and 6.4). The results were discussed and compared to real measurements from the studied trolleybus system.

Chapter 7 defined some of the developed TBSSM's use cases. In Section 7.1, the TBSSM was used as a forecasting tool that could, after adapting the input location of the operating buses, simulate the system state for the next 10 minutes. Furthermore, the simulated energy consumption as well as the SOC of the BTBs were utilised for further optimisation of planning processes. In Sections 7.2 and 7.3, the TBSSM was used to find the optimal locations to install PV systems and BSPSs in an existing trolleybus system, respectively. Finally, the TBSSM was implemented as a tool to support the operation of a monitoring and control system (see Section 7.4).

The presented simulation model of a trolleybus system basically presents an all-in-one simulation tool and thus offers a noteworthy potential for operating and planning of a trolleybus system or similar public transport systems. The TBSSM is developed to mimic a real-world trolleybus system, whereby the movements of all bus fleet are represented discretely with respect to a time step and based on each bus specific schedule. The model considers the traffic situation and road restrictions. Bus consumption was determined based on the bus longitudinal dynamics model and other auxiliary requirements, i.e., HVAC system and the basic auxiliary. Therefore, all the modelling challenges, which were discussed in Section 2.6, have been managed, and cleared from the simulation model.





## 9 References

### 9.1 Bibliography

- [1] Die Bundesregierung:  
**Zweiter Fortschrittsbericht zur Deutschen Anpassungsstrategie an den Klimawandel**  
Berlin, Germany, 2020.
- [2] Europäische Kommission:  
**Europa 2020. Eine Strategie für intelligentes, nachhaltiges und integratives Wachstum**  
Mitteilung der Europäischen Kommission  
Brüssel, Belgien, 2010.
- [3] Federal Ministry for the Environment, Nature Conservation, Building and Nuclear Safety:  
**Climate Action Plan 2050: Principles and goals of the German government's climate policy**  
Bundesministerium für Umwelt, Naturschutz, nukleare Sicherheit und Verbraucherschutz (BMUV)  
Berlin, Germany, 2016.
- [4] I. Kaddoura, R. Ewert, and K. Martins-Turner:  
**Exhaust and non-exhaust emissions from today's and future road transport: A simulation-based quantification for Berlin**  
Transportation Research Procedia, vol. 62, pp. 696–702, 2022.
- [5] Fabian Bergk, Wolfram Knörr, Udo Lambrecht:  
**Climate Protection in Transport–Need for Action in the Wake of the Paris Climate Agreement**  
ifeu - Institut für Energie- und Umweltforschung Heidelberg GmbH  
Heidelberg, Jun. 2017.
- [6] S. Grava:  
**Urban transportation systems: Choices for communities**  
New York, London: McGraw-Hill, 2002  
ISBN: 978-0071384179.
- [7] M. E. Garrett:  
**Encyclopedia of transportation: Social science and policy**  
Los Angeles: SAGE reference, 2014  
ISBN: 9781483389806.

- [8] M. Bartłomiejczyk:  
**Dynamic charging of electric buses**, 1st ed.  
Berlin: De Gruyter Open, 2019  
ISBN: 9783110645088.
- [9] M. Glotz-Richter and H. Koch:  
**Electrification of Public Transport in Cities (Horizon 2020 ELIPTIC Project)**  
Transportation Research Procedia, vol. 14, pp. 2614–2619, 2016.
- [10] F. Meishner and D. Uwe Sauer:  
**Technical and Economic Comparison of Different Electric Bus Concepts Based on Actual Demonstrations in European Cities**  
IET Electrical Systems in Transportation, vol. 10, no. 2, pp. 144–153, 2020.
- [11] M. Bartłomiejczyk:  
**Autonomous Battery Drive in Trolleybuses: an Overview of Practical Examples**  
Proceedings of 21st International Scientific Conference TRANSPORT MEANS, 2017.
- [12] M. Wazifehdust, D. Baumeister, M. Salih, P. Steinbusch, M. Zdrallek, C. von Kalben, and C. Troullier:  
**Grid State Evaluation of a LVDC Traction Network: Methods for the Analysis of Forecast Data**  
in CIRED 2021 - The 26th International Conference and Exhibition on Electricity Distribution, Online Conference, pp. 1236–1240.
- [13] International Electrotechnical Commission:  
**Railway Applications—Supply Voltages of Traction Systems**  
IEC: 60850, Nov. 2014.
- [14] D. Vierling, J. Dworacek, H. Ben Zid, and B. Schmuelling:  
**Smart trolley-bus systems: Why a presumed dead relic makes the difference to re-electrify public transportation**  
in 2016 IEEE International Energy Conference (ENERGYCON), pp. 1–6.
- [15] N. Neusel-Lange:  
**Dezentrale Zustandsüberwachung für intelligente Niederspannungsnetze**  
(Decentralised status control for intelligent low-voltage grids)  
Ph.D. Thesis, Bergische Universität Wuppertal, 2013  
Neue Energie aus Wuppertal, Volume 1.
- [16] Energy and Resources Institute (TERI):  
**TERI Energy & Environment Data Diary and Yearbook (TEDDY) 2019/20**  
New Delhi: The Energy and Resources Institute (TERI), 2021  
ISBN: 9788179936887.

- [17] European Parliament and the Council of the European Union:  
**Directive 2019/1161 on the promotion of clean and energy-efficient road transport vehicles (Clean Vehicles Directive)**  
[Online]. Available: <https://www.eumonitor.eu/9353000/1/j9vvik7m1c3gyxp/vl04czyb9kzs> (accessed: Jun. 1 2022).
- [18] Y. Huang, M. D. Seck, and A. Verbraeck:  
**Component-based light-rail modeling in discrete event systems specification (DEVS) SIMULATION**, vol. 91, no. 12, pp. 1027–1051, 2015.
- [19] A. Capasso, R. Lamedica, and C. Penna:  
**Energy Regeneration in Transportation Systems - Methodologies for Power-Networks Simulation**  
IFAC Proceedings Volumes, vol. 16, no. 4, pp. 119–124, 1983.
- [20] F. Du, J. H. He, L. Yu, M. X. Li, Z. Q. Bo, and A. Klimek:  
**Modeling and Simulation of Metro DC Traction System with Different Motor Driven Trains**  
in 2010 Asia-Pacific Power and Energy Engineering Conference, pp. 1–4.
- [21] F. Mao, Z. Mao, and K. Yu:  
**The Modeling and Simulation of DC Traction Power Supply Network for Urban Rail Transit Based on Simulink**  
Journal of Physics: Conference Series, vol. 1087, p. 42058, 2018.
- [22] Z. Tian, S. Hillmansen, C. Roberts, P. Weston, L. Chen, N. Zhao, S. Su, and T. Xin:  
**Modeling and simulation of DC rail traction systems for energy saving**  
in 17th International IEEE Conference on Intelligent Transportation Systems (ITSC), Qingdao, China, pp. 2354–2359.
- [23] W. S. Chan, B. Mellitt, and N. B. Rambukwella:  
**Whole system simulator for AC railways**  
in International Conference on Main Line Railway Electrification 1989, pp. 368–372.
- [24] J. J. Stickler:  
**Computer Simulation of an Electric Trolley Bus**  
United States. Urban Mass Transportation Administration.
- [25] K. J. Kutsmeda, K. G. Fehrle, and P. J. Trick:  
**Computer modeling, simulation, and validation by field testing of a traction power system for electric trolley buses**  
in Proceedings of the 1995 IEEE/ASME Joint Railroad Conference, Baltimore, MD, USA, pp. 87–91.

- [26] K. Mahmud and G. E. Town:  
**A review of computer tools for modeling electric vehicle energy requirements and their impact on power distribution networks**  
Applied Energy, vol. 172, pp. 337–359, 2016.
- [27] Y. Al-Wreikat and J. R. Sodre:  
**Evaluating the energy consumption of an electric vehicle under real-world driving conditions**  
SAE Technical Paper 0148-7191.
- [28] K. Liu, T. Yamamoto, and T. Morikawa:  
**Impact of road gradient on energy consumption of electric vehicles**  
Transportation Research Part D: Transport and Environment, vol. 54, pp. 74–81, 2017.
- [29] G. Papa, M. Santo Zarnik, and V. Vukašinović:  
**Electric-bus routes in hilly urban areas: Overview and challenges**  
Renewable and Sustainable Energy Reviews, vol. 165, p. 112555, 2022.
- [30] X. Yuan, C. Zhang, G. Hong, X. Huang, and L. Li:  
**Method for evaluating the real-world driving energy consumptions of electric vehicles**  
Energy, vol. 141, pp. 1955–1968, 2017.
- [31] J. Ji, Y. Bie, Z. Zeng, and L. Wang:  
**Trip energy consumption estimation for electric buses**  
Communications in Transportation Research, vol. 2, p. 100069, 2022.
- [32] Y. Al-Wreikat, C. Serrano, and J. R. Sodré:  
**Effects of ambient temperature and trip characteristics on the energy consumption of an electric vehicle**  
Energy, vol. 238, p. 122028, 2022.
- [33] Y. Liu and H. Liang:  
**A Data-Driven Approach for Electric Bus Energy Consumption Estimation**  
IEEE Transactions on Intelligent Transportation Systems, pp. 1–12, 2022.
- [34] M. Weisbach, U. Spaeth, and B. Schmuelling:  
**Energy Consumption Behavior Model for an Urban Transportation System Using Multidimensional Correlation Structures : Applied at the Trolley Bus System in Solingen (North Rhine-Westphalia, Germany)**  
in 2019 4th International Conference on Intelligent Transportation Engineering (ICITE), pp. 152–158.

- [35] M. Gallet, T. Massier, and T. Hamacher:  
**Estimation of the energy demand of electric buses based on real-world data for large-scale public transport networks**  
Applied Energy, vol. 230, pp. 344–356, 2018.
- [36] Z. Gao, Z. Lin, T. J. LaClair, C. Liu, J.-M. Li, A. K. Birky, and J. Ward:  
**Battery capacity and recharging needs for electric buses in city transit service**  
Energy, vol. 122, pp. 588–600, 2017.
- [37] X. He, S. Zhang, W. Ke, Y. Zheng, B. Zhou, X. Liang, and Y. Wu:  
**Energy consumption and well-to-wheels air pollutant emissions of battery electric buses under complex operating conditions and implications on fleet electrification**  
Journal of Cleaner Production, vol. 171, pp. 714–722, 2018.
- [38] M. Xylia, S. Leduc, P. Patrizio, F. Kraxner, and S. Silveira:  
**Locating charging infrastructure for electric buses in Stockholm**  
Transportation Research Part C: Emerging Technologies, vol. 78, pp. 183–200, 2017.
- [39] I. Hurtova, M. Sejkorova, J. Verner, and B. Sarkan:  
**Comparison of electricity and fossil fuel consumption in trolleybuses and buses**  
in 2018 17th International Scientific Conference Engineering for Rural Development, pp. 2079–2084.
- [40] M. Bartłomiejczyk:  
**Practical application of in motion charging: Trolleybuses service on bus lines**  
in 2017 18th International Scientific Conference on Electric Power Engineering (EPE), pp. 1–6.
- [41] Y. Gao, S. Guo, J. Ren, Z. Zhao, A. Ehsan, and Y. Zheng:  
**An Electric Bus Power Consumption Model and Optimization of Charging Scheduling Concerning Multi-External Factors**  
Energies, vol. 11, no. 8, p. 2060, 2018.
- [42] N. A. El-Taweel and H. E. Z. Farag:  
**Incorporation of Battery Electric Buses in the Operation of Intercity Bus Services**  
in 2019 IEEE Transportation Electrification Conference and Expo (ITEC), pp. 1–6.
- [43] N. A. El-Taweel, A. Zidan, and H. E. Z. Farag:  
**Novel Electric Bus Energy Consumption Model Based on Probabilistic Synthetic Speed Profile Integrated With HVAC**  
IEEE Transactions on Intelligent Transportation Systems, vol. 22, no. 3, pp. 1517–1531, 2021.

- [44] L. Li, S. You, and C. Yang:  
**Multi-Objective Stochastic MPC-Based System Control Architecture for Plug-In Hybrid Electric Buses**  
IEEE Transactions on Industrial Electronics, vol. 63, no. 8, pp. 4752–4763, 2016.
- [45] R. N. Jazar:  
**Advanced vehicle dynamics**  
Cham: Springer International Publishing, 2019  
ISBN: 3030130622.
- [46] D. S. Laila, P. Shakouri, A. Ordys, and M. Askari:  
**Longitudinal vehicle dynamics using Simulink/Matlab**  
in UKACC International Conference on CONTROL 2010, Coventry, UK, pp. 955–960.
- [47] N. Lin, C. Zong, and S. Shi:  
**The Method of Mass Estimation Considering System Error in Vehicle Longitudinal Dynamics**  
Energies, vol. 12, no. 1, p. 52, 2019.
- [48] A. Ritter:  
**Optimal Control of Battery-Assisted Trolley Buses**  
Ph.D. Thesis, Institute for Dynamic Systems and Control.
- [49] Š. Hamacek, M. Bartłomiejczyk, R. Hrbáč, S. Mišák, and V. Stýskala:  
**Energy recovery effectiveness in trolleybus transport**  
Electric Power Systems Research, vol. 112, pp. 1–11, 2014.
- [50] G. Stana and V. Brazis:  
**Two Trolleybus Motion Modeling by Calculating Transmission Loss Compensation Currents**  
in 2020 61st International Scientific Conference on Information Technology and Management Science of Riga Technical University (ITMS), pp. 1–6.
- [51] A. Ritter, P. Elbert, and C. Onder:  
**Energy Saving Potential of a Battery-Assisted Fleet of Trolley Buses**  
IFAC-PapersOnLine, vol. 49, no. 11, pp. 377–384, 2016.
- [52] H. Alnuman, D. Gladwin, and M. Foster:  
**Electrical Modelling of a DC Railway System with Multiple Trains**  
Energies, vol. 11, no. 11, p. 3211, 2018.

- [53] A. Jakubowski, L. Jarzebowicz, M. Bartłomiejczyk, J. Skibicki, S. Judek, A. Wilk, and M. Płonka:  
**Modeling of Electrified Transportation Systems Featuring Multiple Vehicles and Complex Power Supply Layout**  
Energies, vol. 14, no. 24, p. 8196, 2021.
- [54] M. Weisbach, U. Spaeth, M. Ghobadi, and B. Schmuelling:  
**Power Demand Prediction of Battery Overhead Line Buses based on a Neural Network Optimization**  
in 2020 IEEE Green Technologies Conference(GreenTech), pp. 133–135.
- [55] J. Ševčík, L. Adam, J. Příkryl, and V. Šmídl:  
**Solvability of the power flow problem in DC overhead wire circuit modeling**  
Appl.Math., vol. 66, no. 6, pp. 837–855, 2021.
- [56] International Electrotechnical Commission:  
**Railway applications – Power supply and rolling stock – Technical criteria for the coordination between power supply (substation) and rolling stock**  
IEC: 62313, Apr. 2009.
- [57] M. Bartłomiejczyk, L. Jarzebowicz, and J. Kohout:  
**Compensation of Voltage Drops in Trolleybus Supply System Using Battery-Based Buffer Station**  
Energies, vol. 15, no. 5, p. 1629, 2022.
- [58] M. Bartłomiejczyk:  
**Potential Application of Solar Energy Systems for Electrified Urban Transportation Systems**  
Energies, vol. 11, no. 4, p. 954, 2018.
- [59] M. Bartłomiejczyk and L. Jarzebowicz:  
**Utility analysis and rating of energy storages in trolleybus power supply system**  
in 2020 Zooming Innovation in Consumer Technologies Conference (ZINC), pp. 237–241.
- [60] I. Diab, B. Scheurwater, A. Saffirio, G. R. Chandra-Mouli, and P. Bauer:  
**Placement and sizing of solar PV and Wind systems in trolleybus grids**  
Journal of Cleaner Production, vol. 352, p. 131533, 2022.
- [61] U. Kreutzer and E. Blocher:  
**Mit Strom auf die Straße: Von der Elektromote zum eHighway**  
[Online]. Available: <https://new.siemens.com/de/de/unternehmen/konzern/geschichte/stories/mit-strom-auf-die-strasse.html> (accessed: Oct. 1 2021).

- [62] **The trolley bus : where it is and where it's going : based on the Workshop on Trolley Bus Applications, August 29-September 1, 1982, Seattle, Washington**  
Washington, D.C.: National Academy of Sciences, 1983.
- [63] W. Reinhardt:  
**Öffentlicher Personennahverkehr: Technik - rechtliche und betriebswirtschaftliche Grundlagen**, 1st ed.  
Wiesbaden: Vieweg + Teubner, 2012  
ISBN: 3834812684.
- [64] D. J. Victor and S. Ponnuswamy:  
**Urban transportation: Planning operation and management**  
New Delhi: Tata McGraw Hill Education Private Limited, 2012  
ISBN: 9781259002731.
- [65] Mattis Schindler:  
**Übersicht Obusbetriebe der Welt: Survey of the trolleybussystems in the world**  
[Online]. Available: <http://docplayer.org/6593167-Uebersicht-obusbetriebe-der-welt-survey-of-the-trolleybussystems-in-the-world.html> (accessed: Oct. 26 2021).
- [66] J. Spousta:  
**Trolleybus intermodal compendium**  
Brno: Centrum dopravního výzkumu, Divize rozvoje dopravy; Magistrát města Brna, Odbor dopravy, 2013  
ISBN: 978-80-86502-50-2.
- [67] Jürgen Lehmann:  
**Der Obus in Solingen - Aktuelle Situation: Der Obus in Solingen - kurzer Rückblick**  
[Online]. Available: <http://obus269.homepage.t-online.de/ObusSolingen.htm>  
(accessed: Oct. 11 2021).
- [68] H. Hondius:  
**E-Mobilität: Welche Rolle kann der Trolleybus spielen?: Stand und Perspektiven eines unterschätzten Verkehrsmittels**  
Der Nahverkehr, vol. 2018, 2018.
- [69] W. Stock:  
**Obus-Anlagen in Deutschland: die Entwicklung der Oberleitungs-Omnibus-Betriebe im Deutschen Reich, in der Bundesrepublik Deutschland und in der Deutschen Demokratischen Republik seit 1930**  
Bielefeld: Busch, 1987  
ISBN: 3-926882-00-X.



- [70] M. Faltenbacher:  
**Hybrid- und Elektrobuss-Projekte in Deutschland: Statusbericht 2015/16 :  
Arbeitsgruppe Innovative Antriebe Bus : erneuerbar mobil**  
Deutschland, Bundesministerium für Verkehr und Digitale Infrastruktur Deutschland,  
Bundesministerium für Umwelt, Naturschutz, Bau und Reaktorsicherheit NOW GmbH  
Berlin.
- [71] Lucien Mathieu:  
**Electric Buses Arrive on Time: Marketplace, Economic, Technology, Environmental  
and Policy Perspectives for Fully Electric Buses in the EU**  
Transport & Environment  
Brussels, Belgium, Nov. 2018  
[Online]. Available: [https://www.transportenvironment.org/sites/te/files/publications/  
Electric%20buses%20arrive%20on%20time.pdf](https://www.transportenvironment.org/sites/te/files/publications/Electric%20buses%20arrive%20on%20time.pdf) (accessed: Nov. 10 2021).
- [72] Sileo GmbH:  
**TECHNICAL SPECIFICATION: SILEO S18**  
[Online]. Available: <https://www.sileo-ebus.com/en/e-bus-models/e-bus-s18/>  
(accessed: Nov. 11 2021).
- [73] F. Bergk, K. Biemann, U. Lambrecht, R. Pütz, and H. Landinger:  
**Potential of In-Motion Charging Buses for the Electrification of Urban Bus Lines**  
J. Earth Sci. Geotech. Eng, vol. 6, pp. 347–362, 2016.
- [74] J. Zavada, J. Blašković Zavada, and K. Miloš:  
**Conditions for Implementing Trolleybuses in Public Urban Transport**  
PROMET, vol. 22, no. 6, pp. 467–474, 2010.
- [75] I. Boldea and S. A. Nasar:  
**The induction machine handbook**  
Boca Raton: CRC Press, 2002  
ISBN: 9781420042658.
- [76] M. Jurczak:  
**Integracja i konkurencja jako sposoby kształtowania publicznego transportu  
zbiorowego na przykładzie aglomeracji poznańskiej**  
Uniwersytet Ekonomiczny w Poznaniu, Poznań, 2013.
- [77] M. Wołek and O. Wyszomirski:  
**The trolleybus as an urban means of transport in the light of the Trolley project**  
Wydawnictwo Uniwersytetu Gdańskiego, Gdańsk, 2013.

- [78] F. Kiessling, R. Puschmann, and A. Schmieder:  
**Contact lines for electric railways: Planning, design, implementation**  
Munich: Publicis, 2001  
ISBN: 3895781525.
- [79] International Electrotechnical Commission:  
**Railway applications - Fixed installations - Electric traction - Copper and copper alloy grooved contact wires**  
IEC: 62917, Apr. 2009.
- [80] F. Kiessling, R. Puschmann, A. Schmieder, and E. Schneider:  
**Contact lines for electric railways: Planning, design, implementation, maintenance**  
Erlangen, Germany: Publicis Publishing, 2018  
ISBN: 9783895784200.
- [81] M. A. Laughton and D. F. Warne:  
**Electrical Engineer's Reference Book**: Elsevier Science, 2002  
ISBN: 9780080523545.
- [82] M. Krail, T. Gnann, S. Funke, S. Körner, E. Fritz, A. Müller, H. Neumann, F. Bartels, M. Steude, M. Franke, J. Elger, M. Balsler, J. Hietzge, P. Strauß, H. Schäuble, C. Hocke, A. Stephan, and R. Kayser:  
**Machbarkeit eines Hybridoberleitungsbusbetriebs – „Berlin-Spandau“**  
Karlsruhe, Dresden, 2019.
- [83] P. Arboleya, B. Mohamed, C. Gonzalez-Moran, and I. El-Sayed:  
**BFS algorithm for voltage-constrained meshed DC traction networks with nonsmooth voltage-dependent loads and generators**  
in 2017 IEEE Power & Energy Society General Meeting, Chicago, IL, p. 1.
- [84] A. Emadi, M. Ehsani, and J. M. Miller:  
**Vehicular electric power systems: Land, sea, air, and space vehicles**  
New York: Marcel Dekker; London : Momenta [distributor], 2004  
ISBN: 0-8247-4751-8.
- [85] D. Baumeister:  
**Betrieb und Planung von Oberleitungsbussystemen**  
(Operation and Planning of Trolleybus Systems)  
Ph.D. Thesis, Bergische Universität Wuppertal, 2022  
Neue Energie aus Wuppertal, Volume 50.

- [86] M. Wazifehdust:  
**Prädiktive Regelung und Optimierung eines Oberleitungsbussystems**  
(Predictive Control and Optimization of a Trolleybus System)  
Ph.D., Bergische Universität Wuppertal, 2023  
Neue Energie aus Wuppertal, Volume 51.
- [87] S. Kratz, B. Krueger, R. Wegener, and S. Soter:  
**Expansion of a Trolleybus Infrastructure towards a 100% Renewable Energy Usage**  
in *IEEE 48th Photovoltaic Specialists Conference (PVSC)*, pp. 233–236.
- [88] A. Bitoleanu, M. Popescu, and C. V. Suru:  
**Bidirectional static system for active D.C. traction substations: Theoretical and experimental evaluation**  
in 2017 5th International Symposium on Electrical and Electronics Engineering (ISEEE), Galati, pp. 1–10.
- [89] M. Lebküchner:  
**Zukunft des Trolleybusbetriebs**  
Infras Forschung und Beratung  
Zürich, 2007.
- [90] D. Jungnickel:  
**Graphs, networks and algorithms**, 4th ed.  
Heidelberg: Springer, 2013  
ISBN: 978-3-642-32278-5.
- [91] K. H. Rosen:  
**Discrete mathematics and its applications**  
New York NY: McGraw-Hill, 2019  
ISBN: 978-1-259-67651-2.
- [92] European Conference of Ministers of Transport (ECMT):  
**Speed Management**  
Paris: OECD Publishing, 2006  
ISBN: 9789282103784.
- [93] K. D. Lee and S. Hubbard:  
**Data structures and algorithms with Python**  
Cham: Springer, 2015  
ISBN: 978-3-319-13072-9.

- [94] H.-L. Dienel:  
**Die neue Nähe: Raumpartnerschaften verbinden Kontrasträume**  
Stuttgart: Steiner, 2004  
ISBN: 3-515-08492-4.
- [95] P. Kirchhoff:  
**Städtische Verkehrsplanung**  
Wiesbaden: Vieweg+Teubner Verlag, 2002  
ISBN: 978-3-519-00351-9.
- [96] J. Hellekes and C. Winkler:  
**Incorporating Passenger Load in Public Transport Systems and its Implementation in Nationwide Models**  
Procedia Computer Science, vol. 184, pp. 115–122, 2021.
- [97] J. Lehmann:  
**Mit dem Obus durch Solingen**  
Nordhorn: Verlag Kenning, 2019  
ISBN: 9783944390109.
- [98] D. Göhlich, T.-A. Fay, D. Jefferies, E. Lauth, A. Kunith, and X. Zhang:  
**Design of urban electric bus systems**  
Des. Sci., vol. 4, 2018.
- [99] D. Perrotta, A. Teixeira, H. Silva, B. Ribeiro, and J. Afonso:  
**Electrical Bus Performance Modeling for Urban Environments**  
SAE Int. J. Alt. Power., vol. 1, no. 1, pp. 34–45, 2012.
- [100] J. Larminie and J. Lowry:  
**Electric vehicle technology explained**  
Chichester, West Sussex, United Kingdom: Wiley, 2012  
ISBN: 978-1-119-94273-3.
- [101] P. D. Walker, S. Abdul Rahman, N. Zhang, W. Zhan, Y. Lin, and B. Zhu:  
**Modelling and Simulation of a Two Speed Electric Vehicle**  
in Sustainable Automotive Technologies 2012, Berlin, Heidelberg, pp. 193–198.
- [102] H.-P. Willumeit:  
**Modelle und Modellierungsverfahren in der Fahrzeugdynamik**  
Wiesbaden: Vieweg+Teubner Verlag, 1998  
ISBN: 978-3-663-12248-7.

- [103] A. Łebkowski:  
**Studies of Energy Consumption by a City Bus Powered by a Hybrid Energy Storage System in Variable Road Conditions**  
Energies, vol. 12, no. 5, p. 951, 2019.
- [104] Y. Li and R. L. West:  
**Rolling resistance revisited**  
Tire Science and Technology, vol. 47, no. 1, pp. 77–100, 2019.
- [105] R. Rajamani:  
**Vehicle dynamics and control**  
New York, Great Britain: Springer, 2006  
ISBN: 9780387263960.
- [106] J. Mwambeleko, T. Kulworawanichpong, and K. Greyson:  
**Tram and Trolleybus Net Traction Energy Consumption Comparison in**  
[Online]. Available: <http://ieeexplore.ieee.org/servlet/opac?punumber=7366880>
- [107] V. R. Vuchic:  
**Urban transit systems and technology**  
Hoboken, N.J.: Wiley; Chichester : John Wiley [distributor], 2007  
ISBN: 9780471758235.
- [108] K. R. Kambly and T. H. Bradley:  
**Estimating the HVAC energy consumption of plug-in electric vehicles**  
Journal of Power Sources, vol. 259, pp. 117–124, 2014.
- [109] Y. Luo, L. Li, and Y. Tan:  
**Electric Air Conditioning Control Method of Electric Bus Based on Driving Conditions**  
MATEC Web Conf., vol. 232, p. 4011, 2018.
- [110] E. Z. E. Conceição, M. C. G. Silva, J. C. S. André, and D. X. Viegas:  
**A Computational Model to Simulate the Thermal Behaviour of the Passengers Compartment of Vehicles**  
SAE Transactions, vol. 108, pp. 1483–1492, 1999  
[Online]. Available: <http://www.jstor.org/stable/44668021>
- [111] Verband Deutscher Verkehrsunternehmen:  
**VDV Recommendation 236: Air Conditioning of Diesel-and Gas-powered Buses as well as Hybrid Buses, Fuel Cell Buses and Electric Buses Operated as Line-service Buses according to Licensing Class I (Urban Line-service Buses) and Licensing Class II (Regional Line-service Buses) 11**  
[Online]. Available: <https://knowhow.vdv.de/documents/236/>

- [112] E. Specht:  
**Der Mensch als wärmetechnisches System: Mess-und Regelungsmechanismus der Betriebstemperatur, Wärmeabgabe, Energieerhaltung, Gewichtsänderung, Behaglichkeit**  
Otto-von-Guericke-Universität Magdeburg, 2005.
- [113] R. Hofstädter:  
**Energy Optimal Control of Thermal Comfort in Trams**  
Ph.D. Thesis, Vienna University of Technology, 2018.
- [114] P. von Böckh and T. Wetzel:  
**Heat transfer: Basics and practice**  
Heidelberg, New York: Springer, 2012  
ISBN: 978-3-642-19182-4.
- [115] N. E. Wijesundera:  
**Principles of Heating, Ventilation and Air Conditioning with Worked Examples:**  
WORLD SCIENTIFIC, 2016  
ISBN: 978-981-4667-76-0.
- [116] J. G. Ingersoll, T. G. Kalman, L. M. Maxwell, and R. J. Niemiec:  
**Automobile Passenger Compartment Thermal Comfort Model - Part I: Compartment Cool-Down/Warm-Up Calculation**  
in SAE Technical Paper Series.
- [117] G. Chiriac, D. D. Lucache, C. Nițucă, A. Dragomir, and S. Ramakrishna:  
**Electric Bus Indoor Heat Balance in Cold Weather**  
Applied Sciences, vol. 11, no. 24, p. 11761, 2021.
- [118] H. Berg:  
**Batteries for Electric Vehicles: Materials and Electrochemistry**  
Cambridge University Press, 2015  
ISBN: 9781107085930.
- [119] M. Pecht and M. Kang:  
**Prognostics and health management of electronics: Fundamentals, machine learning, and internet of things**  
Hoboken NJ: John Wiley & Sons, 2018  
ISBN: 9781119515333.
- [120] B. M. Wilamowski and J. D. Irwin:  
**The industrial electronics handbook. Control and mechatronics**  
Boca Raton, FL: CRC Press, 2016?  
ISBN: 9781439802908.

- [121] Y. Zhang, W. Song, S. Lin, and Z. Feng:  
**A novel model of the initial state of charge estimation for LiFePO<sub>4</sub> batteries**  
Journal of Power Sources, vol. 248, pp. 1028–1033, 2014.
- [122] R. Xiong:  
**Battery Management Algorithm for Electric Vehicles**  
Singapore: Springer Singapore, 2020  
ISBN: 978-981-15-0247-7.
- [123] International Electrotechnical Commission:  
**Insulation co-ordination: Part 2: Application guide**  
IEC: 60071-2, Dec. 1996.
- [124] International Electrotechnical Commission:  
**Insulation co-ordination: Part 1: Definitions, principles and rules**  
IEC: 60071, 1993.
- [125] F. Dorfler, J. W. Simpson-Porco, and F. Bullo:  
**Electrical Networks and Algebraic Graph Theory: Models, Properties, and Applications**  
Proceedings of the IEEE, vol. 106, no. 5, pp. 977–1005, 2018.
- [126] K. Korotkiewicz:  
**Koordinierte, Teilautarke Regelung von Mittelspannungsnetzen unter Einsatz dezentraler Automatisierungslösungen**  
(Partially Autonomous Coordinated Control of Medium-Voltage Networks Using Decentralised Automation Solutions)  
Ph.D. Thesis, Bergische Universität Wuppertal, 2021  
Neue Energie aus Wuppertal, Volume 31.
- [127] F. Dorsemagen:  
**Zustandsidentifikation von Mittelspannungsnetzen für eine übergreifende Automatisierung der Mittel- und Niederspannungsebene**  
(State Recognition of Medium-Voltage Networks for a General Automation of the Medium- and Low-Voltage Level)  
Ph.D. Thesis, Bergische Universität Wuppertal, 2018  
Neue Energie aus Wuppertal, Volume 19.
- [128] P. White:  
**Public transport: Its planning, management and operation**, 5th ed.  
London: Routledge, 2009  
ISBN: 9780203892282.

- [129] M. Salih, D. Baumeister, M. Wazifehdust, P. Steinbusch, M. Zdrallek, S. Mour, P. Deskovic, and T. Küll:  
**Impact Assessment of Integrating Novel Battery-Trolleybuses, PV Units and EV Charging Stations in a DC Trolleybus Network**  
Proceedings of the 2nd E-Mobility Power System Integration Symposium, Stockholm, Sweden (2018).
- [130] R. Uhlig:  
**Nutzung der Ladeflexibilität zur optimalen Systemintegration von Elektrofahrzeugen**  
(Leverage charging flexibility for optimal system integration of electric vehicles)  
Ph.D., Bergische Universität Wuppertal, 2017  
Neue Energie aus Wuppertal, Volume 13.
- [131] M. Motz, J. Huber, and C. Weinhardt:  
**Forecasting BEV charging station occupancy at work places**  
INFORMATIK 2020, Lecture Notes in Informatics (LNI), pp. 771–781, 2021.
- [132] M. S. Islam and N. Mithulananthan:  
**Daily EV load profile of an EV charging station at business premises**  
in 2016 IEEE Innovative Smart Grid Technologies - Asia (ISGT-Asia), pp. 787–792.
- [133] J. Zheng, X. Wang, K. Men, C. Zhu, and S. Zhu:  
**Aggregation Model-Based Optimization for Electric Vehicle Charging Strategy**  
IEEE Trans. Smart Grid, vol. 4, no. 2, pp. 1058–1066, 2013.
- [134] I. Anselmo and H. Mahmood:  
**Modeling and Simulation of EV Unscheduled Charging and its Impact on Distribution Systems**  
in 2021 IEEE PES Innovative Smart Grid Technologies Conference - Latin America (ISGT Latin America), pp. 1–5.
- [135] H J Wang, B Wang, C Fang, W Li, and H W Huang:  
**Charging Load Forecasting of Electric Vehicle Based on Charging Frequency**  
IOP Conference Series: Earth and Environmental Science, vol. 237, no. 6, p. 62008, 2019.
- [136] M. Shepero and J. Munkhammar:  
**Modelling charging of electric vehicles using mixture of user behaviours**  
in 1st e-mobility power system integration symposium, Berlin, Germany  
[Online]. Available: [https://mobilityintegrationsymposium.org/berlin2017/wp-content/uploads/sites/7/2018/06/emob17\\_034\\_posterpaper\\_shepero\\_mahmoud.pdf](https://mobilityintegrationsymposium.org/berlin2017/wp-content/uploads/sites/7/2018/06/emob17_034_posterpaper_shepero_mahmoud.pdf)



- [137] S. Dhameja:  
**Electric vehicle battery systems**  
Boston, Mass., Oxford: Newnes, 2002  
ISBN: 9780750699167.
- [138] J. J. Grainger and W. D. Stevenson:  
**Power system analysis**  
New York: McGraw-Hill, 1994  
ISBN: 0-07-113338-0.
- [139] A. R. Bergen and V. Vittal:  
**Power systems analysis**, 2nd ed.  
Upper Saddle River, N.J.: Prentice Hall; London : Prentice-Hall International, 2000  
ISBN: 0136919901.
- [140] J. D. Glover, T. J. Overbye, and M. S. Sarma:  
**Power system analysis & design**  
Boston MA: Cengage Learning, 2017  
ISBN: 1305632133.
- [141] J. D. Glover, M. S. Sarma, and T. J. Overbye:  
**Power system analysis and design**, 4th ed.  
Australia, Toronto Ont.: Thomson, 2008  
ISBN: 0534548849.
- [142] R. Idema and D. J. P. Lahaye:  
**Computational Methods in Power System Analysis**  
Paris: Atlantis Press; Imprint, 2014  
ISBN: 9789462390645.
- [143] D. P. Kothari and I. J. Nagrath:  
**Modern power system analysis**, 3rd ed.  
New Delhi: Tata McGraw-Hill Pub. Co, 2003  
ISBN: 0070494894.
- [144] L. Powell:  
**Power system load flow analysis**  
New York, London: McGraw-Hill, 2004  
ISBN: 0071447792.
- [145] H. Saadat:  
**Power system analysis**, 3rd ed.  
[United States]: PSA Pub, 2010  
ISBN: 9780984543861.

- [146] X.-F. Wang, Y.-H. Song, and M. Irving:  
**Modern power systems analysis**  
New York: Springer, 2008  
ISBN: 9780387728537.
- [147] B. M. Weedy:  
**Electric power systems**, 5th ed.  
Chichester, West Sussex, UK: John Wiley & Sons, 2012  
ISBN: 9780470682685.
- [148] A. J. Wood and B. F. Wollenberg:  
**Power Generation, Operation, and Control**, 2nd ed.  
New York, NY: John Wiley & Sons, 2012  
ISBN: 9781118585955.
- [149] D. Oeding and B. R. Oswald:  
**Elektrische Kraftwerke und Netze**  
Berlin, Heidelberg: Springer Berlin Heidelberg, 2016  
ISBN: 978-3-662-52702-3.
- [150] B. Stott, J. Jardim, and O. Alsac:  
**DC Power Flow Revisited**  
IEEE Trans. Power Syst., vol. 24, no. 3, pp. 1290–1300, 2009.
- [151] A. Benchaib:  
**Advanced control of AC/DC power networks: System of systems approach based on spatio-temporal scales**  
London, UK: ISTE; Wiley, 2015  
ISBN: 1119135788.
- [152] A. Garces:  
**On the Convergence of Newton's Method in Power Flow Studies for DC Microgrids**  
IEEE Trans. Power Syst., vol. 33, no. 5, pp. 5770–5777, 2018.
- [153] L. F. Grisales-Noreña, O. D. Montoya, W. J. Gil-González, A.-J. Perea-Moreno, and M.-A. Perea-Moreno:  
**A Comparative Study on Power Flow Methods for Direct-Current Networks Considering Processing Time and Numerical Convergence Errors**  
Electronics, vol. 9, no. 12, p. 2062, 2020.
- [154] C. Li, S. K. Chaudhary, T. Dragicevic, J. C. Vasquez, and J. M. Guerrero:  
**Power flow analysis for DC voltage droop controlled DC microgrids**  
in 2014 11th International Multi-Conference on Systems, pp. 1–5.

- [155] O. D. Montoya, V. M. Garrido, W. Gil-Gonzalez, and L. F. Grisales-Noreña:  
**Power Flow Analysis in DC Grids: Two Alternative Numerical Methods**  
IEEE Trans. Circuits Syst. II, vol. 66, no. 11, pp. 1865–1869, 2019.
- [156] O. D. Montoya, L. F. Grisales-Noreña, D. González-Montoya, C. A. Ramos-Paja, and A. Garces:  
**Linear power flow formulation for low-voltage DC power grids**  
Electric Power Systems Research, vol. 163, pp. 375–381, 2018.
- [157] K. F. Schäfer:  
**Netzberechnung**  
Wiesbaden: Springer Fachmedien Wiesbaden, 2020  
ISBN: 978-3-658-26732-2.
- [158] C. T. Tse:  
**Effective loadflow technique with non-constant MVA load for the Hong Kong Mass Transit Railway urban lines power distribution system**  
in APSCOM-97. International Conference on Advances in Power System Control, Operation and Management, Hong Kong, pp. 753–757.
- [159] N. H. van der Blij, D. Chaifouroosh, C. A. Canizares, T. B. Soeiro, L. M. Ramirez-Elizondo, M. T. J. Spaan, and P. Bauer:  
**Improved Power Flow Methods for DC Grids**  
in 2020 IEEE 29th International Symposium on Industrial Electronics (ISIE), Delft, Netherlands, pp. 1135–1140.
- [160] E. Zhou and A. Nasle:  
**Simulation of DC power distribution systems**  
in 1994 Industrial and commercial power systems technical conference, Irvine, CA, USA, pp. 191–195.
- [161] T. Kulworawanichpong:  
**Simplified Newton–Raphson power-flow solution method**  
International Journal of Electrical Power & Energy Systems, vol. 32, no. 6, pp. 551–558, 2010.
- [162] L. O. Chua, C. A. Desoer, and E. S. Kuh:  
**Linear and nonlinear circuits**  
New York, London: McGraw-Hill, 1987  
ISBN: 0070108986.

- [163] M. Salih, M. Koch, D. Baumeister, M. Wazifehdust, P. Steinbusch, and M. Zdrallek:  
**Adapted Newton-Raphson Power Flow Method for a DC Traction Network Including Non-Receptive Power Sources and Photovoltaic Systems**  
in 2019 IEEE PES Innovative Smart Grid Technologies Europe (ISGT-Europe), pp. 1–5.
- [164] R. K. Varma:  
**Smart inverters for PV solar power systems**, 1st ed.  
Hoboken: Wiley-IEEE Press, 2021  
ISBN: 9781119214212.
- [165] D. Baumeister, M. Salih, M. Wazifehdust, M. Koch, M. Zdrallek, P. Steinbusch, C. von Kalben, and J. O. Schumacher:  
**Power Control Model for Conventional and Battery Trolleybuses to Improve Voltage Profile in a DC Traction Network Simulation**  
in CIRED 2021 - The 26th International Conference and Exhibition on Electricity Distribution, Online Conference, pp. 1231–1235.
- [166] P. Arboleya, G. Diaz, and M. Coto:  
**Unified AC/DC Power Flow for Traction Systems: A New Concept**  
IEEE Trans. Veh. Technol., vol. 61, no. 6, pp. 2421–2430, 2012.
- [167] J. Beerten, S. Cole, and R. Belmans:  
**Generalized Steady-State VSC MTDC Model for Sequential AC/DC Power Flow Algorithms**  
IEEE Trans. Power Syst., vol. 27, no. 2, pp. 821–829, 2012.
- [168] M. E. El-Hawary and S. T. Ibrahim:  
**A new approach to AC-DC load flow analysis**  
Electric Power Systems Research, vol. 33, no. 3, pp. 193–200, 1995.
- [169] W. Liu, J. Zhang, H. Wang, T. Wu, Y. Lou, and X. Ye:  
**Modified AC/DC Unified Power Flow and Energy-Saving Evaluation for Urban Rail Power Supply System With Energy Feedback Systems**  
IEEE Trans. Veh. Technol., vol. 70, no. 10, pp. 9898–9909, 2021.
- [170] D. J. Tylavsky:  
**A Simple Approach to the Solution of the ac-dc Power Flow Problem**  
IEEE Trans. Educ., vol. 27, no. 1, pp. 31–40, 1984.
- [171] Y.-S. Tzeng:  
**Unified AC/DC power flow for system simulation in DC electrified transit railways**  
IEE Proc., Electr. Power Appl., vol. 142, no. 6, p. 345, 1995.

- [172] C. L. Pires, S. I. Nabeta, and J. R. Cardoso:  
**DC traction load flow including AC distribution network**  
IET Electr. Power Appl., vol. 3, no. 4, p. 289, 2009.
- [173] S.-L. Shaw:  
**Geographic information systems for transportation: from a static past to a dynamic future**  
Annals of GIS, vol. 16, no. 3, pp. 129–140, 2010.
- [174] M. Loidl, G. Wallentin, R. Cyganski, A. Graser, J. Scholz, and E. Haslauer:  
**GIS and Transport Modeling—Strengthening the Spatial Perspective**  
IJGI, vol. 5, no. 6, p. 84, 2016.
- [175] A. Banos and T. Thévenin:  
**Geographical information and urban transport systems**  
London, Hoboken NJ: ISTE; Wiley, 2011  
ISBN: 9781848212282.
- [176] S. Shekhar and H. Xiong:  
**Encyclopedia of Geographical Information Sciences**  
Berlin: Springer, 2008  
ISBN: 9780387359731.
- [177] B. Mearns:  
**QGIS Blueprints: Develop analytical location-based web applications with QGIS**  
Birmingham: Packt Publishing, 2015  
ISBN: 1785284096.
- [178] F. Ramm and J. Topf:  
**OpenStreetMap: Die freie Weltkarte nutzen und mitgestalten**, 3rd ed.  
Berlin: Lehmanns, 2010  
ISBN: 9783865416353.
- [179] E. Petroustos:  
**Google Maps: Power tools for maximizing the API**  
New York: McGraw-Hill Education, 2014  
ISBN: 9780071823043.
- [180] E. Hossain:  
**Excel Crash Course for Engineers**  
Cham: Springer, 2021  
ISBN: 9783030710354.

- [181] E. E. Mikhailov:  
**Programming with MATLAB for scientists: A beginner's introduction**, 1st ed.  
Boca Raton: CRC Press, 2017  
ISBN: 9781498738309.
- [182] M. Wazifehdust, D. Baumeister, M. Salih, P. Steinbusch, M. Zdrallek, S. Mour, and C. Troullier:  
**Potential Analysis for the Integration of Renewables and EV Charging Stations within a Novel LVDC Smart-Trolleybus Grid** in.
- [183] M. Salih, D. Baumeister, M. Wazifehdust, M. Koch, P. Steinbusch, M. Zdrallek, S. Mour, and C. Troullier, Eds.:  
**Optimized positioning for storage systems in an LVDC traction grid with non-receptive power sources and photovoltaic systems**  
Proceedings of the 9th Solar & Storage Integration Workshop, Dublin, 2018.

## 9.2 Publications of the author

- [I] Wazifehdust, M.; Baumeister, D.; Salih, M.; Zdrallek, M.; von Kalben, C.; Troullier, C.:  
**Modelbased Predictive Control System for Battery-Trolleybuses in a LVDC Traction Network**  
Proceedings of the 2021 IEEE PES Innovative Smart Grid Technologies Asia (ISGT-Asia), Virtual (2021)
- [II] Baumeister, D.; Salih, M.; Wazifehdust, M.; Koch, M.; Zdrallek, M.; Steinbusch, P.; von Kalben, C.; Schumacher, J.-O.:  
**Power Control Model for Conventional and Battery Trolleybuses to Improve Voltage Profile in a DC Traction Network Simulation**  
Proceedings of the International CIRED 2021 Conference, Virtual (2021)
- [III] Wazifehdust, M.; Baumeister, D.; Salih, M.; Steinbusch, P.; Zdrallek, M.; von Kalben, C.; Troullier, C.:  
**Grid State Evaluation of a LVDC Traction Network: Methods for the Analysis of Forecast Data**  
Proceedings of the International CIRED 2021 Conference, Virtual (2021)
- [IV] Baumeister, D.; Salih, M.; Wazifehdust, M.; Zdrallek, M.; von Kalben, C.; Schumacher, J.-O.:  
**Intelligent Trolleybus Guidance System with Short-Term Grid State Forecast**  
Proceedings of the 2021 IEEE PES Innovative Smart Grid Technologies Europe (ISGT-Europe), Virtual (2021)
- [V] Baumeister, D.; Wazifehdust, M.; Salih, M.; Zdrallek, M.; von Kalben C.; Schumacher J.-O.:  
**Optimal Catenary Planning of Trolleybus Systems**  
Proceedings of the International ETG Congress 2021, Virtual (2021)
- [VI] Wazifehdust, M.; Baumeister, D.; Salih, M.; Steinbusch, P.; Zdrallek, M.; von Kalben C.; Schumacher J.-O.:  
**Predictive Flexibility Calculation for Battery-Trolleybuses**  
Proceedings of the International ETG Congress 2021, Virtual (2021)
- [VII] Salih, M.; Baumeister, D.; Wazifehdust, M.; Koch, M.; Steinbusch, P.; Zdrallek, M.; Mour, S.; Troullier, C.:  
**Optimized Positioning for Storage Systems in an LVDC Traction Grid with Non-Receptive Power Sources and Photovoltaic Systems**  
Proceedings of the 9th Solar & Storage Integration Workshop, Dublin (2019)
- [VIII] Baumeister, D.; Salih, M.; Wazifehdust, M.; Koch, M.; Steinbusch, P.; Zdrallek, M.; Mour, S.; Troullier, C.:  
**Scenario Analyses of a Dynamic LVDC Smart-Trolleybus-Network with Battery-Assisted Traction Loads**  
Proceedings of the 3rd E-Mobility Power System Integration Symposium, Dublin (2019)
- [IX] Salih, M.; Koch, M.; Baumeister, D.; Wazifehdust, M.; Steinbusch, P.; Zdrallek, M.:  
**Adapted Newton-Raphson Power Flow Method for a DC Traction Network Including Non-Receptive Power Sources and Photovoltaic Systems**  
Proceedings of the 2019 IEEE PES Innovative Smart Grid Technologies Europe (ISGT-Europe), Bucharest (2019)
- [X] Wazifehdust, M.; Baumeister, D.; Salih, M.; Koch, M.; Steinbusch, P.; Zdrallek, M.; Mour, S.; Troullier, C.:  
**Potential Analysis for the Integration of Renewables and EV Charging Stations within a Novel LVDC Smart-Trolleybus Grid**

- Proceedings of the 25th International Conference on Electricity Distribution (CIRED 2019), Madrid (2019)
- [XI] Salih, M.; Baumeister, D.; Wazifehdust, M.; Steinbusch, P.; Zdrallek, M.; Mour, S.; Deskovic, P.; Küll, T.:  
**Impact Assessment of Integrating Novel Battery-Trolleybuses, PV Units and EV Charging Stations in a DC Trolleybus Network**  
Proceedings of the 2nd E-Mobility Power System Integration Symposium, Stockholm, Sweden (2018)
- [XII] Baumeister, D.; Salih, M.; Wazifehdust, M.; Steinbusch, P.; Zdrallek, M.; Mour, S.; Lenuweit, L.; Deskovic, P.; Ben Zid, H.:  
**Modelling and Simulation of a Public Transport System with Battery-trolleybuses for an Efficient E-mobility Integration**  
Proceedings of the 1st E-Mobility Power System Integration Symposium, Berlin (2017)



## 10 List of Symbols and Abbreviations

### 10.1 Mathematical Formulas and Symbols

$i, j, k, n, m, r, s, e$	indices
$\mathbb{N}_1$	natural number set
$\mathbb{R}$	real numbers set
$\mathbb{Z}$	integral numbers set
$X$	set
$\mathbf{X}$	matrix
$\mathbf{X}^{-1}$	inverse matrix
$x$	variable or set element
$\Delta x$	change in $x$
$\ x\ $	norm of $x$
$\{ \quad , \quad , \dots, \quad \}$	set brackets (set theory)
$\{ \quad   \quad \}$ or $\{ \quad : \quad \}$	set of ... such that ... (set theory)
$(\quad, \quad)$	open interval
$(\quad, \quad]$	left-open interval
$[\quad, \quad)$	right-open interval
$[ \quad, \quad ]$	closed interval
<b>mod</b>	remainder calculation
$diag(\mathbf{X})$	diagonal of matrix $\mathbf{X}$
$\odot$	hadamard product of matrices
$\oslash$	hadamard division of matrices
$ X $	size of set $X$ (set theory)
...	and so forth
$\quad \setminus \quad$	throw out (set theory)
$\in$	is an element of (set theory)
$\notin$	is not an element of (set theory)
$\subset$	is a subset of (set theory)
$\cap$	intersect (set theory)
$\cup$	union (set theory)
$\emptyset$ or $\{ \}$	empty set (set theory)
$\forall$	for all
$\exists$	there is
$\Leftrightarrow$	if and only if

$\wedge$	and
$\vee$	or
$:=$	is equal by definition to

## 10.2 List of Symbols

$A_{BS}$	total surface area
$A_c$	chassis area of the bus
$A_g$	window glass area
$A_f$	frontal area of the bus
$A_{ij}$	elements of the traction network adjacency matrix $A$
$a$	bus acceleration rate
$a'$	bus deceleration rate
$a_r$	bus rolling deceleration rate
$aw_p$	average passenger weight
$B_{at}$	set of arrival time (at bus depot)
$B_{dt}$	set of departure time (from bus depot)
$B_{line}$	bus line number
$B_{sp}$	specification set of given bus maker
$B_{state}$	bus state set
$B_{t,k,1}$	bus $k$ departure trip
$B_{t,k,i}$	bus $k$ trips set
$B_{t,k,n}$	bus $k$ arrival trip
$B_{trips}$	bus daily trips set
$B_{trs}$	travel segment
$BM_k$	bus model for bus $k$
$BS_{name}$	bus stop names set
$BS_{ts}$	bus stop names set
$B_{profile}$	bus profile matrix
$B_{TR}$	bus daily travelling route matrix
$BS_{dis}$	trip distance
$BS_{end}$	name of the last bus stop
$BS_{SP}$	paired of traffic nodes set
$BS_{start}$	name of the first bus stop
$BS_{trip}$	bus stop names along bus trip set
$BS_{trips}$	miscellaneous bus stop names along bus trip set
$d_r$	rolling distance
$C_p$	air specific heat capacity
$CS_{sp}$	EVCS specification set
$c_r$	rolling resistance coefficient
$c_d$	aerodynamic drag coefficient

$D$	distance between two consecutive stops
$D_{\text{paths}}$	corresponding distance of $R_{\text{paths}}$
$DS_{\text{Buses}}$	daily schedule of all buses
$d_b$	braking distance
$d(t)$	travelled distance between two consecutive traffic nodes at time ( $t$ )
$d'(t)$	travelled distance between two consecutive stops at time ( $t$ )
$d''(t)$	the travelled distance between two consecutive traction nodes at time ( $t$ )
$E$	edge
$E'$	energy consumption rate
$E_{\text{CB}}$	bus energy consumption
$E_{\text{sc}}$	battery effective capacity
$E_{\text{tn}}$	traffic branches
$EB_a$	AC branch attributes set
$EF_{a,k}$	AC network terminals attribute set
$EN_a$	AC node attributes set
$F_A$	aerodynamic drag force
$F_{\text{in}}$	inertia force
$F_R$	rolling resistance force
$F_{\text{r}}$	rolling resistance force over bus tire
$F_S$	grade (gravitational) force
$F_T$	tractive (traction) force
$G$	graph
$G_t$	nodal conductance matrices set
$G_{\text{tnw}}$	weighted road network graph
$G_{\text{tn}}$	road network graph
$\mathbf{G}_{t,z}$	nodal conductance matrix in zone $z$
$g$	gravitational acceleration
$g_{z,ii}$	nodal self-conductance in zone $z$
$g_{z,ij}$	mutual conductance between nodes $i$ and $j$ in zone $z$
$h_i$	inside convection coefficients
$h_o$	outside convection coefficients
$I$	indexing set
$Ibz$	indices of the operational buses in zone $z$
$Ibzn$	$Ibz$ corresponding new node Ids in zone $z$

$I_{CSZ}$	traction node Ids of EVCSs in zone $z$
$I_{pvz}$	traction node Ids of the PV systems in zone $z$
$I_{aux}$	bus auxiliary load current
$I_{bs}$	row indices (based on matrix $B_{pro,z}$ ) of buses sharing the same traction branch
$I_M$	bus motor current
$I_{z,i}$	current injection into node $i$ in zone $z$
$I_{ac,B}$	AC branch currents
$I_{ac}$	nodal current vector
$I'_{t,b}$	calculated steady state traction branch currents
$I_{t,z}$	nodal injection current in zone $z$
$J$	Jacobi matrix
$K$	incidence matrix
$K_{OB}$	Set of operational buses
$L_{xy}$	traffic nodes geographic coordinates set
$l$	length
$l_{b,z,o}$	length of the original traction branch in zone $z$
$l_{xy,i}$	traffic node $i$ geographic coordinate
$M$	bus total mass
$M_B$	regimes of motion
$M_{hc}$	control variable of heating system
$m_{et}$	number of traction branches
$m_{max}$	bus maximum mass
$m_{min}$	bus minimum mass
$m_r$	number of traffic nodes in bus daily travelling route
$m_t$	number of traffic branches
$N_{tps}$	traction transformer turns ratio
$N_{type}$	traffic node type numbers set
$N_{zn,z}$	set of new traction node Ids in zone $z$
$n_{bst}$	total number of the miscellaneous bus stop trips
$n_{bt}$	number of bus daily trips
$n_{bus}$	number of buses
$n_{cloud}$	number of the total recorded cloud data sets
$n_{cs}$	number of EVCSs
$n_{eb}$	total number of AC branches
$n_{ef}$	total number of terminals

$n_{en}$	total number of AC nodes
$n_{et,z}$	summation of the zone nodes
$n'_{et,z}$	number of traction nodes in zone $z$ plus $n_{op,z}$
$n_{et}$	number of traction nodes
$n_{op,z}$	number of operational buses in zone $z$
$n_p$	number of passengers in the bus cabin
$n_p$	passenger crowding
$n_s$	number of discrete samples
$n_{sb}$	number of the BSPSs
$n_{ss}$	number of simulation steps
$n_t$	number of traffic nodes
$n_{tps}$	total number of traction substation
$n_{type,et}$	number of all traction node types
$n_z$	number of zones
$n_a$	number of active AC nodes
$n_{type}$	number of traffic node types
$o$	row index of the original traction branch
$P$	power
$PV_{cloud}$	cloud indicator data set
$PA$	passive nodes set
$PC$	nodes with constant power set
$PP$	constant power and passive nodes set
$P_{ac,r}$	traction substation active AC power
$P_{ac}$	power profiles of active AC nodes
$P_{B,lbz}$	powers of the operational buses in zone $z$
$P_b$	regenerative braking power
$P'_B$	bus consumed/produced power
$P_{bat}$	battery power
$P_{baux}$	basic auxiliary power
$P_C$	passenger crowding intervals set
$P_{cal}$	calculated power
$P_{CS}$	expected power profile of EVCS
$P_{dwell}$	dwell probabilities set
$P_{HC}$	heating/cooling power consumption
$P_{HVAC}$	HVCA system total power consumption
$P_M$	bus motor power

$P_{PV,lpvz}$	PV systems power in zone $z$
$P_{PV}$	PV system realistic power profile
$P'_{PV}$	PV system ideal power profile
$P_{SB,icsz}$	powers of the BSPSs in zone $z$
$P_{SB}$	BSPS power
$P_{sc}$	battery charging/discharging power
$P_{T,k}$	total power of bus $k$
$P_{t,p}$	traction substation DC power
$P_t$	node power vectors set
$P_{TB}$	electric traction power
$P'_{TB}$	mechanical traction power
$P'_V$	ventilator power
$P_{z,lbzn}$	updated power of the node power vector $P_{t,z}$
$P_{z,icszn}$	EVCS node powers
$P'_{z,tsn}$	powers of the traction substations in zone $z$
$P_{z,i}$	power injected into node $i$ in zone $z$
$P_{ac,inj}$	injected active powers
$P_{loss}$	wasted powers
$P_{t,z}$	node power vector in zone $z$
$P'_t$	calculated steady state traction node powers
$p$	set of traction substation node Ids (DC traction side)
$Q_D(t)$	energy loss due to opening bus doors at time ( $t$ )
$Q_{HVAC}(t)$	HVAC thermal energy at time ( $t$ )
$Q_L(t)$	conductive and convective thermal losses energy at time ( $t$ )
$Q_P(t)$	passengers heat energy at time ( $t$ )
$Q_V(t)$	energy loss from ventilation at time ( $t$ )
$Q_{ac,inj}$	injected reactive powers
$q_p$	heat gained per passenger
$R'$	resistance per unit length
$RH$	rush hours set
$R_{paths}$	possible paths between two bus stops set
$R_{th,tot}$	total thermal resistance
$r$	set of traction substation node Ids (AC side)
$S_{max}$	maximum permitted speeds set
$S_n$	number of sections in the traction network

$SB_{sp}$	BSPS specifications set
$SM_{int}$	simulation interval set
$SM_{sd}$	simulation start (date and time) set
$SOC_{sb}$	BSPS battery SOC level
$SOC(t')$	new SOC
$SOC(t)$	last time step SOC
$SP$	stopping traffic node Ids set
$SP_{bs}$	traffic node set of type bus stops
$SP_{rj}$	traffic node set of type road junction
$SP_{tl}$	traffic node set of type traffic light
$T_{end}$	arriving time at the last bus stop
$T_i$	bus internal temperature
$T_o$	outside temperature
$T_{start}$	starting time at the first bus stop
$T_{t,u}$	upper comfort temperature
$T_t$	target comfort temperature
$TB_a$	traffic branches attributes set
$TEN_a$	traction nodes attributes set
$TEN_{type}$	traction node types set
$TB_{a1} \dots TB_{a6}$	traffic branches attribute subsets
$TEB_a$	traction branch attributes set
$TEB_{a1} \dots TEB_{a7}$	traction branch attribute subsets
$TEN_{a1} \dots TEN_{a6}$	traction nodes attribute subsets
$TN_a$	traffic node attributes set
$TN_{a1} \dots TN_{a9}$	traffic node attribute subsets
$TPS_i$	traction substation model
$t$	time
$t_{ab,k}$	arrival times of bus $k$
$t_{db,k}$	departure times of bus $k$
$t_{s1}$	stop-to-stop start time
$t_{s2}$	stop-to-stop end time
$t_{se}$	simulation end time
$t_{ss}$	simulation start time
$U$	voltage
$U_B$	bus voltage
$U_{cal}$	calculated voltage



$U_{\max 1}$	highest permanent voltage
$U_{\max 2}$	highest non-permanent voltage
$U_{\min 1}$	lowest permanent voltage
$U_{\min 2}$	lowest non-permanent voltage
$U_{n, MV}$	nominal voltage of medium voltage network
$U_n$	nominal traction network voltage
$U_{sb, low}$	BSPS lower voltage level
$U_{sb, up}$	BSPS upper voltage level
$U_t$	initial nodal voltages set
$U'_{z, zn}$	DC power flow solution of the nodal voltage in zone $z$
$\mathbf{U}_{ac}$	nodal voltage vector
$\mathbf{U}_{t, z}$	initial nodal voltages in zone $z$
$\mathbf{U}'_t$	calculated steady state traction node voltages
$V$	vertex
$VC$	nodes with constant voltage set
$V_b$	air mass inside bus
$V_{tn}$	traffic nodes
$\mathcal{V}_d$	air infiltration flow rate
$v$	velocity
$v(t')$	bus speed at time $(t')$
$v(t)$	bus speed at time $(t)$
$v'$	bus speed
$v_{m3}$	bus speed after utilising $M_B = 3$
$v_{\max}$	maximum permitted speed
$v_r$	bus speed before switching from rolling regime
$WT_{bs}$	dwelling times at bus stops set
$WT_{rj}$	dwelling time at road junction set
$WT_{tl}$	dwelling times at traffic lights set
$w_{tn}$	traffic branch lengths
$\mathbf{Y}_{ac, B}$	diagonal matrix
$\mathbf{Y}_{ac}$	nodal admittance matrix
$Z_{uni}$	zones with unidirectional traction substations
$zn$	set of new traction node Ids in zone $z$

---

$\alpha$	knee point factor
$\alpha_r$	reduction factor
$\Delta I_{z,k}$	mismatch current for traction node $k$ in zone $z$
$\delta d(t')$	change in distance at time ( $t'$ )
$\delta$	voltage angles
$\delta t$	time step
$\eta$	efficiency
$\eta_c$	coulomb efficiency
$\eta_{hc}$	thermal to electrical energy ratio
$\eta_m$	electrical motor efficiency
$\eta_b$	regenerative braking efficiency
$\eta'_b$	overall braking efficiency
$\theta$	gradient of the road
$\rho_{air}$	air density
$\tau_b$	braking interval
$\tau_c$	constant-speed interval
$\tau_{int}$	simulation interval in second
$\tau_r$	rolling interval
$\tau_{rb}$	time interval for both rolling and braking regimes
$\tau_{rw}$	real world time samples set
$\tau_s$	simulation time samples set
$\tau_{ss}$	stop-to-stop travel interval
$\tau_{sb}$	timeframe time sequence set
$\tau_a$	acceleration interval
$\Psi_{sb}$	BSPS operating modes
$\Psi'_{sb}$	BSPS framed operating mode
$\psi_{bat}$	battery operating mode
$\psi_{door}$	condition of the bus doors
$\psi_v$	ventilation system functional condition

### 10.3 Abbreviations

AC	alternate current
BDTRM	bus daily travelling routes model
BEB	battery-electric bus
BF	Backward-Forward
BM	bus model
BPTB	battery-powered trolleybus
BSPS	battery storage power station
BTB	battery-trolleybus
CO <sub>2</sub>	carbon dioxide
CSV	comma-separated values
DC	direct current
DIN	<i>ger.</i> : Deutsches Institut für Normung
DTM	daily timetable model
DTMM	digital terrain map model
EBTB	electric battery-trolleybus
e.g.	for example
EN	European norms
ENM	electric network model
EVCS	electric vehicle charging station
GHG	greenhouse-gas
GIS	geographical information system
GPS	global positioning system
GS	Gauss-Seidel
HVAC	heating, ventilation, and air conditioning
IEC	international electrotechnical commission
IEEE	institute of electrical and electronics engineers
i.e.	that is
IMC	in-motion charging
LiFePO <sub>4</sub>	lithium iron phosphate
LTO	lithium titanate
LVDC	low voltage direct current
MV	medium voltage
MVAC	medium voltage alternating current
NC	normally close
NMC	nickel-manganese-cobalt
NO	normally open

NR	Newton-Raphson
OHCW	overhead contact wire
PV	photovoltaic
RNM	road network model
SNR	simplified Newton-Raphson
SOC	state-of-charge
STS	smart trolleybus system
TB	trolleybus
TBSSM	trolleybus system simulation model
TNM	traffic network model
TNZ	traction network zone
TSM	traffic state model
VDV	<i>ger:</i> Verband Deutscher Verkehrsunternehmen

# 11 Annex

## 11.1 Solingen Digital Terrain Map

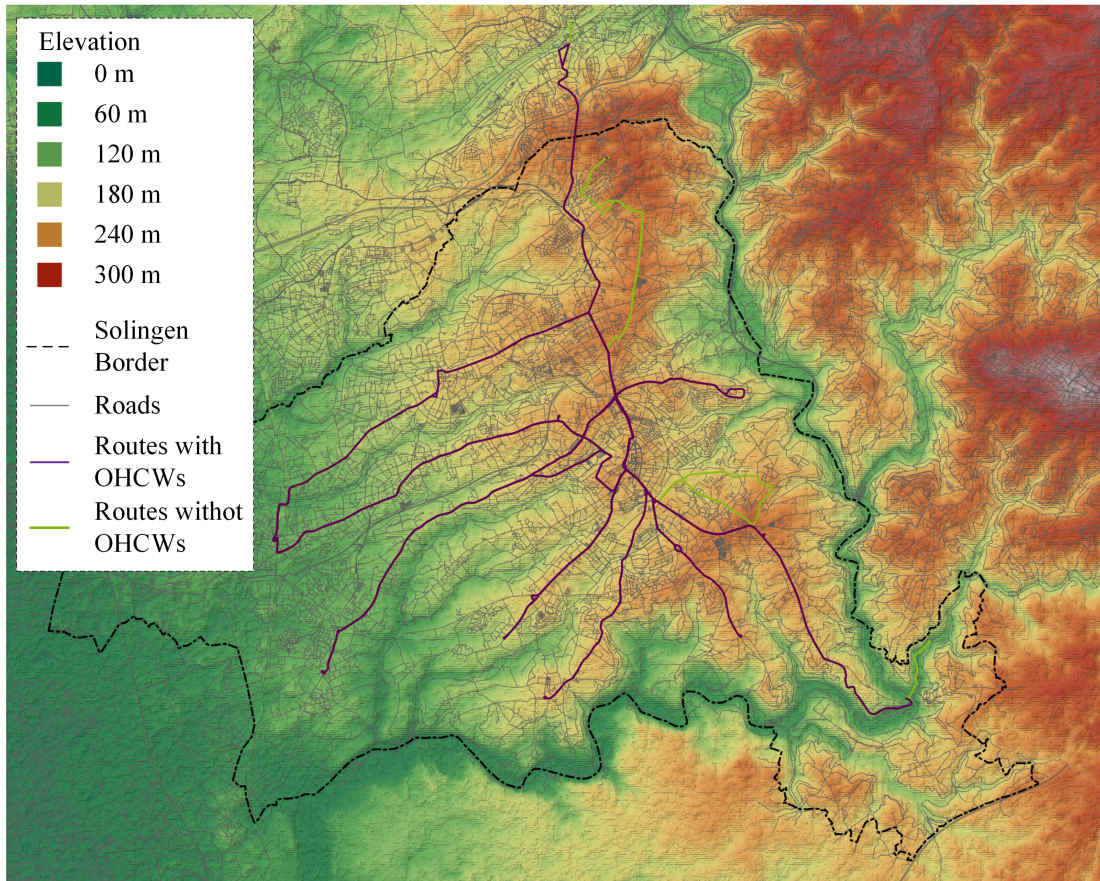


**Figure 11-1: Overview of the entire terrain map of Solingen, including the road network and the trolleybus travel routes (with and without overhead contact wires (OHCWs)).**

## 11.2 Real-World Outside Temperature Data

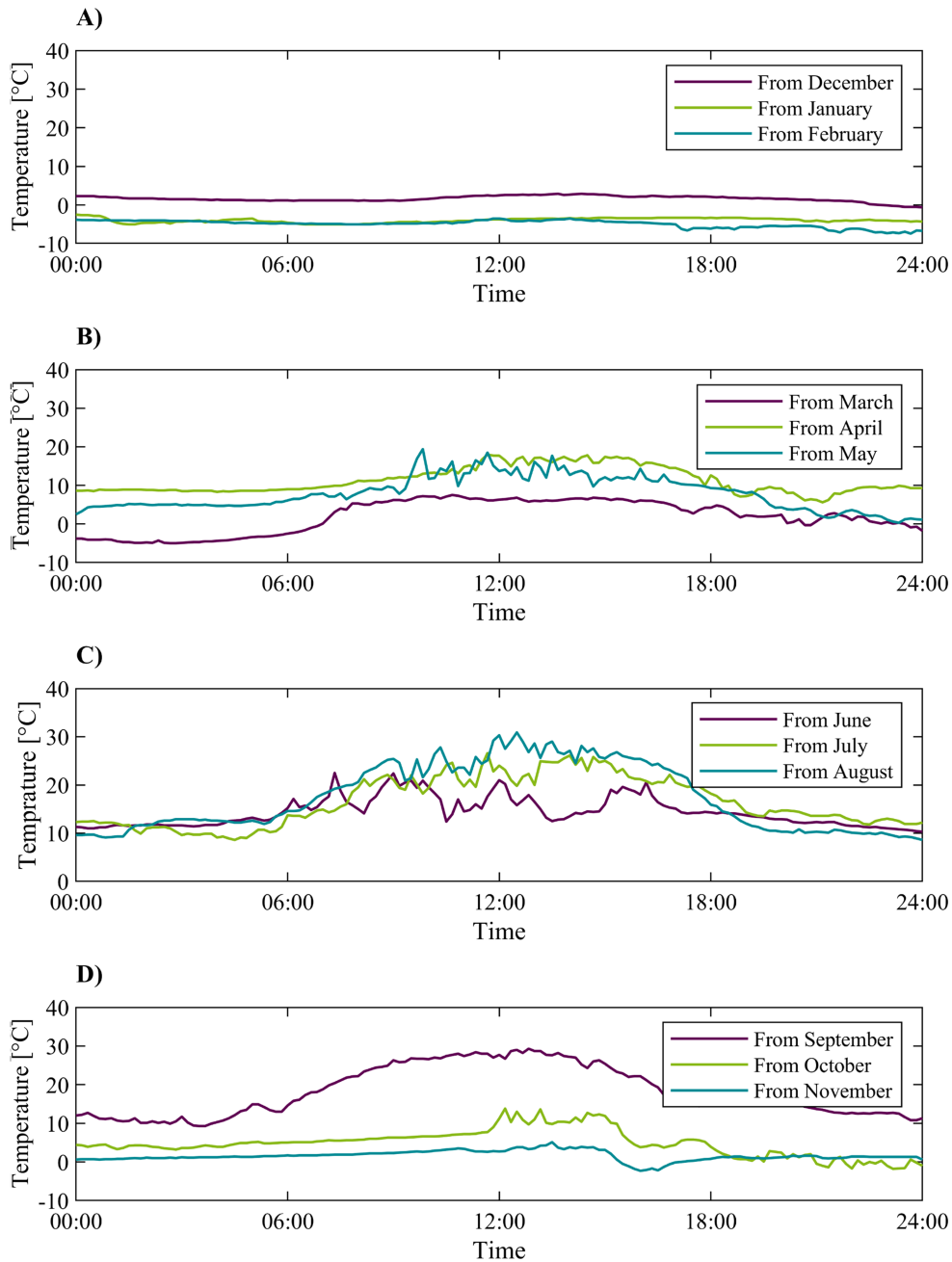


**Figure 11-2:** Various measured real-world temperatures collected from different years. Each curve in the four figures represents the temperature of a random day selected from the measured data within the indicated month.

- A) Temperature during three different days from the winter season.**
- B) Temperature during three different days from the spring season.**
- C) Temperature during three different days from the summer season.**
- D) Temperature during three different days from the autumn season.**

### 11.3 Bus Daily Timetable (Schedule)

Table 11-1: A sample from Solingen bus daily timetable referenced to Equations 3.5, 3.6, and 3.10 input parameters.

$DS_{Buses}$ (Equation 3.10)							
		Bus Line No.	Trip Start Time	First Bus Stop	Trip End Time	Last Bus Stop	Trip Distance
$B_{trips,k}$	$B_{t,k,i}$	$B_{line}$	$T_{start}$	$BS_{star}$	$T_{end}$	$BS_{end}$	$BS_{dis}$
$k = 1$	$i = 1$	Departure	9:01	ELBA	9:05	KLIH	0.960km
	$i = 2$	684/05	9:05	KLIH	9:24	HASS	4.955km
	$i = 3$	684/05	9:27	HASS	9:55	WIDD	7.840km
	$i = 4$	684/05	10:10	WIDD	10:39	HASS	8.060km
	:	684/05	10:42	HASS	11:10	WIDD	7.840km
		684/05	11:25	WIDD	11:54	HASS	8.060km
		684/05	11:57	HASS	12:25	WIDD	7.840km
		684/05	12:40	WIDD	13:09	HASS	8.060km
		684/05	13:12	HASS	13:40	WIDD	7.840km
		684/05	13:55	WIDD	14:24	HASS	8.060km
		684/05	14:27	HASS	14:55	WIDD	7.840km
		684/05	15:10	WIDD	15:39	HASS	8.060km
		684/05	15:42	HASS	16:10	WIDD	7.840km
		684/05	16:25	WIDD	16:54	HASS	8.060km
		684/05	16:57	HASS	17:25	WIDD	7.840km
		684/05	17:40	WIDD	18:09	HASS	8.060km
		684/05	18:12	HASS	18:31	MANG	5.207km
$i = n_{bt,1}$	Arrive	18:31	MANG	18:36	ELBA	0.494km	
$k = 1$	$i = 1$	Departure	5:43	BHOF	5:46	MANG	0.575km
	$i = 2$	685/02	5:46	MANG	6:10	AUFD	9.485km
	$i = 3$	686/02	6:30	AUFD	6:50	GWPL	7.992km
	$i = 4$	685/02	6:52	GWPL	7:10	AUFD	7.567km
	:	:					
:							

**Table 11-2: A sample the miscellaneous bus stop trips referenced to Equations 3.7, 3.8, and 3.9 input parameters.**

$BS_{trips}$ (Equation 3.9)							
	Bus Line No.	First Bus Stop	Last Bus Stop	Trip Distance	Trip Bus Stops		
$BS_{trip,i}$	$B_{line}$	$BS_{start}$	$BS_{end}$	$BS_{dis}$	$BS_{ts}$		
$i = 1$	684	MANG	WIDD	6.361km	Mangenberg A	...	Schule Widdert
$i = 2$	684	WIDD	HASS	8.060km	Schule Widdert	...	Hasselstraße
$i = 3$	684	WIDD	MANG	6.585km	Schule Widdert	...	Mangenberg B
⋮	685	AUFD	GWPL	7.972km	Aufderhöhe B	...	Graf-Wilhelm-Platz D
	685	AUFD	MANG	9.702km	Aufderhöhe B	...	Mangenberg B
	685	GWPL	AUFD	7.567km	Graf-Wilhelm-Platz E	...	Aufderhöhe B
	685	KLIH	AUFD	6.056km	Klingenhalle	...	Aufderhöhe B
	685	MANG	AUFD	9.485km	Mangenberg A	...	Aufderhöhe B
⋮							
⋮							



## 11.4 Buses Specifications

Table 11-3: Bus specifications data for 4 different buses variety referenced to Equation 3.43 and Table 3-1.

Set Element (Table 3-1)		Variety 1 ( $i = 1$ )	Variety 2 ( $i = 2$ )	Variety 3 ( $i = 2$ )	Variety 4 ( $i = 4$ )
$b_{sp1,i}$	$B_{type}$	Berkhof: Premier AT 18	Van Hool: AG 300 T	Carrosserie Hess: Swisstrolley 3	Solaris: Trollino 18.75
$b_{sp2,i}$	$m_{min}$	16,650	16,700	18,000	18,000
$b_{sp3,i}$	$m_{max}$	26,600	26,900	28,000	27,000
$b_{sp4,i}$	$\lambda_m$	1.05	1.05	1.05	1.05
$b_{sp5,i}$	$L_b$	17.96	17.98	17.976	18.75
$b_{sp6,i}$	$W_b$	2.5	2.49	2.55	2.55
$b_{sp7,i}$	$H_m$	3.5	3.5	3.5	3.49
$b_{sp8,i}$	$v_{bs}$	70	65	65	70
$b_{sp9,i}$	$pn_{max}$	160	135	131	150
$b_{sp10,i}$	$a$	0.5	0.5	0.5	0.6
$b_{sp11,i}$	$a'$	-0.5	-0.5	-0.5	-0.6
$b_{sp12,i}$	$c_d$	0.65	0.65	0.65	0.6
$b_{sp13,i}$	$c_r$	0.015	0.015	0.015	0.008
$b_{sp14,i}$	$\eta_m$	0.85	0.85	0.85	0.85
$b_{sp15,i}$	$\eta_b$	0.6	0.6	0.6	0.6
$b_{sp16,i}$	$P_m$	172,000	210,000	320,000	320,000
$b_{sp17,i}$	$P_{BH}$	50440	50440	50440	35000
$b_{sp18,i}$	$P_{BAC}$	30240	30240	30240	55000
$b_{sp19,i}$	$P'_V$	750	750	750	750
$b_{sp20,i}$	$\eta_{hc}$	2.3	2.3	2.3	2.3
$b_{sp21,i}$	$P_{baux}$	150	150	150	150
$b_{sp22,i}$	$\rho_{air}$	1.2041	1.2041	1.2041	1.2041
$b_{sp23,i}$	$C_p$	1005	1005	1005	1005
$b_{sp24,i}$	$L_g$	0.008	0.008	0.008	0.008
$b_{sp25,i}$	$L_c$	0.009	0.009	0.009	0.009
$b_{sp26,i}$	$k_g$	0.0566	0.0566	0.0566	0.0566
$b_{sp27,i}$	$k_c$	0.0738	0.0738	0.0738	0.0738
$b_{sp28,i}$	$P_{bdis}$				300,000
$b_{sp29,i}$	$P_{bcha}$				180,000
$b_{sp30,i}$	$E_{sc}$				45,000
$b_{sp31,i}$	$SOC_{ini}$				1

## 11.5 Traction Substations Specifications

Table 11-4: Traction substations specifications referenced to Equation 4.4 input parameters.

TPS (Equation 4.4)					
Index	Traction Node Id	AC Node Id	Rectifier Type	Number of Transformer	Capacity (kVA)
$i$	$tps_1$	$tps_2$	$tps_3$	$tps_4$	$tps_5$
1	1	301	1	1	1000
2	5	870	1	1	1000
3	19	368	1	1	1000
4	21	679	1	1	500
5	23	775	1	1	1000
6	30	757	1	1	1000
7	11	356	1	1	1000
8	177	259	1	1	1000
9	32	729	1	1	1000
10	80	983	1	1	1000
11	37	160	1	2	2000
12	39	179	1	1	1000
13	106	71	1	1	1000
14	135	243	1	1	1000
15	138	118	1	1	1000
16	124	953	1	2	1600
17	144	908	1	1	1000
18	146	-	1	1	1000
19	143	914	1	1	1000
20	71	214	1	1	1000
21	88	569	1	1	1000
22	91	433	1	1	1000
23	350	294	1	1	360

## 11.6 Photovoltaic Systems Specifications

Table 11-5: PV systems specifications referenced to Equation 4.20 input parameters.

$PV_{sp}$ (Equation 4.20)					
Index	Traction Node Id	Installed Power (kW)	Latitude (degrees)	Altitude (m)	Azimuth (degrees)
$i$	$pv_{sp1}$	$pv_{sp2}$	$pv_{sp3}$	$pv_{sp4}$	$pv_{sp5}$
1	274	87	51	30	0
2	276	30	51	30	0
3	278	59	51	30	0
4	280	21	51	30	0
5	282	24	51	30	0
6	283	30	51	30	0
7	285	96	51	30	0
8	287	30	51	30	0
9	288	72	51	30	0
10	289	22	51	30	0
11	290	52	51	30	0
12	292	22	51	30	0
13	293	63	51	30	0
14	294	29	51	30	0
15	295	92	51	30	0
16	297	50.56	51	30	0

## 11.7 Electric Vehicle Charging Stations Specifications

Table 11-6: EVCSs specifications referenced to Equation 4.24 input parameters.

$CS_{sp}$ (Equaion 4.24)					
Index	Traction Node Id	Maximum Charging Power (kW)	No. of Charging Ports	Location	Occupancy Rate (percent)
$i$	$CS_{sp1}$	$CS_{sp2}$	$CS_{sp3}$	$CS_{sp4}$	$CS_{sp5}$
1	323	22	1	1	90
2	324	22	1	2	90
3	325	22	1	3	90
4	326	22	1	1	90
5	327	22	1	1	80
6	328	22	1	1	60
7	329	22	1	1	90
8	330	22	1	1	90
9	331	22	1	1	70
10	332	22	1	1	100
11	333	22	1	1	60
12	334	22	1	1	70
13	335	22	1	1	90
14	336	22	1	1	90
15	337	22	1	2	90
16	338	22	1	1	90
17	339	22	1	2	90
18	340	22	1	1	90

## 11.8 Battery Storage Power Stations Specifications

Table 11-7: BSPSs specifications referenced to Equation 4.26 input parameters.

$SB_{sp}$ (Equation 4.26)						
Index	Traction Node Id	Discharging Power (W)	Charging Power (W)	Battery Effective Energy (W/h)	Initial SOC (percent)	Operating Setting
$i$	$sb_{sp1}$	$sb_{sp2}$	$sb_{sp3}$	$sb_{sp4}$	$sb_{sp5}$	$sb_{sp6}$
1	301	140000	140000	90000	100	1
2	302	140000	140000	90000	100	1

## **NEUE ENERGIE AUS WUPPERTAL**

Publication series of the Chair of Power Systems Engineering,  
University of Wuppertal

Publisher: Univ.-Prof. Dr.-Ing. Markus Zdrallek

### **Band 1**

Neusel-Lange, Nils:

Dezentrale Zustandsüberwachung für intelligente Niederspannungsnetze

1. Auflage 2013

ISBN 978-3-8442-7401-1

### **Band 2**

Stötzel, Marcus:

Strategische Ressourcendimensionierung von Netzleitstellen in Verteilungsnetzen

1. Auflage 2014

ISBN 978-3-8442-7826-2

### **Band 3**

Zdrallek, Markus (Hrsg.):

Tagungsband zum 2. Wuppertaler Energie-Forum

1. Auflage 2014

### **Band 4**

Oerter, Christian:

Autarke, koordinierte Spannungs- und Leistungsregelung in Niederspannungsnetzen

1. Auflage 2014

ISBN 978-3-7375-1758-4

### **Band 5**

Athamna, Issam:

Zuverlässigkeitsberechnung von Offshore-Windparks

1. Auflage 2015

ISBN 978-3-7375-5678-1

### **Band 6**

Thies, Hans Henning:

Ein übergreifendes Modell zur Optimierung von Netz und Netzbetrieb

1. Auflage 2015

ISBN 978-3-7375-7465-5

### **Band 7**

Zdrallek, Markus (Hrsg.):

Tagungsband zum 3. Wuppertaler Energie-Forum

1. Auflage 2016

### **Band 8**

Harnisch, S.; Steffens, P.; Thies, H.; Monscheidt, J.; Münch, L.; Böse, C.; Gemsjäger, B.:

Planungs- und Betriebsgrundsätze für ländliche Verteilungsnetze - Leitfaden zur

Ausrichtung der Netze an ihren zukünftigen Anforderungen

1. Auflage 2016

### **Band 9**

Pawlowski, Erik:

Realitätsgerechte Zustandsbewertung gasisolierter Hochspannungsschaltanlagen

1. Auflage 2016

ISBN 978-3-7418-1983-4

### **Band 10**

Zdrallek, Markus (Hrsg.):

BUW Seminar „Smart Grids“ - Aufbau und Betrieb von intelligenten Verteilnetzen

1. Auflage 2016

### **Band 11**

Beerboom, Dominik:

Objektive Zustandsbewertung von Mittelspannungsnetzen als Grundlage der Asset-

Optimierung

1. Auflage 2017

ISBN: 978-3-7418-9539-5

### **Band 12**

Tabke, Thorsten:

Entwicklung und Anwendung eines typunabhängigen, minimalinvasiven

Zustandsbewertungsverfahrens für SF6-Hochspannungsschaltanlagen

1. Auflage 2017

ISBN: 978-3-7450-0240-9

### **Band 13**

Uhlig, Roman:

Nutzung der Ladeflexibilität zur optimalen Systemintegration der Elektromobilität

1. Auflage 2017

ISBN: 978-3-7450-5959-5

**Band 14**

Zdrallek, Markus (Hrsg.):  
Tagungsband zum 4. Wuppertaler Energie-Forum  
1. Auflage 2018

**Band 15**

Zdrallek, Markus (Hrsg.):  
Lehrstuhl für Elektrische Energieversorgungstechnik – Portrait  
1. Auflage 2018

**Band 16**

Steffens, Philipp:  
Innovative Planungsgrundsätze für ländliche Mittelspannungsnetze  
1. Auflage, 2018  
ISBN: 978-3-7450-9538-8

**Band 17**

Johae, Christopher:  
Realitätsgerechte Zustandsbewertung von Mittelspannungsanlagen durch Einsatz geeigneter  
Messverfahren  
1. Auflage 2018  
ISBN: 978-3-7467-4381-3

**Band 18**

Meese, Jan:  
Dynamische Stromtarife zur Erschließung von Flexibilität in Industrieunternehmen  
1. Auflage 2018  
ISBN: 978-3-7467-7558-6

**Band 19**

Dorsewagen, Felix:  
Zustandsidentifikation von Mittelspannungsnetzen für eine übergreifende Automatisierung  
der Mittel- und Niederspannungsebene  
1. Auflage 2018  
ISBN: 978-3-7467-7488-6

**Band 20**

Harnisch, Johannes Sebastian:  
Planung von ländlichen Niederspannungsnetzen mit innovativen Lösungsoptionen  
1. Auflage 2019  
ISBN: 978-3-7485-2122-8

### **Band 21**

Nebel, Arjuna:

Auswirkung einer übergeordneten Steuerung dezentraler elektrischer Anlagen auf die Höhe des konventionellen positiven Redispatcheinsatzes in Deutschland

1. Auflage 2019

ISBN: 978-3-7485-1948-5

### **Band 22**

Kornrumpf, Tobias:

Bewertung von Flexibilitätsoptionen in Mittelspannungsnetzen

1. Auflage 2019

ISBN: 978-3-7485-1394-0

### **Band 23**

Zdrallek, Markus (Hrsg.):

BUW Seminar „Smart Grids 2019“ - Aufbau und Betrieb von intelligenten Verteilnetzen

1. Auflage 2019

### **Band 24**

Wolter, Daniel:

Neue Topologiekonzepte für moderne Mittelspannungsnetze

1. Auflage 2019

ISBN: 978-3-7485-8662-3

### **Band 25**

Hopfer, Nikolai:

Nutzen der Breitband-Powerline-Kommunikation zur Erfassung kritischer Kabelzustände in Mittel- und Niederspannungsnetzen

1. Auflage 2020

ISBN: 978-3-7502-7734-2

### **Band 26**

Zdrallek, Markus (Hrsg.):

Tagungsband zum 5. Wuppertaler Energie-Forum

1. Auflage 2020

### **Band 27**

Schäfer, Karl Friedrich:

Netzberechnung - Übungsaufgaben mit Lösungen

1. Auflage 2020

ISBN 978-3-7502-7910-0



### **Band 28**

Dahlmann, Benedikt:

Aktivierung und Vermarktung industrieller Flexibilitätsoptionen mittels eines dynamischen Stromtarifs

1. Auflage 2020

ISBN 978-3-7529-6673-2

### **Band 29**

Ludwig, Marcel:

Automatisierung von Niederspannungsnetzen auf Basis von Multiagentensystemen

1. Auflage 2020

ISBN 978-3-7529-8649-5

### **Band 30**

Zdrallek, Markus (Hrsg.):

Tagungsband BUW Seminar "Elektromobilität in der Netzplanung" - Strategien für Ladeinfrastruktur, Anwendungsfälle und Praxisbeispiele

1. Auflage 2020

### **Band 31**

Korotkiewicz, Kamil:

Koordinierte, teilautarke Regelung von Mittelspannungsnetzen unter Einsatz dezentraler Automatisierungslösungen

1. Auflage 2020

ISBN 978-3-7541-5783-1

### **Band 32**

Steinbusch, Philippe:

Adaptive, aufwandsminimale und fehlerrobuste Automatisierung von Niederspannungsnetzen

1. Auflage 2020

ISBN 978-3-7541-1625-8

### **Band 33**

Möhrke, Fabian:

Auswirkungen der Energiewende auf die Zuverlässigkeit von Nieder- und Mittelspannungsnetzen

1. Auflage 2021

ISBN 978-3-7541-6565-2

### **Band 34**

Wruk, Julian:

An Optimisation Approach to Automated Strategic Network Planning at Low-Voltage Level

1. Auflage 2021

ISBN 978-3-7541-5679-7

### **Band 35**

Wintzek, P.; Ali, S. A.; Monscheidt, J.; Gemsjäger, B.; Slupinski, A.; Zdrallek, M.:

Planungs- und Betriebsgrundsätze für städtische Verteilnetze - Leitfaden zur Ausrichtung der Netze an ihren zukünftigen Anforderungen

1. Auflage 2021

### **Band 36**

Kamps, Kristof:

Auswirkungen von Smart-Grid-Technologien auf die Zuverlässigkeit von Mittel- und Niederspannungsnetzen

1. Auflage 2021

ISBN 978-3-7549-3464-7

### **Band 37**

Cibis, Kevin:

Automatisierte Zielnetzplanung zur Entwicklung von innovativen Planungsgrundsätzen für ländliche Niederspannungsnetze in Europa

1. Auflage 2022

ISBN 978-3-7549-3846-1

### **Band 38**

Stephan, Jessica:

Modulare Netzzustandsprognosen für Mittel- und Niederspannungsnetze

1. Auflage 2021

ISBN 978-3-7549-3272-8

### **Band 39**

Schmidt, Robert:

Gewinnoptimale Vermarktung lastseitiger Flexibilitätsoptionen in Virtuellen Kraftwerken

1. Auflage 2021

ISBN 978-3-7549-3274-2

### **Band 40**

Paulat, Frederik:

Lokale Flexibilitätsmärkte für das präventive Engpassmanagement von Mittelspannungsnetzen

1. Auflage 2022

ISBN 978-3-7549-4406-6

**Band 41**

Zdrallek, Markus (Hrsg.):  
Tagungsband zum 6. Wuppertaler Energie-Forum  
1. Auflage 2022

**Band 42**

Kotthaus, Kevin:  
Marktbasierter Flexibilitätseinsatz zur präventiven Netzengpassbewirtschaftung in Mittel- und Niederspannungsnetzen  
1. Auflage 2022  
ISBN 978-3-7549-5610-6

**Band 43**

Dalamaras, Petros:  
Realitätsgerechte Alterungsmodelle von Mittelspannungs-Netzstationen als Basis optimierter Instandhaltungs- und Erneuerungsstrategien  
1. Auflage 2022  
ISBN 978-3-756516-04-9

**Band 44**

Garzón Real, James Leonardo:  
Ein Netzautomatisierungskonzept für gekoppelte Strom- und Gasverteilnetze  
1. Auflage 2022  
ISBN 978-3-7565-0908-9

**Band 45**

Uhlemeyer, Björn:  
Optimale Eigenversorgung in zellularen Energiesystemen auf Mittel- und Niederspannungsebene  
1. Auflage 2022  
ISBN 978-3-7565-1956-9

**Band 46**

Hobert, Alexander:  
Analyse der Flexibilitätsoptionen zur Optimierung des elektrischen Energiesystems von urbanen Quartieren  
1. Auflage 2022  
ISBN 978-3-7575-1805-9

**Band 47**

Zdrallek, Markus (Hrsg.):  
Tagungsband: NRW Kompetenzzentrum Zustandsbewertung  
1. Auflage 2022

**Band 48**

Azad, Schaugar:

Optimierte Netzzustandsschätzung von Niederspannungsnetzen durch Integration von Smart Meter Daten in Automatisierungssysteme

1. Auflage 2023

ISBN 978-3-7575-1542-3

**Band 47**

Zdrallek, Markus (Hrsg.):

Tagungsband BUW Workshop Sektorenübergreifende Planungs- und Betriebsgrundsätze für Energienetze

1. Auflage 2023

**Band 50**

Baumeister, Dirk:

Betrieb und Planung von Oberleitungsbussystemen

1. Auflage 2023

ISBN 978-3-7575-3977-1

**Band 51**

Wazifehdust, Mahjar:

Prädiktive Regelung und Optimierung eines Oberleitungsbussystems

1. Auflage 2023

ISBN 978-3-7575-3974-0

**Band 52**

Modemann, Marcel:

Adaptive Netzzustandsidentifikation zur Automatisierung von Mittel- und Niederspannungsnetzen

1. Auflage 2023

ISBN 978-3-